frontiers | Research Topics

Physiological and molecular mechanisms of important agronomic traits in plants under various abiotic factors

Edited by
Dongmei Li, Dominik K. Großkinsky and Weiwei Zheng

Coordinated by
Zhibo Wang

Published in
Frontiers in Plant Science

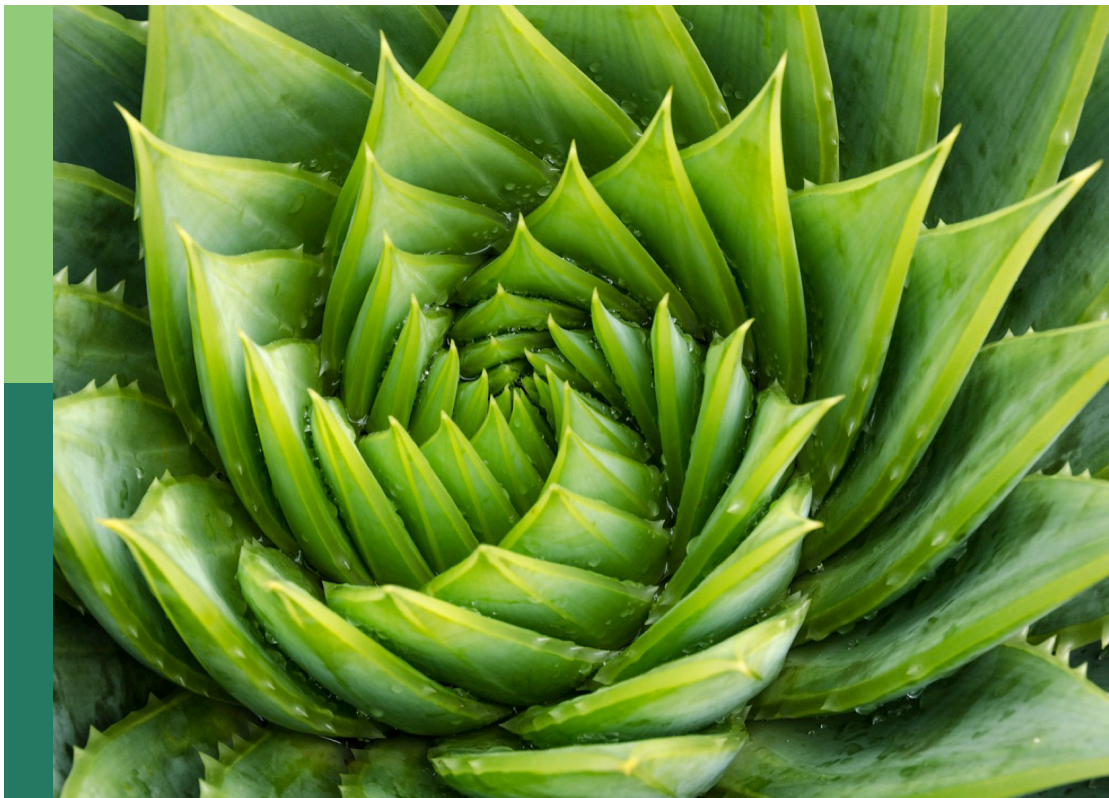

ISSN 1664-8714
ISBN 978-2-8325-5623-8
DOI 10.3389/978-2-8325-5623-8

About Frontiers

Frontiers is more than just an open access publisher of scholarly articles: it is a pioneering approach to the world of academia, radically improving the way scholarly research is managed. The grand vision of Frontiers is a world where all people have an equal opportunity to seek, share and generate knowledge. Frontiers provides immediate and permanent online open access to all its publications, but this alone is not enough to realize our grand goals.

Frontiers journal series

The Frontiers journal series is a multi-tier and interdisciplinary set of open-access, online journals, promising a paradigm shift from the current review, selection and dissemination processes in academic publishing. All Frontiers journals are driven by researchers for researchers; therefore, they constitute a service to the scholarly community. At the same time, the *Frontiers journal series* operates on a revolutionary invention, the tiered publishing system, initially addressing specific communities of scholars, and gradually climbing up to broader public understanding, thus serving the interests of the lay society, too.

Dedication to quality

Each Frontiers article is a landmark of the highest quality, thanks to genuinely collaborative interactions between authors and review editors, who include some of the world's best academicians. Research must be certified by peers before entering a stream of knowledge that may eventually reach the public - and shape society; therefore, Frontiers only applies the most rigorous and unbiased reviews. Frontiers revolutionizes research publishing by freely delivering the most outstanding research, evaluated with no bias from both the academic and social point of view. By applying the most advanced information technologies, Frontiers is catapulting scholarly publishing into a new generation.

What are Frontiers Research Topics?

Frontiers Research Topics are very popular trademarks of the *Frontiers journals series*: they are collections of at least ten articles, all centered on a particular subject. With their unique mix of varied contributions from Original Research to Review Articles, Frontiers Research Topics unify the most influential researchers, the latest key findings and historical advances in a hot research area.

Find out more on how to host your own Frontiers Research Topic or contribute to one as an author by contacting the Frontiers editorial office: frontiersin.org/about/contact

Physiological and molecular mechanisms of important agronomic traits in plants under various abiotic factors

Topic editors
Dongmei Li — Shandong Agricultural University, China
Dominik K. Großkinsky — Austrian Institute of Technology (AIT), Austria
Weiwei Zheng — Zhejiang Agriculture and Forestry University, China

Topic coordinator
Zhibo Wang — Donald Danforth Plant Science Center, United States

Citation
Li, D., Großkinsky, D. K., Zheng, W., Wang, Z., eds. (2024). *Physiological and molecular mechanisms of important agronomic traits in plants under various abiotic factors*. Lausanne: Frontiers Media SA. doi: 10.3389/978-2-8325-5623-8

Table of contents

frontiers | Frontiers in Plant Science

TYPE Editorial
PUBLISHED 18 October 2024
DOI 10.3389/fpls.2024.1502061

OPEN ACCESS

EDITED AND REVIEWED BY
Baris Uzilday,
Ege University, Türkiye

*CORRESPONDENCE
Zhibo Wang
zhibowang@danforthcenter.org

†PRESENT ADDRESS
Zhibo Wang,
Donald Danforth Plant Science Center,
Olivette, MO, United States

RECEIVED 26 September 2024
ACCEPTED 08 October 2024
PUBLISHED 18 October 2024

CITATION
Wang Z, Großkinsky DK, Li D and Zheng W (2024) Editorial: Physiological and molecular mechanisms of important agronomic traits in plants under various abiotic factors.
Front. Plant Sci. 15:1502061.
doi: 10.3389/fpls.2024.1502061

Editorial: Physiological and molecular mechanisms of important agronomic traits in plants under various abiotic factors

Zhibo Wang [1*†], Dominik K. Großkinsky [2], Dongmei Li [3,4] and Weiwei Zheng [5]

[1]School of Plant and Environmental Sciences, Virginia Tech, Blacksburg, VA, United States, [2]Bioresources Unit, Center for Health and Bioresources, AIT Austrian Institute of Technology, Tulln, Austria, [3]College of Horticulture Science and Engineering, Shandong Agricultural University, Taian, China, [4]State Key Laboratory of Crop Biology, Shandong Agricultural University, Taian, China, [5]Key Laboratory of Quality and Safety Control for Subtropical Fruit and Vegetable, Ministry of Agriculture and Rural Affairs, Collaborative Innovation Center for Efficient and Green Production of Agriculture in Mountainous Areas of Zhejiang Province, College of Horticulture Science, Zhejiang A&F University, Hangzhou, China

KEYWORDS

abiotic stress, physiological response, molecular mechanism, agronomic trait, global climate change

Editorial on the Research Topic
Physiological and molecular mechanisms of important agronomic traits in plants under various abiotic factors

The effects of abiotic stress on plant growth, yield, and quality have become increasingly significant in light of global climate change. In this Research Topic, we explore the physiological and molecular mechanisms by which plants respond to various environmental stressors, such as drought, temperature extremes, salinity, metal, chemical, and pollutant exposure. It compiles ten original research articles that provide new insights into how plants adapt and maintain critical agronomic traits in the face of adverse environmental conditions.

Understanding plant responses to abiotic stresses

Plants face an array of environmental challenges, including extreme temperatures, water scarcity, high salinity, and more, all of which negatively impact productivity. These abiotic stresses disrupt cellular homeostasis and alter metabolic pathways, leading to reduced growth, development, and yield. In response, plants have evolved various physiological mechanisms to mitigate these effects. Understanding and evaluating these physiological changes provide critical phenotypic data for investigating genetic mechanisms, which can ultimately aid in molecular breeding efforts.

Two original research studies in this Research Topic focus on plant responses to abiotic stress. Wang et al. explore the response of alfalfa (*Medicago sativa* L.) root systems using a metabolomics approach. They identify amino acids, organic acids, sugars, and alkaloids as key metabolites essential for alfalfa's resistance to drought, including compounds such as 6-gingerol, salicylic acid (SA), indole-3-acetic acid (IAA), gibberellin A4 (GA4), abscisic acid (ABA), trans-cinnamic acid, sucrose, L-phenylalanine, L-tyrosine, succinic acid, and nicotinic acid.

Davoudi et al. investigate the effects of elevated CO_2 levels on the physiology of strawberries and tomatoes. With atmospheric CO_2 levels having increased by more than 20% in the past four decades, this research is highly significant. They found that a three-month exposure to 800 ppm CO_2 increased yields in both strawberry and tomato. Additionally, while both species prioritized fruit development over other sink organs, they were limited by carbon export at elevated CO_2 levels, as new photoassimilates were evenly distributed across various sinks, regardless of CO_2 conditions.

Advances in molecular biology, genetics, and genomics related to abiotic stress adaptation

With food security becoming an increasingly pressing concern, breeding stress-resistant crops has emerged as a critical focus in modern agriculture. This effort is bolstered by advancements in our understanding of the molecular mechanisms and genetic components involved in signaling cascades, transcriptional networks, structural modifications, and biochemical pathways. This Research Topic presents groundbreaking studies that advance molecular biology, genetics, and genomics associated with abiotic stress tolerance, enhancing our ability to dissect plant stress responses.

Tian et al. cloned the *CabHLH18* gene, a specific bHLH transcription factor, from a waterlogging-tolerant pepper cultivar, 'ZHC2'. Compared with wild-type (WT) plants, pepper plants overexpressing *CabHLH18* showed greater water content, amino acid, proline, soluble sugar levels, root viability, and superoxide dismutase activity, while exhibiting lower malondialdehyde content under waterlogging conditions. After 24 hours of waterlogging stress, the fresh weight, amino acid, proline, and soluble sugar levels of the overexpression lines were higher than those of the WT plants. Hence, *CabHLH18* is a promising candidate for breeding waterlogging-tolerant hot pepper varieties.

Liu et al. investigated respiratory burst oxidase homologs (RBOHs), a key enzyme family regulating superoxide production and playing a central role in plant stress responses. Seven *PsRBOH* genes were identified in the pea genome, with tissue-specific expression patterns and functional diversity during growth and stress responses. *PsRBOH4* emerged as a key responsive gene, as its expression was significantly induced under heat, cold, cadmium, drought, and low boron stresses, while *PsRBOH1* primarily responded to salt stress. This study provides valuable insights into the functional roles of pea *RBOH* genes in plant adaptation to climate-related challenges.

Aluminum (Al) toxicity in acidic soils is a major limiting factor affecting crop yield, inhibiting root growth, reducing nutrient and water absorption, and ultimately impairing photosynthesis. Zhang et al. studied potato aluminum-activated malate transporters (ALMTs), which play important roles in responding to Al toxicity, maintaining ion homeostasis, and supporting mineral nutrient distribution. Fourteen *StALMT* genes were identified in the potato genome, unevenly distributed across seven chromosomes. Specific *StALMT* genes were significantly up-regulated in response to Al^{3+} and overexpression of these genes conferred enhanced growth resistance to Al toxicity, highlighting the pivotal role of these genes in combating Al^{3+} toxicity in plants.

Khassanova et al. identified two chickpea zinc finger knuckle genes, *Ca04468* and *Ca07571*, as key candidates in plant responses to drought and dehydration. Various methods, including Sanger sequencing, DArT (Diversity Array Technology) for plant genotyping, molecular marker and gene expression analyses, and field trials, were used to characterize these genes. Associations with 100-seed weight and seed weight per plant were examined, and two SNP molecular markers for both genes were developed and verified. These markers hold potential for marker-assisted selection to improve drought and dehydration tolerance in chickpea, paving the way for the development of novel chickpea cultivars in the future.

These studies collectively highlight the critical advancements in understanding the molecular, genetic, and genomic bases of abiotic stress resistance, providing invaluable tools and knowledge for breeding climate-resilient crop varieties.

Cross-talk between stress responses pinpoints key genetic regulators that serve as central hubs for conferring multiple stress resistance

Under changing climatic conditions, crop plants are increasingly affected by combinations of multiple abiotic stresses rather than individual stress factors. Studies in this Research Topic explore the concept of cross-talk between different abiotic stress responses. Samarina et al. investigate the role of specific transcription factors in regulating stress-responsive genes in tea plants under drought and cold conditions, as well as gene models related to cell wall remodeling. The highlighted key signaling pathways suggest that plants employ shared mechanisms to cope with multiple stressors, providing a molecular basis for breeding tea plants with enhanced tolerance to interactive abiotic stresses.

The frequent co-occurrence of various abiotic stresses highlights the need to identify potential donors resistant to multiple stressors for developing climate-resilient crop varieties. In this context, Kumar et al. screened 41 rice germplasm accessions, including landraces and elite cultivars, for tolerance to drought, salinity, and submergence at the 21-day-old seedling stage over a 10-day period. Specific genotypes were identified as promising

donors for multiple abiotic stress tolerance. Additionally, a set of 30 SSR markers linked to drought, salinity, and submergence QTLs were used to characterize these accessions, providing valuable genomic tools for future breeding efforts.

New insights into interactions between plants and atypical abiotic stress

Continuous agricultural production can also introduce atypical abiotic stress to plants. Zhou et al. reported that continuous cropping of tobacco results in the accumulation of allelopathic compounds in the rhizosphere. Redundancy analysis (RDA) identified eight compounds with autotoxic effects on tobacco growth. These compounds contributed to yield reductions, outbreaks of tobacco black shank, and a decline in beneficial soil flora.

Expanding industrialization and other human activities lead to an increase in the occurrence of sudden environmental pollution accidents (SEPAs), an atypical form of abiotic stress. Developing methods to promptly eliminate pollutants at their source and address the resulting environmental issues is crucial for global ecological health and sustainable human development. Phytoremediation, a biological approach, offers advantages such as simplicity, cost-effectiveness, and the reduction of secondary pollution compared to traditional methods. Li et al. developed a 3D-QSAR pharmacophore model to predict plant resistance and the phytodegradation of polychlorinated biphenyls (PCBs), a class of organic pollutants regulated under the Stockholm Convention due to their persistence, high toxicity, bioaccumulation, and long-range environmental transport. This study provides theoretical support for the application of transgenic plant-based emergency phytoremediation technology.

Future perspectives

As the global climate continues to change, the frequency and intensity of abiotic stresses will likely increase, further challenging global food production systems. This Research Topic provides a foundation for developing stress-tolerant crops that can thrive in adverse conditions. Future work should focus on validating the newly identified molecular mechanisms underlying the physiological responses, integrating these insights into breeding programs and agricultural practices, ensuring that crop yield and quality can be maintained in the face of environmental uncertainties. This Research Topic represents a significant step toward understanding the intricate mechanisms that govern plant stress responses and offers promising avenues for improving crop resilience through innovative biotechnological approaches.

Author contributions

ZW: Writing – review & editing, Writing – original draft. DG: Writing – review & editing. DL: Writing – review & editing. WZ: Writing – review & editing.

Conflict of interest

The authors declare that the research was conducted in the absence of any commercial or financial relationships that could be construed as a potential conflict of interest.

The author(s) declared that they were an editorial board member of Frontiers, at the time of submission. This had no impact on the peer review process and the final decision.

Publisher's note

frontiers | Frontiers in Plant Science

TYPE Original Research
PUBLISHED 10 May 2023
DOI 10.3389/fpls.2023.1145793

OPEN ACCESS

EDITED BY
Guang-Long Wang,
Huaiyin Institute of Technology, China

REVIEWED BY
Wei Zhu,
Institute of Basic Medicine and Cancer (CAS), China
Supriya Ambawat,
Agriculture University, Jodhpur, India

*CORRESPONDENCE
Lidiia Samarina
q11111w2006@yandex.ru

RECEIVED 16 January 2023
ACCEPTED 11 April 2023
PUBLISHED 10 May 2023

CITATION
Samarina L, Wang S, Malyukova L, Bobrovskikh A, Doroshkov A, Koninskaya N, Shkhalakhova R, Matskiv A, Fedorina J, Fizikova A, Manakhova K, Loshkaryova S, Tutberidze T, Ryndin A and Khlestkina E (2023) Long-term cold, freezing and drought: overlapping and specific regulatory mechanisms and signal transduction in tea plant (*Camellia sinensis* (L.) Kuntze).
Front. Plant Sci. 14:1145793.
doi: 10.3389/fpls.2023.1145793

Long-term cold, freezing and drought: overlapping and specific regulatory mechanisms and signal transduction in tea plant (*Camellia sinensis* (L.) Kuntze)

Lidiia Samarina[1,2]*, Songbo Wang[1], Lyudmila Malyukova[1], Alexandr Bobrovskikh[3], Alexey Doroshkov[3], Natalia Koninskaya[1], Ruset Shkhalakhova[1], Alexandra Matskiv[1], Jaroslava Fedorina[1,2], Anastasia Fizikova[1,2], Karina Manakhova[1,2], Svetlana Loshkaryova[1], Tsiala Tutberidze[1], Alexey Ryndin[1] and Elena Khlestkina[2,4]

[1]Federal Research Centre the Subtropical Scientific Centre, Russian Academy of Sciences, Sochi, Russia, [2]Center of Genetics and Life Sciences, Sirius University of Science and Technology, Sirius, Russia, [3]Institute of Cytology and Genetics Siberian Branch, Russian Academy of Sciences, Novosibirsk, Russia, [4]Federal Research Center, N. I. Vavilov All-Russian Institute of Plant Genetic Resources (VIR), Saint Petersburg, Russia

Introduction: Low temperatures and drought are two main environmental constraints reducing the yield and geographical distribution of horticultural crops worldwide. Understanding the genetic crosstalk between stress responses has potential importance for crop improvement.

Methods: In this study, Illumina RNA-seq and Pac-Bio genome resequencing were used to annotate genes and analyze transcriptome dynamics in tea plants under long-term cold, freezing, and drought.

Results: The highest number of differentially expressed genes (DEGs) was identified under long-term cold (7,896) and freezing (7,915), with 3,532 and 3,780 upregulated genes, respectively. The lowest number of DEGs was observed under 3-day drought (47) and 9-day drought (220), with five and 112 genes upregulated, respectively. The recovery after the cold had 6.5 times greater DEG numbers as compared to the drought recovery. Only 17.9% of cold-induced genes were upregulated by drought. In total, 1,492 transcription factor genes related to 57 families were identified. However, only 20 transcription factor genes were commonly upregulated by cold, freezing, and drought. Among the 232 common upregulated DEGs, most were related to signal transduction, cell wall remodeling, and lipid metabolism. Co-expression analysis and network reconstruction showed 19 genes with the highest co-expression connectivity: seven genes are related to cell wall remodeling (*GATL7*, *UXS4*, *PRP-F1*, *4CL*, *UEL-1*, *UDP-Arap*, and *TBL32*), four genes are related to calcium-signaling (*PXL1*, *Strap*, *CRT*, and *CIPK6*), three genes are related to

photo-perception (*GIL1*, *CHUP1*, and *DnaJ11*), two genes are related to hormone signaling (*TTL3* and *GID1C-like*), two genes are involved in ROS signaling (*ERO1* and *CXE11*), and one gene is related to the phenylpropanoid pathway (*GALT6*).

Discussion: Based on our results, several important overlapping mechanisms of long-term stress responses include cell wall remodeling through lignin biosynthesis, o-acetylation of polysaccharides, pectin biosynthesis and branching, and xyloglucan and arabinogalactan biosynthesis. This study provides new insight into long-term stress responses in woody crops, and a set of new target candidate genes were identified for molecular breeding aimed at tolerance to abiotic stresses.

KEYWORDS

tea plant (*Camellia sinensis*), stress tolerance, cell wall biosynthesis, lipid metabolism, light perception, phenilpropanoid pathway, differentially expressed genes, coexpression analysis

1 Introduction

Low temperatures and drought can lead to decreased water potential of plant tissues and induce reactive oxygen species accumulation, which causes severe damage to various cellular components (Chaves et al., 2003; Minhas et al., 2017). Lately, significant progress has been made in the identification of stress-inducible genes and components of signaling pathways involved in a variety of abiotic stresses. Thousands of genes are involved in response to each stressor, and the relationships among genes remain largely unknown (Hao et al., 2018; Xia et al., 2019).

In nature, plants often face several abiotic stresses rather than a particular one at the same time (Ahuja et al., 2010). Cold, freezing, and drought induce common and specific sets of signaling pathways and regulatory mechanisms following biochemical responses affecting plant phenotype (Zhou et al., 2019). Consequently, cold tolerance also promotes drought tolerance in plants, which is consistent with an increase in osmo-regulatory compounds and antioxidant enzyme activities (Li et al., 2019). Thus, it is necessary to better understand the cross-talk genetic mechanisms for the development of cultivars that are tolerant to both environmental factors that can largely contribute to the enhancement of crop productivity under changing climates worldwide (Minhas et al., 2017). Additionally, comparison of the molecular profiles of an organism under different stresses would allow us to identify conserved stress mechanisms in woody crops (Amrine et al., 2015; Muthuramalingam et al., 2017; Chamani Mohasses et al., 2020).

The cross-talk transcriptomic responses between cold and drought have been reported in a few studies. Among them, much more DEGs were upregulated under cold conditions rather than drought in tea plants (Zheng et al., 2015), apples (Li et al., 2019), and maize (Lu et al., 2017). However, a significant number of DEGs were upregulated during drought as compared to cold in cassava (Li et al., 2017). In total, 56% of common genes expressed under drought and cold stresses were related to 43 transcription factor families (primarily *WRKY*, *NAC*, *MYB*, *AP2/ERF*, and *bZIP*) in Arabidopsis (Sharma et al., 2018). Many transcription factors and metabolite-related genes have been shown to be involved in both the cold and drought responses of tree species (Wang et al., 2012; Ban et al., 2017). ABRE-binding proteins and ABRE-binding factor TFs control gene expression in an ABA-dependent manner. *SNF1*-related protein kinases2, group A2C-type protein phosphatases, and ABA receptors were shown to control the ABA signaling pathway. ABA-independent signaling pathways such as *DREB* and *NAC* TFs are also involved in stress responses, including drought, heat, and cold (Nakashima et al., 2014; Pareek et al. 2017). In contrast to Arabidopsis (Matsui et al., 2008; Sham et al., 2014), maize (Shan et al., 2013), and rice (Rabbani et al., 2003). In woody crops, little has been reported about transcriptome dynamics and crosstalk responses to drought, cold, and freezing. Moreover, available data were obtained for short-term stress treatments, but long-term stress and recovery were not sufficiently studied.

Among tree crops, the tea plant (*Camellia sinensis* L.) is one of the most important commercial crops in China, India, Sri Lanka, Kenya, and certain Caucasian and Middle Eastern countries (Turkey, Georgia, Russia, and Azerbaijan). This perennial evergreen crop is grown in more than 60 countries on five continents, from 49°N in Ukraine to 33°S in South Africa (Turkozu and Sanlier, 2017). In the most tea-producing countries, plantations are affected by drought and cold stress, which significantly reduce the yield and decrease the distribution of the crop in colder areas. The available studies on tea plants confirmed that the key cold regulators *ICE*, *CBF*, and *DHN* are related to an ABA-independent responsive pathway and participate in both cold and drought stress and in other abiotic stress responses (Liu et al., 2015; Singh, and Laxmi 2015; Ban et al., 2017; Hu et al., 2020). In addition, several transcription factor families (*AP2/EREBP*, *WRKY*, *bHLH*, *NAC*, *MYB*, *HSP*, *LEA*, *CML*, *bZIP*, *HD-ZIP*, *HSF*, *SCL*, *ARR*, and *SPL*) have been shown to be activated in tea plants in response to cold and drought (Chen et al., 2014; Cao et al., 2015;

Zheng et al., 2015; Wang et al., 2016; Cui et al., 2018; Li et al., 2019; Ma et al., 2019; Zhang et al. 2019a). Additionally, signal transduction pathways are the link between the sensing mechanism and the genetic response, and plants can have multiple stress perception and signal transduction pathways, which may cross-talk at various steps in the pathways (Huang et al., 2012). The pathway analysis indicated that "plant hormone signal transduction," "starch and sucrose metabolism," "peroxisomes," and "photosynthesis" might play a vital role in low temperature responses in tree crops (Zhou et al., 2021).

Due to out-breeding and its long gestation period, the tea plant requires next-generation breeding strategies to improve its drought and cold tolerance through a deeper understanding of key regulators and their variants for precision introgressions to have better yield and quality under stress conditions. Therefore, efforts are needed to elucidate the global transcriptomic dynamics of multiple tea genotypes under drought and cold stress to critically discern key molecular players (Parmar et al., 2019). The North Caucasus' tea germplasm collection is in the border region (44°36′ 40″ N, 40°06′40″ E) of the possible global tea production and can be the source of the most tolerant cultivars; some genotypes of the collection can survive below −20°C, providing a good yield (Samarina et al., 2022). Resequencing of new germplasm outside of the global producing regions can help to discover novel molecular mechanisms of acclimation and domestication of tree crops in the extreme climatic zones. The third-generation sequencing technology represented by PacBio has the advantage of long read lengths (Sun et al., 2020a). PacBio and RNA-seq sequencing technologies are highly complementary to each other. To obtain an overall view of the molecular regulation during cold, freezing, drought, and recovery, we combined PacBio genome sequencing and RNA-Seq to investigate the transcriptome dynamics of *C. sinensis* cv. Kolkhida. This study will provide new data on overlapping and specific regulatory pathways, key functional genes, and signal transduction components involved in short- and long-term cold, freezing, drought, and recovery in perennial tree crops.

2 Materials and methods

2.1 Plant material and stress induction

Three-year-old plants of the elite local tea cultivar Kolkhida (the survival temperature of adult plants is about −10–12°C) obtained by vegetative propagation at the Federal Research Centre, the Subtropical Scientific Centre of the Russian Academy of Sciences (FRC SSC RAS, Sochi, Russia), were used for experiments. Healthy plants grown in 2-liter pots filled with brown forest acidic soil (pH = 5.0) were randomly selected for experiments; 9–15 plants per treatment were replicated three times. The plants were maintained for one month at the following control conditions: temperature +22 ± 2°C, light regime day/night 16/8, light intensity of 3,000 lux, soil water content of 65 ± 5%. To induce cold stress, plants were placed in the cold chamber HF-506 (Liebherr, Denmark) at a temperature of +4 ± 2°C for 14 days. Freezing was induced after 14 days of cold by the following decrease of the temperature by −4°C for 7 days. Recovery was induced by a gradual increase in temperature +10 ± 2°C for 10 days. To induce drought stress, the soil watering was gradually decreased to 15% within 14 days, with a 7-day recovery period. The light regime was day/night 16/8, the light intensity was 3,000 lux, and the soil water content was 65 ± 5 for all treatments (Table 1).

2.2 Phenotypical evaluation of tea plants under stress

For each assessed parameter (relative electrolyte leakage, relative water content, caffeine, theanine, and catechin contents),

TABLE 1 Experimental treatments.

Treatment	Temperature, °C	Light/dark	Soil water content, %	Duration,Days
Control	+22 ± 2	16/8—3,000 lux	65 ± 5	30
Cold12h (12 h)	+4 ± 2	16/8—3,000 lux	65 ± 5	0.5
Cold3d (three days)	+4 ± 2	16/8—3,000 lux	65 ± 5	3
Cold14d (14 days)	+4 ± 2	16/8—3,000 lux	65 ± 5	14
Freezing3d (three days)*	−4 ± 2	16/8—3,000 lux	65 ± 5	3
Freezing7d (seven days)*	−4 ± 2	16/8—3,000 lux	65 ± 5	7
RecoveryC (recovery after freezing)	+10 ± 2	16/8—3,000 lux	65 ± 5	10
Drought3d (three days)	+22 ± 2	16/8—3,000 lux	45 ± 5	3
Drought9d (nine days)	+22 ± 2	16/8—3,000 lux	25 ± 5	9
Drought14d (14 days)	+22 ± 2	16/8—3,000 lux	15 ± 5	14
RecoveryD (recovery after drought)	+22 ± 2	16/8—3,000 lux	65 ± 5	7

*Freezing was followed by a 14-day cold.

2^{nd}, 3^{rd}, and 4^{th} mature leaves from the top of the plant were used for sampling.

Electrolyte leakage indicating the damage of leaf tissues was measured using the conductivity meter ST300C (Ohaus): a leaf sample was immersed in 150 ml of deionized water, and electrical conductivity was evaluated 2 h later (L1) and after 2 h of boiling and cooling (L2). The relative electrolyte leakage (EL, %) was calculated as: $EL = \frac{L1}{L2} \star 100$ (Bajji et al., 2002).

The relative water content (RWC) was determined as follows: fresh leaves were first weighed (FW), then immersed in water solution for 12 h (TW) and dried at 105°C for 5 h (DW). RWC was calculated according to the formula: $RWC = (\frac{(FW-DW)}{(TW-DW)}) \star 100\,\%$ (Yamasaki and Dillenburg, 1999).

Caffeine, L-theanine, and catechins (gallocatechin (GC), epigallocatechin (EGC), epicatechin (EC), epicatechin gallate (ECG), gallocatechin gallate (GCG), and epigallocatechin gallate (EGCG)) (mg g^{-1} dry leaf mass) were evaluated by HPLC using the following extraction protocol: 130–175 mg of dried tea leaf were poured into a 4.0-ml solution of 80% methanol, hermetically closed, and incubated for one week at +4°C in the dark. After that, the vessels with methanol leaf extracts were placed in a UV bath for 30 min and then centrifuged at 13,000 rpm for 10 min. Then, 1 ml of supernatant was injected into the HPLC column. The Agilent Technologies 1100 HPLC chromatographer, equipped with a flow-through vacuum degasser G1379A, a 4th-channel low pressure gradient channel pump G13111A, an automatic injector G1313A, a column thermostat G13116A, and a diode array detector G1316A, was used. The 2.1 × 150 mm column filled with octadecyl silyl sorbent, with agrain size of 3.5 μm, "ZORBAX-XDB C18," was applied. The acetonitrile solution was used for the gradient: the initial composition of the mobile phase, consisting of 90% (v/v) solvent A (0.1% H_3PO4) and 10% of solvent B (90.0% acetonitrile), was maintained for 8 min. After that, solvent A was decreased linearly to 40% at 25 min, 0% at 90 min, and then increased to 100% at 29.1 min to 34 min. The programming was then continued in isocratic mode as follows: 40% A at 70.1 to 75.0 min; 7% A at 75.1 to 90.1 min (the flow rate is 0.30 ml/min, the column temperature is 40°C). The wavelengths for detection were 195 nm (for L-theanine) and 273 nm for caffeine and catechins. Identification of the substances was performed based on the time of holding the standards for respective compounds.

2.3 Pac-Bio genome sequencing, assembly, and annotation of cv. Kolkhida

For the PacBio Hifi sequencing, the 20 kb libraries with the three cells of data were constructed following PacBio's standard protocol and sequenced using the Sequel II platform. For the short reads, DNA samples were sequenced using the Illumina Hiseq platform with 150-bp pair-end reads and an insert size of 350 bp. All the raw sequencing reads were preprocessed to remove low-quality bases, adaptor reads, duplications, and potential contaminants before subsequent analyses. A total of 88.62 Gb (~29-fold) of high-fidelity PacBio reads were sequenced for the Kolkhida tea genome. We assembled reads by Hifiasm (Cheng et al., 2021), and because of the high heterozygosity and repeat sequence number in the tea plant genome, redundant contigs were conducted by Purge_Dups (Guan et al., 2020). To correct the SNP errors and small indel variations, the Pilon tool (Walker et al., 2014) was employed to polish the genome using Illumina short reads. Finally, the assembled genome size was 3.11 Gb with a contig N50 of 4.32 Mb. The BUSCO (Manni et al., 2021) assessment showed 94.3% completeness of core-orthologous genes. Otherwise, the Illumina short reads were mapped to the genome with a 97.57% mapping ratio.

2.4 RNA-sequencing and data analysis

The leaf sampling for the RNA extraction was performed between 10 and 12 am (except for the treatment Cold12h, where it was performed at 10 pm). A total of 48 RNA libraries were constructed for sequencing (three to five biological replicates per treatment, each replicate representing a separate plant) using standard Illumina protocols, and RNA sequencing was performed by Novogene Co., Ltd. (https://en.novogene.com/) using the Illumina Hi-Seq platform. Read quality control was performed using fastp (https://github.com/OpenGene/fastp). The RNA-Seq reads were aligned to the reference genome using the HIS AT2 short read aligner tool (Kim et al., 2019). Intermediate file processing of.sam to sorted.bam conversion was carried out using the SAMTOOLS v.1.9 package (Danecek et al., 2021). Based on the alignment BAM file, the RSEM (https://github.com/deweylab/RSEM) (Li and Dewey, 2011) was employed to calculate and quantify the gene expression using the default parameters. Gene expression was normalized by reads per kilobase of exon per million reads mapped. The differentially expressed genes (DEGs) for each of the compared sample groups were identified by the DEseq2 package (Love et al., 2014) with a P-value<0.05, and those DEGs with |log2FC|>1, FDR<0.1 were defined as having significantly different expression. The Venn diagrams of the DEGs among the compared groups were created by the Venn web tool (https://bioinformatics.psb.ugent.be/webtools/Venn/). GO (http://www.geneontology.org/) and KEGG (https://www.kegg.jp/) enrichment of the DEGs was conducted by the Clusterprofiler (https://bioconductor.org/packages/clusterProfiler/).

2.5 Gene prediction

We combined *de novo*, homology-based, and RNA-seq methods to predict protein-coding genes in the tea plant cv. Kolkhida genome. AUGUSTUS (Stanke et al., 2006) and GENESCAN (Burge and Karlin, 1997) were conducted for *de novo* prediction. First, the TE sequences were masked from the genome. For the AUGUSTUS, we randomly selected 2,000 high quality genes from the homology-based results as the training sets. Arabidopsis parameters were used for Genescan.

For the homology prediction, the proteins derived from *Actinidia chinensis*, *Arabidopsis thaliana*, *Camellia oleifera*,

C. sinensis cv. TGY, *Vitis vinifera*, and uniprot_sprot_plants were used as the inputs for TBLASTN (Altschul et al., 1997) with an E-value threshold of 1e−06. Then the blast hits were linked to candidate gene loci by solar (v.0.9.6) (Li et al., 2010) with parameters "-a prot2genome2 –z". Finally, the Genewise tool (Birney et al., 2004) was employed to construct the intron-exon boundary. Genes with a length of less than 150 bp or with incomplete structures were removed.

For the RNAseq prediction, all the transcript sample data were mapped to the genome using STAR (2.7.9a) (Dobin et al., 2013) and then the alignments were assembled by String (v2.1.7) (Kovaka et al., 2019) with the following parameters: "-j 2 -f 0.01 -c 2 -m 200 -a 10".

Finally, all pieces of evidence resulting from the above three methods were integrated by the Maker tool (v.01.03v 3.01.03) Pipeline (Cantarel et al., 2008), which can integrate predictions based on homology proteins, *de novo* gene models, and transcriptome assembly genes to better annotate protein-coding genes.

2.6 Verification of the RNA-Seq results by qRT-PCR

Total RNA was extracted from the third leaf from the top of the plant in three biological replicates by the Trizol method, according to the manufacturer's protocol (Biolabmix, Russia; https://biolabmix.ru/). The concentration and quality of RNA were evaluated using a Bio-drop μLite (Biochrom, UK) spectrophotometer, and quality was assessed in a 1% agarose gel. The 1,000 ng RNA was treated with 1 μl DNAseI-Buffer and 1 μl DNAseI (Biolabmix, Russia; https://biolabmix.ru/) for 30 min at 37°C, with subsequent DNAse inhibition by heating to 65°C for 10 min. After that, 1,000 ng of RNA was used to prepare 20 μl of cDNA using the M-MuLV–RH-kit (Biolabmix, Russia; https://biolabmix.ru/), with the following quality evaluation by gel electrophoresis and qRT-PCR using LightCycler 96 (Roche Life Sciences; https://lifescience.roche.com/global_en.html). After cDNA preparation, all samples were diluted to the same concentration of 700 ng μl^{-1} according to the standardization achieved by the expression of the reference gene Actin (NCBI Gene ID: 114316878). To analyze gene expression, the 15 μl of the qPCR-mix consisted of 7.5 μl of 2× SybrBlue qRT-PCR-buffer with the hot-start polymerase (Biolabmix, Russia; https://biolabmix.ru/), 0.2 μl of each primer (forward and reverse), 1 μl cDNA, and the rest volume was PCR-water. The two-step amplification program was applied: preheating for 5 min at 95°C, 40 cycles of amplification (10 s at 95°C, 30 s at 56–62°C), final elongation for 5 min at 72°C, and melting for 3 min at 95°C. The relative gene expression level was calculated by the statistical method of Livak and Schmittgen (2001) using the following algorithm: $2^{-\Delta\Delta Cq}$, where:

$$\Delta\Delta Cq = (Cq_{\text{gene of interest}} - Cq_{\text{internal control}})_{\text{treatment}} - (Cq_{\text{gene of interest}} - Cq_{\text{internal control}})_{\text{control}}.$$

2.7 Data analysis and availability

Statistical analyses of the data were carried out using XLSTAT software (free trial version) (https://www.xlstat.com/). A one-way ANOVA and Tukey's HSD were performed to determine significant differences between the respective treatments. Additionally, hierarchical clustering was performed, and dissimilarities were calculated using the DICE coefficient, with agglomeration by Ward's method (Ward 1963). The data were analyzed by Pearson's (n) PCA type. The co-expression analysis was performed by pairwise Pearson correlation coefficients using the function pandas.DataFrame.corr (https://pandas.pydata.org/docs/reference/api/pandas.DataFrame.corr.html). For calculations, we used log2-values of expression changes in response to cold, freezing, and drought. Pairs of co-expressed genes with a pairwise Pearson coefficient >0.94 were selected for the gene network reconstruction. The table with co-expression above the threshold was imported into Cytoscape v. 3.9.1 for further layout and visualization (Shannon et al., 2003). Additionally, the information about homologs in *A. thaliana* was added to the gene network (Supplementary Tables S4, S5).

Raw data from the PacBio HiFi reads and the Illumina short reads, as well as genome assemblies and annotation proteins (gff and fasta) have been deposited in the China National GeneBank Database (project accession number: CNP0004163).

3 Results

3.1 Phenotypical evaluation of stress effect

Cold resulted in increased electrolyte leakage (EL) in five of the nine treatments as compared to control, namely Cold14d, Freezing3d, Freezing7d, Drought14d, and RecoveryC (see Table 1 above for abbreviation decoding). The highest EL (14.0%) was detected under Freezing7d as compared to Control (1.6%). Three other treatments (Cold14d, Freezing3d, and Drought14d) showed about a 3-fold elevation in EL, indicating equal tissue damage in these treatments (Figure 1A). The remarkable decrease in RWC was observed in four treatments (Freezing3d, Freezing14d, RecoveryC, and Drought14d)—57.4%–75.1% as compared to Control, which was at 93.0%. Interestingly, no significant decrease in RWC was detected in the other treatments (Figure 1B). Additionally, RecoveryC showed lower EL and lower RWC as compared to RecoveryD, indicating delayed recovery after freezing as compared to drought.

Under the effects of cold and freezing, the contents of several catechins, namely EGC, GCG, and EGCG, decreased by 30% compared to the control (Figure 1C). The long-term drought has not significantly affected tea quality; however, the short-term drought resulted in a decrease in several catechin contents (EGC, GCG, and EGCG) in tea leaves (Figure 1D). Additionally, no significant changes in GC, EGC, and EC were detected among different drought treatments.

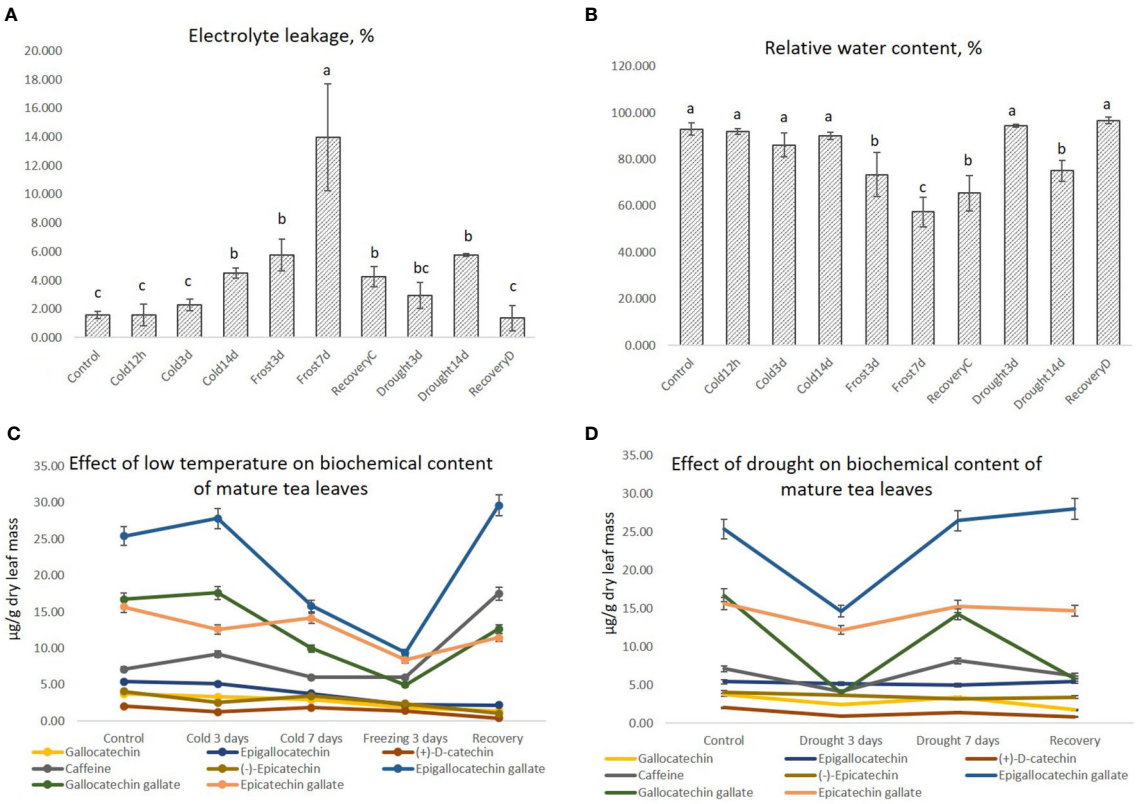

FIGURE 1
The relative electrolyte leakage **(A)**, the relative water content **(B)**, and the catechins and caffeine content **(C, D)** in the tea leaf tissues under cold, freezing, and drought treatments. Small letters represent the significance of the differences at P<0.05 as compared to the control.

3.2 Transcriptome dynamics of tea plants under cold, freezing, drought, and recovery

3.2.1 Biological processes and differentially expressed genes under cold, freezing, drought, and recovery

Among the different treatments, the highest number of DEGs was observed under Freezing7d (7915) and Cold14d (7896), with 3,780 and 3,532 genes upregulated, respectively. The lowest number of DEGs was observed under Drought3d (47) and Drought9d (220), with five and 112 genes upregulated, respectively (Table 2; Supplementary Tables S1, S2). The RecoveryC samples indicated about 6.5 times greater DEG numbers as compared to RecoveryD.

Based on the DEGs dissimilarity, two main significant clusters were identified: the first cluster includes the following samples—Control, Drought3d, Drought9d, and RecoveryD. The second cluster combined all treatments with a pronounced stress response: Cold14d, Drought14d, Freezing3d, Freezing7d, and RecoveryC (Figure 2A). The correlation map corresponds with Figure 2A, indicating three groups of correlated treatments: 1). Control, Drought3d, Drought9d, Cold12h, and RecoveryD; 2). Freezing3d, RecoveryC, and Drought14; and 3). Cold14D, Freezing7D, and Cold3d (Figure 2B). These results correspond with the physiological parameters, confirming the similar stress severity in tea plants subjected to Cold14D, Freezing3d, and Drought14d. Thus, these three treatments were further used to analyze overlapping and specific stress responses.

Analyzing the gene networks, a more pronounced response was observed under Cold14d as compared to Freezing3d and Drought14d (Figure 3). Interestingly, much more DEGs involved in the biosynthesis of the secondary metabolites, carbon metabolism, glyoxylate, and dicarboxylate metabolism were observed under Cold14d, than under Freezing3d and Drought14d.

As for common responses, most of the genes involved in photosynthesis and ribosome assembly were significantly downregulated under Drought14d, Cold14d, and Freezing3d. Most DEGs related to RNA polymerase, plant–pathogen interaction, and metabolic pathways were downregulated under Cold14d and Freezing3d. Many genes involved in the biosynthesis of secondary metabolites were upregulated under Drought14d and Cold14d. As for specific responses, most DEGs related to the MAPK-signaling pathway were specifically downregulated under Freezing3d. However, the big portion of DEGs related to nucleotide excision repair, base excision repair, mismatch repair, DNA replication, and RNA polymerase activity was specifically downregulated under Drought14d. Additionally, many DEGs related to galactose metabolism and metabolic pathways were specifically upregulated under Drought14d.

Subsequently, we classified all upregulated genes into five categories by the fold of elevation to control, where I—genes were upregulated greater than 100 folds and V—genes were upregulated

10.3389/fpls.2023.1145793

TABLE 2 The number of differentially expressed genes in each experimental group.

VS	Upeegulated	Downregulated	Total
Control-VS-Cold12h.DEseq2	701	554	1,255
Control-VS-Cold03d.DEseq2	1,627	1,789	3,416
Control-VS-Cold14d.DEseq2	3,532	4,364	7,896
Control-VS-Frost03d.DEseq2	1,034	2,009	3,043
Control-VS-Frost07d.DEseq2	3,780	41,35	7,915
Control-VS-CRecovey.DEseq2	1,727	1,929	3,656
Control-VS-Drougth03d.DEseq2	5	42	47
Control-VS-Drougth09d.DEseq2	112	108	220
Control-VS-Drougth14d.DEseq2	1,258	667	1,925
Control-VS-DRecovey.DEseq2	130	434	564

up to 2.99 folds (Figure 4A). Interestingly, 45, 4, and 23 genes from category I were induced by Drought14d, Cold14d, and Freezing3d, respectively. However, three to four times greater numbers of genes from categories IV and V were observed in Cold14d as compared to Drought14d and Freezing3d. Among all upregulated DEGs, 12%, 10%, and 5% were overlapping for Cold-Freezing, Cold-Drought, and Cold-Freezing-Drought, respectively (Figure 4B). Only 1% of genes were common for drought and freezing. Remarkably, 72% of genes were specifically upregulated by each treatment. Additionally, many DEGs of certain biological processes were specifically induced by Drought14d, Freezing3D, and Cold14d (Figures 4C, D). For upregulated DEGs, GO terms related to stress and stimulus responses were significantly enriched at all time points. Pathway analysis indicated overlapping GO terms related to thylakoid membranes, photosynthetic membranes, the response to Karrikin, electron transport, and the cytochrome complex play a vital role in tea responses (Figure 4D). Interestingly, GO-term enrichment analysis indicates more specific biological processes detected in the tea drought response as compared to the cold and freezing responses.

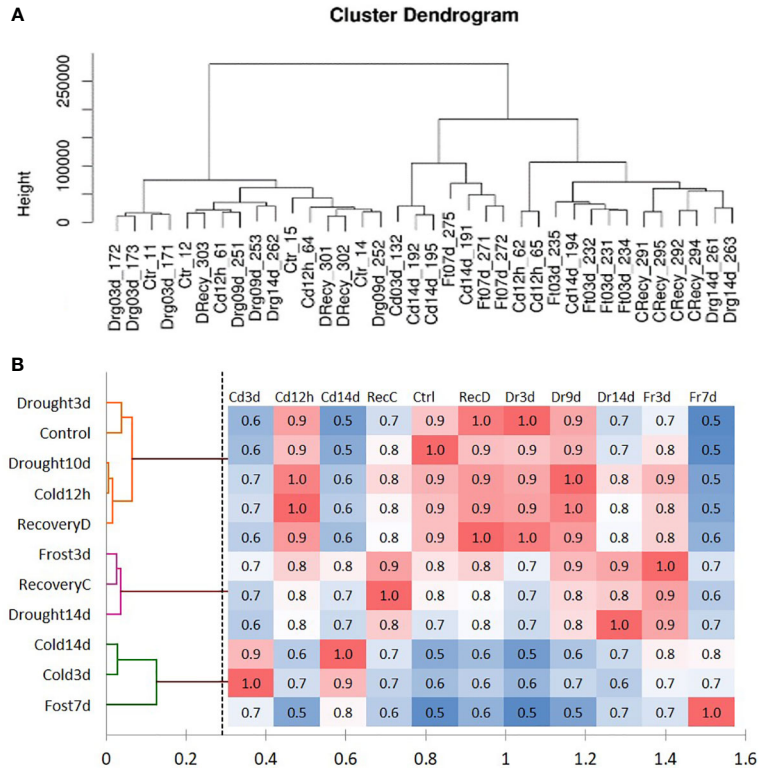

FIGURE 2
(A) UPGMA-clustering of tea transcriptome samples; **(B)** correlation heat map of tea plant stress responses based on transcriptome profiles.

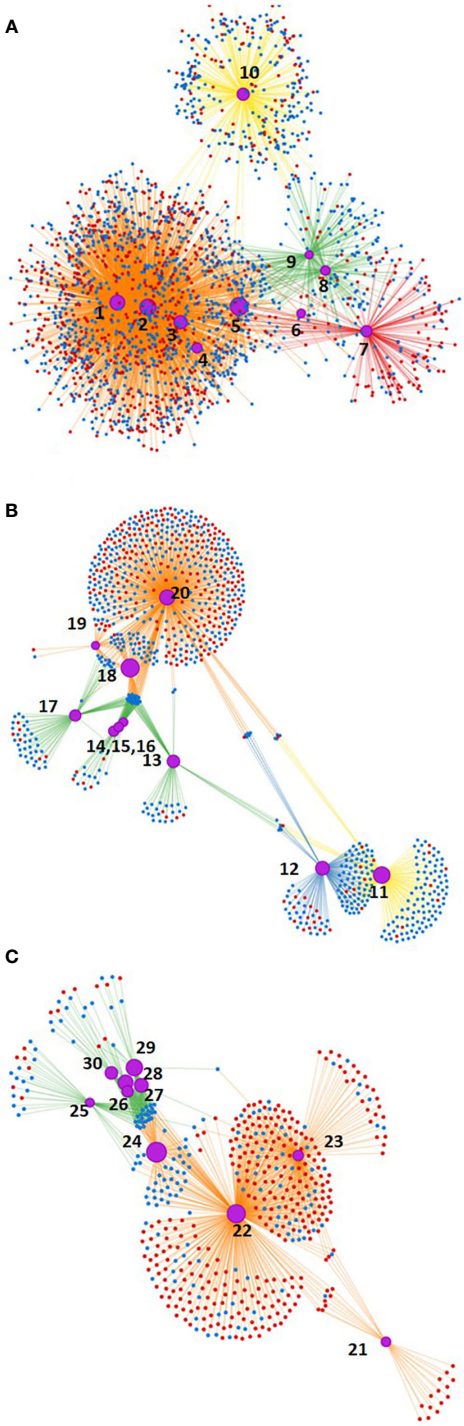

FIGURE 3
Gene networks affected by Cold14d, Freezing3d, and Drought14d: blue dots—downregulated genes, red dots—upregulated genes, purple cycles marked with numbers—biological processes: **(A)** Cold14d: 1—Biosynthesis of secondary metabolites, 2—Metabolic pathways, 3—carbon metabolism, 4—Glyoxylate and dicarboxylate metabolism, 5—Photosynthesis, 6—Photosynthesis antenna proteins, 7—Endocytosis, 8—RNA-polymerase, 9—Ribosome, 10—Plant–pathogen interaction; **(B)** Freezing3d: 11—Plant–pathogen interaction, 12—MAPK-signaling pathway, 13—RNA-polymerase, 14—Base excision repair, 15—DNA-replication, 16—Mismatch repair, 17—Ribosome, 18—Photosynthesis, 19—Oxidative phosphorylation, 20—Metabolic pathways; **(C)** Drought14d: 21—Galactose metabolism, 22—Metabolic pathways, 23—Biosynthesis of secondary metabolites, 24—Photosynthesis, 25—Ribosome, 26—Nucleotide excision repair, 27—Base excision repair, 28—Mismatch repair, 29—DNA-replication, 30—RNA-polymerase.

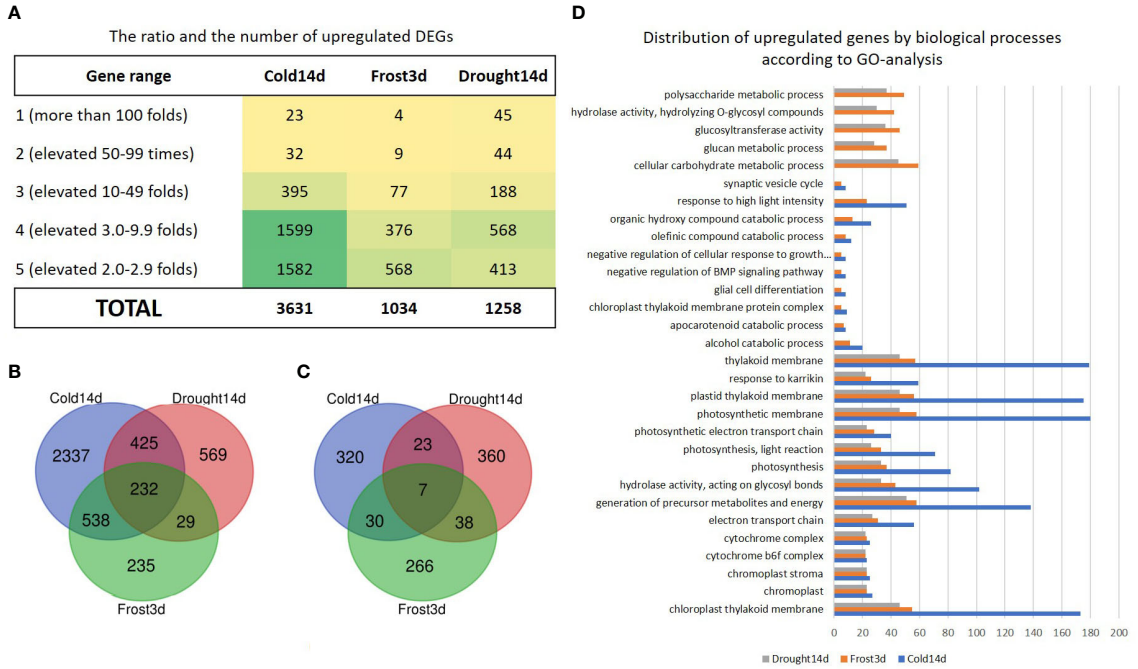

FIGURE 4
The classification of the significantly upregulated genes under Cold14d, Freezing3d, and Drought14d: **(A)** the ratio and the number of upregulated DEGs, **(B)** the number of common and specific DEGs, **(C, D)** the number of common and specific DEGs related to certain biological processes.

Among specifically upregulated genes, 57 genes of categories I and II (dramatically upregulated), were specifically induced by Drought14d (Supplementary Table S3).

3.2.2 Classification of commonly upregulated DEGs under cold, freezing, and drought

In total, 6.3% of overlapping (common) upregulated genes present in 232 genes and appeared to be the core Cold-Drought-Freezing-responsive genes. These genes clustered into four groups (Clusters A, B, C, and D) according to their expression level (Figure 5; Supplementary Table S3).

The group D combined 22 genes with expression increased by 50–100-fold as compared to control, namely, *ELIP1*, *ECP63-like*, *GRF1*, *UGT74B1*, *glucan endo-1,3-beta-glucosidase 11-like*, *12-like*, *phosphoprotein ECPP44*, *sugar transport protein 13-like*, *protein NRT1/PTR FAMILY 1.2-like*, *F-box/kelch-repeat protein SKIP25-like*, *ultraviolet-B receptor UVR8-like*, *11S globulin seed storage protein 2-like*, *EID1-like F-box protein 3*, *=probable protein phosphatase 2C 24*, and seven more that showed no overlap with any annotated genes and can represent novel protein-coding genes). Similarly, the expression groups B and C combined 71 and 46 genes, respectively, which were upregulated up to 49 folds. Additionally, the most abundant expression group A combined 93 genes with a moderate increase of up to 9 folds. Along with well-known regulators of stress response (e.g., *CBF* and *DHN*), we identified novel transcripts that were highly induced by cold, freezing, and drought (e.g., *ELIP1* and *GRF1-interacting factor 1*).

Interestingly, most of the genes in categories IV and V were related to the same category in Cold14d, Freezing3d, and Drought14d, indicating their similar role and co-expression character in the three stress treatments. In addition, transcription factors and metabolism-related genes were observed in each of the expression groups from 1 to 5. Among the 1,492 transcription factor DEGs identified in all treatments, 20 were common in long-term cold, freezing, and drought (Supplementary Table S3).

These 20 transcription factor genes correspond to *CBF1*, *DHN1*, *DHN2*, *DHN3*, *LEA*, *LEA14-A*, *LEA29*, *bHLH*, *WRKY22*, *ZAT10*, *NAC*, *GIF1*, *AP2*, *ERF*, *PIP7a*, *GRAS*, *ECP63*, *HSP70*, *DUF567*, and *COR413PM1-like*, and most of them are known to be related to the ABA-signaling pathway (Supplementary Table S3).

Remarkably, 36 genes related to hormone-, calcium-, and ROS-signaling were revealed among these 232 DEGs. Additionally, 26 genes were related to cell wall remodeling and biosynthesis: 19 DEGs were related to lipid metabolism, 12 DEGs were related to the biosynthesis of polyphenols and anthocyanidins, 11 DEGs were involved in sugar metabolism and transport, nine DEGs were related to photosynthetic activity and stomatal organization, and eight DEGs were related to amino acid biosynthesis and transport. Also, several genes related to signaling pathways, cell wall remodeling and biosynthesis, and amino acid biosynthesis and transport were not functionally annotated. The rest part of upregulated DEGs were related to protein ubiquitination (*UBC24*, *PUB1*, *PUB19*, *PUB14*, *PUB45*, *SKIP25*, *NPL4*, *ALT13*, and *ATL51*) and protein catabolism (*CBP2*, *TIC20-V*, *RPN7*, *APF2*, and *ASPG1*), inorganic ion transport (*NRT2.7*, *NRT1*, *ZIP6*, *ZIP8*, *BOR5*, *ACA1*, *FER3*, *FRO2*, *At1g07590*-like, and two Potassium ion transporters), ABC-transport (*ABCC5*, *ABCC3*, *ABCC13*, *ABCC8*, and *ABCF1*), post transcriptional regulation of gene expression (*SNRPB*, *RCL*, *IWC1*, *CDA1*, and *URT1*), DNA-methylation and chromatin modification (*H3.3*, *H2B.1*, and *PELP1*), and NAD-metabolism (*NDA1*, *NADSYN*, and *GID8*) (Supplementary Table S3).

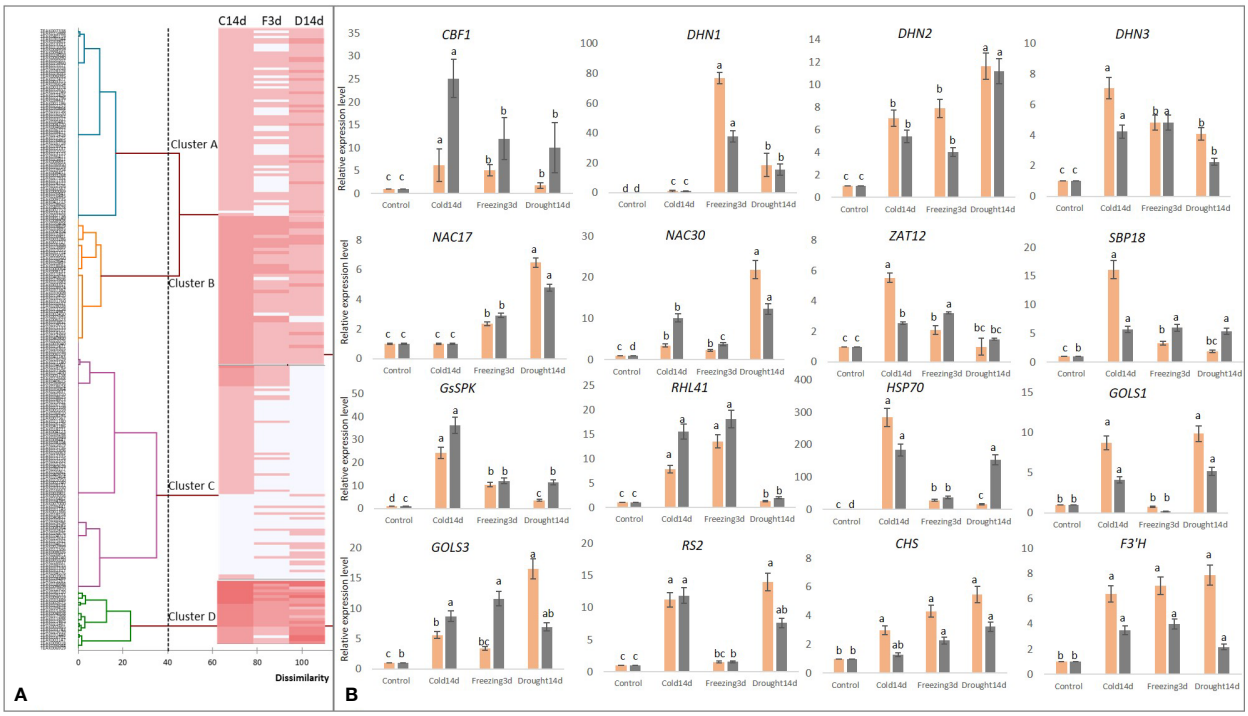

FIGURE 5
Overlapping genes significantly upregulated in tea plants under Cold14d, Freezing3d, and Drought14d as compared to Control: **(A)** the UPGMAdendrogram and the heat-map based on the level of upregulation according to RNAseq data (see Supplementary Table S3 for details); **(B)** the relative expression levels of the several stress-inducible genes assessed by qRT-PCR (gray columns) and RNAseq (orange columns). Small letters represent the significance of the differences at P<0.05 as compared to control.

Interestingly, 27 novel uncharacterized transcripts were found among these 232 overlapping DEGs, which were highly induced by cold, freezing, and drought and were not recognized and not annotated by publicly available databases, namely TEAK032489, TEAK033550, TEAK006579, TEAK006919, TEAK029131, TEAK010562, TEAK012137, TEAK013321, TEAK015517, TEAK016462, TEAK036810, etc. (Supplementary Table S3).

To validate the expression data obtained by RNA-Seq, we performed qRT-PCR analysis of the expression of the set of stress-inducible genes under long-term cold, freezing, and drought (Figure 5). In general, both data sets were congruent. The important regulators of the stress responses in tea showed 10-fold elevated expression during long stress treatments, namely *CBF1*, *DHN1*, *DHN2*, *DHN3*, *ZAT12*, *GS-SPK*, *SBP18*, and *HSP70*. Several stress-inducible sugar-metabolism genes (*GOLS1*, *GOLS3*, and *RS2*) were upregulated up to 10-fold. Two important polyphenol biosynthesis transcripts (*CHS* and *F3'H*) were upregulated 2–8 fold in all treatments as compared to control, which is consistent with RNASeq data. However, GOLS1 and RS2 indicated inhibited expression under freezing.

To summarize overlapping stress responses and to propose new candidate genes for molecular breeding, we performed co-expression analysis and network reconstruction of the 58 key upregulated DEGs related to signal transduction, light perception, and cell wall remodeling. In total, 390 highly correlated pairs (Pearson coefficient >0.94) were revealed for 54 genes. The KEGG annotations of homologs in *A. thaliana* provided the co-expression gene network with corresponding enzyme annotations (Supplementary Table S5). This network contains 56 genes and 415 edges, of which 390 are co-expressed and 25 are enzyme associations (Figure 6). Among them, the central functional cluster of 19 genes was revealed with the highest co-expression connectivity (green color). Among these 19 genes, seven are related to cell wall remodeling (*GATL7*, *UXS4*, *PRP-F1*, *4CL*, *UEL-1*, *UDP-Arap*, and *TBL32*), four are related to Ca^{2+}-signaling (*PXL1*, *Strap*, *CRT*, and *CIPK6*), three are related to photo-perception (*GIL1*, *CHUP1*, and *DnaJ11*), two are related to hormone signaling (*TTL3* and *GID1C-like*), two are related to ROS signaling (*ERO1* and *CXE11*), and one is related to the phenylpropanoid pathway (*GALT6*). This cluster also contains 41 of 79 most significant edges (Pearson coefficient >0.997) that confirms the joint regulation of this core sub-network. Among them, four genes with six most significant neighbors were identified: *GIL1*, *Strap*, *CRT*, and *CXE11*. Additionally, five genes from this cluster are characterized by the highest number of edges in the network: *PXL1*, *PRP-F1*, *GATL7*, *CIPK6*, and *UEL-1* (Supplementary Table S6).

4 Discussion

Tea genetic diversity in the North-Western Caucasus can be considered a useful reservoir of cold-tolerant germplasm useful for the development of new tolerant cultivars. Kolkhida is the best large-leaf local tea cultivar, characterized by high leaf quality for

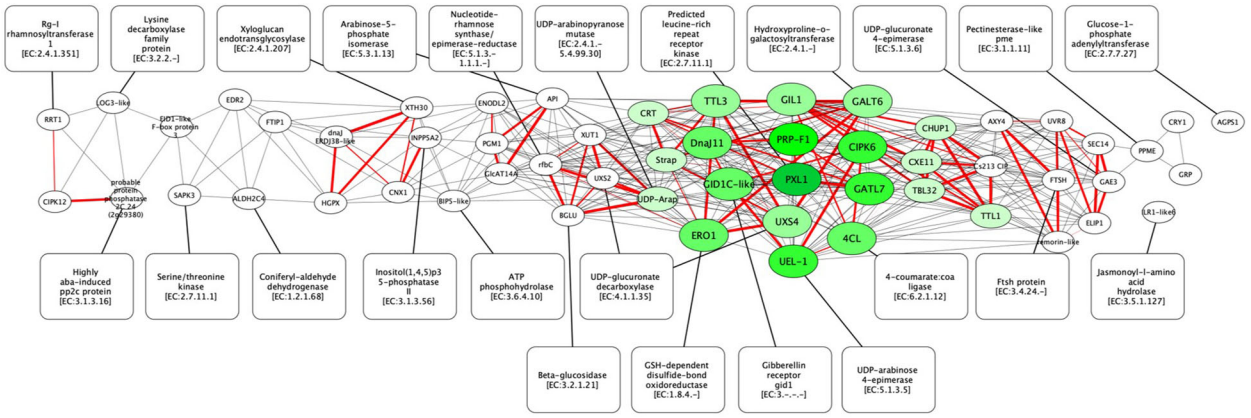

FIGURE 6
Homology based gene co-expression network for *C. sinensis* (N nodes = 58; N edges = 390). Genes are presented as ellipses, and their corresponding enzymes are presented in round rectangles with an EC number. Genes with the greatest number of edges are presented by shades of green (a color legend is shown on the left bottom part of the figure). The thick red line shows the most significant co-expression interactions (Pearson coefficient >0.997).

black and green tea production. In this study, we analyzed the transcriptome dynamics of this cultivar in response to the cold, freezing, drought, and recovery. Many previous studies focused on the short-term stress response. However, the long-term response and recovery mechanisms can be of critical importance for crop hardening. In this study, the emphasis was placed on overlapping genes and pathways because common mechanisms are important to develop new cultivars tolerant to several stresses and showing higher hardening potential. We identified a series of new candidate genes related to different pathways. These genes can be used as new genetic targets for gene editing and marker-assisted selection.

Among the different treatments, the highest number of DEGs was observed under freezing and cold conditions rather than drought (Table 2). In addition, the RecoveryC samples indicated about 6.5 times greater DEG numbers as compared to RecoveryD. These results correspond with several studies that reported that cold induced more DEGs than drought in tea plants (Zheng et al., 2015), apples (Li et al., 2019), maize (Lu et al., 2017), and tomatoes (Zhou et al., 2019). Furthermore, we observed that only 6.3% of upregulated genes were common for Cold14d, Freezing3d, and Drought14d, whereas 7.9% of upregulated DEGs were common for cold and drought. Other studies showed that only 10% of the drought-inducible genes were also induced by cold in Arabidopsis and tomato (Seki et al., 2002; Zhou et al., 2019). However, these researchers evaluated the short-term responses while we focused on the long-term response. Anyway, the percentage of the common upregulated DEGs is not as high as it was expected, and most of the DEGs were specific to a cold or drought response.

4.1 Overlapping biological processes upon cold, freezing, and drought

Our results on pathway analysis are partly consistent with the other studies, which indicated common GO terms of "thylakoid membranes," "photosynthetic membranes," "response to Karrikin," "electron transport," and "cytochrome complex" (Zhu et al., 2013; Guo et al., 2021; Zhou et al., 2021). We speculate that these pathways play a vital role in tea responses to long-term drought, cold, and freezing. According to some other studies, "plant hormone signal transduction," "starch and sucrose metabolism," "peroxisomes," and "photosynthesis" might play a vital role in wild apple responses to freezing stress (Zhou et al., 2021). Additionally, Zheng et al. (2015) reported that "photosynthesis" and "photosynthesis-antenna proteins" were important for the short-term cold response. In cotton, treated with 10 d of drought and 2 d chilling of stress, most of the DEGs were related to "carbohydrate metabolism," "stress/defense response," "nucleic acid metabolism," or "transcriptional regulation" (Zhu et al., 2013), which is consistent with our results on the tea plant. Long-term downregulation of many photosynthesis genes can involve different mechanisms in drought and cold (Hussain et al., 2018). The difference in GO results can be explained by the different lengths of stress treatments used in the studies.

4.1.1 Phenylpropanoid pathway and cell wall remodeling DEGs

Among common upregulated genes, several key genes were related to the phenylpropanoid pathway (*ALDH2C4* and homolog *At1g55270*—regulator of the phenylpropanoid pathway) and the polyphenol biosynthesis pathway (*F3'H* (two genes), *F3'5'H* (two genes), and *CHS1*). Interestingly, along with the increased expression of *CHS1*, *F3'H*, and *F3'5'H*, we observed inhibited expression of their downstream genes (*DFR* and *FLS*), and these results corresponded with the HPLC results (Figure 1C). Thus, it can be suggested that the conversion of dehydroflavonols into the final products is suppressed under long-term stress. Several other transcriptomic studies indicated upregulation of the polyphenol-related DEGs controlled by *WD40-MYB-bHLH* regulatory complexes and could be an important mechanism of plant defense against different abiotic stresses (Chezem and Clay, 2016; Xie et al., 2018; Qari and Tarbiyyah, 2021; Wang et al., 2021).

The phenylpropanoid pathway serves as a rich source of metabolites in plants. It is a starting point for the biosynthesis of lignin, flavonoids, and coumarins (Fraser and Chapple, 2011; Hori et al., 2020; Oliveira et al., 2020). We identified many upregulated genes related to cell wall remodeling and biosynthesis (*UDP-Arap*, *XTH30*, *AGPS1*, *BGLU*, *ENODL2*, *AXY4*, *UEL*-1, *PRP-F1*, *API*, *PPME*, *GALT6*, *GATL7*, *UXS2*, *UXS4*, *TBL32*, *GlcAT14A*, *XUT1*, *GAE3*, *4CL*, *API*, *RRT1*, *rfbC*, glucan endo-1,3-beta-glucosidase 7- and 8-like, etc.), confirming the importance of these pathways for the long-term cold, freezing, and drought responses in tea plants. Recent studies showed upregulation of lignin biosynthesis genes along with the downregulation of cellulose biosynthesis genes under several osmotic stresses (Wildhagen et al., 2018; Chen et al., 2019; Hori et al., 2020). Additionally, an increased level of xyloglucan endotransglucosylase/hydrolase (XTH) and expansin proteins were highlighted (Peña et al., 2012; Gall et al., 2015). These proteins affect the cell wall plasticity and reinforcement of the secondary wall with hemicellulose and lignin to increase cell wall thickening. In our study, the increased expression of beta-glucosidase (BGLU) and several DEGs related to xyloglucan and pectin biosynthesis (*RRT1*, *PPME*, *XTH*, *UXS2*, *UXS4*, *GAE3*, and *XUT1*) was observed. Among them, *RRT1* is required for the synthesis of the RG-I major structural domain of pectin, which is important for both cellular adhesion and cell wall plasticity (Takenaka et al., 2018); *PPME*, participates in apoplastic Ca^{2+}homeostasis, controlling stomatal movements, and regulating the flexibility of the guard cell wall (Wu et al., 2018). Also, the products of *XTH*s cut and re-join hemicellulose chains in the plant cell wall, affecting cellulose deposition (Wu et al., 2018). Additionally, there are *UXS2*, *UXS4*, and *GAE3*, required for the biosynthesis of heteroxylans and xyloglucans and for the side chains of pectin (Kuang et al., 2016; Borg et al., 2021).

Plant cell walls contain hydroxyproline-rich O-glycoproteins (HRGPs), a superfamily that is classified into extensins (EXTs), arabinogalactan-proteins (AGPs), and Hyp/Pro-rich proteins (H/PRPs) (Cassab and Varner, 1988; Basu et al., 2015; Ajayi et al., 2021). According to our results, a set of genes involved in H/PRPs and AGPs metabolism (*AGPS1*, *UEL-1*, *API*, *GALT6*, *GATL7*, *GlcAT14A*, *ENODL2*, *PRP-F1*, etc.) were highly upregulated, suggesting that glycosylation of HRGPs is an important responsive mechanism under long-term stress. Additionally, some genes (*TBL32*, *TBL27*) related to O-acetylation of polysaccharides were upregulated under long-term stresses in the tea plant, which is consistent with some earlier findings (Sun et al., 2020b). O-acetylation of polysaccharides changes their physicochemical properties, and acetyl substituents inhibit the enzymatic degradation of wall polymers (Gall et al., 2015).

To summarize, several important mechanisms of long-term stress responses can be suggested that are directed toward increasing the cell wall's plasticity, thickness, and hydrophobicity: lignin biosynthesis, glycosylation of HRGPs, O-acetylation of polysaccharides, pectin biosynthesis and branching, and xyloglucan and arabinogalactan biosynthesis.

4.1.2 Light-perception- and signal transduction DEGs

According to the KEGG analysis, most of the common biological processes in tea were related to membranes, electron transport, and light perception. Previous studies also reported that cold response is closely associated with light perception, particularly the circadian clock, which affects the expression of *CBF* genes (Chen et al., 2004; Gould et al., 2013; Wisniewski et al., 2014; Estravis-Barcala et al., 2019; Kidokoro et al., 2021; Kidokoro et al., 2022). In accordance with these findings, we revealed increased expression of genes related to red-light perception (*GIL1*), blue and UV-light perception (*CRY1*, *ELIP1*, and *UVR8*), chloroplast relocation (*CHUP1*), regulation of chlorophyll biosynthesis (clone *Cs213* putative cold-inducible protein), stomatal movement (*PGM1*), and PSII-associated light-harvesting complex II (*FTSH*). Interestingly, among all upregulated DEGs, the highest expression level was observed in *ELIP1*, which was upregulated 150–2,000 folds above control under long-term cold, freezing, and drought. Early light-inducible proteins (ELIPs) are present in the thylakoid membranes. These proteins protect photosynthetic machinery from various environmental stresses in higher plants and have been suggested to participate in the phytochrome signaling pathway (Rizza et al., 2011). The induction of *ELIP1/2* expression is mediated *via CRY1* in a blue light intensity-dependent manner (Kleine et al., 2007; Yang et al., 2017). *CRY1* participates in the high temperature response in plants. However, an accumulation of *CRY* transcripts has not been observed in response to short-term cold stress in Arabidopsis (Gould et al., 2013; Ma et al., 2016). Several other genes related to the light perception were upregulated under long-term cold, freezing, and drought. Among them, *EID1*-like F-box protein 3 is related to red-light perception and functions as a negative regulator in phytochrome A (phyA)-specific light signaling (Marrocco et al., 2006). *DnaJ11* and *dnaJ ERDJ3B*-like encode co-chaperone components, responsible for stabilizing the interaction of Hsp70 with client proteins (Ohta and Takaiwa, 2014). Knockout of these genes in *A. thaliana* causes a decrease in photosynthetic efficiency and destabilization of PSII complexes (Chen et al., 2010). Also, the FT-interacting protein 3 *FTIP1* is an essential regulator of FT encoding florigen in plants (Liu et al., 2012). To summarize, it can be suggested that the long-term overlapping stress responses include the activation of several important genes of photo-perception, which probably activate the phenylpropanoid pathway leading to cell wall remodeling. An adjustment in the light harvesting system and reaction centers to capture less light energy for photosynthesis can be an important regulatory mechanism for long-term stress, according to Zhou et al. (2021). We suppose that several light receptor genes, such as *CRY1*, *ELIP1*, *FTIP1*, *EID1*, *ERDJ3B*, and *dnaJ11*, can be new target genes for molecular breeding of the tea plant.

Calcium signaling. Under the long-term stresses, we observed the elevated expression of several genes related to Ca^{2+}-dependent signaling and protein phosphorylation. Among them are *CNX1* and *CRT*, whose products act as molecular chaperones (Liu et al., 2017;

Joshi et al., 2019); *CIPK12* and *CIPK6* products bind to CBLs—which are regulators of Ca^{2+}-signal transduction (Sardar et al., 2017; Czolpinska and Rurek, 2018; Guo et al. 2018; Bai et al., 2022). Additionally, several genes related to Ca^{2+}-signaling were upregulated (Strap, *SAPK3*, *PXL1*, *INPP5A2*, *GRP*, etc.), indicating the important role of the membrane trafficking system in response to long-term cold, freezing, and drought in tea plants. Similarly, in Populus, calcium-dependent protein kinase 10 (*CPK10*) activates both drought- and frost-responsive genes to induce stress tolerance (Chen et al., 2013). In apples, common DEGs encoding protein phosphatases and serine/threonine protein kinases were upregulated in response to different abiotic stresses (Li et al., 2019). In addition, probable protein phosphatase 2C 24 (2g29380) was upregulated in tea plants. PP2C enzymes are key players in plant signal transduction processes such as ABA signal transduction (Rodriguez, 1998). These results confirmed that activation of Ca^{2+}-signaling cascades is relevant for the long-term stress responses in tea plants.

Hormone signaling. Several new DEGs involved in hormone signaling were upregulated in tea plants under long-term stress (*GID1C*-like, *LOG3*-like, *ILR1*-like6, *TTL1*, *TTL3*, and *2g29380*). The product of *GID1* can bind negative regulators of GA responses called DELLA proteins (Hauvermale et al., 2014). *LOG* plays a pivotal role in regulating cytokinin activity (Kuroha et al., 2009). *ILR1* regulates the rates of amido-IAA hydrolysis, resulting in the activation of auxin signaling (Sanchez Carranza et al., 2016). *TTL1* regulates the transcript levels of several dehydration-responsive genes, such as *CBF2*, *ERD1* (early response to dehydration 1), *ERD3*, and *COR15a* (Rosado et al., 2006; Lakhssassi et al., 2012). Our results indicate that jasmonic acid, brassinosteroid-, and the ABA-signaling pathways are consistently upregulated during long-term stress, which is partly consistent with recent studies on woody plants (Wisniewski et al., 2014; Estravis-Barcala et al., 2019; He et al. 2019; Zheng et al., 2022). It is suggested that a highly variable interaction between different hormone signal transduction pathways takes place, leading to a complex transcriptional landscape in response to abiotic stress.

ROS signaling. A well-known effect of abiotic stress in plants is the production of ROS, which can eventually oxidize lipids, proteins, and DNA and thereby trigger cell death (Akula and Ravishankar, 2011; Bartwal et al., 2013; Estravis-Barcala et al., 2019; He et al., 2019). We revealed several new upregulated DEGs related to lipid metabolism. For example, *SEC14* is an important regulator of phospholipid metabolism (de Campos and Schaaf, 2017); *EDR2* is a negative regulator of cell death and acts in opposition to the SA pathway (Vorwerk et al., 2007); *REM* encodes remorin-like proteins of lipid rafts and physically interacts with receptor-like kinases and pathogen effectors (Cai et al., 2020); *HGPX* encodes phospholipid hydroperoxide (glutathione peroxidase), which participates in scavenging of lipid hydroperoxide (Jain and Bhatla, 2014). Also, *ERO1* encodes endoplasmic reticulum oxidoreductin) that participates in protein folding under oxidative stress (Matsusaki et al., 2019). *CXE11* encodes carboxylesterase 11, which is involved in the catabolism of volatile esters and activation of MeJA signaling (Cao et al., 2019). Finally, two luminal-binding protein genes (*BIP5*-like) whose overexpression leads to an increase in anti-oxidative defenses under water stress in transgenic tobacco and soybean (Valente et al., 2009). These results suggest that lipid stabilization can be an important mechanism of long-term stress responses in tea plants.

The co-expression analysis revealed the core functional module of the network (Figure 6), which demonstrates the coordinated regulation of pathways for photo-perception, phenylpropanoid, calcium signaling, cell wall remodeling, ROS, and hormone signaling. Having key knowledge about the presence of such coordinated regulation and its targets opens a new horizon for the discovery of major activators that play a key role in transcriptional stress responses. In comparison to the core gene network of *A. thaliana* in response to high light (Bobrovskikh et al., 2022), our selected gene set includes four corresponding orthologs: *dnaJ ERDJ3B*-like (TEAK028829/AT3G62600), *ELIP1* (TEAK023638/AT3G22840), *CRY1* (TEAK018624/AT4G08920), and *ALDH2C4* (TEAK002753/AT5G42020). However, these genes are not included in the central co-expression cluster, indicating a high specificity of the highlight stress response as well as different genetic mechanisms involved in these responses.

4.1.3 Regulatory mechanisms

Only 19 transcription factor genes were commonly upregulated (*CBF1*, *DHN1*, *DHN2*, *DHN3*, *LEA*, *LEA14-A*, *LEA29*, *ECP63*, *bHLH*, *WRKY22*, *ZAT10*, *NAC*, *AP2*, *ERF*, *GIF1*, *PIP7a*, *HSP70*, *GRAS*, *DUF567*, and *COR413PM1*-like), and most of them are related to the ABA-signaling pathway. Among the well-known genes, we found new COR genes upregulated under long-term cold, freezing, and drought in tea plants. For example, a homolog of *COR413PM1* is a regulator of the ABA response in Arabidopsis, and affects the ABA-induced transient Ca^{2+} oscillation in the plasma membrane (Hu et al., 2021). Additionally, *DUF567* encodes a protein of unknown function (Nabi et al., 2020), *GRAS*, and *GIF1* (GIF1/2/3), which regulate root and shoot development (Tian et al., 2004; Zhang et al., 2018; Liu et al., 2020). Corresponding with our results, cold and drought induce transcription factors of an ABA-dependent response, such as members of the basic-domain leucine zipper (*bZIP*) family, the *MYB* family, and the *WRKY* family (Li et al., 2019; Zhou et al., 2019; Zheng et al., 2022).

4.2 Specific biological processes activated by cold, freezing, and drought

In our experiment, freezing treatment was followed a 14-day cold treatment, leading to the accumulation of the negative effects of low-temperature stress. Most of the DEGs related to the MAPK-signaling pathway were specifically downregulated under freezing, indicating severe damage of the defense system. Mitogen-activated protein kinase cascade (MAPK) is an evolutionarily conserved signal transduction module involved in transducing extracellular signals to the nucleus for appropriate cellular adjustment (Sinha et al., 2011). In strawberries, the freezing stress response was through several pathways: flavonoid biosynthesis, plant hormone signal transduction, MAPK-signaling, starch and sucrose metabolism, and circadian rhythm (Zhang et al., 2019b).

Transcriptomic analysis of *Magnolia wufengensis* under cold stress showed that the response mechanism was related to photosynthesis, plant hormone signal transduction, and primary and secondary metabolism pathways (Deng et al., 2019).

Several specific biological processes were indicated in the tea plant under long-term drought. Interestingly, under long-term drought, downregulation of many DEGs related to nucleotide excision repair, base excision repair, mismatch repair, DNA replication, and RNA polymerase activity was detected. DNA repair mechanisms are important to eliminate errors in replication and maintain genomic integrity of plants under endogenous and exogenous DNA-damaging factors. Nucleotide excision repair is a general repair mechanism employed by both prokaryotic and eukaryotic cells to remove a variety of structurally different DNA lesions (Manova and Gruszka, 2015). Base excision repair is a critical DNA repair mechanism for the removal of damaged bases arising from oxidation, alkylation, or deamination (Krokan and Bjoras, 2013; Roldán-Arjona et al., 2019). The mismatch repair (MMR) mechanism of correction of replication errors (mismatches) or nucleotides accidentally inserted/deleted during replication to prevent mutation accumulation (Belfield et al., 2018). Thus, downregulation of these genes can lead to the accumulation of mutations in plant cells under long-term drought stress. Additionally, many DEGs related to galactose metabolism and metabolic pathways were specifically upregulated in Drought14d, which is consistent with other studies on osmotic stress (Seifert et al., 2002; Zhang et al., 2015; Zhang et al., 2019b).

5 Conclusion

To conclude, only 17.9% of the cold-induced genes were also upregulated by drought, and only 6.3% of upregulated genes were common for long-term cold, freezing, and drought. In total, 1,492 transcription factor genes were identified among all DEGs related to 57 families. However, only 20 transcription factor genes were commonly upregulated by long-term cold, freezing, and drought (*CBF1*, *DHN1*, *DHN2*, *DHN3*, *LEA*, *LEA14-A*, *LEA29*, *ECP63*, *bHLH*, *WRKY22*, *ZAT10*, *NAC*, *AP2*, *ERF*, *GIF1*, *PIP7a*, *HSP70*, *GRAS*, *DUF567*, and *COR413PM1*-like). Coexpression analysis and network reconstruction showed 19 genes with the highest co-expression connectivity: seven genes are related to cell wall remodeling (*GATL7*, *UXS4*, *PRP-F1*, *4CL*, *UEL-1*, *UDP-Arap*, and *TBL32*); four genes are involved in Ca2+-signaling (*PXL1*, *Strap*, *CRT*, and *CIPK6*); three genes are related to photo-perception (*GIL1*, *CHUP1*, and *DnaJ11*); two genes of hormone signaling (*TTL3* and *GID1C-like*); two genes of ROS signaling (*ERO1* and *CXE11*); and one gene of phenylpropanoid pathway (*GALT6*). These genes can be a new target for molecular breeding of tea plants. Several important mechanisms of long-term stress responses include cell wall remodeling through lignin biosynthesis, o-acetylation of polysaccharides, pectin biosynthesis and branching, and xyloglucan and arabinogalactan biosynthesis. These results revealed the important mechanisms of overlapping responses to cold, freezing, and drought stresses and a set of new target candidate genes for the molecular breeding of tea plants aimed at tolerance to abiotic stresses.

Data availability statement

The datasets presented in this study can be found in online repositories. The names of the repository/repositories and accession number(s) can be found below: https://db.cngb.org/, CNP0004163.

Author contributions

LS - conceptualization, experimental design, investigation, data analysis, visualization, funding acquisition, manuscript draft; SW - investigation, data analysis, visualization, manuscript review and editing; LM - funding acquisition, data acquisition, manuscript review and editing; AB and AD - data analysis and interpretation, manuscript critical revision; NK, RS and AM - investigation, data acquisition; JF, KM and AF - results interpretation, formal analysis, manuscript review and editing; SL, TT and AR - results acquisition, revision the work, EK - conceptualization, supervision, formal analysis, manuscript review and editing. All authors approved the final version of the manuscript. All authors agreed to be accountable for all aspects of the work in ensuring that questions related to the accuracy or integrity of any part of the work are appropriately investigated and resolved.

Funding

The study was funded by a grant from the Russian Science Foundation # 18-76-10001 (https://rscf.ru/project/21-76-03003/). Plant material for this study was provided by a program of the Ministry of Science and Higher Education of the Russian Federation (program # FGRW-2021-0008). All experiments with plants were conducted at Federal Research Centre the Subtropical Scientific Centre of the Russian Academy of Sciences. Data analysis and the manuscript processing were conducted at the Sirius University of Science and Technology and the N. I. Vavilov All-Russian Institute of Plant Genetic Resources. Gene network reconstruction was performed at the Institute of Cytology and Genetics.

Conflict of interest

The authors declare that the research was conducted in the absence of any commercial or financial relationships that could be construed as a potential conflict of interest.

Publisher's note

Supplementary material

The Supplementary Material for this article can be found online at: https://www.frontiersin.org/articles/10.3389/fpls.2023.1145793/full#supplementary-material

SUPPLEMENTARY TABLE 1
RPKM per treatment.

SUPPLEMENTARY TABLE 2
All DEGs per treatment.

SUPPLEMENTARY TABLE 3
Upregulated DEGs.

SUPPLEMENTARY TABLE 4
Correlation of DEGs.

SUPPLEMENTARY TABLE 5
Enzymatic Fractions of DEGs.

SUPPLEMENTARY TABLE 6
Gene network details.

References

Ahuja, I., de Vos, R. C., Bones, A. M., and Hall, R. D. (2010). Plant molecular stress responses face climate change. *Trends Plant Sci.* 15, 664–674. doi: 10.1016/j.tplants.2010.08.002

Ajayi, O. O., Held, M. A., and Showalter, A. M. (2021). Three β-glucuronosyltransferase genes involved in arabinogalactan biosynthesis function in arabidopsis growth and development. *Plants* 10 (6), 1172. doi: 10.3390/plants10061172

Akula, R., and Ravishankar, G. A. (2011). Influence of abiotic stress signals on secondary metabolites in plants. *Plant Signaling Behav.* 6 (11), 1720–1731. doi: 10.4161/psb.6.11.17613

Altschul, S. F., Madden, T. L., Schäffer, A. A., Zhang, J., Zhang, Z., Miller, W., et al. (1997). Gapped BLAST and PSI-BLAST: a new generation of protein database search programs. *Nucleic Acids Res.* 25, 3389–3402. doi: 10.1093/nar/25.17.3389

Amrine, K. C. H., Blanco-Ulate, B., and Cantu, D. (2015). Discovery of core biotic stress responsive genes in arabidopsis by weighted gene co-expression network analysis. *PloS One* 10 (3), e0118731. doi: 10.1371/journal.pone.0118731

Bai, X., Ji, J., Wang, W., Gu, C., Yu, Q., Jiang, J., et al. (2022). Characterization of CBL-interacting protein kinases' gene family and expression pattern reveal their important roles in response to salt stress in poplar. *Forests* 13, 1353. doi: 10.3390/f13091353

Bajji, M., Kinet, J. M., and Lutts, S. (2002). The use of the electrolyte leakage method for assessing cell membrane stability as a water stress tolerance test in durum wheat. *Plant Growth Regul.* 36, 61–10. doi: 10.1023/A:1014732714549

Ban, Q., Wang, X., Pan, C., Wang, Y., Kong, L., Jiang, H., et al. (2017). Comparative analysis of the response and gene regulation in cold resistant and sensitive tea plants. *PloS One* 12 (12), e0188514.

Bartwal, A., Mall, R., Lohani, P., Guru, S. K., and Arora, S. (2013). Role of secondary metabolites and brassinosteroids in plant defense against environmental stresses. *J. Plant Growth Regul.* 32, 216–232. doi: 10.1007/s00344-012-9272-x

Basu, D., Tian, L., Wang, W., Bobbs, S., Herock, H., Travers, A., et al. (2015). A small multigene hydroxyproline-o-galactosyltransferase family functions in arabinogalactan-protein glycosylation, growth and development in arabidopsis. *BMC Plant Biol.* 15, 295. doi: 10.1186/s12870-015-0670-7

Belfield, E. J., Ding, Z. J., Jamieson, F. J., Visscher, A. M., Zheng, S. J., Mithani, A., et al. (2018). DNA Mismatch repair preferentially protects genes from mutation. *Genome Res.* 28, 1–9. doi: 10.1101/gr.219303.116

Birney, E., Clamp, M., and Durbin, R. (2004). GeneWise and genomewise. *Genome Res.* 14, 988–995. doi: 10.1101/gr.1865504

Bobrovskikh, A. V., Zubairova, U. S., Bondar, E. I., Lavrekha, V. V., and Doroshkov, A. V. (2022). Transcriptomic data meta-analysis sheds light on high light response in arabidopsis thaliana l. *Int. J. Mol. Sci.* 23, 4455. doi: 10.3390/ijms23084455

Borg, A. J., Dennig, A., Weber, H., and Nidetzky, B. (2021). Mechanistic characterization of UDP-glucuronic acid 4-epimerase. *FEBBS J.* 288 (4), 1163–1178. doi: 10.1111/febs.15478

Burge, C., and Karlin, S. (1997). Prediction of complete gene structures in human genomic DNA. *J. Mol. Biol.* 268, 78–94. doi: 10.1006/jmbi.1997.0951

Cai, J., Chen, T., Wang, Y., Qin, G., and Tian, S. (2020). SlREM1 triggers cell death by activating an oxidative burst and other regulators. *Plant Physiol.* 183 (2), 717–732. doi: 10.1104/pp.20.00120

Cantarel, B. L., Korf, I., Robb, S. M., Parra, G., Ross, E., Moore, B., et al. (2008). MAKER: an easy-to-use annotation pipeline designed for emerging model organism genomes. *Genome Res.* 18, 188–196. doi: 10.1101/gr.6743907

Cao, X., Duan, W., Wei, C., Chen, K., Grierson, D., and Zhang, B. (2019). Genome-wide identification and functional analysis of carboxylesterase and methylesterase gene families in peach (Prunus persica l. batsch). *Fron.t Plant Sci.* 10. doi: 10.3389/fpls.2019.01511

Cao, H., Wang, L., Hao, X., Wang, X., and Yang, Y. (2015). Isolation and expression analysis of 18 CsbZIP genes implicated in abiotic stress responses in the tea plant (Camellia sinensis). *Plant Physiol. Biochem.* 97, 432–442. doi: 10.1016/j.plaphy.2015.10.030

Cassab, G. I., and Varner, J. E. (1988). Cell wall proteins. *Annu. Rev. Plant Biol.* 39 (1), 321–353. doi: 10.1146/annurev.pp.39.060188.001541

Chamani Mohasses, F., Solouki, M., Ghareyazie, B., Fahmideh, L., and Mohsenpour, M. (2020). Correlation between gene expression levels under drought stress and synonymous codon usage in rice plant by in-silico study. *PloS One* 15 (8), e0237334. doi: 10.1371/journal

Chaves, M. M., Maroco, J. P., and Pereira, J. S. (2003). Understanding plant responses to drought – from genes to the whole plant. *Funct. Plant Biol.* 30, 239–264.

Chen, M., Chory, J., and Fankhauser, C. (2004). Light signal transduction in higher plants. *Annu. Rev. Genet.* 38, 87–117. doi: 10.1146/annurev.genet.38.072902.092259

Chen, K. M., Holmström, M., Raksajit, W., Suorsa, M., Piippo, M., and Aro, E. M. (2010). Small chloroplast-targeted DnaJ proteins are involved in optimization of photosynthetic reactions in arabidopsis thaliana. *BMC Plant Biol.* 10, 43. doi: 10.1186/1471-2229-10-43

Chen, X., Wang, H., Li, X., Ma, K., Zhan, Y., and Zeng, F. (2019). Molecular cloning and functional analysis of 4-Coumarate:CoA ligase 4 (4CL-like 1)from fraxinus mandshurica and its role in abiotic stress tolerance and cell wall synthesis. *BMC Plant Biol.* 19, 231. doi: 10.1186/s12870-019-1812-0

Chen, J., Xue, B., Xia, X., and Yin, W. (2013). A novel calcium-dependent protein kinase gene from populus euphratica, confers both drought and cold stress tolerance. *Biochem. Biophy.s Res. Commun.* 441 (3), 630–636. doi: 10.1016/j.bbrc.2013.10.103

Chen, J., Yin, W., and Xia, X. (2014). Transcriptome profiles of populus euphratica upon heat shock stress. *Curr. Genomics* 15 (5), 326–340. doi: 10.2174/1389202915051411061018 35

Cheng, H., Concepcion, G. T., Feng, X., Zhang, H., and Li, H. (2021). Haplotype-resolved *de novo* assembly using phased assembly graphs with hifiasm. *Nat. Methods* 18, 170–175. doi: 10.1038/s41592-020-01056-5

Chezem, W. R., and Clay, N. K. (2016). Regulation of plant secondary metabolism and associated specialized cell development by MYBs and bHLHs. *Phytochemistry* 131, 26–43. doi: 10.1016/j.phytochem.2016.08.006

Czolpinska, M., and Rurek, M. (2018). Plant glycine-rich proteins in stress response: an emerging, still prospective story. *Front. Plant Sci.* 9. doi: 10.3389/fpls.2018.00302

Cui, X., Wang, Y.-X., Liu, Z.-W., Wang, W.-L., Li, H., and Zhuang, J. (2018). Transcriptome-wide identification and expression profile analysis of the bHLH family genes in camellia sinensis. *Funct. Integr. Genomics* 18 (5), 489–503. doi: 10.1007/s10142-018-0608-x

Danecek, P., Bonfield, J. K., Liddle, J., Marshall, J., Ohan, V., Pollard, M. O., et al. (2021). Twelve years of SAMtools and BCFtools. *Gigascience* 10 (2), giab008. doi: 10.1093/gigascience/giab008

de Campos, M. K., and Schaaf, G. (2017). The regulation of cell polarity by lipid transfer proteins of the SEC14 family. *Curr. Opin. Plant Biol.* 40, 158–168. doi: 10.1016/j.pbi.2017.09.007

Deng, S., Ma, J., Zhang, L., Chen, F., Sang, Z., and Jia, Z. (2019). *De novo* Transcriptome sequencing and gene expression profiling of magnolia wufengensis in response to cold stress. *BMC Plant Biol.* 19, 321. doi: 10.1186/s12870-019-1933-5

Dobin, A., Davis, C. A., Schlesinger, F., Drenkow, J., Zaleski, C., Jha, S., et al. (2013). STAR: ultrafast universal RNA-seq aligner. *Bioinformatics* 29 (1), 15–21. doi: 10.1093/bioinformatics/bts635

Estravis-Barcala, M., Mattera, M. G., Soliani, C., Bellora, N., Opgenoorth, L., Heer, K., et al. (2019). Molecular bases of responses to abiotic stress in trees. *J. Exp. Bot.* 71 (13), 3765–3779. doi: 10.1093/jxb/erz532

Fraser, C. M., and Chapple, C. (2011). The phenylpropanoid pathway in arabidopsis. *Arabidopsis Book* 9, e0152. doi: 10.1199/tab.0152

Gall, H. L., Philippe, F., Domon, J. M., Gillet, F., Pelloux, J., and Rayon, C. (2015). Cell wall metabolism in response to abiotic stress. *Plants* 4 (1), 112–166. doi: 10.3390/plants4010112

Gould, P. D., Ugarte, N., Domijan, M., Costa, M., Foreman, J., MacGregor, D., et al. (2013). Network balance *via* CRY signaling controls the arabidopsis circadian clock over ambient temperatures. *Mol. Syst. Biol.* 9, 650. doi: 10.1038/msb.2013.7

Guan, D., McCarthy, S. A., Wood, J., Howe, K., Wang, Y., and Durbin, R. (2020). Identifying and removing haplotypic duplication in primary genome assemblies. *Bioinformatics* 36 (9), 2896–2898. doi: 10.1093/bioinformatics/btaa025

Guo, Q., Li, X., Niu, L., Jameson, P. E., and Zhou, W. (2021). Transcription-associated metabolomic adjustments in maize occur during combined drought and cold stress. *Plant Physiol.* 186, 677–695. doi: 10.1093/plphys/kiab050

Guo, X., Liu, D., and Chong, K. (2018). Cold signaling in plants: insights into mechanisms and regulation. *J. Integr. Plant Biol.* 60 (9), 745–756. doi: 10.1111/jipb.12706

Hao, X., Wang, L., Zeng, J., Yang, Y., and Wang, X. (2018). "Response and adaptation mechanisms of tea plant to low-temperature stress," in *Stress physiology of tea in the face of climate change*. Eds. W.-Y. Han, L. Xin and ,. A. Golam Jalal (Singapore: Springer Nature Pte Ltd), 39–61.

Hauvermale, A. L., Ariizumi, T., and Steber, C. M. (2014). The roles of the GA receptors GID1a, GID1b, and GID1c in sly1-independent GA signaling. *Plant Signal. Behav.* 9 (2), e28030. doi: 10.4161/psb.28030

He, F., Li, H. G., Wang, J. J., Su, Y., Wang, H. L., Feng, C. H., et al. (2019). PeSTZ1, a C2H2-type zinc finger transcription factor from populus euphratica, enhances freezing tolerance through modulation of ROS scavenging by directly regulating PeAPX2. *Plant Biotechnol. J.* 17 (11), 2169–2183. doi: 10.1111/pbi.13130

Hori, C., Yu, X., Mortimer, J. C., Sano, R., Matsumoto, T., Kikuchi, J., et al. (2020). Impact of abiotic stress on the regulation of cell wall biosynthesis in populus trichocarpa. *Plant Biotechnol.* 37, 273–283. doi: 10.5511/plantbiotechnology.20.0326a

Hu, X., Liu, J., Liu, E., Qiao, K., Gong, S., Wang, J., et al. (2021). Arabidopsis cold-regulated plasma membrane protein Cor413pm1 is a regulator of ABA response. *Biochem. Biophys. Res. Commun.* 561, 88–92. doi: 10.1016/j.bbrc.2021.05.032

Hu, Z., Ban, Q., Hao, J., Zhu, X., Cheng, Y., Mao, J., et al. (2020). Genome-wide characterization of the c-repeat binding factor (CBF) gene family involved in the response to abiotic stresses in tea plant (Camellia sinensis). *Front. Plant Science.* 11. doi: 10.3389/fpls.2020.00921

Huang, G. T., Ma, S. L., Bai, L. P., Zhang, L., Ma, H., Jia, P., et al. (2012). Signal transduction during cold, salt, and drought stresses in plants. *Mol. Biol. Rep.* 239, 969–987. doi: 10.1007/s11033-011-0823-1

Hussain, H. A., Hussain, S., Khaliq, A., Ashraf, U., Anjum, S. A., Men, S., et al. (2018). Chilling and drought stresses in crop plants: implications, cross talk, and potential management opportunities. *Front. Plant Sci.* 9. doi: 10.3389/fpls.2018.00393

Jain, P., and Bhatla, S. C. (2014). Signaling role of phospholipid hydroperoxide glutathione peroxidase (PHGPX) accompanying sensing of NaCl stress in etiolated sunflower seedling cotyledons. *Plant Signal. Behav.* 9 (12), e977746. doi: 10.4161/15592324.2014.977746

Joshi, R., Paul, M., Kumar, A., and Pandey, D. (2019). Role of calreticulin in biotic and abiotic stress signaling and tolerance mechanisms in plants review. *Gene* 714, 144004. doi: 10.1016/j.gene.2019.144004

Kidokoro, S., Hayashi, K., Haraguchi, H., Ishikawa, T., Soma, F., Konoura, I., et al. (2021). Posttranslational regulation of multiple clock-related transcription factors triggers cold-inducible gene expression in arabidopsis. *Proc. Natl. Acad. Sci.* 118 (10), e2021048118. doi: 10.1073/pnas.2021048118

Kidokoro, S., Shinozaki, K., and Yamaguchi-Shinozaki, K. (2022). Transcriptional regulatory network of plant cold-stress responses. *Trends Plant Sci.* 27 (9), 922–935. doi: 10.1016/j.tplants.2022.01.008

Kim, D., Paggi, J. M., Park, C., Bennett, C., and Salzberg, S. L. (2019). Graph-based genome alignment and genotyping with HISAT2 and HISAT-genotype. *Nat. Biotechnol.* 37 (8), 907–915. doi: 10.1038/s41587-019-0201-4

Kleine, T., Kindgren, P., Benedict, C., Hendrickson, L., and Strand, A. (2007). Genome-wide gene expression analysis reveals a critical role for CRYPTOCHROME1 in the response of arabidopsis to high irradiance. *Plant Physiol.* 144 (3), 1391–1406. doi: 10.1104/pp.107.098293

Kolde, R. (2019) *Package 'pheatmap'*. Available at: https://cran.r-project.org/web/packages/pheatmap/index.html (Accessed November 13, 2022).

Kovaka, S., Zimin, A. V., Pertea, G. M., Razaghi, R., Salzberg, S. L., and Pertea, M. (2019). Transcriptome assembly from long-read RNA-seq alignments with StringTie2. *Genome Biol.* 20, 278. doi: 10.1186/s13059-019-1910-1

Krokan, H. E., and Bjoras, M. (2013). Base excision repair. *Cold Spring Harb Perspect. Biol.* 5 (4), a012583. doi: 10.1101/cshperspect.a012583

Kuang, B., Zhao, X., Zhou, C., Zeng, W., Ren, J., Ebert, B., et al. (2016). Role of UDP-glucuronic acid decarboxylase in xylan biosynthesis in arabidopsis. *Mol. Plant* 9, 1119–1131. doi: 10.1016/j.molp.2016.04.013

Kuroha, T., Tokunaga, H., Kojima, M., Ueda, N., Ishida, T., Nagawa, S., et al. (2009). Functional analyses of LONELY GUY cytokinin-activating enzymes reveal the importance of the direct activation pathway in arabidopsis. *Plant Cell* 21 (10), 3152–3169. doi: 10.1105/tpc.109.068676

Lakhssassi, N., Doblas, V. G., Rosado, A., del Valle, A. E., Posé, D., Jimenez, A. J., et al. (2012). The arabidopsis TETRATRICOPEPTIDE THIOREDOXIN-LIKE gene family is required for osmotic stress tolerance and Male sporogenesis. *Plant Physiol.* 158 (3), 1252–1266. doi: 10.1104/pp.111.188920

Li, B., and Dewey, C. N. (2011). RSEM: accurate transcript quantification from RNA-seq data with or without a reference genome. *BMC Bioinf.* 12, 323. doi: 10.1186/1471-2105-12-323

Li, R., Fan, W., Tian, G., Zhu, H., He, L., Cai, J., et al. (2010). The sequence and *de novo* assembly of the giant panda genome. *Nature* 463, 311–317. doi: 10.1038/nature08696

Li, X., Li, M., Zhou, B., Yang, Y., Wei, Q., and Zhang, J. (2019). Transcriptome analysis provides insights into the stress response crosstalk in apple (Malus × domestica) subjected to drought, cold and high salinity. *Sci. Rep.* 9, 9071. doi: 10.1038/s41598-019-45266-0

Li, S., Yu, X., Lei, N., Cheng, Z., Zhao, P., He, Y., et al. (2017). Genome-wide identification and functional prediction of cold and/or drought-responsive lncRNAs in cassava. *Sci. Rep.* 7, 45981. doi: 10.1038/srep45981

Liu, Z., Li, N., Zhang, Y., and Li, Y. (2020). Transcriptional repression of GIF1 by the KIX-PPD-MYC repressor complex controls seed size in arabidopsis. *Nat. Commun.* 11, 1846. doi: 10.1038/s41467-020-15603-3

Liu, L., Liu, C., Hou, X., Xi, W., Shen, L., Tao, Z., et al. (2012).). FTIP1 is an essential regulator required for florigen transport. *PloS Biol.* 10 (4), 6e1001313. doi: 10.1371/journal.pbio.1001313

Liu, D. Y., Smith, P., Barton, D. A., Day, D. A., and Overall, R. L. (2017). Characterisation of arabidopsis calnexin 1 and calnexin 2 in the endoplasmic reticulum and at plasmodesmata. *Protoplasma* 254 (1), 125–136. doi: 10.1007/s00709-015-0921-3

Liu, Z., Xin, M., Qin, J., Peng, H., Ni, Z., Yao, Y., et al. (2015). Temporal transcriptome profiling reveals expression partitioning of homeologous genes contributing to heat and drought acclimation in wheat *(Triticum aestivum* l.). *BMC Plant Biol.* 15, 152. doi: 10.1186/s12870-015-0511-8

Livak, K. J., and Schmittgen, T. D. (2001). Analysis of relative gene expression data using realtime quantitative PCR and the 2-ΔΔCT method. *Methods* 25 (4), 402–408.

Love, M. I., Huber, W., and Anders, S. (2014). Moderated estimation of fold change and dispersion for RNA-seq data with DESeq2. *Genome Biol.* 15, 550. doi: 10.1186/s13059-014-0550-8

Lu, X., Zhou, X., Cao, Y., Zhou, M., McNeil, D., Liang, S., et al. (2017). RNA-seq analysis of cold and drought responsive transcriptomes of zea mays ssp. mexicana l. *Front. Plant Sci.* 8. doi: 10.3389/fpls.2017.00136

Ma, Q., Zhou, Q., Chen, C., Cui, Q., Zhao, Y., Wang, K., et al. (2019). Isolation and expression analysis of CsCML genes in response to abiotic stresses in the tea plant (Camellia sinensis). *Sci. Rep.* 9 (1), e8211.

Ma, D., Li, X., Guo, Y., Chu, J., Fang, S., Yan, C., et al. (2016). Cryptochrome 1 interacts with PIF4 to regulate high temperature-mediated hypocotyl elongation in response to blue light. *PNAS* 113 (1), 224–229. doi: 10.1073/pnas.1511437113

Manni, M., Berkeley, M. R., Seppey, M., and Zdobnov, E. M. (2021). BUSCO: assessing genomic data quality and beyond. *Curr. Protoc.* 1, e323. doi: 10.1002/cpz1.323

Manova, V., and Gruszka, D. (2015). DNA Damage and repair in plants – from models to crops. *Front. Plant Sci.* 6. doi: 10.3389/fpls.2015.00885

Marrocco, K., Zhou, Y., Bury, E., Dieterle, M., Funk, M., Genschik, P., et al. (2006). Functional analysis of EID1, an f-box protein involved in phytochrome a-dependent light signal transduction. *Plant J.* 45 (3), 423–438. doi: 10.1111/j.1365-313X.2005.02635.x

Matsui, A., Ishida, J., Morosawa, T., Mochizuki, Y., Kaminuma, E., Endo, T. A., et al. (2008). Arabidopsis transcriptome analysis under drought, cold, high-salinity and ABA treatment conditions using a tiling array. *Plant Cell Physiol.* 49 (8), 1135–1149. doi: 10.1093/pcp/pcn101

Matsusaki, M., Okuda, A., Matsuo, K., Gekko, K., Masuda, T., Naruo, Y., et al. (2019). Regulation of plant ER oxidoreductin 1 (ERO1) activity for efficient oxidative protein folding. *J. Biol. Chem.* 294 (49), 18820–18835. doi: 10.1074/jbc.RA119.010917

Minhas, P. S., Rane, J., and Pasala, R. K. (2017). *Abiotic stress management for resilient agriculture* (Singapore: Springer).

Muthuramalingam, P., Krishnan, S. R., Pothiraj, R., and Ramesh, M. (2017). Global transcriptome analysis of combined abiotic stress signaling genes unravels key players in oryza sativa l.: an in silico approach. *Front. Plant Sci.* 8. doi: 10.3389/fpls.2017.00759

Nabi, R. B. S., Tayade, R., Imran, Q. M., Hussain, A., Shahid, M., and Yun, B. W. (2020). Functional insight of nitric-oxide induced DUF genes in arabidopsis thaliana. *Front. Plant Sci.* 11. doi: 10.3389/fpls.2020.01041

Nakashima, K., Yamaguchi-Shinozaki, K., and Shinozaki, K. (2014). The transcriptional regulatory network in the drought response and its crosstalk in abiotic stress responses including drought, cold, and heat. *Front. Plant Sci.* 4. doi: 10.3389/fpls.2014.00170

Ohta, M., and Takaiwa, F. (2014). Emerging features of ER resident J-proteins in plants. *Plant Signal. Behav.* 9 (3), e28194. doi: 10.4161/psb.28194

Oliveira, D. M., Mota, T. R., Salatta, F. V., Sinzker, R. C., Končitíková, R., Kopečný, D., et al. (2020). Cell wall remodeling under salt stress: insights into changes in polysaccharides, feruloylation, lignification, and phenolic metabolism in maize. *Plant Cell Environ.* 43 (9), 2172–2191. doi: 10.1111/pce.13805

Pareek, A., Khurana, A., K Sharma, A., and Kumar, R. (2017). An overview of signaling regulons during cold stress tolerance in plants. *Curr. Genomics* 18, 498–511. doi: 10.2174/1389202918666170228141345

Parmar, R., Seth, R., Singh, P., Singh, G., Kumar, S., and Sharma, R. K. (2019). Transcriptional profiling of contrasting genotypes revealed key candidates and nucleotide variations for drought dissection in camellia sinensis (L.) o. kuntze. *Sci. Rep.* 9 (1), 1–12. doi: 10.1038/s41598-019-43925-w

Peña, M. J., Kong, Y., York, W. S., and O'Neill, M. A. (2012). A galacturonic acid-containing xyloglucan is involved in arabidopsis root hair tip growth. *Plant Cell* 24 (11), 4511–4524. doi: 10.1105/tpc.112.103390

Qari, S. H., and Tarbiyyah, I. (2021). The genetic regulation of secondary metabolic pathways in response to salinity and drought as abiotic stresses. *Appl. Sci.* 11 (15), 6668. doi: 10.3390/app11156668

Rabbani, M. A., Maruyama, K., Abe, H., Khan, M. A., Katsura, K., Ito, Y., et al. (2003). Monitoring expression profiles of rice genes under cold, drought, and high-salinity stresses and abscisic acid application using cDNA microarray and RNA gel-blot analyses. *Plant Physiol.* 133, 1755–1767. doi: 10.1104/pp.103.025742

Rizza, A., Boccaccini, A., Lopez-Vidriero, I., Costantino, P., and Vittorioso, P. (2011). Inactivation of the ELIP1 and ELIP2 genes affects arabidopsis seed germination. *New Phytol.* 190 (4), 896–905. doi: 10.1111/j.1469-8137.2010.03637.x

Rodriguez, P. L. (1998). Protein phosphatase 2C (PP2C) function in higher plants. *Plant Mol. Biol.* 38 (6), 919–927. doi: 10.1023/a:1006054607850

Roldán-Arjona, T., Ariza, R. R., and Córdoba-Cañero, D. (2019). DNA Base excision repair in plants: an unfolding story with familiar and novel characters. *Front. Plant Sci.* 10. doi: 10.3389/fpls.2019.01055

Rosado, A., Schapire, A. L., Bressan, R. A., Harfouche, A. L., Hasegawa, P. M., and Valpuesta, V. (2006). The arabidopsis tetratricopeptide repeat-containing protein TTL1 is required for osmotic stress responses and abscisic acid sensitivity. *Plant Physiol.* 142 (3), 1113–1126. doi: 10.1104/pp.106.085191

Samarina, L. S., Matskiv, A. O., Koninskaya, N. G., Shkhalakhova, R. M., Gvasaliya, M. V., Tsaturyan, G. A., et al. (2022). Genetic diversity and genome size variability in germplasm collection of tea plant (Camellia sinensis l. kuntze) in russia. *Front. Plant Sci.* doi: 10.3389/fpls.2021.800141

Sanchez Carranza, A. P., Singh, A., Steinberger, K., Panigrahi, K., Palme, K., Dovzhenko, A., et al. (2016). Hydrolases of the ILR1-like family of arabidopsis thaliana modulate auxin response by regulating auxin homeostasis in the endoplasmic reticulum. *Sci. Rep.* 6, 24212. doi: 10.1038/srep24212

Sardar, A., Nandi, A. K., and Chattopadhyay, D. (2017). CBL-interacting protein kinase 6 negatively regulates immune response to pseudomonas syringae in arabidopsis. *J. Exp. Bot.* 68 (13), 3573–3584. doi: 10.1093/jxb/erx170

Seifert, G. J., Barber, C., Wells, B., Dolan, L., and Roberts, K. (2002). Galactose biosynthesis in arabidopsis: genetic evidence for substrate channeling from UDP-D-Galactose into cell wall polymers. *Curr. Biol.* 12 (21), 1840–1845. doi: 10.1016/S0960-9822(02)01260-5

Seki, M., Narusaka, M., Ishida, J., Nanjo, T., Fujita, M., Oono, Y., et al. (2002). Monitoring the expression profiles of 7000 arabidopsis genes under drought, cold, and high-salinity stresses using a full-length cDNA microarray. *Plant J.* 31, 279–292. doi: 10.1046/j.1365-313X.2002.01359.x

Sham, A., Al-Azzawi, A., Al-Ameri, S., Al-Mahmoud, B., Awwad, F., Al-Rawashdeh, A., et al. (2014). Transcriptome analysis reveals genes commonly induced by botrytis cinerea infection, cold, drought and oxidative stresses in arabidopsis. *PloS One* 9 (11), e113718. doi: 10.1371/journal.pone.0113718

Shannon, P., Markiel, A., Ozier, O., Baliga, N. S., Wang, J. T., Ramage, D., et al. (2003). Cytoscape: a software environment for integrated models of biomolecular interaction networks. *Genome Research* 13 (11), 2498–2504.

Sharma, R., Singh, G., Bhattacharya, S., and Singh, A. (2018). Comparative transcriptome meta-analysis of arabidopsis thaliana under drought and cold stress. *PloS One* 13 (9), e0203266. doi: 10.1371/journal.pone.0203266

Shan, X., Li, Y., Jiang, Y., Jiang, Z., Hao, W., and Yuan, Y. (2013). Transcriptome profile analysis of maize seedlings in response to high-salinity, drought and cold stresses by deep sequencing. *Plant Mol. Biol. Rep.* 31 (6), 1485–1491. doi: 10.1007/s11105-013-0622-z

Singh, D., and Laxmi, A. (2015). Transcriptional regulation of drought response: a tortuous network of transcriptional factors. *Front. Plant Sci.* 6. doi: 10.3389/fpls.2015.00895

Sinha, A. K., Jaggi, M., Raghuram, B., and Tuteja, N. (2011). Mitogen-activated protein kinase signaling in plants under abiotic stress. *Plant Signal Behav.* 6 (2), 196–203. doi: 10.4161/psb.6.2.14701

Stanke, M., Keller, O., Gunduz, I., Hayes, A., Waack, S., and Morgenstern, B. (2006). AUGUSTUS: ab initio prediction of alternative transcripts. *Nucleic Acids Res.* 34 (2), W435–W439. doi: 10.1093/nar/gkl200

Sun, M., Huang, D., Zhang, A., Khan, I., Yan, H., Wang, X., et al. (2020a). Transcriptome analysis of heat stress and drought stress in pearl millet based on pacbio full-length transcriptome sequencing. *BMC Plant Biol.* 20 (1), 15. doi: 10.1186/s12870-020-02530-0

Sun, A., Yu, B., Zhang, Q., Peng, Y., Yang, J., Sun, Y., et al. (2020b). MYC2-activated TRICHOME BIREFRINGENCE-LIKE37 acetylates cell walls and enhances herbivore resistance. *Plant Physiol.* 184 (2), 1083–1096. doi: 10.1104/pp.20.00683

Takenaka, Y., Kato, K., Ogawa-Ohnishi, M., Tsuruhama, K., Kajiura, H., Yagyu, K., et al. (2018). Pectin RG-I rhamnosyltransferases represent a novel plant-specific glycosyltransferase family. *Nat. Plants* 4 (9), 669–676. doi: 10.1038/s41477-018-0217-7

Tian, C., Wan, P., Sun, S., Li, J., and Chen, M. (2004). Genome-wide analysis of the GRAS gene family in rice and arabidopsis. *Plant Mol. Biol.* 54 (4), 519–532. doi: 10.1023/B:PLAN.0000038256.89809.57

Turkozu, D., and Sanlier, N. (2017). L-theanine, unique amino acid of tea, and its metabolism, health effects, and safety. *Crit. Rev. Food Sci. Nutr.* 57 (8), 1681–1687.

Valente, M. A. S., Faria, J. A., Soares-Ramos, J. R., Reis, P. A., Pinheiro, G. L., Piovesan, N. D., et al. (2009). The ER luminal binding protein (BiP) mediates an increase in drought tolerance in soybean and delays drought-induced leaf senescence in soybean and tobacco. *J. Exp. Bot.* 60 (2), 533–546. doi: 10.1093/jxb/ern296

Vorwerk, S., Schiff, C., Santamaria, M., Koh, S., Nishimura, M., Vogel, J., et al. (2007). EDR2 negatively regulates salicylic acid-based defenses and cell death during powdery mildew infections of arabidopsis thaliana. *BMC Plant Biol.* 7, 35. doi: 10.1186/1471-2229-7-35

Walker, B. J., Abeel, T., Shea, T., Priest, M., Abouelliel, A., Sakthikumar, S., et al. (2014). Pilon: an integrated tool for comprehensive microbial variant detection and genome assembly improvement. *PloS One* 9, e112963. doi: 10.1371/journal.pone.0112963

Wang, Y., Li, X. Y., Li, C. X., He, Y., Hou, X. Y., and Ma, X. R. (2021). The regulation of adaptation to cold and drought stresses in poa crymophila keng revealed by integrative transcriptomics and metabolomics analysis. *Front. Plant Sci.* 12. doi: 10.3389/fpls.2021.631117

Wang, Y., Jiang, C.-J., Li, Y.-Y., Wei, C.-L., and Deng, W.-W. (2012). CsICE1 and CsCBF1: two transcription factors involved in cold responses in camellia sinensis. *Plant Cell Rep.* 31 (1), 27–34. doi: 10.1007/s00299-011-1136-5

Wang, Y.-X., Liu, Z.-W., Wu, Z.-J., Li, H., and Zhuang, J. (2016). Transcriptome-wide identification and expression analysis of the NAC gene family in tea plant [Camellia sinensis (L.) o. kuntze]. *PloS One* 11 (11), e0166727. doi: 10.1371/journal.pone.0166727

Ward, J. H. Jr. (1963). Hierarchical grouping to optimize an objective function. *J. Am. Stat. Assoc.* 58 (301), 236–244. doi: 10.1080/01621459.1963.10500845

Wildhagen, H., Paul, S., Allwright, M., Smith, H. K., Malinowska, M., Schnabel, S. K., et al. (2018). Genes and gene clusters related to genotype and drought-induced variation in saccharification potential, lignin content and wood anatomical traits in populus nigra. *Tree Physiol.* 38 (3), 320–339. doi: 10.1093/treephys/tpx054

Wisniewski, M., Nassuth, A., Teulieres, C., Marque, C., Rowland, J., Cao, P. B., et al. (2014). Genomics of cold hardiness in woody plants. *Crit. Rev. Plant Sci.* 33 (2-3), 92–124. doi: 10.1080/07352689.2014.870408

Wu, H. C., Bulgakov, V. P., and Jinn, T. L. (2018). Pectin methylesterases: cell wall remodeling proteins are required for plant response to heat stress. *Front. Plant Sci.* 9. doi: 10.3389/fpls.2018.01612

Xia, E. H., Tong, W., Wu, Q., Wei, S., Zhao, J., Zhang, Z. Z., et al. (2019). Tea plant genomics: achievements, challenges and perspectives. *Horticulture Res.* 7 (7). doi: 10.1038/s41438-019-0225-4

Xie, Y., Chen, P., Yan, Y., Bao, C., Li, X., Wang, L., et al. (2018). An atypical R2R3 MYB transcription factor increases cold hardiness by CBF-dependent and CBF-independent pathways in apple. *New Phytol.* 218 (1), 201–218. doi: 10.1111/nph.14952

Yamasaki, S., and Dillenburg, L. R. (1999). Measurements of leaf relative water content in araucaria angustifolia. *Rev. Bras. Fisiologia Vegetal* 11 (2), 69–75.

Yang, Z., Liu, B., Su, J., Liao, J., Lin, C., and Oka, Y. (2017). Cryptochromes orchestrate transcription regulation of diverse blue light responses in plants. *Photochem. Photobiol.* 93 (1), 112–127. doi: 10.1111/php.12663

Zhang, Y., Li, D., Zhou, R., Wang, X., Dossa, K., Wang, L., et al. (2019a). Transcriptome and metabolome analyses of two contrasting sesame genotypes reveal the crucial biological pathways involved in rapid adaptive response to salt stress. *BMC Plant Biol.* 19, 66. doi: 10.1186/s12870-019-1665-6

Zhang, B., Liu, J., Yang, Z. E., Chen, E. Y., Zhang, C. J., Zhang, X. Y., et al. (2018). Genome-wide analysis of GRAS transcription factor gene family in gossypium hirsutum l. *BMC Genomics* 19, 348. doi: 10.1186/s12864-018-4722-x

Zhang, G. Y., Liu, R. R., Zhang, C. Q., Tang, K. X., Sun, M. F., Yan, G. H., et al. (2015). Manipulation of the rice l-galactose pathway: evaluation of the effects of transgene overexpression on ascorbate accumulation and abiotic stress tolerance. *PloS One* 10 (5), e0125870. doi: 10.1371/journal.pone.0125870

Zhang, Y., Zhang, Y., Lin, Y., Luo, Y., Wang, X., Chen, Q., et al. (2019b). Transcriptomic analysis reveals diverse regulatory networks that respond to cold stress in strawberry (Fragaria×ananassa). *Int. J. Genomics* 2019, 7106092. doi: 10.1155/2019/7106092

Zheng, L., Zhao, Y., Gan, Y., Li, H., Luo, S., Liu, X., et al. (2022). Full-length transcriptome sequencing reveals the impact of cold stress on alternative splicing in quinoa. *Int. J. Mol. Sci.* 23, 5724. doi: 10.3390/ijms23105724

Zheng, C., Zhao, L., Wang, Y., Shen, J., Zhang, Y., Jia, S., et al. (2015). Integrated RNA-seq and sRNA-seq analysis identifies chilling and freezing responsive key molecular players and pathways in tea plant (Camellia sinensis). *PloS One* 10 (4), e0125031. doi: 10.1371/journal.pone.0125031

Zhou, P., Li, X., Liu, X., Wen, X., Zhang, Y., and Zhang, D. (2021). Transcriptome profiling of malus sieversii under freezing stress after being cold acclimated. *BMC Genomics* 22, 681. doi: 10.1186/s12864-021-07998-0

Zhou, R., Yu, X., Zhao, T., Ottosen, C. O., Rosenqvist, E., and Wu, Z. (2019). Physiological analysis and transcriptome sequencing reveal the effects of combined cold and drought on tomato leaf. *BMC Plant Biol.* 19, 377. doi: 10.1186/s12870-019-1982-9

Zhu, Y. N., Shi, D. Q., Ruan, M. B., Zhang, L. L., Meng, Z. H., Liu, J., et al. (2013). Transcriptome analysis reveals crosstalk of responsive genes to multiple abiotic stresses in cotton (Gossypium hirsutum l.). *PloS One* 8 (11), e80218. doi: 10.1371/journal.pone.0080218

frontiers | Frontiers in Plant Science

TYPE Original Research
PUBLISHED 20 November 2023
DOI 10.3389/fpls.2023.1274260

OPEN ACCESS

EDITED BY
Dongmei Li,
Shandong Agricultural University, China

REVIEWED BY
Kocsy Gábor,
Hungarian Academy of Sciences (MTA), Hungary
Shengjun Feng,
Zhejiang Agriculture and Forestry University, China

*CORRESPONDENCE
Yanlin An
17855124165@163.com
Moli Chu
molixm@126.com

RECEIVED 08 August 2023
ACCEPTED 03 November 2023
PUBLISHED 20 November 2023

CITATION
Zhang F, Jiang S, Li Q, Song Z, Yang Y, Yu S, Nie Z, Chu M and An Y (2023) Identification of the *ALMT* gene family in the potato (*Solanum tuberosum* L.) and analysis of the function of *StALMT6/10* in response to aluminum toxicity. *Front. Plant Sci.* 14:1274260. doi: 10.3389/fpls.2023.1274260

Identification of the *ALMT* gene family in the potato (*Solanum tuberosum* L.) and analysis of the function of *StALMT6/10* in response to aluminum toxicity

Feng Zhang[1], Sixia Jiang[1], Qiong Li[2], Zhiying Song[1], Ying Yang[1], Shirui Yu[1], Zongyue Nie[3], Moli Chu[4]* and Yanlin An[1]*

[1]Department of Food Science and Engineering, Moutai Institute, Renhuai, Guizhou, China, [2]Department of Brewing Engineering, Moutai Institute, Renhuai, Guizhou, China, [3]Agriculture Science Institute of Bijie, Bijie, Guizhou, China, [4]Anhui Provincial Key Laboratory of the Conservation and Exploitation of Biological Resources/College of Life Sciences, Anhui Normal University, Wuhu, Anhui, China

Introduction: Aluminum (Al)-activated malate transporters (ALMTs) play an important role in the response to Al toxicity, maintenance of ion homeostasis balance, mineral nutrient distribution, and fruit quality development in plants. However, the function of the *StALMT* gene family in potato remains unknown.

Methods and results: In this study, 14 *StALMT* genes were identified from the potato genome, unevenly distributed on seven different chromosomes. Collinearity and synteny analyses of *ALMT* genes showed that potatoes had 6 and 22 orthologous gene pairs with Arabidopsis and tomatoes, respectively, and more than one syntenic gene pair was identified for some *StALMT* gene family members. Real-time quantitative polymerase chain reaction (qPCR) results showed differential expression levels of *StALMT* gene family members in different tissues of the potato. Interestingly, *StALMT1*, *StALMT6*, *StALMT8*, *StALMT10*, and *StALMT12* had higher expression in the root of the potato cultivar Qingshu No. 9. After being subjected to Al^{3+} stress for 24 h, the expression of *StALMT6* and *StALMT10* in roots was evidently increased, displaying their decisive role in Al^{3+} toxicity.

Discussion: In addition, overexpression of *StALMT6* and *StALMT10* in Arabidopsis enhanced its tolerance to Al toxicity. These results indicate that *StALMT6* and *StALMT10* impart Al^{3+} resistance in the potato, establishing the foundation for further studies of the biological functions of these genes.

KEYWORDS

StALMT family, potato, StALMT6, StALMT10, Al toxicity

1 Introduction

Acidic soil accounts for 30%–40% of the world's arable land, and this proportion is even higher in subtropical regions, reaching approximately 70% (Kochian et al., 2015). Previous studies have shown that aluminum (Al) toxicity in acidic soils is an important limiting factor affecting crop yield. It inhibits the growth of main root crops, promotes lateral root growth, hinders the absorption of water and other nutrients, reduces photosynthesis, and ultimately leads to crop yield reduction (Zheng, 2010; Magalhaes et al., 2018; Chen et al., 2022). The aluminum-activated malate transporter (ALMT) is a class of membrane proteins present in plants that plays a vital role in the plasma membrane transport of plant malic acid. The *ALMT* gene family has been identified and depicted in different plants and crops. For instance, 14 members of the *AtALMT* gene family have been identified in the Arabidopsis genome (Kovermann et al., 2007). In the soybean genome, 34 members of the *GmALMT* gene family have been identified, and studies have demonstrated that GmALMT5 is a plasma membrane protein that mediates malate efflux from the roots (Peng et al., 2018). In sugarcane, 11 members of the *ALMT* gene family were recognized, and six of these genes played a role in Al toxicity (Ribeiro et al., 2021). Additionally, the *ALMT* gene family in Chinese white pear and apple was identified, which plays a key role in various physiological functions such as malate accumulation and organic acid efflux (Lin et al., 2018; Ma et al., 2018). In hydrangea (*Hydrangea macrophylla* [Thunb.] Ser.), 11 *ALMT* gene family members were recognized based on transcriptome data. Furthermore, the expression of three genes (*HmALMT5*, *HmALMT9*, and *HmALMT11*) in yeast increased tolerance to Al toxicity (Qin Z. et al., 2022).

The main functions of the ALMT family include tolerance to Al toxicity, regulation of stomatal resistance, transportation of mineral nutrition, microbial interactions, and seed development (Sharma et al., 2016). *TaALMT* was the first Al-activated malate transporter gene discovered and identified in wheat (*Triticum aestivum* L.). The main function of *TaALMT1* is to enable the transport of malate to bind with Al ions outside the cell, preventing Al ions from entering the root-tip cells (Sasaki et al., 2004). Subsequently, *AtALMT1* (Hoekenga et al., 2006), *BnALMT1* and *BnALM2* (Ligaba et al., 2006), *ScALMT1* (Collins et al., 2008), *ZmALMT1* (Piñeros et al., 2008) and *ZmALMT2* (Ligaba et al., 2012), *GmALMT1* and *HlALMT1* (Chen et al., 2013), *MsALMT1* (Chen et al., 2013), *SlALMT9* (Ye et al., 2017), and *BoALMT1* (Zhang et al., 2018) were also cloned. In Zea mays, *ZmALMT1* plays a significant role in mineral nutrition and ion homeostasis modes, rather than controlling a distinctive Al-activated citrate excretion reaction in the root (Piñeros et al., 2008). *ZmALMT2* is not related to Al stress but plays a significant role in mineral nutrient absorption and allocation (Ligaba et al., 2012). Interestingly, *AtALMT1* is responsible for mediating Al-activated malate secretion and responding to multiple signals indicating indole-3-acetic acid (IAA), abscisic acid (ABA), low pH, and hydrogen peroxide (Kobayashi et al., 2013). Furthermore, *HvALMT1* has been shown to be unrelated to Al resistance in barley (*Hordeum vulgare*) and functions as an anion channel to promote organic anion transportation in stomatal function and expanding cells (Gruber et al., 2010). Other members of the *ALMT* gene families code for anion channels, but the effects of substrate specificity, plasma membrane presence, and the dynamic balance of different functions including malic acid, osmotic regulation, and function of guard cells have significant differences (Kovermann et al., 2007; Xu et al., 2015).

There are 16 *ALMT* gene family members identified and analyzed in the tomato plant, which belongs to the *Solanaceae* family along with the potato. *SlALMT4* and *SlALMT5* are localized in the vascular bundles, and these two proteins secrete malate efflux (Sasaki et al., 2016). *SlALMT9* (Solyc06g072910–Solyc06g072920) was included in a genome-wide association study with 272 tomato accessions, demonstrating that tonoplast-localized was responsible for deciding the malic acid content of the fruit (Ye et al., 2017). Furthermore, the tomato-response Al toxicity and jasmonic acid (JA)-regulated mechanism revealed that *SlALMT3* is responsible for the regulatory mechanism underlying the crosstalk between Al and JA, and six *SlWRKYs* may act as upstream regulators of *SlALMT3* in this crosstalk response (Wang et al., 2020). In addition, *ALMT* (Solyc01g096140.3) was reported to be negatively correlated with the sugar/organic acid ratio in the tomato fruit (Li et al., 2021). Next, *SlALMT15* was confirmed to be related to the stomatal density of leaves and further affects photosynthesis and drought tolerance in the tomato (Ye et al., 2021). Finally, *SlALMT11* expressed in tomato leaf guard cells was associated with external malate-induced stomatal closure, but not with abscisic acid (Sasaki et al., 2022).

The edible part of the potato is in direct contact with the soil, and it is also the first contact site for high Al toxicity. High Al toxicity on potato growth and yield refers to the negative impact of excessive Al content in the soil on the growth and yield of potato crops. Al ions in the soil can harm the root system and reduce the uptake of essential nutrients by the potato plants. This stress can lead to stunted growth, reduced tuber formation, and lower yields. The function of the *StALMT* gene family in the potato remains correspondingly unknown. In this study, we identified and analyzed members of the *StALMT* gene family from the potato genome. Our study focused on chromosome distribution, gene nomenclature, physicochemical properties, subcellular localization, evolutionary relationship, and analysis of cis-acting elements of the members of the *StALMT* gene family. Additionally, we researched the expression of the *StALMT* gene family, the response of the potato cultivar to $Al3^{+}$ toxicity, the relationship between malate secretion in the potato and Al toxicity, and the role of *StALMT6* and *StALMT10* in response to Al toxicity.

2 Materials and methods

2.1 Plant materials and growth conditions

The potato cultivar 'Qingshu No. 9' was used to analyze Al toxicity. Qingshu No. 9 was obtained from the Institute of Vegetables and Flowers, Chinese Academy of Agricultural Sciences. After germinating at 22°C, pre-elite seeds were transferred to 1/4 potato Murashige and Skoog (MS) basal salts

with vitamins (Coolaber) non-buffered solutions at an initial pH of 5.5. The potatoes were grown at 25°C in growth chambers with a 12-h light/12-h dark photoperiod.

Arabidopsis thaliana Columbia-0 (Col-0) was obtained from the School of Life Sciences, Nanjing University. For growth experiments, Col-0 seeds were sterilized with 10% sodium hypochlorite for 4 min, washed in double-distilled water four times, and sown on MS or 1/4 MS medium containing 1% sucrose (Aldrich-Sigma) and solidified with 1% agar (Aldrich-Sigma). Our previous study specified the experimental methods for Al-tolerant growth phenotypes in Arabidopsis [30]. The plates were incubated at 4°C in darkness for 2 days and then positioned vertically. On day 10 after germination, the seedlings were imaged to measure primary root lengths using ImageJ (http://rsb.info.nih.gov/ij/) or were collected to weigh the biomass.

2.2 Identification and analysis of the ALMT gene family

The protein sequence of the reference genome "PGSC DM v4.03" was obtained from the Spud DB database (http://spuddb.uga.edu/). Then, the members of the potato *ATML* gene family were identified by gene annotation and BLASTp homology alignment. The MW and pI values of the ALMT family proteins were predicted using the ExPASy website (https://www.expasy.org/). Furthermore, the cis-acting elements were predicted by PlantCARE online software (https://bioinformatics.psb.ugent.be/webtools/plantcare/html/). Subsequently, the structural features of all candidate *ALMT* genes, i.e., protein motifs and cis-acting elements in the promoter region, are displayed using TBtools. Subcellular localization prediction of the StALMT family proteins was performed using WoLF PSORT (https://wolfpsort.hgc.jp/) (Horton et al., 2007). Both SOPMA database (https://npsa-prabi.ibcp.fr/cgi-bin/npsa_automat.pl?page=/NPSA/npsa_server.html) and Phyre2 (http://www.sbg.bio.ic.ac.uk/phyre2/html/page.cgi?id=index) software were used to predict the secondary and tertiary structures of the proteins, respectively (Gasteiger et al., 2005; Kelley et al., 2015).

2.3 Phylogenetic analysis and motif identification

All protein sequences were aligned using ClustalW in MEGA 7, and then the neighbor-joining (NJ) phylogenetic tree was constructed based on Poisson model with a bootstrap value of 1,000. All protein sequence motifs were predicted using MEME (http://meme-suite.org/) (Lu et al., 2021).

2.4 Chromosomal distribution, gene duplication, and synteny analysis

The location information of all gene family members is obtained from the GFF file of reference genome v4.03, and then the distribution of these genes on chromosomes is drawn based on the online web service of MG2C (http://mg2c.iask.in/mg2c_v2.1/). Using the multicollinearity scanning function module built in the TBtools software, gene duplication and collinearity analysis were completed and visualized (An et al., 2022).

2.5 RT-PCR and qRT-PCR

Total RNA was extracted from potato and Arabidopsis roots using TRIzol reagent (Invitrogen), followed by synthesis of poly (dT) complementary DNA using M-MLV Reverse Transcriptase (Promega). Reverse transcription–quantitative PCR (RT-qPCR) was performed using the SYBR Green I Master kit (Roche Diagnostics) according to the manufacturer's instructions on a CFX Connect Real-Time System (Bio-Rad). Primer Premier 5.0 was used to design RT-qPCR primers for 14 members of the StALMT gene family, and Actin (PGSC0003DMT400047481) was used as the internal reference gene in PCR analyses. All primers used are listed in Supplementary Table S2. Three biological replicates were performed for each sample, and differential expression was calculated using the 2 [-Delta Delta C(T)] method (Livak and Schmittgen, 2001).

2.6 Cloning of the full-length CDS sequence of the StALMT6 and StALMT10 genes

The Qingshu No. 9 root was selected for the extraction of RNA material, and total RNA was extracted using the extraction kit [Tiangen Biochemical Technology (Beijing) Co., Ltd.]. Subsequently, cDNA was synthesized using reverse transcription. PCR amplification was performed using the cDNA as a template. The primers used were St-ALMT6-F1, St-ALMT6-R1, St-ALMT10-F1, and S-tALMT10-R1 (Supplementary Table S1). Amplified products were separated by electrophoresis using 1% agarose gel. The *StALMT6* and *StALMT10* fragments were tested for concentration after recovery using DNA Gel Extraction Kit. The recovered products were tailed with polyA using Taq enzyme and then ligated to the pMD 19-T vector and transformed into Escherichia coli DH 5 α competent cells. Growth and culture were coated on screening medium containing antibiotics. Finally, monoclonal colonies were picked for PCR, corrected and verified by sequencing.

2.7 Overexpression vector construction and Arabidopsis transformation

To construct expression vectors for the *StALMT6* and *StALMT10* transgenic expression vector, *StALMT6* and *StALMT10* CDSs were amplified from cDNA of Bishu No. 4 roots. For the Arabidopsis transformation, *StALMT6* and *StALMT10* sequences were cloned into the NcoI/SpeI sites of the plant expression vector pCAMBIA1302, and the plant overexpression vectors for pCAMBIA1302-35S-StALMT6 and pCAMBIA1302-35S-StALMT10

were obtained. The above obtained carriers were transferred into *Agrobacterium tumefaciens* strain GV3101, and Arabidopsis Col-0 plants were transformed by the floral dip method (Clough and Bent, 1998). Seeds were sterilized and then sown on solid 1/2 MS medium containing 35 μg mL^{-1} kanamycin. After 4 days of cultivation at 4°C, the seeds were transferred to a growth chamber with a light cycle of 16 h of light and 8 h of darkness at 25°C for 8 days. Subsequently, the plants were transplanted into soil. Specific primers (Supplementary Table S2) were designed for PCR identification of transgenic Arabidopsis to screen for positive plants. Three overexpressing homozygous T3 transgenic lines (OE strains) were obtained for each gene, and the best expressing OE strain was selected for subsequent Al toxicity experiments.

2.8 Morin fluorescence staining and measurements of Al contents by ICP-MS

Morin is a naturally occurring flavonoid compound derived from plants. It has the remarkable ability to form a fluorescent chelator when combined with aluminum ions, making it an ideal tool for aluminum ion fluorescence staining imaging. The method for morin fluorescence assay was previously described in our research (Zhang et al., 2019). In short, 7-day-old seedlings were incubated in 1/2 MS basal salts with vitamin solutions at pH 4.5, supplemented with 0 or 300 μM $Al_2(SO_4)_3$ for 6 h. They were then stained with 1/6 MS solutions, without Al^{3+} (pH 4.5), containing 100 μM morin (Aldrich-Sigma) for 30 min. After rinsing with water thrice, the root tips were observed under a microscope (BX53, Olympus).

Three-week-old Arabidopsis seedlings were transferred onto 1/6-strength MS solutions (pH 5.0) without or with 300 μM $Al_2(SO_4)_3$. After a 72-h treatment, Col-0, OE-*StALMT6-#2*, and OE-*StALMT10-#3* seedlings were collected and pooled into roots and shoots. After washing with distilled water three times, the samples were dried for 48 h at 100°C, milled to fine powder, weighed, and digested with concentrated HNO_3 (Aldrich-Sigma) in a digester (DigiBlock ED16, LabTech). Ion concentration was measured by inductively coupled plasma mass spectrometry (ICP-MS; NexION 300, Perkin-Elmer). Each sample was tested at least three times.

2.9 Measurements of malate content

Root malate exudation was detected as previously described (Ding et al., 2013). Briefly, 3-week-old Col-0, OE-*StALMT6-#2*, and OE-*StALMT10-#3* seedlings were transferred onto 400 mL 1/6 MS basal salts with vitamin solutions (pH 5.0) without or with 300 μM $Al_2(SO_4)_3$. After 3 days of incubation, the solutions were collected and passed through cation and anion exchange columns filled with 8 g resin-001X and 5 g DOWEX 1 × 8 chloride form (100–200 mesh, Aldrich-Sigma). After eluting with 10 mL of 1 M hydrochloric acid, the elate was concentrated in a rotary evaporator at 40°C. The residue was redissolved in 1 mL deionized ultrapure water and was used to detect malate and citrate concentration by high-performance liquid chromatography (HPLC; Model 1200SL, Agilent Technologies).

2.10 Statistical analysis

For all experiments in this paper, we performed at least three independent replications. The data obtained were statistically analyzed using the Student's t-test ($p < 0.05$).

3 Results

3.1 Analysis of the StALMT family

A study showed that Arabidopsis has 14 members of the ALMT family (Kovermann et al., 2007). The tomato and potato, which belong to the *Solanaceae* family, have 16 members of the ALMT protein family (Sasaki et al., 2016). In order to ascertain the number of ALMT protein family members in the potato, we used the information from the potato ALMT protein family in NCBI and Spud DB databases to obtain the sequence of StALMT proteins and related homologous proteins (Xu et al., 2011). A total of 14 ALMT family member proteins were identified in the potato, which were named StALMT1~14 based on their location on the chromosome (Supplementary Table S1). StALMT proteins were found to be 310~665 amino acids long and contain 3–7 transmembrane domains, and subcellular localization prediction showed that StALMT proteins are well distributed in the plasma membrane (Plas), endoplasmic reticulum (ER), cytolysosome (Cyto), chloroplast (Chlo), vacuole (Vacu), Golgi complex (Golg), and mitochondria (Mito). Interestingly, *StALMT1* is localized on the cytolysosome; StALMT2, StALMT4, StALMT6, and StALMT9 are localized on the plasma membrane; StALMT3 is localized in the vacuole; StALMT12 is localized in the chloroplast; StALMT7, StALMT8, and StALMT11 are distributed in both the plasma membrane and endoplasmic reticulum; StALMT10 and StALMT14 are localized on both the plasma membrane and vacuole. However, StALMT5 is distributed across the cytolysosome, endoplasmic reticulum, and mitochondria; StALMT13 is distributed across the plasma membrane, Golgi complex, and vacuole. Furthermore, as shown in Figure 1, these proteins are unevenly distributed on seven different chromosomes. Among them, chromosome 1 contains five StALMT members (StALMT 1~5), while chromosomes 3 (StALMT 6, 7), 6 (StALMT 9, 10), and 11 (StALMT 13, 14) all contain two StALMT members.

3.2 Prediction and analysis of the spatial structure of the StALMT protein family members

To further investigate the StALMT protein family, we have predicted its secondary structures. Secondary structure analysis of StALMT proteins showed that all proteins comprised three structural units: α-helix, random coil, and extended strand, but the percentage and order distribution of these three structural units in these proteins were different (Figure 2). The highest percentage of α-helix was from 48.88% to 65.16%, followed by random coils from

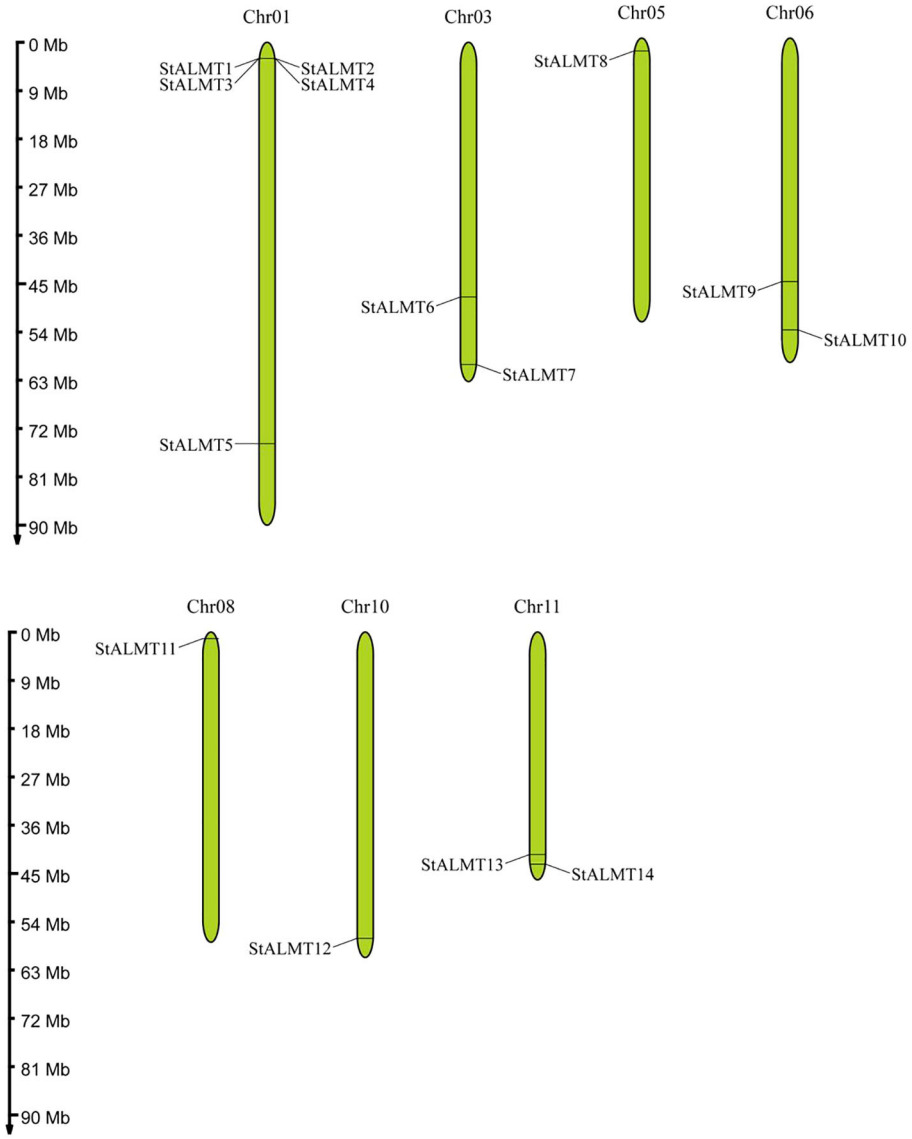

FIGURE 1
Chromosomal distribution of *StALMTs*. The scale bar on the left represents the length (Mb) of the potato chromosomes, and *StALMTs* are marked on both sides of the respective chromosome.

24.52% to 37.03%. The percentage of the extended chains in each protein varied from 6.35% to 14.09%. Interestingly, the StALMT3 had the highest percentage of α-helices and the lowest percentage of random coils among all of the StALMT proteins. StALMT9 had exactly the opposite percentage of α-helices and random coils as StALMT3. The highest percentage of the extended strand was in StALMT9 and the lowest was in StALMT5 (Figure 2A). In addition, based on the publicly reported cryo-electron microscopy (cryo-EM) structure of AtALMT1 (c7vq5B)and GmALMT12 (c7w6Ka) (Qin L. et al., 2022; Wang et al., 2022), we predicted the tertiary structure of the StALMT protein family by using Phyre2 online software. The results showed that the tertiary structures of StALMT6, StALMT10, and StALMT11 were similar to that of Arabidopsis AtALMT1 (ID: c7vq5B) (Figures 3F, J, O). On the other hand, the tertiary structures of StALMT7 and StALMT13 were more similar to that of soybean GmALMT12 (c7w6kA) (Figures 3G, M, P). These predicted results provide a basis for further studying the functions and mechanisms of StALMT6 and StALMT10, and in the future, these predictions can be validated through experiments to further elucidate the relationship between their structure and function.

3.3 Phylogenetic and syntenic analysis of the potato StALMT proteins

In the tomato, 16 SlALMT proteins can be classified into four clades (Sasaki et al., 2016). To elucidate the functional and evolutionary relationship of the StALMT family, we obtained a phylogenetic tree of ALMT family proteins of the potato (Supplementary Table S3), and 14 members of the StALMT family

A

Protein	Proportion of secondary structure element (%)		
	Alpha helix	Extended strand	Random coil
StALMT1	61.71	9.76	28.54
StALMT2	56.39	10.08	33.53
StALMT3	65.16	10.32	24.52
StALMT4	53.38	10.53	36.09
StALMT5	58.84	6.35	34.81
StALMT6	59.19	8.58	32.22
StALMT7	56.29	7.95	35.76
StALMT8	59.78	7.64	32.59
StALMT9	48.88	14.09	37.03
StALMT10	55.52	8.19	36.30
StALMT11	57.25	10.78	31.97
StALMT12	60.93	9.83	29.24
StALMT13	62.47	8.47	29.06
StALMT14	63.93	7.96	28.10

B

Distribution of secondary structure elements

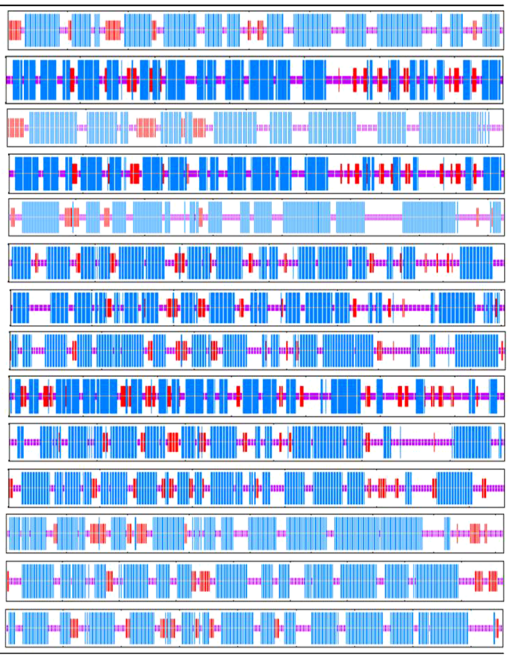

FIGURE 2
The secondary structure properties of the StALMT family members. **(A)** The proportion of the three protein secondary structure units in each StALMT family member. **(B)** The distribution of the three protein secondary structure units in each StALMT family member. The blue line in the figure indicates the alpha helix, the purple line indicates the random coil, and the red line indicates the extended chain.

can be classified into five clades (Figure 4A). The results showed that the potato genome contains 14 *ALMT* genes with seven members in clade II, including *StALMT6*, *StALMT7*, *StALMT8*, and *StALMT10*. Interestingly enough, *StALMT6* (PGSC0003DMG400000543) and *StALMT10* (PGSC0003DMG400027029) are highly homologous in clade II and should belong to the same group (Figure 4A). Collinearity analysis in the genome revealed three collinear gene pairs, namely, *StALMT1/StALMT12*, *StALMT6/StALMT10*, and *StALMT9/StALMT11* (Figure 4B).

3.4 Collinearity and phylogenetic analysis of ALMT genes in the potato

To further study the syntenic relationship between the potato *StALMT* gene and other plant genomes, two comparative syntenic maps were constructed using the TBtools software. The results showed that potatoes had 6 and 22 orthologous gene pairs with Arabidopsis and tomatoes, respectively, and more than one syntenic gene pair was identified for some of the *StALMT* family members. For instance, *StALMT7* and Arabidopsis AT3G18440.1 and AT1G68600.1 were associated, while *StALMT13* was orthologous with tomato Solyc01g007080, Solyc06g074100, Solyc10g081890, and Solyc11g068970. This means that the evolutionary relationship between the potato and tomato genomes is closer and has a wider range of collinearity compared to Arabidopsis. We further examined the evolutionary history of the *StALMT* family and its subfamily classification; we acquired a total of 30 ALMT protein sequences from Arabidopsis and tomato for alignment (Figure 5A).

In the tomato, SlALMT4 and SlALMT5 genes are expressed mainly in the vascular bundles of the fruit during development, and both proteins possess malate efflux functions (Sasaki et al., 2016). Furthermore, researchers performed a genome-wide association study (GWAS) with 272 tomato accessions, revealing that tonoplast-localized SlALMT9 was involved in determining the malic acid content of the fruit (Ye et al., 2017). To investigate the evolutionary relationships of ALMT in different plants, the amino acid sequences from the tomato (16 members of the ALMT protein family), the potato (14 members of the ALMT protein family), and Arabidopsis (14 members of the ALMT protein family) were used to generate the phylogenetic tree. The analysis showed that the 44 ALMT proteins can be classified into five clades, with potato StALMT6 and StALMT10 proteins being highly homologous to tomato SlALMT4 (Solyc03g096820) and SlALMT9 (Solyc06g072920) proteins, respectively (Figure 5B, Supplementary Figure S1).

3.5 Phylogenetic, conserved protein motif, cis-regulatory element, and gene structure analysis of the StALMT family

The phylogenetic tree constructed using the protein sequences of 14 *StALMT* genes showed that these genes can be divided into two categories (Figure 6A). Conservative motif analysis showed that

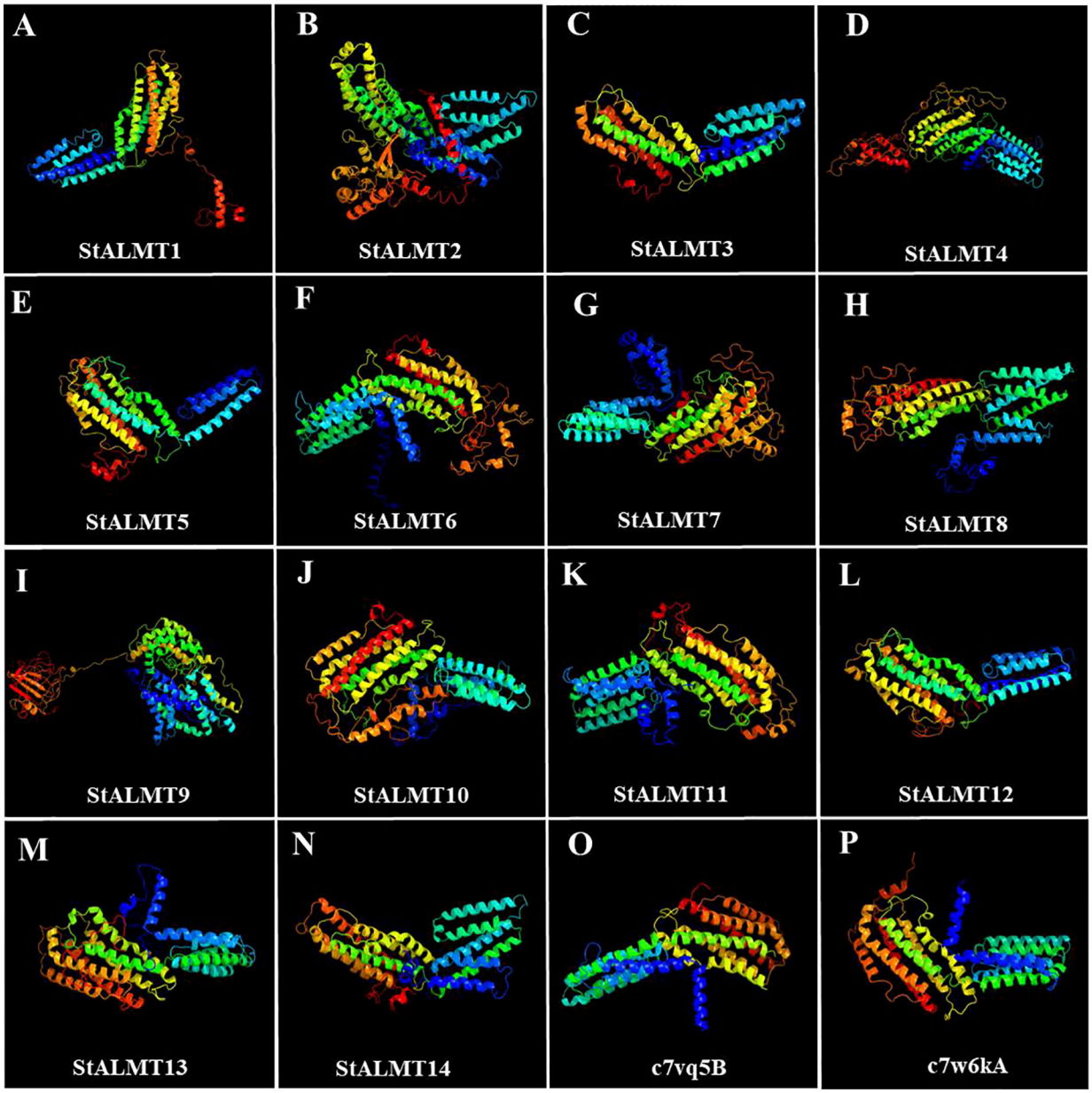

FIGURE 3
The tertiary structure properties of the StALMT family members. Tertiary structure of **(A)** StALMT1, **(B)** StALMT2, **(C)** StALMT3, **(D)** StALMT4, **(E)** StALMT5, **(F)** StALMT6, **(G)** StALMT7, **(H)** StALMT8, **(I)** StALMT9, **(J)** StALMT10, **(K)** StALMT11, **(L)** StALMT12, **(M)** StALMT13, **(N)** and StALMT14. **(O)** Cryo-EM structure of AtALMT1 with ID number c7vq5B derived from the fold library. **(P)** Cryo-EM structure of the GmALMT12/QUAC1 anion channel with ID number c7w6kA derived from the fold library.

the *StALMT* family contained 10 different types of motifs, among which motif 6 and motif 9 were identified in all family members. Unlike eight members in class I, the distance between motif 6 and motif 9 of six members in class II is larger. Cis-acting elements can interact with transcription factors to regulate the growth and development of plants and play an important role in responding to various biotic or abiotic stresses. Therefore, we extracted sequences 2 kb upstream (5′) of the 14 *StALMT* genes to identify cis-acting elements using the PlantCARE web service. The results showed that in addition to a large number of light-responsive core promoter element and common cis-acting elements, many promoter regions of *StALMT* family members contained numerous cis-acting originals of hormone response (Figure 6B). At the same time, some genes contain cis-acting originals related to stress responses such as drought. Interestingly, *StALMT10* also contains a cis-acting element, i.e., the MYB-binding site involved in the regulation of flavonoid biosynthetic genes. Abundant regulatory elements indicate the diversity of potential gene functions. Furthermore, structural analysis shows that different *StALMT* genes contain 4–6 CDS regions (Figure 6C).

10.3389/fpls.2023.1274260

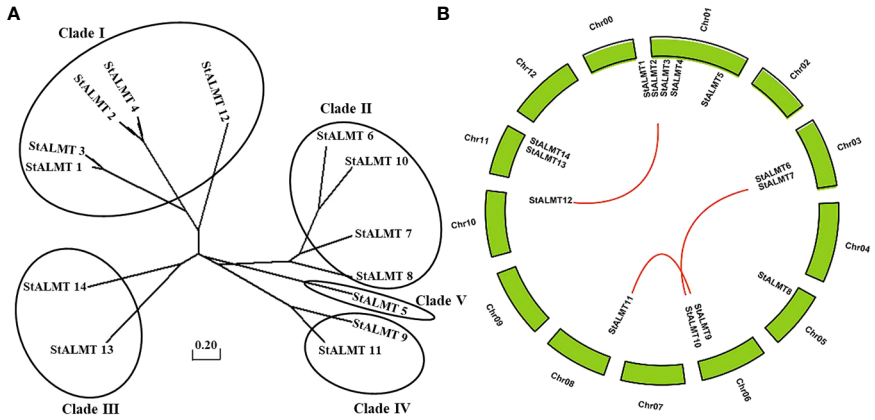

FIGURE 4
Phylogenetic and syntenic analysis of the potato StALMT genes. **(A)** The phylogenetic tree of the ALMT family of proteins in the potato (*Solanum tuberosum* L.) was obtained from the *Solanum tuberosum* genome v4.03. Amino acid sequence was aligned using the ClustalW program of the MEGA software. **(B)** Syntenic relationships of the *StALMT* genes. Potato chromosomes are displayed as green lines. The putative orthologous *StALMT* genes of the potato are symbolized by red lines.

3.6 StALMT family expression analysis in different tissues

To understand the different tissue expression patterns of the *ALMT* family in the potato, the roots, stems, and leaves of potato cultivar Qingshu No. 9 were analyzed by RT-qPCR. The results showed that *StALMT1*, *StALMT6*, *StALMT8*, *StALMT10*, and *StALMT12* had higher expression in potato roots; *StALMT3*, *StALMT4*, *StALMT13*, and *StALMT14* were highly expressed in stems; *StALMT2*, *StALMT8*, *StALMT10*, *StALMT12*, *StALMT13*, and *StALMT14* had extremely low expression in leaves; and *StALMT3*, *StALMT4*, *StALMT7*, *StALMT8*, and *StALMT11* were highly expressed in flowers. The expression of *StALMT6*, *StALMT8*, *StALMT10*, and *StALMT12* in leaves was lower than that in roots (Figure 7). These results suggested that *StALMT* genes have different functions in different tissues.

3.7 Expression analysis of StALMTs in the potato in case of Al toxicity

In the current study, we found that *StALMT1*, *StALMT6*, *StALMT8*, *StALMT10*, and *StALMT12* had higher expression in potato roots (Figure 7). In addition, phylogenetic analysis showed that StALMT6 was highly homologous to SlALMT4, and StALMT10 to SlALMT9 (Figure 5B, Supplementary Figure S1). Therefore, we assessed the expression patterns of *StALMT1*, *StALMT6*, *StALMT8*, *StALMT10*, and *StALMT12* due to Al toxicity. The experimental results showed that under Al ion stress, the expression levels of *StALMT6* and *StALMT10* genes were significantly upregulated, while *StALMT1*, *StALMT8*, and *StALMT12* genes did not show significant changes. Compared with the control group, the relative expression level of *StALMT6* increased 2-fold, and the relative expression level of *StALMT10* increased 1.5-fold. These findings indicate that potatoes respond to Al ion toxicity by upregulating the expression of *StALMT6* and *StALMT10* genes under Al ion stress (Figure 8).

3.8 The growth of OE-StALMT6 and OE-StALMT10 after Al^{3+} treatment

To explore whether *StALMT6* and *StALMT10* respond to Al toxicity, we overexpressed the *StALMT6* and *StALMT10* genes of the potato in Arabidopsis (Col-0) by gene transformation and subsequently screened the progeny for overexpression lines of these genes (Supplementary Figure S3). The Col-0, OE-*StALMT6-#2*, and OE-*StALMT10-#3* plants grew comparably on the normal medium. Under higher Al^{3+} conditions (300 μM), *StALMT6* and *StALMT10* overexpressors displayed longer primary roots than Col-0 did, indicating that *StALMT6* and *StALMT10* are involved in Al resistance in the potato (Figure 9A). The fresh weight measurements show and are consistent with the degree of difference in root length probably because the main toxic site of Al toxicity is the root, so the difference between the two seedlings is not obvious, and the shoots of seedlings account for a greater proportion of the overall fresh weight (Figures 9B, C).

The fluorescent reagent morin can emit green fluorescence after binding to small amounts of Al, which can be observed under a fluorescence microscope; morin specifically binds Al in the plant cytoplasm (Eggert, 1970; Oh et al., 2014). To further clarify the role of *StALMT6 a*nd *StALMT10* in Al resistance in the potato, we examined Al accumulation in the roots of Col-0, OE-*StALMT6-#2*, and OE-*StALMT10-#3* using morin fluorescence analysis. Without Al^{3+} treatment, the Col-0, OE-*StALMT6-#2*, and OE-*StALMT10-#3* roots have the same bright fluorescence intensity. However, after being exposed to 300 μM Al^{3+}, Col-0 has more fluorescence intensity than OE-*StALMT6-#2* and OE-*StALMT10-#3* (Figure 9D). These results suggest that *StALMT6-#2* and *StALMT10-#3* may play a role in Al resistance in the potato.

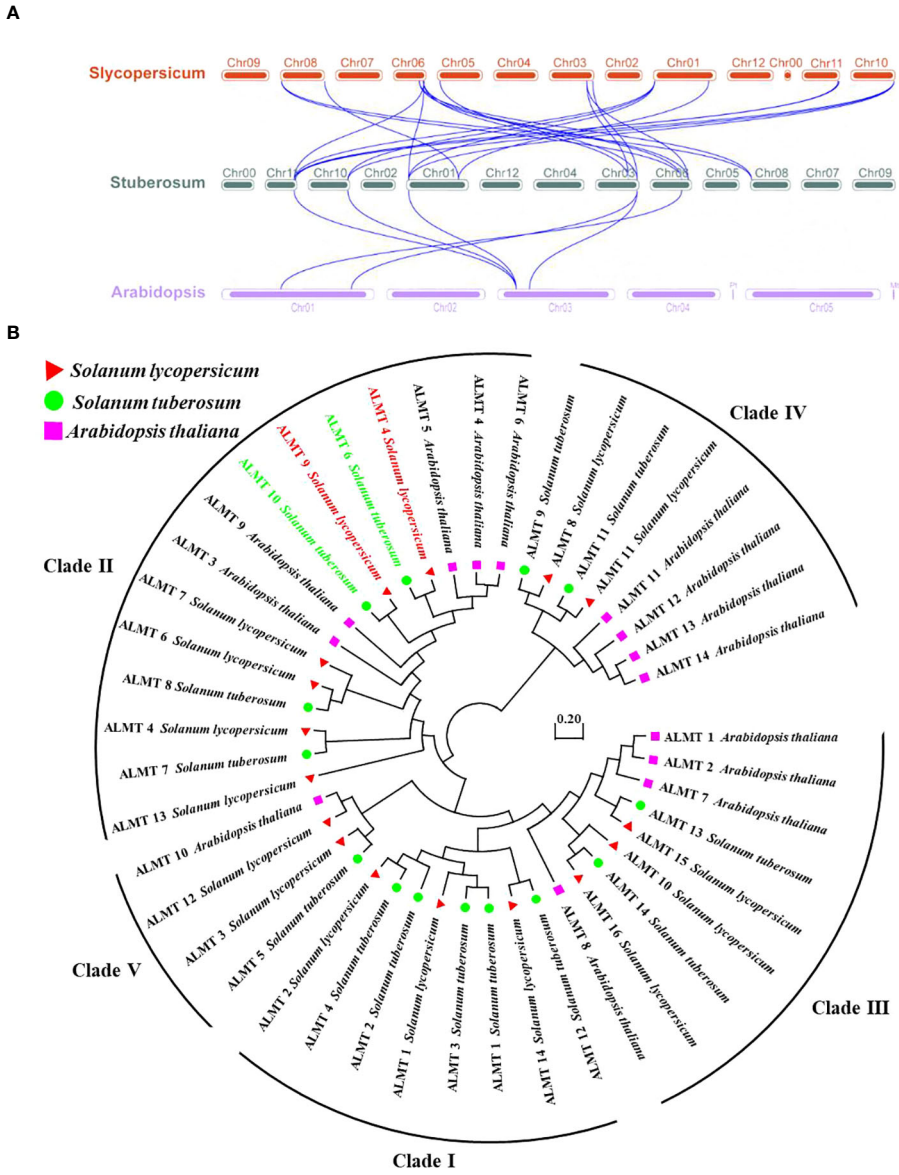

FIGURE 5
Collinearity and phylogenetic analysis of aluminum-activated malate transporter (ALMT) in the tomato, the potato, and Arabidopsis. **(A)** Collinearity analysis of *ALMT* genes in the tomato, the potato, and Arabidopsis. Chromosomes of the tomato, the potato, and Arabidopsis are represented as red, dark green, and purple, respectively. The blue curve indicates *ALMT* genes with collinearity. **(B)** Phylogenetic analysis of the ALMT proteins from the tomato, the potato, and Arabidopsis using the complete protein sequences. The neighbor-joining (NJ) tree was constructed using the MEGA software with the pairwise deletion option, and 1,000 bootstrap replicates were used to assess tree reliability. The ALMT proteins of the tomato, the potato, and Arabidopsis are represented as red triangles, green circles, and purple squares, respectively.

3.9 Relationship between malate secretion and Al toxicity

In the study of external rejection mechanism of plant resistance to Al toxicity, the secretion of malate efflux from plant roots has been considered to be one of the important mechanisms of resistance to Al toxicity (Deng et al., 2022; Wang et al., 2023). In order to evaluate whether there was a correlation between malate efflux and its Al toxicity, we examined the malate content in Col-0, OE-*StALMT6-#2*, and OE-*StALMT10-#3* root exudates using HPLC. First, we obtained standard curves of malate (Figure 10A). In the absence of Al treatment, Col-0, OE-*StALMT6-#2*, and OE-*StALMT10-#3* roots released the same amount of malate. However, after being exposed to 300 μM Al^{3+}, OE-*StALMT6-#2* and OE-*StALMT10-#3* roots secreted more malate than Col-0 roots did (Figure 10B). These results indicate that the Al^{3+} toxicity growth phenotype OE-*StALMT6-#2* and OE-*StALMT10-#3* may be related to enough malate secretion.

In order to investigate the mechanism of Al resistance in plants overexpressing StALMT6 and StALMT10, the Al content in the different plant lines was measured using ICP-MS in this study. After

10.3389/fpls.2023.1274260

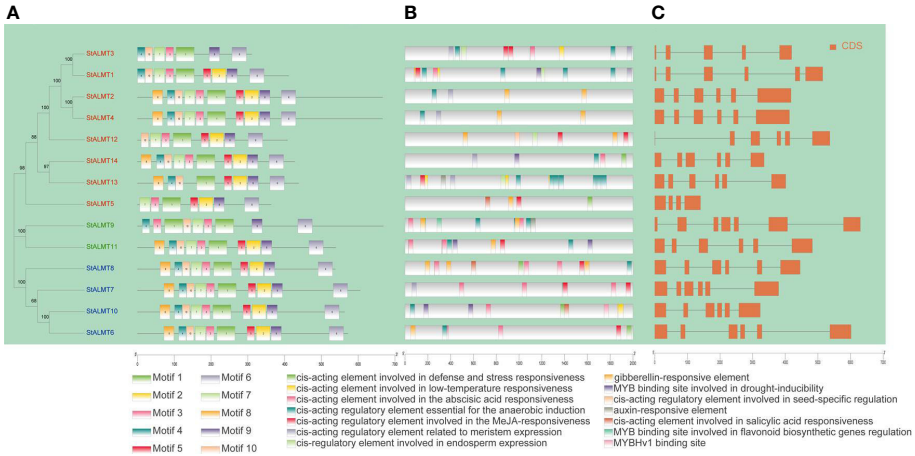

FIGURE 6
Analysis of the cis-regulatory element distribution in the ALMT promoters. **(A)** Protein sequence motifs in ALMT marked by different colors. **(B)** The number of cis-elements in different categories. **(C)** Structural analysis showing the different StALMT genes containing 4–6 CDS regions.

treatment with 300 μM Al^{3+} for 3 days, the Al content in the roots of both Col-0 and overexpression plants showed a significant increase. However, the Al accumulation in the Col-0 plants was much higher compared to the overexpression plants (Figure 10C). In contrast, there was no significant change in the Al content in the stems and leaves of both Col-0 and overexpression plants, and the Al contents were similar after treatment with the same concentration of Al^{3+} (Figure 10C). These results suggest that the Al-resistant growth phenotype observed in the OE-*StALMT6-#2* and OE-*StALMT10-#3* plants may be attributed to reduced Al^{3+} accumulation.

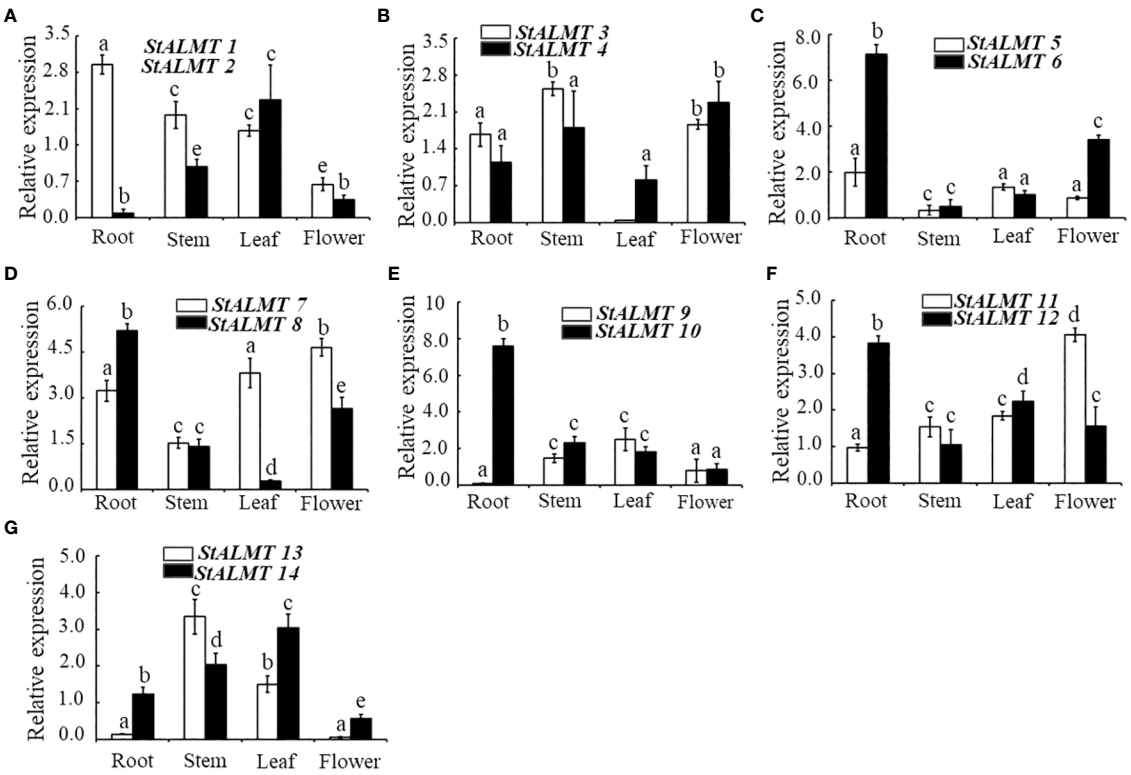

FIGURE 7
Expression of the *StALMT* family members in different tissues. The expression of **(A)** *StALMT1* and *StALMT2*, **(B)** *StALMT3* and *StALMT4*, **(C)** *StALMT5* and *StALMT6*, **(D)** *StALMT7* and *StALMT8*, **(E)** *StALMT9* and *StALMT10*, **(F)** *StALMT11* and *StALMT12*, and **(G)** *StALMT13* and *StALMT14* in a 7-week-old potato. Actin (PGSC0003DMT400047481) was used as an internal standard. Statistical data are presented as the mean ± standard deviation of three replicate experiments. Different letters indicate significant differences ($p < 0.05$).

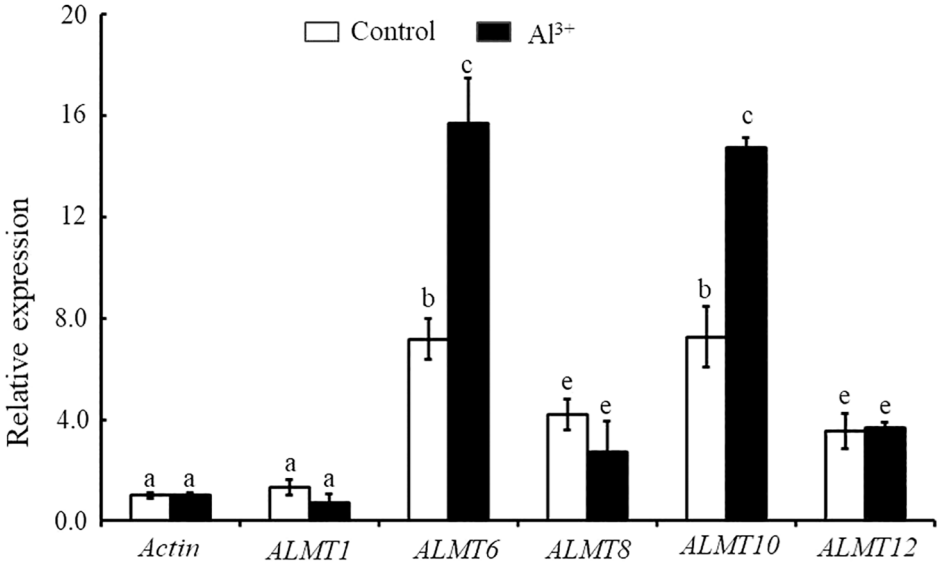

FIGURE 8
The expression of *StALMT1*, *StALMT6*, *StALMT8*, *StALMT10*, and *StALMT12* genes related to Al^{3+} toxicity in the potato after treatment. Actin (PGSC0003DMT400047481) was used as an internal standard. Statistical data are presented as the mean ± standard deviation of three replicate experiments. Different letters indicate significant differences ($p < 0.05$).

4 Discussion

A total of 14 potato genome *StALMT* family members are consistent with corresponding members in the publicly reported Arabidopsis (Kovermann et al., 2007). More than 12 *ALMT* family members in peach and Chinese plum (Lin et al., 2018), 16 *ALMT* family members in strawberry (Lin et al., 2018) and tomato (Sasaki et al., 2016), 21 family members in apple (Lin et al., 2018), 25 family members in European pear (Lin et al., 2018), 27 family members in Chinese white pear (Lin et al., 2018), 30 family members in common tobacco (Zhang et al., 2020), and 34 family members in soybean have been identified (Peng et al., 2018). In our study, we found 14 *ALMT* family members in the potato that are distributed on seven different chromosomes (Figure 1); this is similar to the findings reported on the chromosomal distribution of ALMT family members in other species (Ma et al., 2018). The N-terminus of potato ALMT family members contains 3–7 transmembrane domains (Supplementary Table S1), which is consistent with previous reports on apple (6–7 transmembrane domains) (Ma et al., 2018) and tobacco (4–6 transmembrane domains) (Zhang et al., 2020).

The structure of proteins plays a crucial role in their function and activity. The cryo-EM structure of AtALMT1 bound to malate under neutral or acidic pH conditions has been resolved in Arabidopsis (Wang et al., 2022). By using bioinformatics online tools to analyze and predict the amino acid sequences of StALMT6 and StALMT10, this study successfully obtained their tertiary structure models (Figure 3). These predictive results provide important clues for further understanding the functions and regulatory mechanisms of these two genes. In addition, this study also used a protein structure prediction software to predict the secondary structure of the amino acid sequences of StALMT6 and StALMT10. The results showed that the secondary structure of these two genes mainly consists of α-helices and β-sheets (Figure 2). This is consistent with the secondary structure features of many studied transport proteins, indicating that StALMT6 and StALMT10 may have similar structures and functions. These predictive results provide valuable information for further studying the functions and regulatory mechanisms of these two genes. Future research can validate these predictive results through experiments and further explore the relationship between the structure and function of StALMT6 and StALMT10.

The tomato and potato belong to the *Solanaceae* family; a total of 16 members of the *SlALMT* family have been identified, and two genes (*SlALMT4* and *SlALMT9*) function to generate the malate efflux (Sasaki et al., 2016; Ye et al., 2017). We used bioinformatics to perform collinearity and phylogenetic analysis on the *ALMT* genes in the potato, the tomato, and Arabidopsis (Figure 2). The phylogenetic evolutionary analysis of StALMT6 and StALMT10 proteins with the tomato ALMT family proteins revealed 98% homology between StALMT6 and SlALMT4 (Sasaki et al., 2016), and StALMT10 and SlALMT9 (Ye et al., 2017) (Supplementary Figure S1). Furthermore, qRT-PCR showed that *StALMT1*, *StALMT6*, *StALMT8*, *StALMT10*, and *StALMT12* had higher expression in potato roots (Figure 7). These results suggest that *StALMT6* and *StALMT10* may play important roles in Al resistance and malate secretion in the potato.

Upregulation of the *AtALMT1* gene promotes the efflux of malate in Arabidopsis cells, thereby alleviating the toxic effects of Al ions (Ding et al., 2013). In this study, we analyzed the gene expression of potatoes under Al ion stress, with a particular focus on the expression of the *StALMT6* and *StALMT10* genes. The experimental results showed that the expression levels of the *StALMT6* and *StALMT10* genes were significantly upregulated

10.3389/fpls.2023.1274260

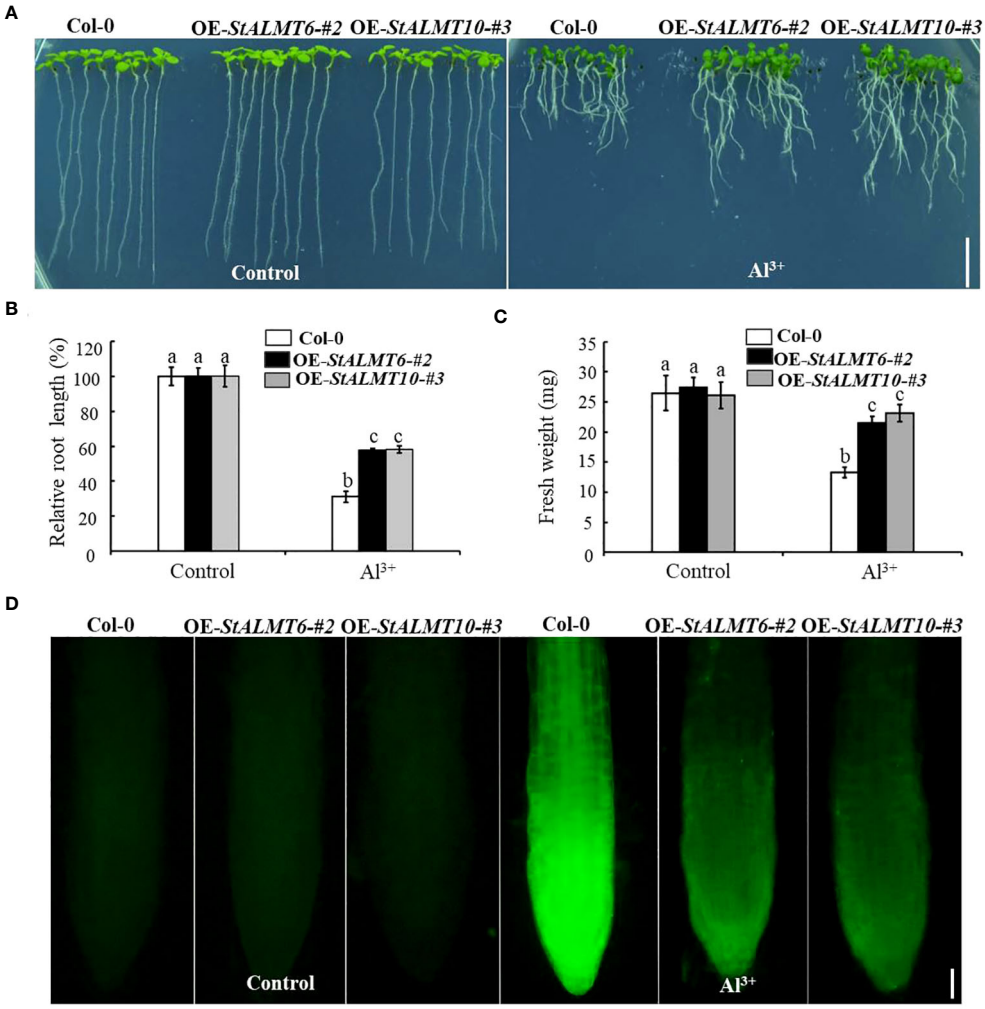

FIGURE 9
The growth phenotype of Col-0, OE-*StALMT6-#2*, and OE-*StALMT10-#3* after Al^{3+} treatment. **(A)** The growth phenotype of Col-0, OE-*StALMT6-#2*, and OE-*StALMT10-#3* after Al^{3+} treatment (0 and 300 μM), which was sourced from $Al_2(SO_4)_3$. **(B)** Relative root length statistics. **(C)** Fresh weight statistics. Pictures were taken on the sixth day after cultivation. Scale bar = 1.0 cm. Statistical data are presented as the mean ± standard deviation of three replicate experiments. Different letters indicate significant differences ($p < 0.05$). **(D)** Morin fluorescence staining of the root tips of Col-0, OE-*StALMT6-#2*, and OE-*StALMT10-#3* after 0 and 300 μM Al^{3+} treatment for 6 **(h)** Scale bar = 100 μm.

under Al ion stress, while the *StALMT1*, *StALMT8*, and *StALMT12* genes did not show significant changes (Figure 8). Compared to the control group, the relative expression levels of the *StALMT6* and *StALMT10* genes increased more than 2-fold. These findings indicate that potatoes respond to Al ion toxicity by upregulating the expression of the *StALMT6* and *StALMT10* genes.

This regulatory mechanism can minimize the damage of Al ions to the plant root system, thus enhancing the plant's resistance to Al toxicity. Morin fluorescence happens through the reaction of the dye with Al, and this method is usually used to evaluate whether the plants are resistant to Al toxicity (Rincón and Gonzales, 1992; Eticha et al., 2005). In order to study the Al toxicity function of the *StALMT6* and *StALMT10* genes, this study successfully transferred the *StALMT6* and *StALMT10* genes into *A. thaliana* plants, obtaining overexpression lines. The presence of the *StALMT6* and *StALMT10* genes in the transgenic plants was confirmed by RT-PCR technique, laying the foundation for further research on the function of these two genes under Al toxicity conditions (Supplementary Figure S3). Furthermore, this study compared the phenotypes of wild-type plants with transgenic lines that overexpressed the *StALMT6* and *StALMT10* genes under Al toxicity conditions. The experimental results clearly demonstrated that, under identical Al toxicity conditions, the transgenic lines exhibited significantly reduced root inhibition compared to the wild-type plants (Figure 9A). However, the statistical analysis of root length and weight aligned with the growth phenotype (Figures 9B, C), suggesting that overexpression of the *StALMT6* and *StALMT10* genes can effectively alleviate the inhibitory effects of Al toxicity on the roots. In addition, by measuring the fluorescence intensity of Al ions, it was found that the accumulation of Al ions in the roots of the *StALMT6* and *StALMT10* gene overexpression lines under Al toxicity conditions was significantly lower than that in wild-type plants (Figures 9D, 10C). This suggests that the overexpression of the *StALMT6* and *StALMT10* genes can inhibit the accumulation of Al ions in plants, thereby reducing the damage caused by Al toxicity.

10.3389/fpls.2023.1274260

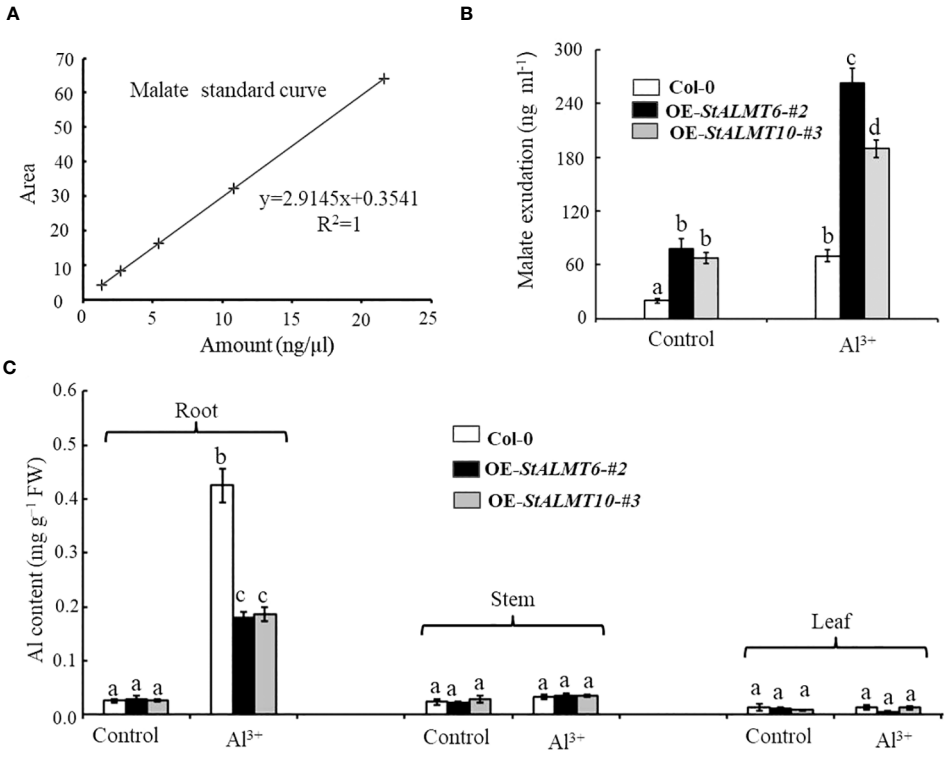

FIGURE 10
The overexpression plants excrete malate in response to Al toxicity. **(A)** Standard curves of malate detected by HPLC. **(B)** Malate exudate from the 3-week-old Col-0, OE-*StALMT6-#2*, and OE-*StALMT10-#3* incubated in the normal solutions (Control) and solution containing 300 μM Al^{3+} for 72 (h) **(C)** Al contents in the root and shoot of Col-0, OE-*StALMT6-#2*, and OE-*StALMT10-#3* on day 3 after transferring to the solutions without or with 300 μM Al^{3+}. Data are means ± SD of three independent plant samples in three replicates. Different letters indicate significant differences ($p < 0.05$).

The secretion of organic acids (OAs), such as citrate, malate, and oxalate, in response to Al toxicity is a well-documented mechanism that helps plants resist Al toxicity (Yang et al., 2019; Ofoe et al., 2023) We analyzed the malate content in root exudates of Col-0, OE-*StALMT6-#2*, and OE-*StALMT10-#3* using HPLC (Figures 10A, B). In the absence of Al treatment, all three lines released similar amounts of malate (Figure 10B). However, after exposure to 300 μM Al^{3+}, OE-*StALMT6-#2* and OE-*StALMT10-#3* secreted more malate than Col-0 did (Figure 10B). In addition, we conducted ICP-MS analysis of Col-0, OE-*StALMT6-#2*, and OE-*StALMT10-#3* to quantify the Al content in various tissues under Al-treated and nontreated conditions. It found that the roots of OE-*StALMT6-#2* and OE-*StALMT10-#3* contained lower levels of Al compared to those of Col-0 after Al treatment, while no significant differences were observed in the stems and leaves (Figure 10C). In conclusion, through the study of heterologous overexpression lines of the *StALMT6* and *StALMT10* genes, it was found that the overexpression of these two genes can significantly alleviate the inhibition of Al toxicity on plant roots and reduce the accumulation of Al ions. The findings of the study suggest that StALMT6 and StALMT10 do not function in aluminum ion transport but instead regulate aluminum ion uptake by promoting the excretion of organic acids. These results provide an important theoretical basis for further research on the molecular mechanisms of Al toxicity and breeding improvement.

In summary, we have performed a systematic analysis and functional validation of the potato *ALMT* family. A total of 14 *StALMT* genes were identified, which were unevenly distributed on seven chromosomes. Phylogenetic analysis showed that the *StALMT* family can be divided into two classes and five subfamilies, among which *StALMT6* and *StALMT10* are highly homologous genetically to the tomato for evolutionary purposes. Expression analysis showed that most *StALMTs* were expressed mainly in the roots, where the expression changes of *StALMT6* and *StALMT10* were most pronounced under Al toxicity conditions. Arabidopsis overexpression plants transgenic for *StALMT6* and *StALMT10* genes were found to display a growth phenotype resistant to Al toxicity. These results not only provide useful information for illuminating the functions of the *ALMT* gene family in potato but also establish a basis for understanding the molecular mechanisms involved in the response of some of their members to abiotic stresses, especially Al toxicity.

Data availability statement

The original contributions presented in the study are included in the article/Supplementary Material, further inquiries can be directed to the corresponding author/s.

Author contributions

YA: Writing – review & editing, Writing – original draft. FZ: Writing – original draft, Conceptualization, Formal Analysis, Methodology, Resources, Software, Writing – review & editing. SJ: Formal Analysis, Writing – original draft, Methodology, Writing – review & editing. QL: Formal Analysis, Writing – original draft. ZS: Data curation, Writing – review & editing. YY: Data curation, Formal Analysis, Methodology, Writing – original draft. SY: Funding acquisition, Visualization, Writing – review & editing. ZN: Resources, Writing – review & editing. MC: Writing – original draft, Investigation.

Funding

The author(s) declare financial support was received for the research, authorship, and/or publication of this article. This research was supported by the National Natural Science Foundation of China (32160441) and Zunyi Technology Bureau, Moutai Institute Joint Science and Technology Research and Development Project (ZSKHHZ [2021] No.332 and ZSKHHZ [2022] No.166).

Conflict of interest

The authors declare that the research was conducted in the absence of any commercial or financial relationships that could be construed as a potential conflict of interest.

Publisher's note

Supplementary material

The Supplementary Material for this article can be found online at: https://www.frontiersin.org/articles/10.3389/fpls.2023.1274260/full#supplementary-material

References

An, Y., Xia, X., Jing, T., and Zhang, F. (2022). Identification of gene family members and a key structural variation reveal important roles of OVATE genes in regulating tea (Camellia sinensis) leaf development. *Front. Plant Sci.* 13. doi: 10.3389/fpls.2022.1008408

Chen, W., Tang, L., Wang, J., Zhu, H., Jin, J., Yang, J., et al. (2022). Research advances in the mutual mechanisms regulating response of plant roots to phosphate deficiency and Al toxicity. *Int. J. Mol. Sci.* 23 (3), 1137. doi: 10.3390/ijms23031137

Chen, Z. C., Yokosho, K., Kashino, M., Zhao, F. J., Yamaji, N., and Ma, J. F. (2013). Adaptation to acidic soil is achieved by increased numbers of cis-acting elements regulating ALMT1 expression in Holcus lanatus. *Plant J.* 76 (1), 10–23. doi: 10.1111/tpj.12266

Clough, S. J., and Bent, A. F. (1998). Floral dip: a simplified method for Agrobacterium-mediated transformation of Arabidopsis thaliana. *Plant J.* 16 (6), 735–743. doi: 10.1046/j.1365-313x.1998.00343.x

Collins, N. C., Shirley, N. J., Saeed, M., Pallotta, M., and Gustafson, J. P. (2008). An ALMT1 gene cluster controlling aluminum tolerance at the Alt4 locus of rye (Secale cereale L). *Genetics* 179 (1), 669–682. doi: 10.1534/genetics.107.083451

Deng, X., Li, Y., Yao, K., Qiao, J., Wang, J., and Lin, J. (2022). Advances in the mechanism of plant adaptation to acid aluminum stress. *Sheng Wu Gong Cheng Xue Bao* 38 (8), 2754–2766. doi: 10.13345/j

Ding, Z. J., Yan, J. Y., Xu, X. Y., Li, G. X., and Zheng, S. J. (2013). WRKY46 functions as a transcriptional repressor of ALMT1, regulating aluminum-induced malate secretion in Arabidopsis. *Plant J.* 76 (5), 825–835. doi: 10.1111/tpj.12337

Eggert, D. A. (1970). The use of morin for fluorescent localization of aluminum in plantissues. *Stain Technol.* 45 (6), 301–303. doi: 10.3109/10520297009067806

Eticha, D., Stass, A., and Horst, W. J. (2005). Localization of aluminium in the maize root apex: can morin detect cell wall-bound aluminium? *J. Exp. Bot.* 56 (415), 1351–1357. doi: 10.1093/jxb/eri136

Gasteiger, E., Hoogland, C., Gattiker, A., Duvaud, S. E., Wilkins, M. R., Appel, R. D., et al. (2005). "Protein identification and analysis tools on the ExPASy server," in *The Proteomics Protocols Handbook*. Ed. J. M. Walker (Totowa, NJ: Humana Press), 571–607.

Gruber, B. D., Ryan, P. R., Richardson, A. E., Tyerman, S. D., Ramesh, S., Hebb, D. M., et al. (2010). HvALMT1 from barley is involved in the transport of organic anions. *J. Exp. Bot.* 61 (5), 1455–1467. doi: 10.1093/jxb/erq023

Hoekenga, O. A., Maron, L. G., Piñeros, M. A., Cançado, G. M. A., Shaff, J., Kobayashi, Y., et al. (2006). AtALMT1, which encodes a malate transporter, is identified as one of several genes critical for aluminum tolerance in Arabidopsis. *Proc. Natl. Acad. Sci. U.S.A* 103 (25), 9738–9743. doi: 10.1073/pnas.0602868103

Horton, P., Park, K. J., Obayashi, T., Fujita, N., Harada, H., and Adams-Collier, C. J. (2007). Nakai K. WoLF PSORT: protein localization predictor. *Nucleic Acids Res.* 35 (Web Server issue), W585–W587. doi: 10.1093/nar/gkm259

Kelley, L. A., Mezulis, S., Yates, C. M., Wass, M. N., and Sternberg, M. J. (2015). The Phyre2 web portal for protein modeling, prediction and analysis. *Nat. Protoc.* 10 (6), 845–858. doi: 10.1038/nprot.2015.053

Kobayashi, Y., Sugimoto, M., Lakshmanan, V., Iuchi, S., Kobayashi, M., Bais, H. P., et al. (2013). Characterization of the complex regulation of AtALMT1 expression in response to phytohormones and other inducers. *Plant Physiol.* 162 (2), 732–740. doi: 10.1104/pp.113.218065

Kochian, L., Pifieros, M., Liu, J., and Magalhaes, J. (2015). Plant adaptation to acid soils:the molecular basis for crop aluminum resistance. *Annu. Rev. Plant Biol.* 66, 571–598. doi: 10.1146/annurev-arplant-043014-114822

Kovermann, P., Meyer, S., Hörtensteiner, S., Picco, C., Scholz-Starke, J., Ravera, S., et al. (2007). The Arabidopsis vacuolar malate channel is a member of the ALMT family. *Plant J.* 52 (6), 1169–1180. doi: 10.1111/j.1365-313X.2007.03367

Li, N., Wang, J., Wang, B., Huang, S., Hu, J., Yang, T., et al. (2021). Identification of the carbohydrate and organic acid metabolism genes responsible for brix in tomato fruit by transcriptome and metabolome analysis. *Front. Genet.* 12. doi: 10.3389/fgene.2021.714942

Ligaba, A., Katsuhara, M., Ryan, P. R., Shibasaka, M., and Matsumoto, H. (2006). The BnALMT1 and BnALMT2 genes from rape encode aluminum-activated malate transporters that enhance the aluminum resistance of plant cells. *Plant Physiol.* 142 (3), 1294–1303. doi: 10.1104/pp.106.085233

Ligaba, A., Maron, L., Shaff, J., Kochian, L., and Piñeros, M. (2012). Maize ZmALMT2 is a root anion transporter that mediates constitutive root malate efflux. *Plant Cell Environ.* 35 (7), 1185–1200. doi: 10.1111/j.1365-3040.2011.02479

Lin, X., Xin, Q., Ming, Y. Z., and Shao, Z. (2018). Genome-Wide analysis of aluminum-activated malate transporter family genes in six rosaceae species, and expression analysis and functional characterization on malate accumulation in Chinese white pear. *Plant Sci.* 274, 451–465. doi: 10.1016/j.plantsci.2018.06.022

Livak, K. J., and Schmittgen, T. D. (2001). Analysis of relative gene expression data using real-time quantitative PCR and the 2(-Delta Delta C(T)) Method. *Methods* 25 (4), 402–408. doi: 10.1006/meth.2001.1262

Lu, J., Du, J., Tian, L., Li, M., Zhang, X., Zhang, S., et al. (2021). Divergent response strategies of CsABF facing abiotic stress in tea plant: perspectives from drought-tolerance studies. *Front. Plant Sci.* 12. doi: 10.3389/fpls.2021.763843

Ma, B., Yuan, Y., Gao, M., Qi, T., Li, M., and Ma, F. (2018). Genome-wide identification, molecular evolution, and expression divergence of aluminum-activated malate transporters in apples. *Int. J. Mol. Sci.* 19 (9), 2807. doi: 10.3390/ijms19092807

Magalhaes, J. V., Piñeros, M. A., Maciel, L. S., and Kochian, L. V. (2018). Emerging pleiotropic mechanisms underlying aluminum resistance and phosphorus acquisition on acidic soils. *Front. Plant Sci.* 9. doi: 10.3389/fpls.2018.01420

Ofoe, R., Thomas, R. H., Asiedu, S. K., Wang-Pruski, G., Fofana, B., and Abbey, L. (2023). Aluminum in plant: Benefits, toxicity and tolerance mechanisms. *Front. Plant Sci.* 13. doi: 10.3389/fpls.2022.1085998

Oh, M. W., Roy, S. K., Kamal, A. H., Cho, K., Cho, S. W., Park, C. S., et al. (2014). Proteome analysis of roots of wheat seedlings under aluminum stress. *Mol. Biol. Rep.* 41 (2), 671–681. doi: 10.1007/s11033-013-2905-8

Peng, W., Wu, W., Peng, J., Li, J., Lin, Y., Wang, Y., et al. (2018). Characterization of the soybean GmALMT family genes and the function of GmALMT5 in response to phosphate starvation. *J. Integr. Plant Biol.* 60 (3), 216–231. doi: 10.1111/jipb.12604

Piñeros, M. A., Cançado, G. M., Maron, L. G., Lyi, S. M., Menossi, M., and Kochian, L. V. (2008). Not all ALMT1-type transporters mediate aluminum-activated organic acid responses: the case of ZmALMT1 - an anion-selective transporter. *Plant J.* 53 (2), 352–367. doi: 10.1111/j.1365-313X.2007.03344

Qin, L., Tang, L. H., Xu, J. S., Zhang, X. H., Zhu, Y., Zhang, C. R., et al. (2022). Cryo-EM structure and electrophysiological characterization of ALMT from Glycine max reveal a previously uncharacterized class of anion channels. *Sci. Adv.* 8 (9), eabm3238. doi: 10.1126/sciadv.abm3238

Qin, Z., Chen, S., Feng, J., Chen, H., Qi, X., Wang, H., et al. (2022). Identification of aluminum-activated malate transporters (ALMT) family genes in hydrangea and functional characterization of HmALMT5/9/11 under aluminum stress. *PeerJ* 10, e13620. doi: 10.7717/peerj.13620

Ribeiro, A. P., Vinecky, F., Duarte, K. E., Santiago, T. R., das Chagas Noqueli Casari, R. ,. A., Hell, A. F., et al. (2021). Enhanced aluminum tolerance in sugarcane: evaluation of SbMATE over-expression and genome-wide identification of ALMTs in Saccharum spp. *BMC Plant Biol.* 21 (1), 300. doi: 10.1186/s12870-021-02975-x

Rincón, M., and Gonzales, R. A. (1992). Aluminum partitioning in intact roots of aluminum-tolerant and aluminum-sensitive wheat (Triticum aestivum L.) cultivars. *Plant Physiol.* 99 (3), 1021–1028. doi: 10.1104/pp.99.3.1021

Sasaki, T., Ariyoshi, M., Yamamoto, Y., and Mori, I. C. (2022). Functional roles of ALMT-type anion channels in malate-induced stomatal closure in tomato and Arabidopsis. *Plant Cell Environ.* 45 (8), 2337–2350. doi: 10.1111/pce.14373

Sasaki, T., Tsuchiya, Y., Ariyoshi, M., Nakano, R., Ushijima, K., Kubo, Y., et al. (2016). Two Members of the Aluminum-Activated Malate Transporter Family, SlALMT4 and SlALMT5, are Expressed during Fruit Development, and the Over-expression of SlALMT5 Alters Organic Acid Contents in Seeds in Tomato (Solanum lycopersicum). *Plant Cell Physiol.* 57 (11), 2367–2379. doi: 10.1093/pcp/pcw157

Sasaki, T., Yamamoto, Y., Ezaki, B., Katsuhara, M., Ahn, S. J., Ryan, P. R., et al. (2004). A wheat gene encoding an aluminum-activated malate transporter. *Plant J.* 37 (5), 645–653. doi: 10.1111/j.1365-313x.2003.01991.x

Sharma, T., Dreyer, I., Kochian, L., and Piñeros, M. A. (2016). The ALMT family of organic acid transporters in plants and their involvement in detoxification and nutrient security. *Front. Plant Sci.* 7. doi: 10.3389/fpls.2016.01488

Wang, Z., Liu, L., Su, H., Guo, L., Zhang, J., Li, Y., et al. (2020). Jasmonate and aluminum crosstalk in tomato: Identification and expression analysis of WRKYs and ALMTs during JA/Al-regulated root growth. *Plant Physiol. Biochem.* 154, 409–418. doi: 10.1016/j.plaphy.2020.06.026

Wang, P., Wan, N., Horst, W. J., and Yang, Z. B. (2023). From stress to responses: Aluminium-induced signalling in the root apex. *J. Exp. Bot.* 74 (5), erac516. doi: 10.1093/jxb/erac516

Wang, J., Yu, X., Ding, Z. J., Zhang, X., Luo, Y., Xu, X., et al. (2022). Structural basis of ALMT1-mediated aluminum resistance in Arabidopsis. *Cell Res.* 32 (1), 89–98. doi: 10.1038/s41422-021-00587-6

Xu, X., Pan, S., Zhang, S., Mu, B., Ni, D., Zhang, P., et al. (2011). Genomesequence and analysis of the tuber crop potato. *Nature* 475 (7355), 189–195. doi: 10.1038/nature10158

Xu, M., Gruber, B. D., Delhaize, E., White, R. G., James, R. A., You, J., et al. (2015). The barley anion channel, HvALMT1, has multiple roles in guard cell physiology and grain metabolism. *Physiol. Plant* 153 (1), 183–193. doi: 10.1111/ppl.12234

Yang, J. L., Fan, W., and Zheng, S. J. (2019). Mechanisms and regulation of aluminum-induced secretion of organic acid anions from plant roots. *J. Zhejiang Univ Sci. B.* 20 (6), 513–527. doi: 10.1631/jzus.B1900188

Ye, J., Wang, X., Hu, T., Zhang, F., Wang, B., Li, C., et al. (2017). An InDel in the promoter of Al-ACTIVATED MALATE TRANSPORTER9 selected during tomato domestication determines fruit malate contents and aluminum tolerance. *Plant Cell.* 29 (9), 2249–2268. doi: 10.1105/tpc.17.00211

Ye, J., Wang, X., Wang, W., Yu, H., Ai, G., Li, C., et al. (2021). Genome-wide association study reveals the genetic architecture of 27 agronomic traits in tomato. *Plant Physiol.* 186 (4), 2078–2092. doi: 10.1093/plphys/kiab230

Zhang, H., Li, Z. F., and Xu, G. Y. (2020). Identification and expression analysis of ALMT gene family in Nicotiana tabacum. *Tobacco Sci. Technol.* 53 (5), 1–9. doi: 10.16135/j.issn1002-0861.2019.0079

Zhang, L., Wu, X. X., Wang, J. F., Qi, C. D., Wang, X. Y., Wang, G., et al. (2018). BoALMT1, an Al-induced malate transporter in cabbage, enhances aluminum tolerance in Arabidopsis thaliana. *Front. Plant Sci.* 8. doi: 10.3389/fpls.2017.02156

Zhang, F., Yan, X. Y., Han, X. B., Tang, R. J., Chu, M. L., Yang, Y., et al. (2019). A defective vacuolar proton pump enhances aluminum tolerance by reducing vacuole sequestration of organic acids. *Plant Physiol.* 181 (2), 743–761. doi: 10.1104/pp.19.00626

Zheng, S. J. (2010). Crop production on acidic soils: overcoming aluminium toxicity and phosphorus deficiency. *Ann. Bot.* 106 (1), 183–184. doi: 10.1093/aob/mcq134

frontiers | Frontiers in Plant Science

TYPE Original Research
PUBLISHED 12 December 2023
DOI 10.3389/fpls.2023.1321952

OPEN ACCESS

EDITED BY
Dongmei Li,
Shandong Agricultural University, China

REVIEWED BY
Yuan Huang,
Huazhong Agricultural University, China
Juan de Dios Alché,
Spanish National Research Council (CSIC), Spain

*CORRESPONDENCE
Min Yu
yumin@fosu.edu.cn
Sergey Shabala
sergey.shabala@uwa.edu.au
Gangjun Zhao
zhaogangjun@gdaas.cn

RECEIVED 15 October 2023
ACCEPTED 27 November 2023
PUBLISHED 12 December 2023

CITATION
Liu M, Zhang Y, Pan T, Li Y, Hong Y, Chen W, Yang Y, Zhao G, Shabala S and Yu M (2023) Genome-wide analysis of respiratory burst oxidase homolog gene family in pea (*Pisum sativum* L.). *Front. Plant Sci.* 14:1321952. doi: 10.3389/fpls.2023.1321952

Genome-wide analysis of respiratory burst oxidase homolog gene family in pea (*Pisum sativum* L.)

Minmin Liu[1], Yu Zhang[1], Ting Pan[1], Yuanyuan Li[1], Youheng Hong[1], Wenjie Chen[1], Yao Yang[1], Gangjun Zhao[2]*, Sergey Shabala[1,3]* and Min Yu[1]*

[1]International Research Centre for Environmental Membrane Biology and Department of Horticulture, Foshan University, Foshan, China, [2]Guangdong Key Laboratory for New Technology Research of Vegetables, Vegetable Research Institute, Guangdong Academy of Agricultural Sciences, Guangzhou, China, [3]School of Biological Science, University of Western Australia, Crawley, WA, Australia

Plant respiratory burst oxidase homologs (RBOHs) are key enzymes regulating superoxide production, which is important for plant development and responses to biotic and abiotic stresses. This study aimed to characterize the *RBOH* gene family in pea (*Pisum sativum* L.). Seven *PsRBOH* genes were identified in the pea genome and were phylogenetically clustered into five groups. Collinearity analyses of the *RBOHs* identified four pairs of orthologs between pea and soybean. The gene structure analysis showed that the number of exons ranged from 6 to 16. Amino acid sequence alignment, conserved domain, and conserved motif analyses showed that all seven PsRBOHs had typical features of plant RBOHs. The expression patterns of *PsRBOH* genes in different tissues provided suggested their roles in plant growth and organ development. In addition, the expression levels of *PsRBOH* genes under different abiotic stresses were analyzed *via* reverse transcription-quantitative polymerase chain reaction (RT-qPCR). The results demonstrated that *PsRBOH* genes exhibited unique stress-response characteristics, which allowed for functional diversity in response to different abiotic stresses. Furthermore, four PsRBOHs had a high probability of localization in the plasma membrane, and PsRBOH6 was localized to the plasma membrane and endoplasmic reticulum. The results of this study provide valuable information for further functional analysis of pea *RBOH* genes and their role in plant adaptation to climate-driven environmental constraints.

KEYWORDS

reactive oxygen species, abiotic stress, plasma membrane, drought, salinity, cadmium, boron

Introduction

Abiotic stress tolerance of major staple crops was significantly weakened or even lost during their domestication (Palmgren et al., 2015; Rawat et al., 2022). Major abiotic stresses such as drought, salinity, flooding, and extreme temperatures are increasing due to the current climate changes driven by global warming (Liu et al., 2020). Therefore, improving abiotic stress tolerance in crops is critical for future food security.

Despite different plants having different mechanisms for adapting to abiotic stresses, these stresses increase superoxide levels in all plants, and the superoxide is transformed into reactive oxygen species (ROS) *via* different pathways in different cellular compartments (Sandalio et al., 2021). ROS were initially considered toxic byproducts of aerobic metabolism and deemed harmful to plants; however, their central role in complex adaptive signaling networks has been recently reported (Mittler et al., 2011). While excessive ROS accumulation is toxic, causing DNA backbone damage, protein and lipid oxidation, and inducing apoptosis (Patel et al., 2018; Wang et al., 2020), transient stress-induced ROS spikes are considered central to systemic signaling and adaptation in plants (Bostock et al., 2014; Zhang et al., 2022).

Superoxide can be produced in various cellular compartments, including cytosolic and apoplastic compartments. Respiratory Burst Oxidase Homologues (RBOH) play a key role in apoplastic superoxide production (Suzuki et al., 2011; Zhang et al., 2022). The first identified plant *RBOH* gene was *OsRBOHA* in rice (Groom et al., 1996). With the recent increase in whole-genome sequencing of more plant species, *RBOH* genes have been functionally characterized in various plant species. These plants include *Arabidopsis thaliana* (Torres et al., 1998; Torres et al., 2002), *Lycopersicon esculentum* (Sagi et al., 2004), *Olea europaea* (Jimenez-Quesada et al., 2019), *Glycine max* (Liu et al., 2019), *Brassica rapa* (Li et al., 2019), *Capsicum annuum* (Zhang et al., 2021), *Pyropia yezoensis* (Gui et al., 2022), and *Solanum melongena* (Du et al., 2023).

Previous studies showed that many plants have multiple RBOH members, and different members exhibit different expression profiles with distinct functions. For example, there are ten RBOHs in *Arabidopsis* (AtRBOHA-J) (Sagi and Fluhr, 2006) and nine in rice (OsNox1-9) (Wang et al., 2013). Additional studies showed that *AtRBOHD* and *AtRBOHF* were expressed throughout the plant, while *AtRBOHA-C*, *AtRBOHG* and *AtRBOHI* were specifically expressed in the roots. Moreover, *AtrbohH* and *AtrbohJ* were specifically expressed in pollens and are thus required for normal pollen tube growth (Sagi and Fluhr, 2006; Kaya et al., 2014). *OsNox1-2*, *OsNox5-6*, and *OsNox9* were ubiquitously expressed, while *OsNox3*, *OsNox4*, *OsNox7*, and *OsNox8* showed tissue-specific expression in rice (Wang et al., 2013). Moreover, *OsNox9* were associated with root development (Takeda et al., 2008; Yamauchi et al., 2017).

These studies also provided evidence for the involvement of RBOHs in plant signal transduction during abiotic stress responses and development. Plant RBOHs are involved in several signaling pathways, including Ca^{2+}-dependent protein kinases (CDPKs) (Dubiella et al., 2013), mitogen-activated protein kinases (MAPKs) (Asai et al., 2008), receptor-activated C-kinases (RACKs) (Nakashima et al., 2008), phosphatidylinositol, phospholipase Dα1and phosphatidic acid (Zhang et al., 2009), nitric oxide (NO) (Delledonne et al., 2002), cGMP (Li et al., 2011), extracellular ATP-mediated signaling pathways (Song et al., 2006), and hormonal signaling networks (abscisic acid, salicylic acid, jasmonic acid, and ethylene) (Overmyer et al., 2003). AtRBOHD and AtRBOHF regulate ABA-mediated stomatal closure (Kwak et al., 2003) and salt stress tolerance in *Arabidopsis* (Chung et al., 2008; Xie et al., 2011).

As a classic model plant and the second most important grain legume, pea (*Pisum sativum* L., 2n = 14) has been widely used in genetics and developmental biology studies since Mendel (Kreplak et al., 2019; Chen et al., 2022; Chen et al., 2023; Li et al., 2023). Pea has become an important legume crop and green vegetable favored by many people worldwide. Fresh pea is rich in soluble protein, starch, carotenoid, and flavonoids (Yang et al., 2022). However, pea is sensitive to most common abiotic stresses (e.g., drought, cold, high temperatures, and salinity), which cause massive yield losses.

Given the critical role of RBOH in plant adaptive responses to abiotic stresses, in this work we aimed to provide a comprehensive analysis of pea *RBOH* genes. This study analyzed the chromosomal distribution, developmental evolution, gene structure, conserved domains, subcellular location, and description of cis-acting elements of pea *RBOH* genes. We also studied the tissue specificity and expression patterns of pea *RBOH* genes under different abiotic stresses. The reported data provide valuable information for an in-depth understanding of the biological functions of the *RBOH* gene family in pea, paving the way for improving its abiotic stress tolerance.

Materials and methods

Identification of the *PsRBOH* genes in pea

The DNA sequences and annotation files of the pea genome were downloaded from the Pea Genome Database (https://www.peagdb.com/). In addition, 17 soybean, 8 tomato, and 10 *Arabidopsis* RBOH protein sequences were downloaded from the phytozome (https://phytozome-next.jgi.doe.gov/), Sol Genomics Network (https://www.sgn.cornell.edu/) and TAIR (www.arabidopsis.org/) databases, respectively. *Arabidopsis* is a model plant widely used in various plant studies, including gene family identification studies. Tomato is a horticultural crop that has been widely studied and is one of the most widely eaten vegetables in the world. Its molecular biology research is relatively in-depth. Soybeans, like peas, are important leguminous plants with high protein levels. The domain sequences (HMM model file) of the NADPH oxidase (PF08414), NAD binding (PF08030), FAD binding (PF08022), and Ferric reductase domains (PF01794) were downloaded from the Pfam database (http://pfam.xfam.org/) and used as the seed files to search the RBOH proteins in the pea genome file *via* a hidden Markov model (HMM) search (e-value

0.01). The conserved domains were verified using CD-Search (https://www.ncbi.nlm.nih.gov/Structure/cdd/wrpsb.cgi).

Analysis of the chromosomal location, phylogenetics, collinearity, gene structure, conserved motifs, and cis-elements

The online software MG2C (http://mg2c.iask.in/mg2c_v2.0/) was used for the chromosome localization analysis. The phylogenetic tree was constructed using the IQ-Tree Wrapper program in TBtools software (Chen et al., 2020) with 1000 bootstrap replicates. The collinearity between pea and soybean sequences was determined using TBtools software (Chen et al., 2020). The Gene Structure Display Server (http://gsds.gao-lab.org) was used to generate the gene structure map, and the online software MEME (http://meme-suite.org/tools/meme) was used to search for conserved motifs with the maximum conserved motif search value set to 10. The 2000-bp sequences upstream of *PsRBOH* genes were obtained from the pea genome database and used as the promoter, and the cis-regulatory elements of these promoters were identified using PlantCARE (http://bioinformatics.psb.ugent.be/webtools/plantcare/html/).

Plant materials, stress treatments and tissue expression analysis

P. sativum cultivar Zhongwan6 (ZW6) were obtained from the pea seed breeding center in China (Gu'an, Hebei). The seeds were germinated in a liquid culture using a quarter (1/4)-strength modified Hoagland nutrient solution (pH 5.5) in a growth chamber under 25 ± 2°C with a 16 h/8 h light/dark cycle. The four-leaf stage seedlings were treated with 1/4-strength modified Hoagland nutrient solution [$Ca(NO_3)_2{\cdot}4H_2O$ 236.25 mg/L+KNO_3 126.25 mg/L+ NH_4NO_3 20 mg/L+ $KH_2PO_4{\cdot}2H_2O$ 34 mg/L+ $MgSO_4{\cdot}7H_2O$ 123.25 mg/L, pH 5.5] supplemented with 100 mM NaCl for the salt-stress treatment, 10% (w/v) polyethylene glycol (PEG) for the drought stress treatment, and 6 μM $CdCl_2$ for the cadmium (Cd) treatment. For the heat and cold stress, the seedlings were treated with 1/4-strength modified Hoagland nutrient solution (pH 5.5) at 38°C and 4°C, respectively. For the low-boron stress treatment, seedlings were initially pretreated with the modified Hoagland nutrient solution containing 0.025 μM boric acid (H_3BO_3) (B treatment) at the first stage of culture to diminish variations in B concentrations in seeds. Subsequently, the low-boron-treated plants were treated with the modified Hoagland nutrient solution containing 0.025 μM H_3BO_3, and the controls were treated with the modified Hoagland nutrient solution with 25 μM H_3BO_3 at the four-leaf-stage seedlings (Li et al., 2018). The treatments were conducted in triplicates with five seedlings per replicate. The leaves of treated seedlings were sampled after 0.5, 3, 6, 12, 24, 36, 48, and 72 h of stress treatment. Pea roots, leaves, stems, flowers, tendrils, one-week-old pea seeds, one-week-old pod, and two-week-old pea seeds were sampled for tissue expression analysis. All the harvested samples were frozen in liquid nitrogen and stored at −80°C until analysis. Each treatment had three independent biological replicates.

RNA isolation and RT-qPCR analysis

Total RNA was isolated from the samples using FreeZol Reagent R711 (Nanjing Vazyme Biotech Co., Ltd.), according to the manufacturer's instructions. Briefly, 50 mg of the ground sample was added into 500 μl of FreeZol Reagent for lysis. The lysate was centrifuged, and the supernatant was collected. A dilution buffer was added to the supernatant, and the mixture was precipitated with isopropanol. After centrifugation, the supernatant was discarded, and the pellet was washed with 75% ethanol and dissolved in RNase-free double distilled water (ddH_2O). The quality and concentrations of the isolated RNA samples were determined *via* 1% agarose gel electrophoresis and a NanoDrop 2000 Spectrophotometer (Thermo Fisher Scientific, Wilmington, DE, USA). Reverse transcription PCR was conducted on a QuantStudio™ 6Flex Real-Time PCR System (Applied Biosystems™, Carlsbad, CA, USA) using HiScript® III RT SuperMix for qPCR with (+gDNA wiper) (R323-01) (Vazyme, Nanjin) and ChamQTM Universal SYBR® qPCR Master Mix (Q711) (Vazyme). Three technical replicates were set for each biological sample, and the reaction conditions were as follows: 95°C for 30 s, followed by 40 cycles at 95°C for 10 s and 65°C for 20 s. A melting curve was generated by cooling from 95°C to 65°C then ramping to 95°C, followed by the final cooling to 50°C for 30 s. *PsACT* (Knopkiewicz and Wojtaszek, 2019) was used as the internal control. The expression level of each *PsRBOH* gene was calculated using the delta-delta Ct ($2^{-\Delta\Delta CT}$) method (Livak and Schmittgen, 2001). All analyses were conducted in three biological replicates and three technical replicates. All primer sequences used in this study were designed by Primer Premier 6.0 and are listed in Supplementary Table S1.

Subcellular localization analysis

The coding sequence (CDS) of RBOH6 was amplified from the ZW6 and fused to the N terminus of the green fluorescent protein (GFP) in the pAN580 (GFP) vector. To determine the subcellular localization of RBOH6, the RBHO6-GFP vector was transiently co-expressed with endoplasmic reticulum (ER) marker mCherry-HDEL into *Arabidopsis* protoplasts (Ishikawa et al., 2018). And, the FM4-64 dye was used to marked plasma membrane. The fluorescent signals were observed using a confocal microscope (Leica SP8, Germany). Fluorescence signals were detected using the following excitation and emission wavelengths: GFP (488 nm/507 nm), FM4-64 (515 nm/640 nm) and mCherry (587 nm/610 nm).

Results

Chromosomal localization analysis of the *RBOH* gene family in pea

Seven putative *PsRBOH* genes were retrieved from the pea genome after removing the redundant and repeat sequences. We named these *PsRBOH1–7* (Figure 1 and Supplementary Table S2) based on their localization in the *P. sativum* genome. The distribution of these *RBOH* genes did not show a certain regularity. There was one *RBOH* gene on chromosomes chr1LG5 (*RBOH1*), chr5LG3 (*RBOH4*), and chr6LG2 (*RBOH5*) each, while two were on chromosomes chr3LG5 (*RBOH2* and *3*) and chr7LG2 (*RBOH6* and *7*) each.

Phylogenetic analysis of the *PsRBOHs*

To investigate the evolutionary relationships of *RBOHs* among pea, soybean, tomato, and *Arabidopsis*, we constructed a neighbor-joining phylogenetic tree using the alignments of seven pea RBOH proteins, 17 soybean RBOH proteins, eight tomato RBOH proteins, and ten *Arabidopsis* RBOH proteins (Figure 2A). The results showed that 42 RBOHs from pea, soybean, tomato, and *Arabidopsis* were divided into five groups (I, II, III, IV, and V). Groups I, II, III, IV, and V contained 8, 6, 2, 6, and 20 RBOH proteins, respectively, and 1, 1, 0, 1 and 4 PsRBOHs were clustered in groups I, II, III, IV, and V, respectively.

Collinearity analyses of the *PsRBOHs*

To explore the evolution of RBOH genes, we analyzed the synteny relationship of RBOHs between pea and soybean (Figure 2B). Four ortholog pairs were identified between pea and soybean. *PsRBOH2* paired with *GmRBOHB1*, *GmRBOHB2*, *GmRBOHI1*, and *GmRBOHI2*, while *PsRBOH4* paired with *GmRBOHC1*, *GmRBOHC2*, *GmRBOHE1*, and *GmRBOHE2*. *PsRBOH6* paired with *GmRBOHA1*, *GmRBOHA2*, *GmRBOHF1*, and *GmRBOHF2*, and *PsRBOH7* paired with *GmRBOHC1*, *GmRBOHC2*, *GmRBOHE1*, and *GmRBOHE2*.

Gene structure, conserved motif and conserved domain analysis of the *PsRBOHs*

A gene structure map of *PsRBOHs* was constructed based on the pea genome sequence (Figure 3A). The *PsRBOHs* had varying structures with different numbers of untranslated regions (UTRs) and exons. All *PsRBOHs* but *PsRBOH1* and *PsRBOH4* had no UTRs, and the number of exons ranged from six (*PsRBOH1*) to 14 (*PsRBOH6*). Ten conserved motifs were identified *via* the MEME online tool and were used to gain a deeper understanding of various motif compositions of the PsRBOHs. As shown in Figure 3B and Supplementary Figure S1, PsRBOH proteins contained 10 motifs, except PsRBOH1 and PsRBOH4, which had 4 and 9 motifs, respectively. Moreover, all PsRBOH proteins, except PsRBOH1, had four typical conserved domains, including the NADPH-Ox, Ferri-reduction, FAD-binding, and NAD-binding domains (Figure 3C). PsRBOH1 lacked the FAD-binding and NAD-binding domains, and all RBOH proteins contained the EF-hand domain.

Cis-element analysis of the putative *PsRBOH* promoters

To further explore the function of *PsRBOH* genes in peas, we predicted the cis-elements of the promoters of these using the PlantCARE database (Figure 3D). The results showed that the light-responsive elements (LREs) were the most abundant (84) among the seven *PsRBOH* promoter sequences and widely distributed in all promoter sequences, followed by ethylene-responsive elements (EREs) (20), which was also distributed in all promoter sequences

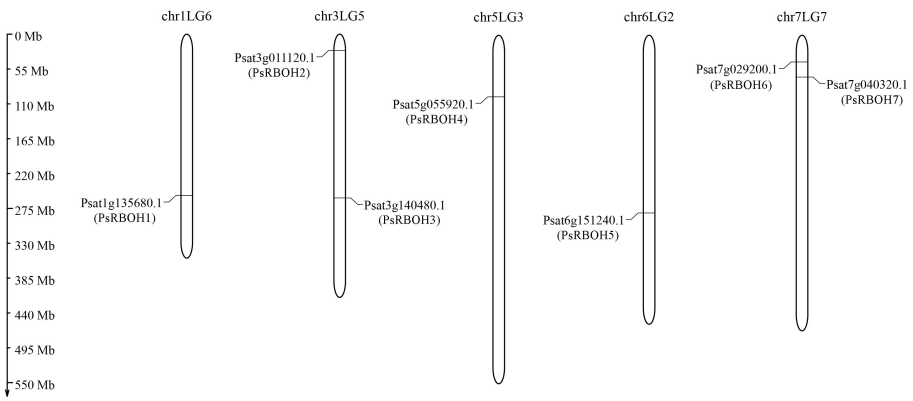

FIGURE 1
Genomic distribution of the *RBOH* genes in pea chromosomes.

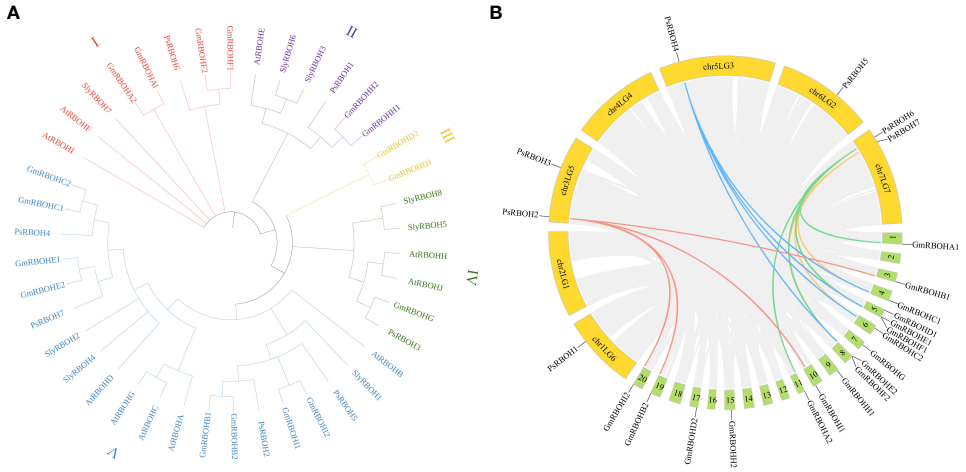

FIGURE 2
Phylogenetic and collinearity analyses of the *PsRBOHs*. **(A)** Phylogenetic analysis of *RBOHs* of pea, soybean, tomato, and *Arabidopsis*. **(B)** Collinearity analysis of *RBOHs* between pea and soybean. The colored lines represent *RBOHs* collinearity between species, and the gray lines are collinearity of all gene members between species. Yellow and green boxes represent pea and soybean chromosomes, respectively.

(Figure 3D). We also found that the promoter sequences of *PsRBOH* genes contained three hormone-responsive elements, [abscisic acid-responsive element (ARE, 17), MeJA-responsive element (MeJARE, 16) and salicylic acid-responsive elements (SARE, 5)] and two abiotic response elements [drought-inducible elements (DRE, 4) and low temperature-responsive element (LTR, 4)].

Tissue-specific expression of *PsRBOHs* in pea

To determine the expression patterns of the *PsRBOH* genes in different tissues, we studied the tissue-specific transcriptional activity of seven genes in the root, stem, tendril, leaf, flower, pod,

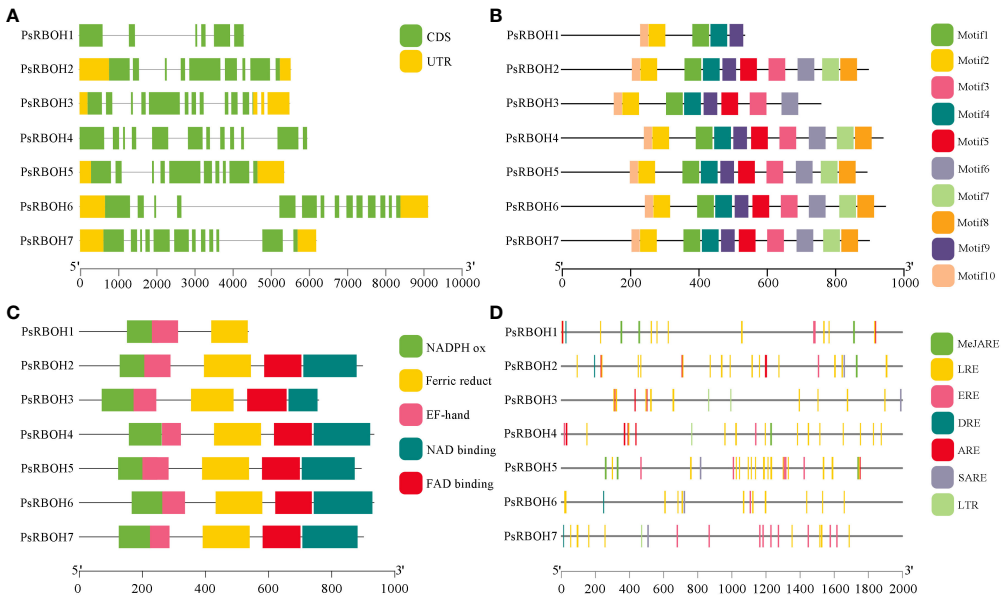

FIGURE 3
The gene structures, conserved motifs, conserved domain, and cis-elements analysis of putative promoters of PsRBOHs. **(A)** Gene structure of *PsRBOHs*. The green block represents the coding sequence (CDS), the yellow block shows the 5′ or 3′ untranslated regions (UTRs), and the black line indicates the intron. The scale bar indicates the length of the DNA sequences. **(B)** The conserved motifs in PsRBOHs were identified by MEME tools. Each motif is indicated by a rectangular box of a different color and the motifs are numbered from 1 to 10. The black line scale represents the length of amino acids. **(C)** Conserved domain compositions of PsRBOHs. Only major domains are presented in the figure based on our searches in the Pfam database. The black line scale represents the length of amino acids. **(D)** Cis-elements analysis of putative promoters of *PsRBOHs*. The black line scale represents the length of promoter amino acids. The cis-elements are as follows: MeJA-responsive elements (MeJARE), light-responsive elements (LREs), ethylene-responsive elements (EREs), drought-inducible elements (DRE), abscisic acid-responsive element (ARE), salicylic acid-responsive elements (SARE), and low temperature-responsive element (LTR).

one-week-old pea seeds (Pea1W), and two-weeks-old pea seeds (Pea2W) of pea (Figure 4). The results showed that the expressions of the *PsRBOH* genes had significant differences in different tissues. *PsRBOH5* was highly expressed in the roots, while *PsRBOH4*, *PsRBOH6*, and *PsRBOH7* were highly expressed in the stem. *PsRBOH2* was highly expressed in all tissues. *PsRBOH6* was highly expressed in the leaves, but *PsRBOH3* was not detected in the leaves. Moreover, *PsRBOH1* and *PsRBOH3* were highly expressed in tendrils, and all seven *PsRBOH* genes had relatively lower expression levels in the pod and Pea1W. *PsRBOH5* and *PsRBOH7* were highly expressed in the roots and Pea2W, respectively, but *PsRBOH1* was not expressed in flowers and pods.

Expression of *PsRBOHs* under different abiotic stresses

To further elucidate the expression patterns of pea *RBOH* genes under different abiotic stresses, we evaluated the expression profiles of *PsRBOHs* in the leaves and roots under heat stress, cold stress, salt stress, Cd stress, PEG-induced drought stress (PEG), and low-boron (LB) stress at various time points after the treatment.

The abiotic stresses induced or inhibited the expression of genes in a highly specific manner, with the most significant changes occurring at the early stages of stress treatment (Figure 5). The expression levels of all genes increased in the leaves in all six treatments (Figures 5A–F), except for *PsRBOH4* under salt stress (Figure 5C) and *PsRBOH5* under Cd stress (Figure 5D). All *PsRBOH* genes were up-regulated at 6 h under all treatments (Figures 5A–F) except for *PsRBOH4* under cold stress (Figure 5B), *PsRBOH5* under Cd stress (Figure 5D) and *PsRBOH4-6* under salt stress (Figure 5C). *PsRBOH1* was up-regulated at 3 h under all six treatments but down-regulated at 24 h under heat (Figure 5A), cold (Figure 5B) and Cd stresses (Figure 5D). *PsRBOH3* was not expressed in the leaves under all treatments (Figures 5A–F). Furthermore, *PsRBOH4* was down-regulated from 0.5 to 48 h but up-regulated at 72 h under salt stress (Figure 5C). *PsRBOH5* was induced at 0.5 h under heat stress (Figure 5A) but down-regulated at 12 h under heat (Figure 5B), salt (Figure 5C), Cd (Figure 5D), and PEG (Figure 5E) stresses. In addition, *PsRBOH6* was induced at 6 h under LB stress (Figure 5F) and down-regulated at all time points except 3 h and 6 h under salt stress (Figure 5C).

The expression patterns of *PsRBOHs* had similarities and differences in the roots and leaves. In the roots, *PsRBOH5* was induced at 0.5 h under heat (Figure 6A), salt (Figure 6C), PEG (Figure 6E), and LB (Figure 6F) stresses and maintained the high expression until 72 h under salt (Figure 6C), PEG (Figure 6E) and LB (Figure 6F) stresses. *PsRBOH1* was up-regulated at 3 h and maintained a high expression level until 72 h under cold (Figure 6B) and salt stresses (Figure 6C) except at 12 h under cold stress.

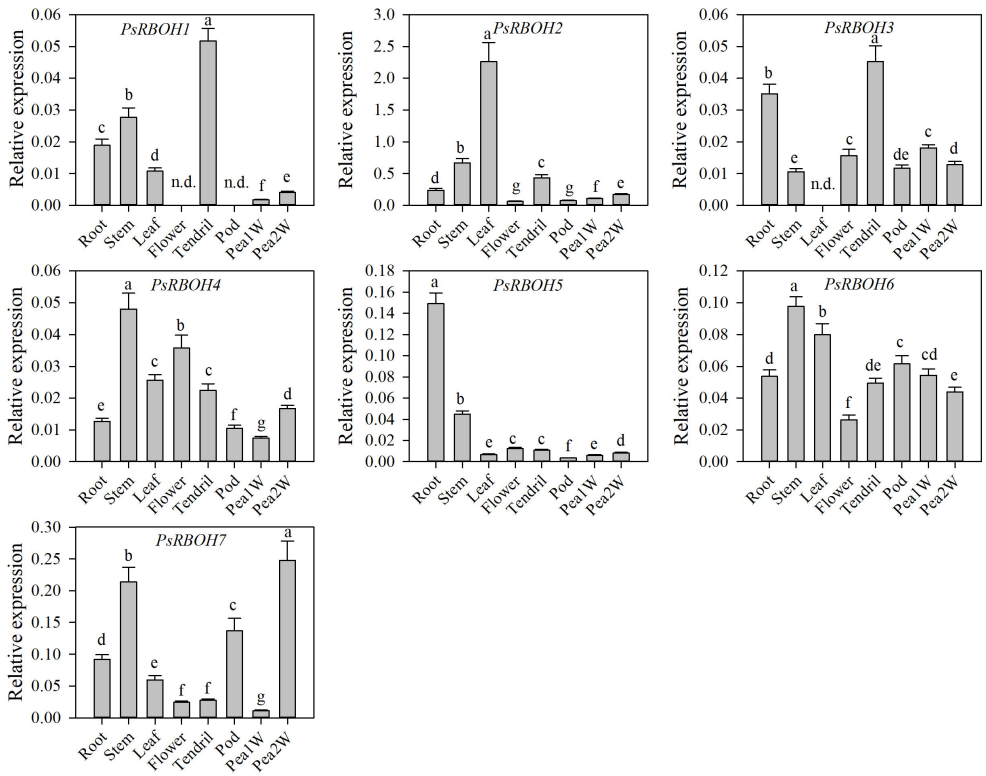

FIGURE 4
Expression patterns of *PsRBOH* genes in different tissues. Pea1W: One-week-old pea seeds; Pea2W: Two-week-old pea seeds. Error bars represent standard deviations for three biological replicates. Different letters indicating significant differences among tissues ($p<0.05$, Duncan's test). n.d.: Not detected.

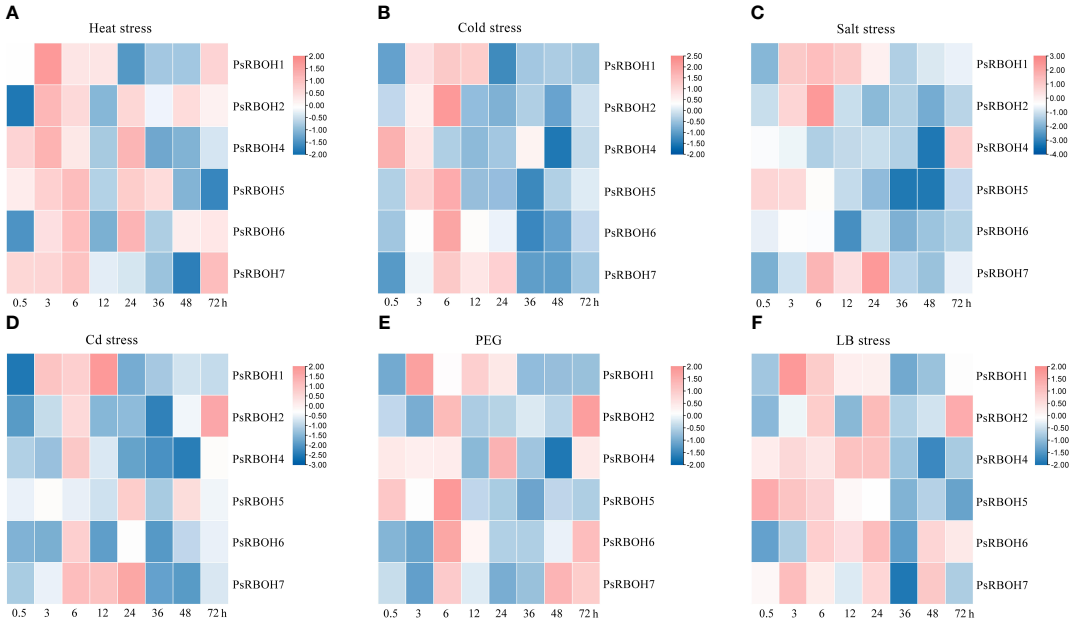

FIGURE 5
Leaf expression of *PsRBOHs* under heat stress **(A)**, cold stress **(B)**, salt stress **(C)**, cadmium (Cd) stress **(D)**, polyethylene glycol (PEG)-induced drought stress (PEG) **(E)**, and low boron (LB) stress **(F)**. The log-transformed relative expression levels were used to generate the heatmaps. The color scale is shown on the right.

However, *PsRBOH1* was down-regulated at all time points under LB treatment (Figure 6F). *PsRBOH6* was induced at 0.5 h under salt (Figure 6C) and Cd (Figure 6D) treatments but down-regulated from 6 to 72 h under Cd (Figure 6D) and LB (Figure 6F) treatments. Additionally, *PsRBOH6* had a similar expression pattern with *PsRBOH1* under LB stress, except at the 3 h time-point (Figure 6F).

Subcellular localization analysis

The subcellular localization of pea RBOH proteins was predicted using WoLFPSORT (Table 1). The results indicated that four PsRBOH proteins were highly likely to be located in the plasma membrane. PsRBOH4 and PsRBOH5 were presumably

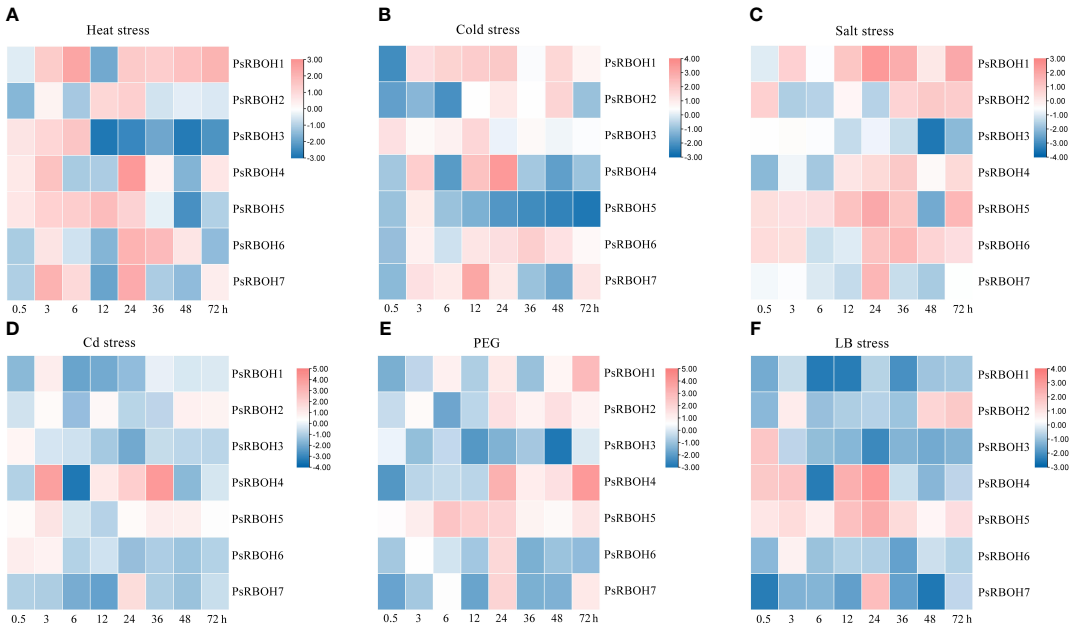

FIGURE 6
Root expression of *PsRBOHs* under heat stress **(A)**, cold stress **(B)**, salt stress **(C)**, cadmium (Cd) stress **(D)**, polyethylene glycol (PEG)-induced drought stress (PEG) **(E)**, and low boron (LB) stress **(F)**. The log-transformed relative expression levels were used to generate the heatmaps. The color scale is shown on the right.

located in the nucleus, and PsRBOH4 in the cytosol. Evolutionary analysis showed that PsRBOH6 was homologous to AtRBOHF and GmRBOHF1/2. It has been shown that multiple calcineurin B-like (CBL) interacting protein kinases (CIPKs) target *Arabidopsis* RBOHF by directly binding Ca^{2+} to its EF-hands to fine-tune superoxide production in response to different stimuli (Drerup et al., 2013; Han et al., 2019). Since AtRBOHF localizes in the plasma membrane (Drerup et al., 2013), PsRBOH6 was selected for a transient expression assay using *Arabidopsis* mesophyll protoplasts (Figure 7). The PsRBOH6-GFP plasmid was transiently co-expressed with the plasma membrane and endoplasmic reticulum markers, FM4-64 (Figure 7A) and mCherry-HDEL (Figure 7B), in *Arabidopsis* leaf protoplasts, respectively. As shown in Figure 7, GFP-PsRBOH6 fluorescent signals were extensively co-localized with FM4-64 and mCherry-HDEL, suggesting that PsRBOH6 localizes in the plasma membrane and endoplasmic reticulum.

Discussion

RBOH genes are involved in plant signal transmission, morphogenesis and development, and responses to biotic and abiotic stresses. However, the *RBOH* gene family has been identified in various plants but not in pea. These studies will be useful for understanding the role of *RBOH* genes in plant responses to abiotic stresses.

The present study analyzed the *RBOH* gene family in pea and identified seven *RBOH* genes were identified in the pea genome. The identified *RBOH* genes were fewer than those of *Arabidopsis* (10) (Sagi and Fluhr, 2006), rice (9) (Groom et al., 1996), *Pyropia yezoensis* (11) (Gui et al., 2022), *Solanum melongena* (8) (Du et al., 2023), and soybean (17) (Liu et al., 2019), but same those of strawberry (7) (Zhang et al., 2018) and alfalfa (7) (Marino et al., 2011). The chromosomal distribution of *RBOH* genes did not show a certain regularity, the same as in other plants (Selvi et al., 2020; Gui et al., 2022; Du et al., 2023). Gene structure analysis revealed that the number of *PsRBOH* exons varied between 6-16 and harbored in 9-12, similar to that of *Arabidopsis* and rice, which were harbored in 10-14 (Zhang et al., 2018). *PsRBOH1* had the lowest number of exons (6), while *PsRBOH6* had the most exons (16), indicating that *PsRBOHs* experienced both conservation and diversification during their evolution.

Determining the phylogenetic relationships among species is fundamental for many biological studies (Kapli et al., 2020). Phylogenetic analysis indicated that members of the *RBOH* gene families in pea, soybean, tomato, and *Arabidopsis* could be divided into five groups, indicating that RBOHs are conserved in various species (Chang et al., 2020; Chen and Yang, 2020; Gui et al., 2022; Du et al., 2023).

In soybeans, the ancestral *Papilionoideae* whole-genome duplication event and *Glycine*-specific duplication event resulted in nearly 75% of the genes present in multiple copies (Schmutz et al., 2010). While there has no a recent whole-genome duplication but reflects the ancestral *Papilionoideae* whole-genome duplication event in pea (Kreplak et al., 2019). This also explains why the amount of *RBOHs* in pea is less than that in soybean and the collinear gene pairs of four *PsRBOHs* (*PsRBOH2*, *PsRBOH4*, *PsRBOH6*, and *PsRBOH7*) in soybean.

In *Arabidopsis*, all ten RBOHs had four typical conserved domains: NADPH-Ox, Ferri-reduction, FAD-binding, and NAD-binding domains (Sagi and Fluhr, 2006). However, in wheat, 4 out of 36 NADPH oxidases had the NADPH_Ox domain but lacked one or two other conserved domains (Hu et al., 2018). In eggplant, 5 out of 8 *SmRBOHs* lacked the FAD-binding domain, which was substituted by the NOX_Duox_like_FAD_NADP domain (Du et al., 2023). In this study, all PsRBOHs, except PsRBOH1, had the four typical conserved domains. PsRBOH1 lacked the FAD-binding and NAD-binding domains which are crucial for electron transfer and ROS production (Wang et al., 2022). Therefore, the possible function of RBOH1 in the production of superoxide needs further verification.

The tissue-specific expression of genes is crucial for plant growth and development and provides important insights into understanding gene function. The tissue-specific expression patterns of the *RBOHs* have been reported in many plants; however, the expression patterns are distinct in different plants. Two out of ten, four out of seven, and all seven *RBOH* genes were expressed throughout *Arabidopsis* (Sagi and Fluhr, 2006), strawberry (Zhang et al., 2018) and grape (Cheng et al., 2013), respectively. However, only four out of ten *AtRBOH* genes were specifically expressed in the roots and elongation zone (Sagi and

TABLE 1 The detailed information of PsRBOH members.

Gene	Annotated	Genomic position	CDS	AA	Subcellular localization
PsRBOH1	Psat1g135680.1	chr1LG6:268211884- 268216192	1608	535	plas: 5, E.R.: 5, mito: 2, chlo: 1
PsRBOH2	Psat3g011120.1	chr3LG5:26369259-26374797	2694	897	cyto: 5, nucl: 3, plas: 3, chlo: 1, vacu: 1
PsRBOH3	Psat3g140480.1	chr3LG5:273226086-273231589	2277	758	plas: 8, E.R.: 2, chlo: 1, nucl: 1, mito: 1
PsRBOH4	Psat5g055920.1	chr5LG3:101924110-101930071	2823	940	nucl: 5, plas: 3, cyto: 2, chlo: 1, vacu: 1, E.R.: 1
PsRBOH5	Psat6g151240.1	chr6LG2:294961062-294966418	2682	893	nucl: 7, cyto: 3, plas: 2, chlo: 1
PsRBOH6	Psat7g029200.1	chr7LG7:45297780-45306906	2844	947	plas: 11, nucl: 3
PsRBOH7	Psat7g040320.1	chr7LG7:69319366-69325556	2703	900	plas: 9, cyto: 4

Chr, chromosome; CDS, length of coding sequence; AA, number of amino acids; The subcellular location of pea RBOH proteins was predicted using WoLF PSORT (http://www.genscript.com/psort/wolf_psort.html). Nucl, nucleus; Mito, mitochondria; Chlo, chloroplast; Cyto, cytosol; E.R, endoplasmic reticulum; Plas, plasma membrane.

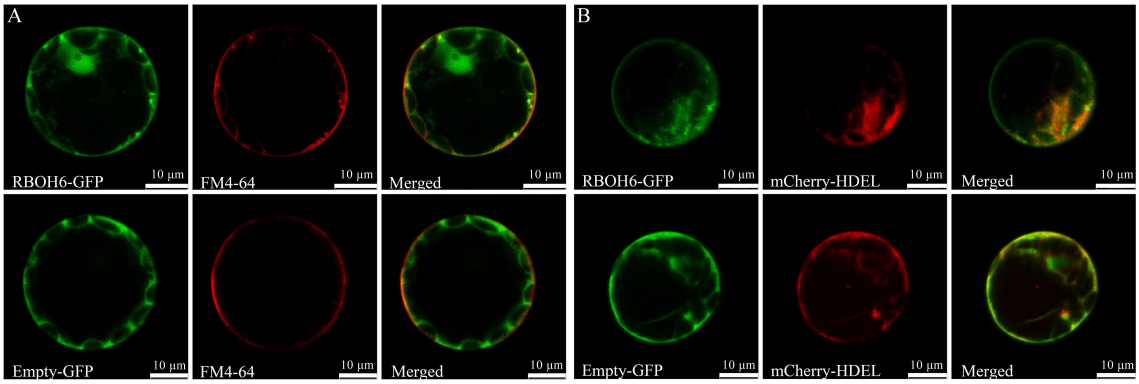

FIGURE 7
Subcellular localization of PsRBOH6 protein. **(A)** The plasma membrane was stained by FM4-64. **(B)** Transient co-expression of PsRBOH6-GFP with endoplasmic reticulum marker mCherry-HDEL. Empty vector was as control. Scale bar = 10 μm. Single optical sections obtained by CLSM.

Fluhr, 2006). In this study, five *RBOHs* (*PsRBOH2* and *PsRBOH4-7*) were expressed in all tissues, while *PsRBOH1* was not detected in the flowers and pods, and *PsRBOH3* was not expressed in the leaves. In addition, the expression of *PsRBOH2* was higher in all tissues, especially in the leaves. In soybeans, *GmRBOHB1*, which was orthologous with *PsRBOH2* and clustered in one cluster, was highly expressed in the leaves (Liu et al., 2019). These results indicated the tissue specificity of the *PsRBOH* genes, suggesting that these genes may have different functions during plant development.

Cis-acting elements regulate the expression of target genes by binding the trans-acting factors (Yamaguchi-Shinozaki and Shinozaki, 2005). It has been reported that *RBOH* family members in various plants are induced by different abiotic stress stimuli, such as drought (Duan et al., 2009), salt (Xie et al., 2011), heat (Li et al., 2014; Xia et al., 2014), wounding (Sagi et al., 2004), and cold stress (Zhang et al., 2018). Moreover, *RBOHs* respond to environmental stimuli through hormonal signaling networks involving abscisic, salicylic, jasmonic acid, and ethylene (Overmyer et al., 2003). In the present study, many hormone-responsive elements (such as ARE, ERE, MeJARE, and SARE) and abiotic response elements (such as DRE and LTR) were found in the promoter of *PsRBOHs*, indicating their potential roles in pea response to phytohormones and stresses.

The involvement of the *RBOH* gene family members in abiotic stress responses has been reported in many plants. In grapes, *VvRBOHs* were significantly increased under salt, drought, powdery mildew, salicylic acid, and abscisic acid treatments (Cheng et al., 2013). It was reported that the expression level of *AtRBOHD* was significantly increased in *Arabidopsis* at an early stage in response to hypoxia (Sagi and Fluhr, 2006). Soybean *RBOH* genes were significantly induced by salt, PEG, cold, and Cu stresses, and *GmRBOHD2* was significantly induced by salt, polyethylene glycol, low temperature, and Cu toxicity in the roots (Liu et al., 2019). In the present study, all *PsRBOH* genes responded to all six stresses. Moreover, *PsRBOH3*, which had a close evolutionary relationship with *GmRBOHD2*, was expressed in the roots and not in leaves, and its expression occurred earlier (0.5 - 6 h) after heat, cold, and LB stress treatments. The expression of *PsRBOH1* was up-regulated in the leaves 3 h after the abiotic stress treatments and lasted for up to 24 h, after which it was down-regulated under heat, cold, salt and Cd treatments. However, *PsRBOH1* was up-regulated in the roots by heat, cold and NaCl treatments but down-regulated by LB treatment. A similar phenomenon was also observed in cotton (Wang et al., 2020). These results indicate that the *PsRBOH* gene family could be involved in the abiotic stress response, but the regulatory mechanisms are still unclear.

Superoxide can be synthesized in different cellular compartments, such as chloroplasts (Foyer and Hanke, 2022), mitochondria (Postiglione and Muday, 2022), peroxisome (Sandalio et al., 2021), and the plasma membrane oxidoreductase system (Lherminier et al., 2009; Jiménez-Quesada et al., 2022; Miller and Mittler, 2023). In leaves from pea plants grown with 50 μm $CdCl_2$, the accumulation of H_2O_2 was observed mainly in the plasma membrane of transfer, mesophyll and epidermal cells, as well as in the tonoplast of bundle sheath cells (Romero-Puertas et al., 2004). RBOH is present in the plasma membrane systems of almost all animals and plants (Chen and Yang, 2020). Subcellular location is a key characteristic that determines the function of many proteins, indicating that proteins in different subcellular locations have different functions (Koroleva et al., 2005). All the RBOHs in *Arabidopsis* (Sagi and Fluhr, 2006), rice (Groom et al., 1996) and wheat (Hu et al., 2018) were predicted to localize to the plasma membrane. Some RBOHs were shown to localize to the chloroplast thylakoid membrane of grapes (Cheng et al., 2013) and strawberry (Zhang et al., 2018). Moreover, in *Gossypium* barbadense, 71 out of 87 RBOHs were located in the cytoplasm (Chang et al., 2020). Tobacco RBOHD was localized in the plasma membrane and Golgi cisternae (Noirot et al., 2014). In *P. vulgaris*, PvRBOHA was localized in the plasma membrane of root hair (Arthikala et al., 2017), whereas PvRBOHB was localized in the central apical dome (Montiel et al., 2012). These different subcellular distributions of RBOHs in root hairs resulted in two models that explain root hair development (Arthikala et al., 2017). In pea, four out of the seven

RBOHs had a high probability of being localized in the plasma membrane, indicating similar functions. Two of the PsRBOHs were presumably located in the nucleus, while PsRBOH6 was localized in the cell membrane and endoplasmic reticulum, suggesting that they may regulate ROS production at different subcellular locations (Lee et al., 2023).

Conclusions

This study comprehensively analyzed the *RBOH* gene family in the pea genome. Seven *PsRBOH* genes were identified and were divided into five groups, which were distributed on five chromosomes. In addition, we analyzed collinearity, gene structure, conserved domains, conserved motifs, cis-elements, and subcellular distribution of the *PsRBOH* genes. The *PsRBOHs* exhibited tissue specificity and functional diversity during plant growth and response to different abiotic stresses. Overall, these results provide valuable information which could be used for further functional analysis of pea *RBOH* genes in response to climate-driven environmental constraints.

Data availability statement

The original contributions presented in the study are included in the article/Supplementary Material. Further inquiries can be directed to the corresponding authors.

Author contributions

ML: Formal Analysis, Visualization, Writing – original draft, Writing – review & editing, Conceptualization, Funding acquisition, Supervision. YZ: Formal Analysis, Visualization, Writing – original draft, Validation. TP: Formal Analysis, Writing – review & editing. YL: Investigation, Writing – review & editing. YH: Investigation, Writing – review & editing. WC: Investigation, Writing – review & editing. YY: Investigation, Writing – review & editing. GZ: Writing – review & editing, Formal Analysis, Visualization, Writing – original draft. SS: Writing – review & editing. MY: Writing – review & editing.

Funding

The author(s) declare financial support was received for the research, authorship, and/or publication of this article. This work was supported by the National Natural Science Foundation of China (31902017, 32172672), Guangdong Basic and Applied Basic Research Foundation (2021A1515011020, 2019A1515110070), the Higher Education Department of Guangdong Province (Grant No. 2020KCXTD025), Special fund for scientific innovation strategy-construction of high-level Academy of Agriculture Science (R2022PY-QY002).

Conflict of interest

The authors declare that the research was conducted in the absence of any commercial or financial relationships that could be construed as a potential conflict of interest.

Publisher's note

Supplementary material

The Supplementary Material for this article can be found online at: https://www.frontiersin.org/articles/10.3389/fpls.2023.1321952/full#supplementary-material

SUPPLEMENTARY FIGURE 1
Amino acid sequence of predicted motif.

References

Arthikala, M.-K., Montiel, J., Sánchez-López, R., Nava, N., Cárdenas, L., and Quinto, C. (2017). Respiratory burst oxidase homolog gene A is crucial for rhizobium infection and nodule maturation and function in common bean. *Front. Plant Sci.* 8, 2003. doi: 10.3389/fpls.2017.02003

Asai, S., Ohta, K., and Yoshioka, H. (2008). MAPK signaling regulates nitric oxide and NADPH oxidase-dependent oxidative bursts in *Nicotiana benthamiana*. *Plant Cell* 20 (5), 1390–1406. doi: 10.1105/tpc.107.055855

Bostock, R. M., Pye, M. F., and Roubtsova, T. V. (2014). Predisposition in plant disease: exploiting the nexus in abiotic and biotic stress perception and response. *Annu. Rev. Phytopathol.* 52 (1), 517–549. doi: 10.1146/annurev-phyto-081211-172902

Chang, Y., Li, B., Shi, Q., Geng, R., Geng, S., Liu, J., et al. (2020). Comprehensive analysis of respiratory burst oxidase homologs (Rboh) gene family and function of gbRboh5/18 on verticillium wilt resistance in gossypium barbadense. *Front. Genet.* 11, 788. doi: 10.3389/fgene.2020.00788

Chen, C., Chen, H., Zhang, Y., Thomas, H. R., Frank, M. H., He, Y., et al. (2020). TBtools: An integrative toolkit developed for interactive analyses of big biological data. *Mol. Plant* 13 (8), 1194–1202. doi: 10.1016/j.molp.2020.06.009

Chen, X., Humphreys, J. L., Ru, Y., He, Y., Wu, F., Mai, J., et al. (2022). Jasmonate signaling and remodeling of cell wall metabolism induced by boron deficiency in pea shoots. *Environ. Exp. Bot.* 201, 104947. doi: 10.1016/j.envexpbot.2022.104947

Chen, X., Ru, Y., Takahashi, H., Nakazono, M., Shabala, S., Smith, S. M., et al. (2023). Single-cell transcriptomic analysis of pea shoot development and cell-type-specific responses to boron deficiency. *Plant J.* doi: 10.1111/tpj.16487

Chen, Q., and Yang, G. (2020). Signal function studies of ROS, especially RBOH-dependent ROS, in plant growth, development and environmental stress. *J. Plant Growth Regul.* 39 (1), 157–171. doi: 10.1007/s00344-019-09971-4

Cheng, C., Xu, X., Gao, M., Li, J., Guo, C., Song, J., et al. (2013). Genome-wide analysis of *respiratory burst oxidase homologs* in grape (*Vitis vinifera* L.). *Int. J. Mol. Sci.* 14 (12), 24169–24186. doi: 10.3390/ijms141224169

Chung, J.-S., Zhu, J.-K., Bressan, R. A., Hasegawa, P. M., and Shi, H. (2008). Reactive oxygen species mediate Na^+-induced *SOS1* mRNA stability in *Arabidopsis*. *Plant J.* 53 (3), 554–565. doi: 10.1111/j.1365-313X.2007.03364.x

Delledonne, M., Murgia, I., Ederle, D., Sbicego, P. F., Biondani, A., Polverari, A., et al. (2002). Reactive oxygen intermediates modulate nitric oxide signaling in the plant hypersensitive disease-resistance response. *Plant Physiol. Bioch.* 40 (6), 605–610. doi: 10.1016/S0981-9428(02)01397-9

Drerup, M. M., Schlücking, K., Hashimoto, K., Manishankar, P., Steinhorst, L., Kuchitsu, K., et al. (2013). The calcineurin B-like calcium sensors CBL1 and CBL9 together with their interacting protein kinase CIPK26 regulate the arabidopsis NADPH oxidase RBOHF. *Mol. Plant* 6 (2), 559–569. doi: 10.1093/mp/sst009

Du, L., Jiang, Z., Zhou, Y., Shen, L., He, J., Xia, X., et al. (2023). Genome-Wide Identification and Expression Analysis of Respiratory Burst Oxidase Homolog (RBOH) Gene Family in Eggplant (Solanum melongena L.) under Abiotic and Biotic Stress. *Genes* 14 (9), 1665. doi: 10.3390/genes14091665

Duan, Z.-Q., Bai, L., Zhao, Z.-G., Zhang, G.-P., Cheng, F.-M., Jiang, L.-X., et al. (2009). Drought-stimulated activity of plasma membranenicotinamide adenine dinucleotide phosphate oxidase and its catalytic properties in rice. *J. Integr. Plant Biol.* 51 (12), 1104–1115. doi: 10.1111/j.1744-7909.2009.00879.x

Dubiella, U., Seybold, H., Durian, G., Komander, E., Lassig, R., Witte, C.-P., et al. (2013). Calcium-dependent protein kinase/NADPH oxidase activation circuit is required for rapid defense signal propagation. *P. Natl. Acad. Sci.* 110 (21), 8744–8749. doi: 10.1073/pnas.1221294110

Foyer, C. H., and Hanke, G. (2022). ROS production and signalling in chloroplasts: cornerstones and evolving concepts. *Plant J.* 111 (3), 642–661. doi: 10.1111/tpj.15856

Groom, Q. J., Torres, M. A., Fordham-Skelton, A. P., Hammond-Kosack, K. E., Robinson, N. J., and Jones, J. D. G. (1996). *rbohA*, a rice homologue of the mammalian gp91phox respiratory burst oxidase gene. *Plant J.* 10 (3), 515–522. doi: 10.1046/j.1365-313X.1996.10030515.x

Gui, T.-Y., Gao, D.-H., Ding, H.-C., and Yan, X.-H. (2022). Identification of respiratory burst oxidase homolog (Rboh) family genes from pyropia yezoensis and their correlation with archeospore release. *Front. Plant Sci.* 13. doi: 10.3389/fpls.2022.929299

Han, J.-P., Köster, P., Drerup, M. M., Scholz, M., Li, S., Edel, K. H., et al. (2019). Fine-tuning of RBOHF activity is achieved by differential phosphorylation and Ca^{2+} binding. *New Phytol.* 221 (4), 1935–1949. doi: 10.1111/nph.15543

Hu, C.-H., Wei, X.-Y., Yuan, B., Yao, L.-B., Ma, T.-T., Zhang, P.-P., et al. (2018). Genome-wide identification and functional analysis of *NADPH oxidase* family genes in wheat during development and environmental stress responses. *Front. Plant Sci.* 9, 906. doi: 10.3389/fpls.2018.00906

Ishikawa, K., Tamura, K., Ueda, H., Ito, Y., Nakano, A., Hara-Nishimura, I., et al. (2018). Synaptotagmin-associated endoplasmic reticulum-plasma membrane contact sites are localized to immobile ER tubules. *Plant Physiol.* 178 (2), 641–653. doi: 10.1104/pp.18.00498

Jiménez-Quesada, M. J., Castro, A. J., Lima-Cabello, E., and Alché, J. (2022). Cell localization of DPI-dependent production of superoxide in reproductive tissues of the olive tree (Olea europaea L.). *Oxygen* 2 (2), 79–90. doi: 10.3390/oxygen2020007

Jimenez-Quesada, M. J., Traverso, J. A., Potocký, M., Žárský, V., and Alché, J. (2019). Generation of superoxide by oeRbohH, a NADPH oxidase activity during olive (Olea europaea L.) pollen development and germination. *Front. Plant Sci.* 10. doi: 10.3389/fpls.2019.01149

Kapli, P., Yang, Z., and Telford, M. J. (2020). Phylogenetic tree building in the genomic age. *Nat. Rev. Genet.* 21 (7), 428–444. doi: 10.1038/s41576-020-0233-0

Kaya, H., Nakajima, R., Iwano, M., Kanaoka, M. M., Kimura, S., Takeda, S., et al. (2014). Ca^{2+}-activated reactive oxygen species production by *Arabidopsis* RbohH and RbohJ is essential for proper pollen tube tip growth. *Plant Cell* 26 (3), 1069–1080. doi: 10.1105/tpc.113.120642

Knopkiewicz, M., and Wojtaszek, P. (2019). Validation of reference genes for gene expression analysis using quantitative polymerase chain reaction in pea lines (*Pisum sativum*) with different lodging susceptibility. *Anna Appl. Biol.* 174 (1), 86–91. doi: 10.1111/aab.12475

Koroleva, O. A., Tomlinson, M. L., Leader, D., Shaw, P., and Doonan, J. H. (2005). High-throughput protein localization in *Arabidopsis* using Agrobacterium-mediated transient expression of GFP-ORF fusions. *Plant J.* 41 (1), 162–174. doi: 10.1111/j.1365-313X.2004.02281.x

Kreplak, J., Madoui, M.-A., Cápal, P., Novák, P., Labadie, K., Aubert, G., et al. (2019). A reference genome for pea provides insight into legume genome evolution. *Nat. Genet.* 51 (9), 1411–1422. doi: 10.1038/s41588-019-0480-1

Kwak, J. M., Mori, I. C., Pei, Z.-M., Leonhardt, N., Torres, M. A., Dangl, J. L., et al. (2003). NADPH oxidase *AtrbohD* and *AtrbohF* genes function in ROS-dependent ABA signaling in *Arabidopsis*. *EMBO J.* 22 (11), 2623–2633. doi: 10.1093/emboj/cdg277

Lee, J., Han, M., Shin, Y., Lee, J. M., Heo, G., and Lee, Y. (2023). How extracellular reactive oxygen species reach their intracellular targets in plants. *Mol. Cells* 46 (6), 329–336. doi: 10.14348/molcells.2023.2158

Lherminier, J., Elmayan, T., Fromentin, J., Elaraqui, K. T., Vesa, S., Morel, J., et al. (2009). NADPH oxidase-mediated reactive oxygen species production: subcellular localization and reassessment of its role in plant defense. *Mol. Plant* 22 (7), 868–881. doi: 10.1094/MPMI-22-7-0868

Li, X., Li, Y., Mai, J., Tao, L., Qu, M., Liu, J., et al. (2018). Boron alleviates aluminum toxicity by promoting root alkalization in transition zone *via* polar auxin transport. *Plant Physiol.* 177 (3), 1254–1266. doi: 10.1104/pp.18.00188

Li, H., Liu, S.-S., Yi, C.-Y., Wang, F., Zhou, J., Xia, X.-J., et al. (2014). Hydrogen peroxide mediates abscisic acid-induced HSP70 accumulation and heat tolerance in grafted cucumber plants. *Plant Cell Environ.* 37 (12), 2768–2780. doi: 10.1111/pce.12360

Li, X., Ou, M., Li, L., Li, Y., Feng, Y., Huang, X., et al. (2023). The wall-associated kinase gene family in pea (*Pisum sativum*) and its function in response to B deficiency and Al toxicity. *J. Plant Physiol.* 287, 154045. doi: 10.1016/j.jplph.2023.154045

Li, J., Wang, X., Zhang, Y., Jia, H., and Bi, Y. (2011). cGMP regulates hydrogen peroxide accumulation in calcium-dependent salt resistance pathway in *Arabidopsis thaliana* roots. *Planta* 234 (4), 709–722. doi: 10.1007/s00425-011-1439-3

Li, D., Wu, D., Li, S., Dai, Y., and Cao, Y. (2019). Evolutionary and functional analysis of the plant-specific NADPH oxidase gene family in *Brassica rapa* L. *R. Soc Open Sci.* 6 (2), 181727. doi: 10.1098/rsos.181727

Liu, J., Lu, H., Wan, Q., Qi, W., and Shao, H. (2019). Genome-wide analysis and expression profiling of respiratory burst oxidase homologue gene family in *Glycine max*. *Environ. Exp. Bot.* 161, 344–356. doi: 10.1016/j.envexpbot.2018.07.015

Liu, M., Pan, T., Allakhverdiev, S. I., Yu, M., and Shabala, S. (2020). Crop halophytism: an environmentally sustainable solution for global food security. *Trends Plant Sci.* 25 (7), 630–634. doi: 10.1016/j.tplants.2020.04.008

Livak, K. J., and Schmittgen, T. D. (2001). Analysis of relative gene expression data using real-time quantitative PCR and the $2^{-\Delta\Delta CT}$ method. *Methods* 25 (4), 402–408. doi: 10.1006/meth.2001.1262

Marino, D., Andrio, E., Danchin, E. G. J., Oger, E., Gucciardo, S., Lambert, A., et al. (2011). A *Medicago truncatula* NADPH oxidase is involved in symbiotic nodule functioning. *New Phytol.* 189 (2), 580–592. doi: 10.1111/j.1469-8137.2010.03509.x

Miller, G., and Mittler, R. (2023). "Plant NADPH oxidases," in *NADPH Oxidases Revisited: From Function to Structure*. Ed. E. Pick (Cham, Switzerland: Springer International Publishing), 445–465.

Mittler, R., Vanderauwera, S., Suzuki, N., Miller, G., Tognetti, V. B., Vandepoele, K., et al. (2011). ROS signaling: the new wave? *Trends Plant Sci.* 16 (6), 300–309. doi: 10.1016/j.tplants.2011.03.007

Montiel, J., Nava, N., Cárdenas, L., Sánchez-López, R., Arthikala, M.-K., Santana, O., et al. (2012). A phaseolus vulgaris NADPH oxidase gene is required for root infection by rhizobia. *Plant Cell Physiol.* 53 (10), 1751–1767. doi: 10.1093/pcp/pcs120

Nakashima, A., Chen, L., Thao, N. P., Fujiwara, M., Wong, H. L., Kuwano, M., et al. (2008). RACK1 functions in rice innate immunity by interacting with the Rac1 immune complex. *Plant Cell* 20 (8), 2265–2279. doi: 10.1105/tpc.107.054395

Noirot, E., Der, C., Lherminier, J., Robert, F., Moricova, P., Kiêu, K., et al. (2014). Dynamic changes in the subcellular distribution of the tobacco ROS-producing enzyme RBOHD in response to the oomycete elicitor cryptogein. *J. Exp. Bot.* 65 (17), 5011–5022. doi: 10.1093/jxb/eru265

Overmyer, K., Brosché, M., and Kangasjärvi, J. (2003). Reactive oxygen species and hormonal control of cell death. *Trends Plant Sci.* 8 (7), 335–342. doi: 10.1016/S1360-1385(03)00135-3

Palmgren, M. G., Edenbrandt, A. K., Vedel, S. E., Andersen, M. M., Landes, X., Østerberg, J. T., et al. (2015). Are we ready for back-to-nature crop breeding? *Trends Plant Sci.* 20 (3), 155–164. doi: 10.1016/j.tplants.2014.11.003

Patel, R., Rinker, L., Peng, J., and Chilian, W. M. (2018). "Reactive oxygen species: The good and the bad," in *Reactive oxygen species (ROS) in living cells*. Ed. C. Albu (IntechOpen, Rijeka, London), 216.

Postiglione, A. E., and Muday, G. K. (2022). Abscisic acid increases hydrogen peroxide in mitochondria to facilitate stomatal closure. *Plant Physiol.* 192 (1), 469–487. doi: 10.1101/2022.01.11.475946

Rawat, N., Wungrampha, S., Singla-Pareek, S. L., Yu, M., Shabala, S., and Pareek, A. (2022). Rewilding staple crops for the lost halophytism: Toward sustainability and profitability of agricultural production systems. *Mol. Plant* 15 (1), 45–64. doi: 10.1016/j.molp.2021.12.003

Romero-Puertas, M. C., Rodriquez-Serrano, M., Corpas, F. J., Gomez, M., Rio, D., and L.A.andSandalio, L. M. (2004). Cadmium-induced subcellular accumulation of O2·– and H_2O_2 in pea leaves. *Plant Cell Environ.* 27 (9), 1122–1134. doi: 10.1111/j.1365-3040.2004.01217.x

Sagi, M., Davydov, O., Orazova, S., Yesbergenova, Z., Ophir, R., Stratmann, J. W., et al. (2004). Plant respiratory burst oxidase homologs impinge on wound responsiveness and development in *Lycopersicon esculentum*. *Plant Cell* 16 (3), 616–628. doi: 10.1105/tpc.019398

Sagi, M., and Fluhr, R. (2006). Production of reactive oxygen species by plant NADPH oxidases. *Plant Physiol.* 141 (2), 336–340. doi: 10.1104/pp.106.078089

Sandalio, L. M., Peláez-Vico, M. A., Molina-Moya, E., and Romero-Puertas, M. C. (2021). Peroxisomes as redox-signaling nodes in intracellular communication and stress responses. *Plant Physiol.* 186 (1), 22–35. doi: 10.1093/plphys/kiab060

Schmutz, J., Cannon, S. B., Schlueter, J., Ma, J., Mitros, T., Nelson, W., et al. (2010). Genome sequence of the palaeopolyploid soybean. *Nature* 463 (7278), 178–183. doi: 10.1038/nature08670

Selvi, A., Devi, K., Manimekalai, R., and Prathima, P. T. (2020). Comparative analysis of drought-responsive transcriptomes of sugarcane genotypes with differential tolerance to drought. *3 Biotech.* 10 (6), 236. doi: 10.1007/s13205-020-02226-0

Song, C. J., Steinebrunner, I., Wang, X., Stout, S. C., and Roux, S. J. (2006). Extracellular ATP induces the accumulation of superoxide *via* NADPH oxidases in *Arabidopsis*. *Plant Physiol.* 140 (4), 1222–1232. doi: 10.1104/pp.105.073072

Suzuki, N., Miller, G., Morales, J., Shulaev, V., Torres, M. A., and Mittler, R. (2011). Respiratory burst oxidases: the engines of ROS signaling. *Curr. Opin. Plant Biol.* 14 (6), 691–699. doi: 10.1016/j.pbi.2011.07.014

Takeda, S., Gapper, C., Kaya, H., Bell, E., Kuchitsu, K., and Dolan, L. (2008). Local positive feedback regulation determines cell shape in root hair cells. *Science* 319 (5867), 1241–1244. doi: 10.1126/science.1152505

Torres, M. A., Dangl, J. L., and Jones, J. D. G. (2002). *Arabidopsis* gp91phox homologues AtrbohD and AtrbohF are required for accumulation of reactive oxygen intermediates in the plant defense response. *P. Natl. Acad. Sci.* 99 (1), 517–522. doi: 10.1073/pnas.012452499

Torres, M. A., Onouchi, H., Hamada, S., Machida, C., Hammond-Kosack, K. E., and Jones, J. D. G. (1998). Six *Arabidopsis thaliana* homologues of the human respiratory burst oxidase ($gp91^{phox}$). *Plant J.* 14 (3), 365–370. doi: 10.1046/j.1365-313X.1998.00136.x

Wang, W., Chen, D., Liu, D., Cheng, Y., Zhang, X., Song, L., et al. (2020). Comprehensive analysis of the *Gossypium hirsutum* L. *respiratory burst oxidase homolog* (*Ghrboh*) gene family. *BMC Genomics* 21 (1), 91. doi: 10.1186/s12864-020-6503-6

Wang, J., Chitsaz, F., Derbyshire, M. K., Gonzales, N. R., Gwadz, M., Lu, S., et al. (2022). The conserved domain database in 2023. *Nucleic Acids Res.* 51 (D1), D384–D388. doi: 10.1093/nar/gkac1096

Wang, G.-F., Li, W.-Q., Li, W.-Y., Wu, G.-L., Zhou, C.-Y., and Chen, K.-M. (2013). Characterization of rice *NADPH oxidase* genes and their expression under various environmental conditions. *Int. J. Mol. Sci.* 14 (5), 9440–9458. doi: 10.3390/ijms14059440

Xia, X.-J., Gao, C.-J., Song, L.-X., Zhou, Y.-H., Shi, K., and Yu, J.-Q. (2014). Role of H_2O_2 dynamics in brassinosteroid-induced stomatal closure and opening in *Solanum lycopersicum*. *Plant Cell Environ.* 37 (9), 2036–2050. doi: 10.1111/pce.12275

Xie, Y.-J., Xu, S., Han, B., Wu, M.-Z., Yuan, X.-X., Han, Y., et al. (2011). Evidence of *Arabidopsis* salt acclimation induced by up-regulation of HY1 and the regulatory role of RbohD-derived reactive oxygen species synthesis. *Plant J.* 66 (2), 280–292. doi: 10.1111/j.1365-313X.2011.04488.x

Yamaguchi-Shinozaki, K., and Shinozaki, K. (2005). Organization of cis-acting regulatory elements in osmotic- and cold-stress-responsive promoters. *Trends Plant Sci.* 10 (2), 88–94. doi: 10.1016/j.tplants.2004.12.012

Yamauchi, T., Yoshioka, M., Fukazawa, A., Mori, H., Nishizawa, N. K., Tsutsumi, N., et al. (2017). An NADPH oxidase RBOH functions in rice roots during lysigenous aerenchyma formation under oxygen-deficient conditions. *Plant Cell* 29 (4), 775–790. doi: 10.1105/tpc.16.00976

Yang, Y., Yuan, Z., Ning, C., Zhao, B., Wang, R., Zheng, X., et al. (2022). The pea *R2R3-MYB* gene family and its role in anthocyanin biosynthesis in flowers. *Front. Genet.* 13, 936051. doi: 10.3389/fgene.2022.936051

Zhang, Y., Li, Y., He, Y., Hu, W., Zhang, Y., Wang, X., et al. (2018). Identification of *NADPH oxidase* family members associated with cold stress in strawberry. *FEBS Open Bio.* 8 (4), 593–605. doi: 10.1002/2211-5463.12393

Zhang, J., Xie, Y., Ali, B., Ahmed, W., Tang, Y., and Li, H. (2021). Genome-wide identification, classification, evolutionary expansion and expression of Rboh family genes in pepper (Capsicum annuum L.). *Trop. Plant Biol.* 14 (3), 251–266. doi: 10.1007/s12042-021-09286-3

Zhang, H., Zhu, J., Gong, Z., and Zhu, J.-K. (2022). Abiotic stress responses in plants. *Nat. Rev. Genet.* 23 (2), 104–119. doi: 10.1038/s41576-021-00413-0

Zhang, Y., Zhu, H., Zhang, Q., Li, M., Yan, M., Wang, R., et al. (2009). Phospholipase Dα1 and phosphatidic acid regulate NADPH oxidase activity and production of reactive oxygen species in ABA-mediated stomatal closure in *Arabidopsis*. *Plant Cell* 21 (8), 2357–2377. doi: 10.1105/tpc.108.062992

frontiers | Frontiers in Plant Science

TYPE Original Research
PUBLISHED 12 January 2024
DOI 10.3389/fpls.2023.1285198

OPEN ACCESS

EDITED BY
Dongmei Li,
Shandong Agricultural University, China

REVIEWED BY
Neftali Ochoa-Alejo,
Centro de Investigación y de Estudios Avanzados del Instituto Politécnico Nacional, Mexico
Zhoubin Liu,
Hunan Agricultural University, China

*CORRESPONDENCE
Guangdong Geng
genggd213@163.com
Suqin Zhang
zsqin2002@163.com

†These authors have contributed equally to this work

RECEIVED 29 August 2023
ACCEPTED 18 December 2023
PUBLISHED 12 January 2024

CITATION
Tian H, Fan G, Xiong X, Wang H, Zhang S and Geng G (2024) Characterization and transformation of the *CabHLH18* gene from hot pepper to enhance waterlogging tolerance.
Front. Plant Sci. 14:1285198.
doi: 10.3389/fpls.2023.1285198

Characterization and transformation of the *CabHLH18* gene from hot pepper to enhance waterlogging tolerance

Huaizhi Tian[1,2†], Gaoling Fan[3†], Xingwei Xiong[1], Hui Wang[1], Suqin Zhang[1*] and Guangdong Geng[1*]

[1]College of Agriculture, Guizhou University, Guiyang, Guizhou, China, [2]Institute of Pepper, Zunyi Academy of Agricultural Sciences, Zunyi, Guizhou, China, [3]Institute of Pepper, Guizhou Academy of Agricultural Sciences, Guiyang, Guizhou, China

Basic helix–loop–helix (bHLH) proteins are important in abiotic stress control. Here, a specific bHLH transcription factor gene, *CabHLH18*, from a strong waterlogging-tolerant pepper cultivar, 'ZHC2', was successfully cloned. The *CabHLH18* gene presented a coding sequence length of 1,056 bp, encoding 352 amino acids, and the protein was the closest to *Capsicum annuum* XM016694561.2 protein. The CabHLH18 protein was located in the nucleus. The transformation of the *CabHLH18* overexpression vector into the plumules of hot peppers, 'DFZJ' and 'ZHC1', exhibited 21.37% and 22.20% efficiency, respectively. The root length, plant height, and fresh weight of the 'DFZJ' overexpression lines were greater than those of wild-type (WT) plants under waterlogging conditions. Compared with the WT plants, the overexpression lines generally showed greater contents of water, the amino acid, proline, soluble sugar, root viability, and superoxide dismutase activity, but lower malondialdehyde content under waterlogging conditions. Plant fresh weight, amino acids, proline, and soluble sugar levels of the overexpression lines were 39.17%, 45.03%, 60.67%, and 120.18% greater, respectively, compared with the WT plants at 24 h after waterlogging stress. Therefore, the *CabHLH18* gene could be implicated in conferring waterlogging tolerance in hot peppers and holds promise for enhancing their overall waterlogging tolerance.

KEYWORDS

***Capsicum annuum*, CabHLH18, gene cloning, characterization, waterlogging tolerance**

Introduction

Capsicum annuum of the Solanaceae family is a vegetable crop of worldwide importance. In 2020, global production was approximately 39.28 million tons (FAO, 2020). Waterlogging is a major abiotic stress that affect plants (Mickelbart et al., 2015). Waterlogging obviously decreases crop production by 32.9% on average (Tian et al., 2021). The annual economic loss

is more than billions of dollars (Sauter, 2013; Voesenek and Bailey-Serres, 2015). Waterlogging stress causes physiological and biochemical changes in plants, leading to inhibition of growth and development (Perata and Voesenek, 2007; Bailey-Serres and Voesenek, 2008; Vidoz et al., 2010; Phukan et al., 2016). Under waterlogging stress, the inhibition of plant aerobic respiration limits energy metabolism, thus restraining plant growth and development, including seed germination, vegetative growth, and reproductive growth (Pan et al., 2021). Plants also respond to waterlogging stress by regulating their morphology, energy metabolism, hormone biosynthesis, and signal transduction (Shinozaki and Yamaguchi-Shinozaki, 2007; Hirabayashi et al., 2013; Kuroh et al., 2018). Pepper is a shallow root plant with weak roots and poor waterlogging resistance and can die after a few hours under water, seriously affecting the yield and quality (Molla et al., 2022). Consequently, increasing research to improve the waterlogging resistance of peppers has been conducted. At present, research on waterlogging stress has been focused on wheat, rice, and corn. Most of the studies related to waterlogging stress in peppers have concentrated on morphological observations, physiological examinations, and biochemical analyses, devoting limited attention to waterlogging tolerance mechanisms (Kato et al., 2020; Kaur et al., 2021; Komatsu et al., 2022). Basic helix–loop–helix (bHLH) proteins play important roles in regulating plant resistance to stress, which belong to a superfamily of regulatory proteins present in eukaryotes, having highly conserved bHLH domains (Toledo-Ortiz et al., 2003; Upadhyay et al., 2018). The HLH domain is located at the carboxyl-terminus and consists of two hydrophobic residues in a helical–ring–helical structure, which promotes protein–protein interactions (Murre et al., 1989). bHLH proteins regulate plant growth and development, and biological and abiotic stress responses by suppressing or activating the expression of related downstream genes through transcriptional regulation or nuclear localization. Many bHLH transcription factor genes have been identified from different plants including *Arabidopsis* (Bailey et al., 2003). Zhang et al. (2020) identified 122 members of the bHLH transcription factor family in peppers, among which a few were noted to be involved in responses to cold, heat, drought, and salt stress (Zhang et al., 2020). Low temperature stress can induce significant upregulation of *WbHLH046* gene expression in wheat and improve the expression of the rice *bHLH* gene (*RsICE1*) (Man et al., 2017). *Arabidopsis bHLH122* positively regulates drought tolerance, salt tolerance, and osmotic signaling (Liu et al., 2013), and *CdICE1* of the chrysanthemum bHLH family regulates tolerance to low temperature, drought, and salt stress (Chen et al., 2012). Pepper bHLH transcription factor CabHLH035 can enhance salt tolerance by regulating ion homeostasis and proline biosynthesis (Zhang et al., 2022), and *OrbHLH18* overexpression in *Arabidopsis* can significantly improve cold resistance (Li et al., 2010). The *CsbHLH18* gene of sweet orange enhances cold tolerance in transgenic tobacco (Geng and Liu, 2018). *MebHLH18* expression can increase peroxidase activity, decrease reactive oxygen species (ROS), and change the abscission rate of cassava leaves at low temperatures (Liao et al., 2023). However, no studies have been reported on the waterlogging tolerance effects of the *bHLH* gene in plants.

bHLH genes are involved in regulating plant tolerance to abiotic stresses, such as drought, salinity, and low temperature. However, there are no reports on the *bHLH* gene function in hot pepper under waterlogging stress. In the present study, an important bHLH transcription factor gene, *CabHLH18*, in hot pepper was successfully cloned. Next, the sequence characteristics, evolutionary relationship, expression pattern, and subcellular localization of the *CabHLH18* gene were examined. Subsequently, the growth and physiological response of *CabHLH18* overexpression lines under waterlogging stress were analyzed, and the function of the *CabHLH18* gene was preliminarily explored. The results provide a reference for generating waterlogging-tolerant peppers.

Materials and methods

Plant materials and treatment

Three hot pepper cultivars, 'ZHC2' (waterlogging-tolerant), 'ZHC1', and 'DFZJ' (waterlogging-sensitive) were used in this study. 'ZHC2' and 'ZHC1' are inbred lines, which were donated by the Zunyi Academy of Agricultural Sciences (Zunyi, China), and 'DFZJ' is a local inbred line from Guizhou province. Pepper seedlings were planted in plastic pots (length × width × depth: 32 × 24 × 13 cm, with one seedling per pot) filled with sand and cultured at 25 ± 2/20 ± 2°C for a 10-h/14-h light/dark photoperiod with an irradiance of 270 μmol m^{-2} s^{-1}. Before and after the formation of two leaves, the pepper seedlings were watered with 1/2 Hoagland solution (only macroelements halved, while microelements were not) and further Hoagland solution once a day. After the formation of five leaves, seedlings with uniform growth were transferred to trays for waterlogging treatment and placed into 2-cm-deep water above the sand surface. The seedlings were subjected to three treatments as follows: 6 h (T1) and 24 h (T2) of waterlogging stress and 1 h of recovery (R) after 24 h of waterlogging stress according to the preliminary experiments. Normal culture (no waterlogging stress) conditions served as the control (CK). At each stage, leaf, stem, and root samples were selected from 10 plants, mixed, immediately frozen in liquid nitrogen, and stored in a −80°C freezer until use for gene cloning. The phenotype and physiology of T_3 pure transgenic hot pepper 'DFZJ' and wild-type (WT) plants were determined and cultured as mentioned earlier. Three biological replicates with 10 plants per replicate were established for the experiments.

RNA reverse transcription, *CabHLH18* amplification, and construction of overexpression vector

RNA was reverse-transcribed into cDNA using a PrimeScript RT kit (Takara, Dalian, China). The full-length coding sequence of the *CabHLH18* gene was amplified from the hot pepper 'ZHC2' (under 24 h of waterlogging stress) cDNA, using primers with *Bsa*I restriction sites at the 5′- and 3′-ends. The primers used for

amplification are shown in Table 1. The amplified fragment was digested with *Sac*I/*Spe*I and *BamH*I/*Kpn*I and inserted into the pEGOEPubi-H vector (modified to contain the green fluorescence protein (*GFP*) gene), using T4-DNA ligase (Takara), according to the manufacturer's protocol. The inserted sequence was driven by a corn UBI promoter.

Bioinformatics analysis of the *CabHLH18* gene

The *CabHLH18* gene sequence was compared using the DNAMAN global alignment method (Tsai et al., 2006). The NCBI Open Reading Frame (ORF) Finder was used to analyze the ORF of the *CabHLH18* gene and predict its amino acid sequence. Expert Protein Analysis System (Expasy) (https://web.expasy.org/protscale/) was used for hydrophobicity prediction, and NetPhos 2.0 (http://www.cbs.dtu.dk/services/NetPhos/) and CPHmodels 3.2 (http://www.cbs.dtu.dk/services/CPHmodels/) were employed for phosphorylation site analyses. The homologous sequences of the CabHLH18 proteins were retrieved by BLAST search in the NCBI database (accession numbers in Supplementary Table S1). A phylogenetic tree was constructed using MEGA 7 (Mega Limited, Auckland, New Zealand) with maximum-likelihood method of 1,000 bootstraps (Kumar et al., 2016). MODELLER9.22 (https://salilab.org/modeller/) was adopted for homology modeling of the CabHLH18 protein (Benjamin and Andrej, 2016), using the X-ray crystal structure of a putative bHLH protein, 5gnj.1.A, as the template. The predicted model was analyzed using SAVES (https://servicesn.mbi.ucla.edu/SAVES/). GROMACS software (http://www.gromacs.org/) was employed for calculating root-mean-square deviation and the potential energy value of the model protein (Hess et al., 2008). Ramachandran plots were examined using Rampage server (http://mordred.bioc.cam.ac.ukrapper/rampage.php) (Lovell et al., 2003).

Subcellular localization of CabHLH18 protein

Subcellular localization of CabHLH18 protein was analyzed after transient expression in *Nicotiana benthamiana* leaf epidermal cells. The plasmid containing the target gene was amplified and spliced to the 1300-GFP vector by seamless cloning methodology. *Agrobacterium* GV3101 containing the 1300-*CabHLH18*-GFP vector plasmid was cultured. The bacterial cells were suspended in 10 mM $MgCl_2$ buffer to an optical density of 600 nm (OD_{600}) of 1.0. Two microliters of 100 mM 2-morpholino ethane sulfonic acid was added to the bacterial suspension, which was then incubated for more than 3 h. Subsequently, the prepared bacterial suspension was inoculated into the lower epidermal layer of 3–4-week-old *N. benthamiana* leaves and incubated for 72 h for transformation. As the control, leaf transformation of the 1300-GFP vector with no target gene was used. After transformation and 20 min of 1 μM 4′-6-diamino-2-phenylindole (DAPI) staining, the samples were observed using laser confocal fluorescence microscopy (FV1000 Olympus Corp., Tokyo, Japan). The excitation and emission spectra used for DAPI were 405 nm and 455–470 nm, respectively. For GFP analyses, the excitation and emission spectra were 488 nm and 507 nm, respectively. At least three fields of view from three leaves were examined.

TABLE 1 Primers used in this study.

Primer role	Primer sequence (5′–3′)
CabHLH18 amplification	ActagggtctcGcaccATGGAATATTATGGCT TTAATCAACAATGG ActagggtctcTcgccTATAACCATTTTGAGA GCTGTGTGCAA
PCR identification of transformant	TTAGCCCTGCCTTCATACGC GACACGCTGAACTTGTGG
Control *18S*	TCGGGATCGGAGTAATGA TTCGCAGTTGTTCGTCTT

Gene transformation and identification

Agrobacterium rhizobiae strain LBA4404 containing the *CabHLH18* gene was inoculated onto Luria broth (LB) solid medium (with 20 mg/L rifampicin and 50 mg/L kanamycin sulfate) and incubated in the dark for 24 h at 28°C. Then, single colonies were selected and inoculated into LB medium for 24 h under constant shaking. Subsequently, 50 μL of the bacterial culture was inoculated into 50 mL of fresh LB medium and incubated in a shaker (180 rpm, 28°C) for 12 h until OD_{600} of 0.5–0.6 was reached.

After germination of the seeds of hot peppers 'DFZJ' and 'ZHC1' to a radicle length of 1–2 mm, the seed coats were removed to expose their plumules and placed into the suspension of *Agrobacterium* containing the *CabHLH18* gene, with 200 μL/L SILWET1-77 surfactant and 1 mL/L acetoeugenone under 15 kPa pressure for 5 min. Then, the bacterial suspension was removed, and the seedlings were placed in a clean dish, cultured in dark for 3 days at 28°C, and planted in cell trays with peat substrate. Three biological replicates with 100 seeds per replicate were employed for germination and gene transformation. The T_0 transgenic seedlings containing the *GFP* reporter gene were detected at the cotyledon stage using a hand-held lamp (LUYOR-3415RG, Shanghai, China). The leaves of the three-leaf stage putative transformants were identified by multiple PCR with specific primers for the UBI promoter and *GFP* gene, and primers for the housekeeping gene *18S* were used as an internal control (Table 1). The PCR products were separated on 1% (w/v) agarose gels.

Analysis of phenotypes and physiological indicators

The T_3 lines were segregating after self-fertilization of T_0 transgenic plants. The T_3 pure overexpression lines of hot pepper were screened by PCR and hygromycin tolerance. The T_3 lines of hot pepper and WT plants were cultured using the abovementioned

method. After the growth of five leaves, samples were collected after 0 h (CK), 6 h (T1), and 24 h (T2) of waterlogging stress, and at 1 h (R1) after recovery. The primary root length, seedling height, fresh weight, water content, and root viability (CAS No. G0124F, Geruisi, Suzhou, China); root proline content (CAS No. BC0295, Solarbio, Beijing, China); and amino acid (not including proline and hydroxyproline, CAS No. BC1575, Solarbio), soluble sugar (CAS No. BC0035, Solarbio), and malondialdehyde (MDA; CAS No. BC0025, Solarbio) levels, and superoxide dismutase (SOD; CAS No. BC0175, Solarbio) activity were analyzed according to the instructions provided in the respective kits. Plant water content was calculated as: plant fresh weight – plant dry weight)/plant fresh weight × 100%.

Statistical analyses

Statistical software (SPSS 20.00, IBM Inc., Armonk, NY, USA) and graphics software (Origin 2017, OriginLab Inc., Northampton, MA, USA) were used for the data analysis and figure construction, respectively. The Duncan's multiple range test was performed to determine significant differences between means at a significance level of $p < 0.05$, after showing a significant effect using one-way analysis of variance.

Results

Cloning and bioinformatics analysis of the *CabHLH18* gene

A 1,056-bp cDNA sequence from 'ZHC2' was amplified by PCR (Figure 1A) using LOC107879909-specific primers, and named *CabHLH18*. Bioinformatics analyses revealed that *CabHLH18* is a hydrophilic protein encoding 352 amino acids (Figure 1B) and has a bHLH_AtNAI1-like conserved domain at 170–242 at the C-terminus (Figure 1C), which mediates endoplasmic reticulum formation and may play a role in plant tolerance to abiotic stress. Phylogenetic tree analyses based on amino acid sequences of various plant species found that CabHLH18 protein had maximum similarity with *Capsicum annuum* XM 016694561.2 protein (Figure 2A) and that their domains were similar. The prediction model revealed that the similarity between the 3D structure model of CabHLH18 and the template 5gnj.1.A was as high as 99.6% and that both proteins had a bHLH-binding domain and belonged to the bHLH family, indicating good model quality (Figure 2B). The root-mean-square deviation curve reached equilibrium after 2,750 ps, with fluctuations in the range of 1.66–2.24 nm. These results showed that *CabHLH18* had a stable structure (Figure 2C). The Ramachandran diagram verification of the protein denoted its suitability because there were no residues in the disallowed regions (Figure 2D).

Subcellular localization of CabHLH18 protein

To determine the subcellular localization of CabHLH18 protein, the 1300-*CabHLH18*-GFP fusion protein was expressed transiently in *N. benthamiana* mesophyll cells. The infective solution was injected into *N. benthamiana* from the lower epidermis of the leaves, and the sample was analyzed after 72 h. CabHLH18 protein was localized in the nucleus, while the empty vector GFP signal was distributed throughout the cell, indicating that CabHLH18 might have a regulatory role as a transcription factor (Figure 3).

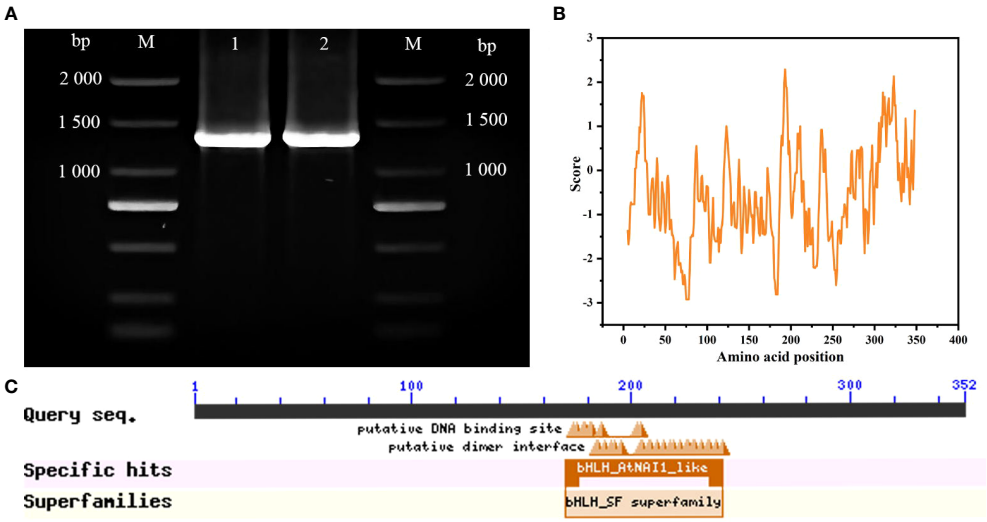

FIGURE 1
Molecular identification of *CabHLH18* gene in 'ZHC2'. **(A)** Amplification of bands using 'ZHC2' cDNA as template. M: 2,000-bp DNA marker; 1-2: 'ZHC2' cDNA. **(B)** Hydrophilic analysis of CabHLH18 protein. **(C)** CabHLH18 protein domains.

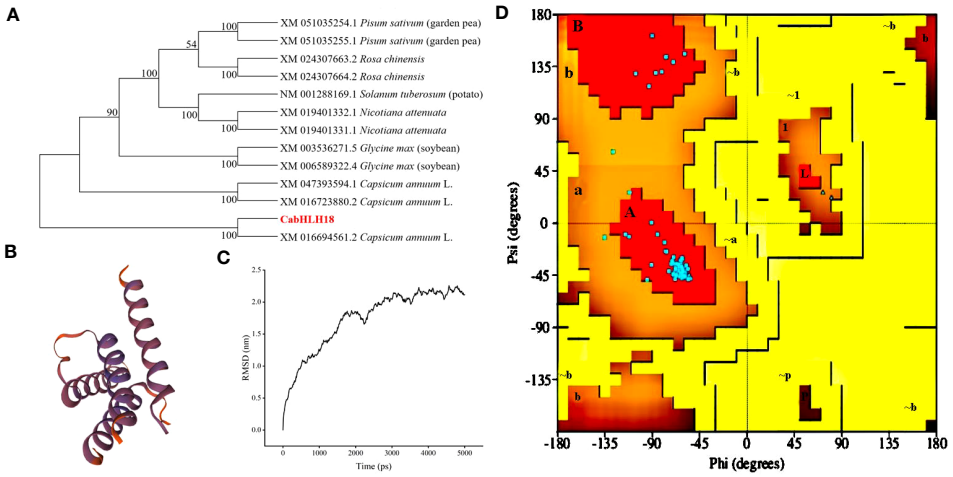

FIGURE 2
Phylogenetic tree, homology modeling, and molecular simulation of CabHLH18 protein. **(A)** Phylogenetic tree of bHLH proteins in various plant species with bHLH homologs. **(B)** Homology modeling of CabHLH18 protein using MODELLER9.22. **(C)** Molecular dynamics simulation. Backbone of root mean squared deviation (RMSD) plotted versus time (in ps). **(D)** Ramachandran plot analysis. A, B, and L regions: most favored residues; a, b, l, and p regions: additional allowed residues; ~a, ~b, ~l, and ~p regions: generously allowed residues.

Transformation and identification of *CabHLH18* gene in hot pepper

To investigate the function of *CabHLH18* gene, *CabHLH18* overexpression vector was transformed into the plumules of hot pepper. The specific primers of *CabHLH18* and housekeeping gene *18S* were identified by multiple PCR analyses. The seedlings of hot peppers 'DFZJ' and 'ZHC1' were selected for transformation, which presented efficiencies of 21.37% and 22.20%, respectively, indicating that this transformation technique was stable and repeatable (Figure 4A). The housekeeping primers amplified in all plant samples, indicating that the DNAs were of good quality. Lanes 1, 4, 7, and 9 showed amplification with construct-specific primer sets, indicating that these plants had incorporated the transgene (Figure 4B).

Overexpression of *CabHLH18* gene improved waterlogging tolerance in hot pepper

After 7 days of waterlogging stress, the leaf wilted degree of hot pepper 'DFZJ' overexpression lines was lower than that of the WT plants (Figure 5), whereas the root length, seedling height, and fresh

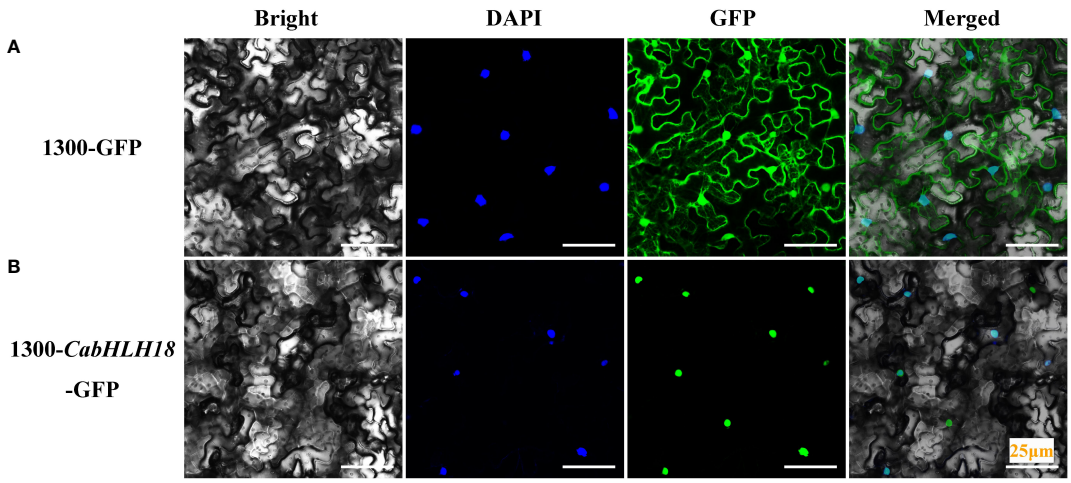

FIGURE 3
Subcellular localization of CabHLH18 protein in *N. benthamiana* mesophyll cells. **(A)** Vector 1300-GFP was introduced into tobacco leaves. **(B)** Fusion protein 1300-*CabHLH18*-GFP was introduced into tobacco leaves. The sample was observed under a confocal laser-scanning microscope. Green fluorescent protein (GFP), nuclear fluorescence (blue), combined images (green and blue), and bright-field, phase-contrast images are displayed. Bar = 25 μm.

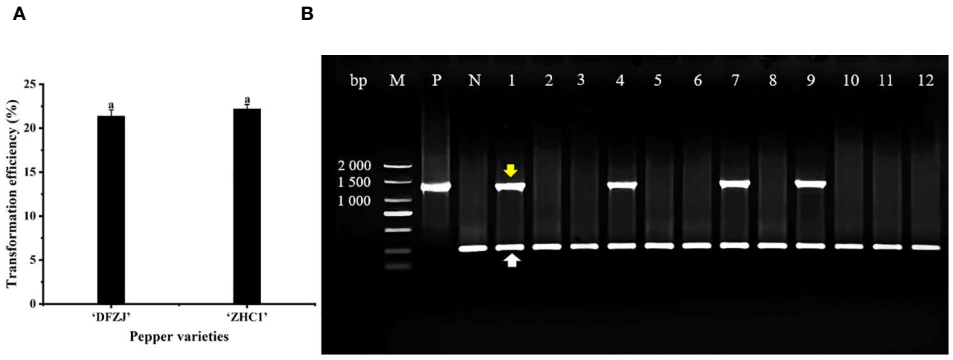

FIGURE 4
Transformation and identification of *CabHLH18* gene in hot pepper. **(A)** Transformation of *CabHLH18* overexpression vector into the plumules of two pepper cultivars. **(B)** PCR identification of *CabHLH18* transgenic plants. PCR detection of *CabHLH18* gene in the genomic DNA of transgenic T_0 plant leaves. The yellow arrow indicates the target fragment of the *CabHLH18* gene. The white arrow shows the amplification band of the housekeeping gene *18S*. M: 2,000-bp DNA marker; lanes 1, 4, 7, and 9: transgenic plants; lanes 2, 3, 5, 6, 8, and 10–12: non-transformed plants; P: positive control (*CabHLH18* recombinant plasmid); N: negative control (wild-type DNA).

weight of the overexpression lines reached 1.29-, 1.17-, and 1.39-fold that of the WT plants at the T2 (24 h after waterlogging stress) stage, respectively (Figures 6A–C). The overexpression lines showed greater height and longer roots than the WT plants (Figures 6A, B). Under normal culture conditions, no difference was observed in the water content between the overexpression lines and WT plants. However, at the T1 and T2 stages, the water content in the WT plants was less than that in the overexpression lines, showing reductions of 0.70% and 2.69%, respectively. At the R stage, the water content in both the overexpression lines and WT plants increased, and the overexpression lines had higher water content than the WT plants (Figure 6D). At the T2 and R stages, the root viability of the overexpression lines was 28.14% and 26.56%, respectively, when compared with the WT plants (Figure 6E).

Under waterlogging stress, the amino acid content (Figure 6F), proline level (Figure 6G), and soluble sugar level (Figure 6H) in the roots of the overexpression lines reached a peak at the T2 stage and were 45.03%, 60.67%, and 120.18% higher, respectively, than those in the roots of the WT plants. However, at the R stage, the amino acid content, proline level, and soluble sugar level decreased in the overexpression lines, and the decrease was more rapid than that noted in the WT plants, indicating that the overexpression lines responded more sensitively to waterlogging stress and recovery.

The SOD activity of both the overexpression lines and WT plants increased under waterlogging stress, peaked at the T2 stage, and decreased at the R stage (Figure 6I). In particular, the SOD activity of the overexpression lines was higher than that of the WT plants under waterlogging conditions, indicating that the overexpression lines had

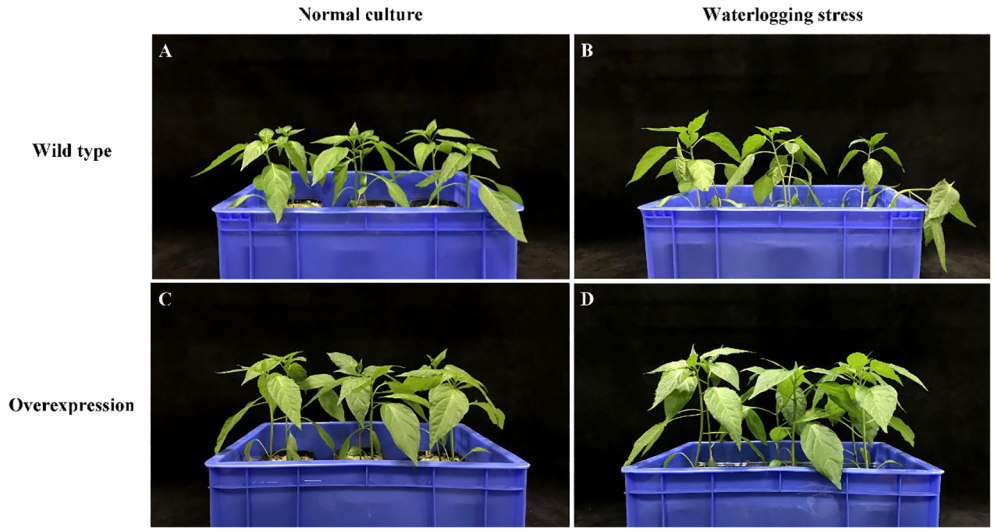

FIGURE 5
Effects of waterlogging stress on hot pepper 'DFZJ' overexpressing *CabHLH18* gene. **(A, B)** Growth of WT pepper under normal and waterlogging stress conditions, respectively. **(C, D)** Growth of overexpression lines under normal and waterlogging stress conditions, respectively.

10.3389/fpls.2023.1285198

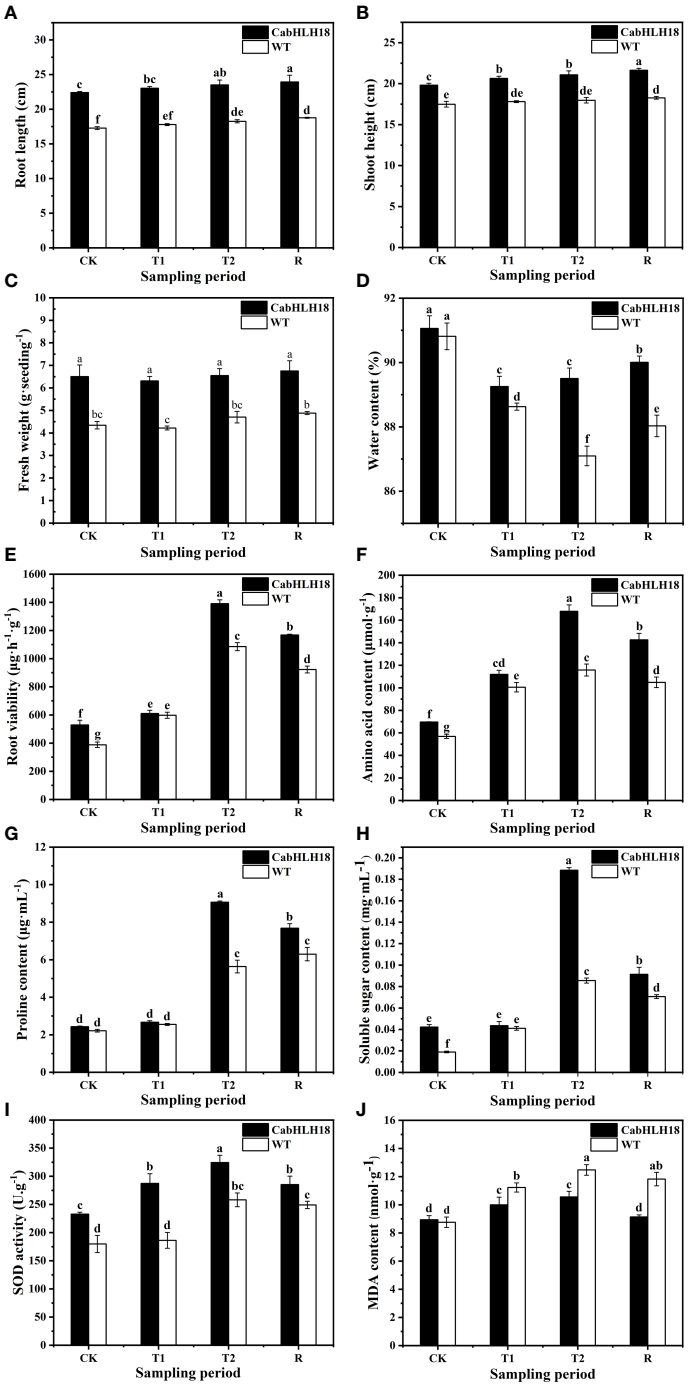

FIGURE 6
Effects of waterlogging stress and recovery on the **(A)** root length, **(B)** seedling height, **(C)** fresh weight, **(D)** water content, **(E)** root viability, **(F)** amino acid content, **(G)** proline content, **(H)** soluble sugar content, **(I)** SOD activity, and **(J)** MDA content of the overexpression line. CK, T1, T2, and R denote control, 6 h after waterlogging stress, 24 h after waterlogging stress, and 1 h after recovery, respectively. The column represents mean value of SD (n = 3), and values with different letters are significantly different ($p < 0.05$).

better ROS scavenging ability. After a longer waterlogging stress period, the MDA content in both the overexpression lines and WT plants increased, reaching a peak at the T2 stage and decreasing at the R stage (Figure 6J). However, the MDA content in the overexpression lines was lower than that in the WT plants under both waterlogging stress and recovery conditions, with the overexpression lines presenting greater MDA decline rates than the WT plants after recovery.

Discussion

Cloning and expression characteristics of the *CabHLH18* gene

The bHLH family of transcription factors responds to plant abiotic stresses (Kiribuchi et al., 2004; Zhang et al., 2020). A novel

bHLH transcription factor, PtrbHLH66, from Triloba orange has been reported to actively regulate plant drought tolerance by root growth effects and ROS clearance (Liang et al., 2022). *Arabidopsis* AtbHLH122 positively regulates plant responses to drought and salt stress by inhibiting *CYP707A3* expression and increasing abscisic acid levels (Liu et al., 2015). Overexpression of *SlbHLH22* in tomato has been observed to increase secondary metabolites and osmoregulatory substances, enhance ROS scavenging ability, and improve drought and salinity tolerance (Waseem et al., 2019). Zhang et al. (2020) identified 122 members of the bHLH transcription factor family in *C. annuum*, among which only a few were noted to regulate plant responses to stresses, such as cold, heat, drought, and salt stress (Zhang et al., 2020). The bHLH transcription factor gene *CabHLH035* in peppers has been found to improve salt tolerance by regulating ion homeostasis and proline biosynthesis (Zhang et al., 2022). Currently, most of the studies related to waterlogging stress on peppers have only concentrated on morphological observation, physiological examination, and biochemical analysis, devoting limited attention to waterlogging tolerance mechanisms (Kato et al., 2020; Kaur et al., 2021; Komatsu et al., 2022). In the present study, the *CabHLH18* gene was cloned from hot pepper 'ZHC2' with strong waterlogging tolerance. Phylogenetic tree analyses of bHLH proteins from different plant species showed that CabHLH18 and capsicum-related proteins clustered together, thus suggesting that they might have close genetic relationships in evolution and function.

Subcellular localization of CabHLH18 protein

A majority of the bHLH transcription factor proteins are located in the nucleus and might have nuclear protein functions. For instance, bHLH122 is localized in the nucleus and plays an important role in drought resistance, osmotic stress resistance, and inhibition of *Arabidopsis* abscisic acid catabolism (Liu et al., 2013). The *ThBHLH1*-encoded protein of the *bHLH* gene of *Salix sphinx* is localized in the nucleus and improves abiotic stress tolerance by increasing osmotic potential and reducing ROS accumulation (Ji et al., 2016). The wheat transcription factor TabHLH39 is located in the nucleus and improves the tolerance of transgenic plants to abiotic stress (Zhai et al., 2016). In the present study, CabHLH18 protein was also localized in the nucleus, indicating that it may predominantly function in the nucleus and might regulate gene expression and control plant responses to waterlogging stress.

Establishment of the plumules transformation system of hot pepper

The transformation complexity of peppers restricts their development of genetic engineering, breeding, and molecular biology (Mahto et al., 2018). Owing to high genotype dependence and tenacity of pepper (Kothari et al., 2010), it is difficult to achieve a stable transformation system, impeding the development of pepper transgenic technology development (Heidmann and Boutilier, 2015). The transformation of peppers mainly uses *Agrobacterium*-mediated and gene-gun methodologies. For example, cotyledon (Kim et al., 2017) and hypocotyl (Kumar et al., 2012) were used as explants to establish an *Agrobacterium*-mediated transformation system of *Capsicum*; however, this method was unstable and not only required complicated tissue culture processes but also needed specific plant materials to achieve regeneration. Currently, achieving a highly efficient hot pepper transformation system is particularly important, and transgenic plants obtained without tissue culture can significantly reduce the cost. In one study, plant meristems were induced to produce shoots with targeted DNA modifications, and targeted genes were transmitted to the progeny, which sidesteps the need for tissue culture (Maher et al., 2020). Cao et al. (2023) achieved the transformation of several plant species by using a cut–dip–budding delivery system to transform plant genes without tissue culture (Cao et al., 2023). In our study, the seed coats of hot pepper were removed to expose the plumules and then infected with *Agrobacterium* containing the target gene. Effective transformation of peppers could be achieved with radicle length of 1–2 mm, *Agrobacterium* density (OD_{600}) of 0.50–0.60 nm, at 15 kPa. Two pepper cultivars ('ZHC1' and 'DFZJ') were transformed by this method, and no significant difference was found in the transformation efficiency, indicating that the transformation system was stable in the hot peppers. This transformation method does not depend on tissue culture, thus avoiding some problems associated with tissue culture such as contamination, browning, and soma clonal variation, and the efficient transformation system might provide strong technical support for pepper genetics and breeding studies.

Effect of the *CabHLH18* gene on waterlogging tolerance of transgenic peppers

Waterlogging stress inhibits root respiration and ATP synthesis, blocking the generation of water potential gradients and ion transport systems on the root endodermis and causing plant withering (Sairam et al., 2008). Under well-watered conditions, the overexpression of the *Populus euphratica* gene, *oxPebHLH35*, in *Arabidopsis* resulted in longer taproots, higher leaf numbers, and increased leaf area, thus improving the plant water stress tolerance, when compared with the vector control plants (Waseem et al., 2019). After treatment with 100 mM and 150 mM NaCl, the roots of the *CabHLH035* transgenic tobacco lines were longer than those of the WT plants. In comparison with the WT plants, the *CabHLH035* transgenic lines had substantially lower water loss (Zhang et al., 2022). In our study, under waterlogging stress, the WT pepper plants exhibited higher leaf wilting degree and lodging at the T2 stage and had lower water content, when compared with those noted in the overexpression lines. Furthermore, the seedlings of the overexpression lines were stronger than the WT plants under the same growth conditions (Figures 6A–E). These results are similar to those reported in a previous study (Waseem et al., 2019; Zhang et al., 2022). Thus, under waterlogging stress, the growth of the WT

pepper plants was inhibited, whereas the overexpression lines adapted to this stress and maintained normal growth.

Plants can adapt to waterlogging stress through the accumulation of proline and soluble sugar (Nanjo et al., 1999; Hildebrandt et al., 2015; Hildebrandt, 2018; Khan et al., 2020). Proline is a main solute molecule involved in plant osmotic regulation and is also a free radical scavenger, protecting the plant's photosynthetic activity and cells from damage, to ensure sustained plant growth under long-term stress (Silva-Ortega et al., 2008; Kavi Kishor and Sreenivasulu, 2014). The increase in higher proline content regulates the osmotic potential and improves abiotic stress tolerance (Ji et al., 2016). The *ThbHLH1* gene has been reported to activate proline biosynthesis by inducing the expression of *P5CS* and *BADH/ALDH* (Ji et al., 2016). Overexpression of *VvbHLH1* in *Arabidopsis* has been found to increase the proline content, maintain osmotic balance between intracellular and extracellular environments, and protect membrane integrity, thus enhancing salt and drought tolerance (Wang et al., 2016). Furthermore, *TabHLH39* transgenic plants have been noted to exhibit higher levels of soluble sugars and proline and lower levels of electrolyte leakage. The TabHLH39 protein in the transgenic plants can protect the plant cells by increasing the soluble sugar content to provide energy and redistribute the soluble osmotic sugars and improve plant stress resistance by promoting proline accumulation. The soluble sugars and proline act as osmotic regulators and molecular chaperones to protect the protein integrity and enhance enzyme activity, thus improving *Arabidopsis* resistance to abiotic stress (Zhai et al., 2016). The synthesis of soluble sugars and other substances can provide sufficient reducing sugars under waterlogging stress (Sairam et al., 2009). In the present study, the contents of proline, soluble sugar, and amino acid levels in *CabHLH18* overexpression lines were significantly higher than those in the WT plants under waterlogging stress. The overexpression lines accumulated more substances involved in osmotic regulation and energy supply, leading to stronger osmotic regulation ability and adequate energy supply, which mitigated the damage caused by waterlogging stress.

Limited oxygen levels can cause ROS accumulation under waterlogging stress, resulting in membrane lipid peroxidation, structural changes in proteins and nucleic acids (Mittler et al., 2004; Bansal and Srivastava, 2012; Mittler, 2017), decreased activity of antioxidant enzymes, and increased MDA. Plants maintain ROS homeostasis to adapt to abiotic stress by activating the antioxidant system, and the increased SOD activity can enhance plant resistance (Tavanti et al., 2021). Zhang et al. (2022) reported CabHLH035-protected plants from oxidative damage by removing ROS through increased expression of the SOD gene (Zhang et al., 2022). In the present study, SOD activity was higher, and MDA content was lower in the overexpression lines, when compared with those in the WT plants under waterlogging stress, indicating that *CabHLH18* overexpression lines could reduce the damage caused by ROS under waterlogging stress.

Conclusion

In this study, the *CabHLH18* gene was found to contain a 1,056-bp ORF and encode 352 amino acids. The CabHLH18 protein was determined to be located in the nucleus. Subsequently, an effective transformation system of hot pepper was established, with an efficiency of 22.20%. Under waterlogging stress, *CabHLH18* overexpression lines showed significantly greater root length, plant height, fresh weight, water content, and root viability, when compared with WT plants. The contents of amino acids, proline, soluble sugars, and SOD activity were also significantly higher, but the MDA level was lower in the overexpression lines, when compared to the WT plants. Thus, the *CabHLH18* gene could enhance waterlogging tolerance of *CabHLH18*-overexpressing hot pepper and might be a valuable gene for improving waterlogging tolerance of crops.

Data availability statement

The datasets presented in this study can be found in online repositories. The names of the repository/repositories and accession number(s) can be found in the article/Supplementary Material.

Author contributions

HT: Software, Writing – original draft, Data curation, Investigation. GF: Writing – original draft, Investigation. XX: Investigation, Writing – original draft. HW: Writing – original draft, Data curation. SZ: Conceptualization, Writing – review & editing. GG: Writing – review & editing, Conceptualization, Funding acquisition.

Funding

The author(s) declare financial support was received for the research, authorship, and/or publication of this article. This research was funded by the National Natural Science Foundation of China, grant number "32260760", the Science and Technology Program of Guizhou Province, grant numbers "20201Y116, 2022050, 20201Z002, and 20202102", and the Science and Technology Bureau of Zunyi, grant number "20216".

Acknowledgments

We thank Hao Tian (Zunyi Academy of Agricultural Sciences) for providing experimental materials. We thank International Science Editing (http://www.internationalscienceediting.com) for editing this manuscript.

Conflict of interest

The authors declare that the research was conducted in the absence of any commercial or financial relationships that could be construed as a potential conflict of interest.

Publisher's note

All claims expressed in this article are solely those of the authors and do not necessarily represent those of their affiliated organizations, or those of the publisher, the editors and the reviewers. Any product that may be evaluated in this article, or claim that may be made by its manufacturer, is not guaranteed or endorsed by the publisher.

Supplementary material

The Supplementary Material for this article can be found online at: https://www.frontiersin.org/articles/10.3389/fpls.2023.1285198/full#supplementary-material

References

Bailey, P. C., Martin, C., Toledo-Ortiz, G., Quail, P. H., Huq, E., Heim, M. A., et al. (2003). Update on the basic helix-loop-helix transcription factor gene family in *Arabidopsis thaliana*. *Plant Cell.* 15 (11), 2497–2502. doi: 10.1105/tpc.151140

Bailey-Serres, J., and Voesenek, L. A. C. J. (2008). Flooding stress: Acclimations and genetic diversity. *Annu. Rev. Plant Biol.* 59, 313–339. doi: 10.1146/annurev.arplant.59.032607.092752

Bansal, R., and Srivastava, J. P. (2012). Antioxidative defense system in pigeon pea roots under waterlogging stress. *Acta Physiologiae Plantarum.* 34, 1595–1595. doi: 10.1007/s11738-012-0977-z

Benjamin, W., and Andrej, S. (2016). Comparative protein structure modeling using Modeller. *Curr. Protoc. Bioinf.* 47, 1–32. doi: 10.1002/cpbi.3

Cao, X. S., Xie, H. T., Song, M. L., Lu, J. H., Ma, P., Huang, B. Y., et al. (2023). Cut–dip–budding delivery system enables genetic modifications in plants without tissue culture. *Innovation.* 4 (1), 100345. doi: 10.1016/j.xinn.2022.100345

Chen, L., Chen, Y., Jiang, J. F., Chen, S. M., Chen, F. D., Guan, Z. Y., et al. (2012). The constitutive expression of *Chrysanthemum dichrum ICE1* in *Chrysanthemum grandiflorum* improves the level of low temperature, salinity and drought tolerance. *Plant Cell Rep.* 31 (9), 1747–1758. doi: 10.1007/s00299-012-1288-y

Food and Agriculture Organization of the United Nations (2020). *Crops* (Roma, Italy).

Geng, J. J., and Liu, J. H. (2018). The transcription factor CsbHLH18 of sweet orange functions in modulation of cold tolerance and homeostasis of reactive oxygen species by regulating the antioxidant gene. *J. Exp. Bot.* 69 (10), 2677–2692. doi: 10.1093/jxb/ery065

Heidmann, I., and Boutilier, K. (2015). Pepper, sweet (*Capsicum annuum*). *Methods Mol. Biol.* 1223, 321–334. doi: 10.1007/978-1-4939-1695-5_26

Hess, B., Kutzner, C., van der Spoel, D., and Lindahl, E. (2008). GROMACS 4: algorithms for highly efficient, load-balanced, and scalable molecular simulation. *J. Chem. Theory Computation.* 4 (3), 435–447. doi: 10.1021/ct700301q

Hildebrandt, T. M. (2018). Synthesis versus degradation: Directions of amino acid metabolism during *Arabidopsis* abiotic stress response. *Plant Mol. Biol.* 98 (1-2), 121–135. doi: 10.1007/s11103-018-0767-0

Hildebrandt, T. M., Nunes, N. A., Araújo, W. L., and Braun, H. P. (2015). Amino acid catabolism in plants. *Mol. Plant* 8 (11), 1563–1579. doi: 10.1016/j.molp.2015.09.005

Hirabayashi, Y., Mahendran, R., Koirala, S., Konoshima, L., Yamazaki, D., Watanabe, S., et al. (2013). Global flood risk under climate change. *Nat. Climate Change.* 3, 816–821. doi: 10.1038/s41558-020-00952-0

Ji, X. Y., Nie, X. G., Liu, Y. J., Zheng, L., Zhao, H. M., Zhang, B., et al. (2016). A bHLH gene from *Tamarix hispida* improves abiotic stress tolerance by enhancing osmotic potential and decreasing reactive oxygen species accumulation. *Tree Physiol.* 36 (2), 193–207. doi: 10.1093/treephys/tpv139

Kato, Y., Collard, B. C. Y., Septiningsih, E. M., and Ismail, A. M. (2020). Increasing flooding tolerance in rice: combining tolerance of submergence and of stagnant flooding. *Ann. Botany.* 124 (7), 1199–1210. doi: 10.1093/aob/mcz118

Kaur, G., Vikal, Y., Kaur, L., Kalia, A., Mittal, A., Kaur, D., et al. (2021). Elucidating the morpho-physiological adaptations and molecular responses under long-term waterlogging stress in maize through gene expression analysis. *Plant Science.* 304, 110823. doi: 10.1016/j.plantsci.2021.110823

Kavi Kishor, P. B., and Sreenivasulu, N. (2014). Is proline accumulation per se correlated with stress tolerance or is proline homeostasis a more critical issue? *Plant Cell Environment.* 37 (2), 300–311. doi: 10.1111/pce.12157

Khan, N., Ali, S., Zandi, P., Mehmood, A., Ullah, S., Ikram, M., et al. (2020). Role of sugars, amino acids and organic acids in improving plant abiotic stress tolerance. *Pakistan J. Botany.* 52, 355–363. doi: 10.30848/PJB2020-2(24

Kim, J., Park, M., Jeong, E. S., Lee, J. M., and Choi, D. (2017). Harnessing anthocyanin-rich fruit: A visible reporter for tracing virus-induced gene silencing in pepper fruit. *Plant Methods* 13, 1–10. doi: 10.1186/s13007-016-0151-5

Kiribuchi, K., Sugimori, M., Takeda, M., Otani, T., Okada, K., Onodera, H., et al. (2004). *RERJ1*, a jasmonic acid-responsive gene from rice, encodes a basic helix-loop-helix protein. *Biochem. Biophys. Res. Commun.* 325 (3), 857–863. doi: 10.1016/j.bbrc.2004.10.126

Komatsu, S., Yamaguchi, H., Hitachi, K., Tsuchida, K., Rehman, S. U., and Ohno, T. (2022). Morphological, biochemical, and proteomic analyses to understand the promotive effects of plant-derived smoke solution on wheat growth under flooding stress. *Plants.* 11 (11), 1508. doi: 10.3390/plants11111508

Kothari, S. L., Joshi, A., Kachhwaha, S., and Ochoa-Alejo, N. (2010). Chilli peppers-A review on tissue culture and transgenesis. *Biotechnol. Advances.* 28 (1), 35–48. doi: 10.1016/j.bioteChadv.2009.08.005

Kumar, R. V., Sharma, V. K., Chattopadhyay, B., and Chakraborty, S. (2012). An improved plant regeneration and *Agrobacterium*-mediated transformation of red pepper (*Capsicum annuum* L.). *Physiol. Mol. Biol. Plants.* 18 (4), 357–364. doi: 10.1007/s12298-012-0132-8

Kumar, S., Stecher, G., and Tamura, K. (2016). MEGA7: molecular evolutionary genetics analysis version 7.0 for bigger datasets. *Mol. Biol. Evolution.* 33 (7), 1870–1874. doi: 10.1093/molbev/msw054

Kuroh, T., Nagai, K., Gamuyao, R., Wang, D. R., Furuta, T., Nakamori, M., et al. (2018). Ethylene-gibberellin signaling underlies adaptation of rice to periodic flooding. *Science.* 361 (6398), 181–186. doi: 10.1126/science.aat1577

Li, F., Guo, S. Y., Zhao, Y., Chen, D. Z., Chong, K., and Xu, Y. Y. (2010). Overexpression of a homopeptide repeat-containing bHLH protein gene (*OrbHLH001*) from Dongxiang wild rice confers freezing and salt tolerance in transgenic *Arabidopsis*. *Plant Cell Rep.* 29 (9), 977–986. doi: 10.1007/s00299-010-0883-z

Liang, B. B., Wan, S. G., Ma, Q. L., Yang, L., Hu, W., Kuang, L. Q., et al. (2022). A novel bHLH transcription factor PtrbHLH66 from trifoliate orange positively regulates plant drought tolerance by mediating root growth and ROS scavenging. *Int. J. Mol. Sci.* 23 (23), 15053. doi: 10.3390/ijms232315053

Liao, W., Cai, J., Xu, H., Wang, Y., Cao, Y., Ruan, M., et al. (2023). The transcription factor MebHLH18 in cassava functions in decreasing low temperature induced leaf abscission to promote low-temperature tolerance. *Front. Plant Science.* 13. doi: 10.3389/fpls.2022.1101821

Liu, Y. J., Ji, X. Y., Nie, X. G., Qu, M., Zheng, L., Tan, Z. L., et al. (2015). *Arabidopsis* AtbHLH112 regulates the expression of genes involved in abiotic stress tolerance by binding to their E-box and GCG-box motifs. *New Phytologist.* 207 (3), 692–709. doi: 10.1111/nph.13387

Liu, W., Tai, H., Li, S., Gao, W., Zhao, M., Xie, C., et al. (2013). *bHLH122* is important for drought and osmotic stress resistance in *Arabidopsis* and in the repression of ABA catabolism. *New phytologist.* 201 (4), 1192–1204. doi: 10.1111/nph.12607

Lovell, S. C., Davis, I. W., Arendall, W. B. III, Bakker, P. I. W., Word, J. M., Prisant, M. G., et al. (2003). Structure validation by Cα geometry: ϕ, ψ and Cβ deviation. *Proteins.* 50 (3), 437–450. doi: 10.1002/prot.10286

Maher, M. F., Nasti, R. A., Vollbrecht, M., Starker, C. G., Clark, M. D., and Voytas, D. F. (2020). Plant gene editing through *de novo* induction of meristems. *Nat. Technology.* 38, 84–89. doi: 10.1038/s41587-019-0337-2

Mahto, B. K., Sharma, P., Rajam, M. V., Reddy, P. M., and Dhar-Ray, S. (2018). An efficient method for *Agrobacterium*-mediated genetic transformation of chili pepper (*Capsicum annuum* L.). *Indian J. Plant Physiol.* 23 (3), 573–581. doi: 10.1007/s40502-018-0389-1

Man, L. L., Xiang, D. J., Wang, L. N., Zhang, W. W., Wang, X. D., and Qi, G. C. (2017). Stress-responsive gene *RsICE1* from *Raphanus sativus* increases cold tolerance in rice. *Protoplasma.* 254 (2), 945–956. doi: 10.1007/s00709-016-1004-9

Mickelbart, M. V., Hasegawa, P. M., and Bailey-Serres, J. (2015). Genetic mechanisms of abiotic stress tolerance that translate to crop yield stability. *Nat. Rev. Genet.* 16 (4), 237–251. doi: 10.1038/nrg3901

Mittler, R. (2017). ROS are good. *Trends Plant Science.* 22 (1), 11–19. doi: 10.1016/j.tplants.2016.08.002

Mittler, R., Vanderauwera, S., Gollery, M., and Van-Breusegem, F. (2004). Reactive oxygen gene network of plants. *Trends Plant Science.* 9 (10), 490–498. doi: 10.1016/j.tplants.2004.08.009

Molla, R. M., Rohman, M. M., Islam, M. R., Hasanuzzaman, M., and Hassan, L. (2022). Screening and evaluation of chilli (*Capsicum annuum* L.) genotypes for waterlogging tolerance at seedling stage. *Biocell.* 46, 1613–1627. doi: 10.32604/biocell.2022.019243

Murre, C., McCaw, P. S., and Baltimore, D. (1989). A new DNA binding and dimerization motif in immunoglobulin enhancer binding, *daughterless*, *MyoD*, and *myc* proteins. *Cell.* 56 (5), 777–783. doi: 10.1016/0092-8674(89)90682-x

Nanjo, T., Kobayashi, M., Yoshiba, Y., Sanada, Y., Wada, K., Tsukaya, H., et al. (1999). Biological functions of proline in morphogenesis and osmotolerance revealed in antisense transgenic *Arabidopsis thaliana*. *Plant J.* 18 (2), 185–193. doi: 10.1046/j.1365-313x.1999.00438.x

Pan, J., Sharif, R., Xu, X., and Chen, X. (2021). Mechanisms of waterlogging tolerance in plants: research progress and prospects. *Front. Plant Science.* 11. doi: 10.3389/fpls.2020.627331

Perata, P., and Voesenek, L. A. C. J. (2007). Submergence tolerance in rice requires *Sub1A*, an ethylene-response-factor-like gene. *Trends Plant Science.* 12 (2), 43–46. doi: 10.1016/j.tplants.2006.12.005

Phukan, U. J., Mishra, S., and Shukla, R. K. (2016). Waterlogging and submergence stress: Affects and acclimation. *Crit. Rev. Biotechnol.* 36 (5), 956–966. doi: 10.3109/07388551.2015.1064856

Sairam, R. K., Dharmar, K., Chinnusamy, V., and Meena, R. C. (2009). Waterlogging-induced increase in sugar mobilization, fermentation, and related gene expression in the roots of mung bean (*Vigna radiata*). *J. Plant Physiol.* 166 (6), 602–616. doi: 10.1016/j.jplph.2008.09.005

Sairam, R. K., Kumutha, D., Ezhilmathi, K., Deshmukh, P. S., and Srivastava, G. C. (2008). Physiology and biochemistry of waterlogging tolerance in plants. *Biol. Plantarum.* 52, 401–412. doi: 10.1007/s10535-008-0084-6

Sauter, M. (2013). Root responses to flooding. *Curr. Opin. Plant Biol.* 16 (3), 282–286. doi: 10.1016/j.pbi.2013.03.013

Shinozaki, K., and Yamaguchi-Shinozaki, K. (2007). Gene networks involved in drought stress response and tolerance. *J. Exp. Botany.* 58 (2), 221–227. doi: 10.1093/jxb/erl164

Silva-Ortega, C. O., Ochoa-Alfaro, A. E., Reyes-Agüero, J. A., Aguado-Santacruz, G. A., and Jiménez-Bremont, J. F. (2008). Salt stress increases the expression of *p5cs* gene and induces proline accumulation in cactus pear. *Plant Physiol. Biochem.* 46 (1), 82–92. doi: 10.1016/j.plaphy.2007.10.011

Tavanti, T. R., Melo, A. A. R. D., Moreira, L. D. K., Sanchez, D. E. J., Silva, R. D., Silva, R. M. D., et al. (2021). Micronutrient fertilization enhances ROS scavenging system for alleviation of abiotic stresses in plants. *Plant Physiol. Biochem.* 160, 386–396. doi: 10.1016/j.plaphy.2021.01.040

Tian, L. X., Zhang, Y. C., Chen, P. L., Zhang, F. F., Li, J., Yan, F., et al. (2021). How does the waterlogging regime affect crop yield? A global meta-analysis. *Front. Plant Science.* 12. doi: 10.3389/fpls.2021.634898

Toledo-Ortiz, G., Huq, E., and Quai, P. H. (2003). The *Arabidopsis* basic/helix-loop-helix transcription factor family. *Plant Cell.* 15 (8), 1749–1770. doi: 10.1105/tpc.013839

Tsai, W. S., Shih, S. L., Green, S. K., Rauf, A., Hidayat, S. H., and Jan, F. J. (2006). Molecular characterization of pepper yellow leaf curl Indonesia virus in leaf curl and yellowing diseased tomato and pepper in Indonesia. *Plant Disease.* 90 (2), 247. doi: 10.1094/PD-90-0247B

Upadhyay, A., Gaonkar, T., Upadhyay, A. K., Jogaiah, S., Shinde, M. P., Kadoo, N. Y., et al. (2018). Global transcriptome analysis of grapevine (*Vitis vinifera* L.) leaves under salt stress reveals differential response at early and late stages of stress in table grape cv. Thompson Seedless. *Plant Physiol. Biochem.* 129, 168–179. doi: 10.1016/j.plaphy.2018.05.032

Vidoz, M. L., Loreti, E., Mensuali, A., Alpi, A., and Perata, P. (2010). Hormonal interplay during adventitious root formation in flooded tomato plants. *Plant J.* 63 (4), 551–562. doi: 10.1111/j.1365-313X.2010.04262.x

Voesenek, L. A. C. J., and Bailey-Serres, J. (2015). Flood adaptive traits and processes: An overview. *New Phytologist.* 206 (1), 57–73. doi: 10.1111/nph.13209

Wang, F. B., Zhu, H., Chen, D. H., Li, Z. J., Peng, R. H., and Yao, Q. H. (2016). A grape bHLH transcription factor gene, *VvbHLH1*, increases the accumulation of flavonoids and enhances salt and drought tolerance in transgenic *Arabidopsis thaliana*. *Plant Cell Tissue Organ Culture.* 125, 387–398. doi: 10.1007/s11240-016-0953-1

Waseem, M., Rong, X. Y., and Li, Z. G. (2019). Dissecting the role of a basic helix-loop-helix transcription factor, *SlbHLH22*, under salt and drought stresses in transgenic *Solanum lycopersicum* L. *Front. Plant Science.* 10. doi: 10.3389/fpls.2019.00734

Zhai, Y. Q., Zhang, L. C., Xia, C., Fu, S. L., Zhao, G. Y., Jia, J. Z., et al. (2016). The wheat transcription factor, TabHLH39, improves tolerance to multiple abiotic stressors in transgenic plants. *Biochem. Biophys. Res. Commun.* 473 (4), 1321–1327. doi: 10.1016/j.bbrc.2016.04.071

Zhang, H. F., Guo, J. B., Chen, X. Q., Zhou, Y. Y., Pei, Y. P., Chen, L., et al. (2022). Pepper bHLH transcription factor *CabHLH035* contributes to salt tolerance by modulating ion homeostasis and proline biosynthesis. *Horticulture Res.* 9, uhac203. doi: 10.1093/hr/uhac203

Zhang, Z. S., Chen, J., Liang, C. L., Liu, F., Hou, X. L., and Zou, X. X. (2020). Genome-wide identification and characterization of the bHLH transcription factor family in pepper (*Capsicum annuum* L.). *Front. Genet.* 11. doi: 10.3389/fgene.2020.570156

frontiers | Frontiers in Plant Science

TYPE Original Research
PUBLISHED 25 January 2024
DOI 10.3389/fpls.2024.1341826

OPEN ACCESS

EDITED BY
Dominik K Großkinsky,
Austrian Institute of Technology (AIT), Austria

REVIEWED BY
Małgorzata Rudnicka,
University of Silesia in Katowice, Poland
Kocsy Gábor,
Hungarian Academy of Sciences (MTA), Hungary

*CORRESPONDENCE
Li-Li Nan
958032689@qq.com

RECEIVED 21 November 2023
ACCEPTED 08 January 2024
PUBLISHED 25 January 2024

CITATION
Wang K, Nan L-L, Xia J, Wu S-W and Yang L-L (2024) Metabolomics reveal root differential metabolites of different root-type alfalfa under drought stress. *Front. Plant Sci.* 15:1341826. doi: 10.3389/fpls.2024.1341826

Metabolomics reveal root differential metabolites of different root-type alfalfa under drought stress

Kun Wang, Li-Li Nan *, Jing Xia, Shi-Wen Wu and Li-Li Yang

Key Laboratory of Grassland Ecosystem of Ministry of Education, College of Pratacultural Science, Gansu Agricultural University, Lanzhou, China

Introduction: Alfalfa (*Medicago sativa* L.) is the favored premium feed ingredient in animal husbandry production which is in serious jeopardy due to soil moisture shortages. It is largely unknown how different root types of alfalfa respond to arid-induced stress in terms of metabolites and phytohormones.

Methods: Therefore, rhizomatous rooted *M. sativa* 'Qingshui' (or QS), tap-rooted *M. sativa* 'Longdong' (or LD), and creeping rooted *M. varia* 'Gannong No. 4' (or GN) were investigated to identify metabolites and phytohormones responses to drought conditions.

Results: We found 164, 270, and 68 significantly upregulated differential metabolites were categorized into 35, 38, and 34 metabolic pathways in QS, LD, and GN within aridity stress, respectively. Amino acids, organic acids, sugars, and alkaloids were the four categories of primary differential metabolites detected, which include 6-gingerol, salicylic acid (SA), indole-3-acetic acid (IAA), gibberellin A_4 (GA_4), abscisic acid (ABA), trans-cinnamic acid, sucrose, L-phenylalanine, L-tyrosine, succinic acid, and nicotinic acid and so on, turns out these metabolites are essential for the resistance of three root-type alfalfa to aridity coercing.

Discussion: The plant hormone signal transduction (PST) pathway was dramatically enriched after drought stress. IAA and ABA were significantly accumulated in the metabolites, indicating that they play vital roles in the response of three root types of alfalfa to water stress, and QS and LD exhibit stronger tolerance than GN under drought stress.

KEYWORDS

alfalfa, drought stress, differential metabolites, phytohormones, amino acids

1 Introduction

Alfalfa (or Lucerne) (*Medicago sativa* L.), as a high-protein legume and more drought-resistant than other forage, is extensively grown in semi-arid and arid regions of China (Nan et al., 2019; Li et al., 2022), but still the growing drought poses a main threat to alfalfa acreage and output (Wu et al., 2017; Wasaya et al., 2021). Therefore, improving the water use efficiency and drought-resistance breeding of alfalfa are the keys to increasing alfalfa yield.

The root types of alfalfa that are currently known can be grouped into four types: tap-rooted, branch-rooted, creeping-rooted and rhizomatous-rooted types. The alfalfa root system is the main organ for absorbing soil moisture and nutrients and exploits a non-substitutable role in improving soil macroporosity. Many alfalfa varieties are tap-rooted and the gene sources come from *Medicago sativa* L. Rhizomatous-rooted, branch-rooted, and creeping-rooted alfalfa own the genes of wild *M. falcata* L. to varying degrees, with have strong resistance to drought and severe cold. Previously, numerous studies have focused on crown characteristics (Nan et al., 2012), root development ability (Nan et al., 2014), stress resistance (Nan et al., 2011), root types, and yield (Nan et al., 2012), and rhizosphere microorganisms of different root-type alfalfa (Wang et al., 2023a). However, there were few reports on the root metabolites and phytohormones of different root-type alfalfa under drought stress.

Soil moisture content is a key abiotic factor limiting plant distribution, growth, and development (Raza et al., 2023). Decreasing the rate of growth in plants, accumulating a large number of osmotic stress substances, enhancing the amount of antioxidant enzymes in the tissues, stimulating the production of secondary metabolites, and regulating gene expression have become commonly used under drought stress (Li et al., 2021; Mubarik et al., 2021; Raza et al., 2022; Raza et al., 2023). Previous research on the adaptation mechanisms of alfalfa to water stress has primarily concentrated on the above-ground part (Zhang et al., 2019b; Kang et al., 2023), nevertheless, the root system is critical for plant production (Thorup-Kristensen et al., 2020) and has just recently received more attention (Soba et al., 2019; Zhang et al., 2019a). Since there is close contact between plant roots and soil, they can sense symptoms of water scarcity and adjust their physiology, biochemistry, and structure to respond to the alterations in the surroundings (Raza et al., 2023). Low soil moisture content induces modifications in plant root metabolism at both the macro and micro levels (Raza et al., 2022). The morphology, physiology, and bioprocesses of plants are affected by water scarcity (Li et al., 2021; Mubarik et al., 2021), which can also inhibit the root of the plant absorbing nutrient elements and the regulation of relevant functional and structural genes (Epie et al., 2019).

Metabolites not only control changes in plant phenotype but also serve as a bridge between phenotype and gene relationships (Yang et al., 2019). Metabolomics can reflect changes in metabolites and reveal the reaction mechanisms of plants to stressful conditions, which is a useful technique for studying plant environmental stress (Han et al., 2023). The same is true for secondary metabolites, which are indispensable to plant signaling, defense, and safety (Savoi et al., 2016; Kumar et al., 2021; Nicolas-Espinosa et al., 2023). It has been discovered that plants accumulate more than 2×10^5 secondary metabolites, which serve as essential to their biological growth (Wang et al., 2015; Ma et al., 2016). Furthermore, some primary metabolites (carbohydrates, amino acids, nucleic acids, and organic acids) and several secondary metabolites (alkaloids, phenolics, quinones, flavonoids, and terpenoids) are also closely related to plant adversity resistance (Ma et al., 2016; Tschaplinski et al., 2019). The production of proteins, osmoregulatory and defensive metabolites, and reactive oxygen species-scavenging systems are some of the strategies used by plants to withstand the effects of dryness (Ma et al., 2016; Mubarik et al., 2021), which is an intricate biological mechanism involving various metabolic changes (Wasaya et al., 2021). Compared to controlling genes and other metabolic pathways, metabolites may result in more adjustments in plant response to arid stress and can be more direct targets for strengthening drought tolerance in plants. Long-term insufficient water absorbed in plants caused a noticeable rise in the contents of amino acids, tricarboxylic acid cycle (TCA) metabolites, and secondary metabolites in *Pinus sylvestris* leaves (Ma et al., 2021). Osmotic stressors, such as polyol (mannitol and sorbitol), sugars, and amino acids (proline), accumulated throughout drought and showed notable variations among tea trees with varying drought tolerance (Nyarukowa et al., 2016).

Currently, we have insufficient understanding regarding the relationship between drought resistance and modifications in alfalfa metabolites. Key secondary metabolites such as IAA, GAs, ABA, and cytokinins (CTKs) participate in plant stress regulation (Marquez-Lopez et al., 2019; Raza et al., 2022). Metabolites are the basis of biological phenotype, which can improve our ability to intuitively and efficiently understand biological processes and their mechanisms. The alteration of metabolites is the most important way for plants to respond to stress, which is achieved by regulating the metabolic network and leading to the synthesis and production of certain metabolites. In recent years, mass spectrometry (LC-MS) has been acknowledged as a vital instrument (Tang et al., 2017; Huang et al., 2018; Gao et al., 2019) for the identification of various plant species, allowing the investigation of changes in metabolites due to genetic modifications and the environment (Kumar et al., 2021; Zhang et al., 2021a). In this work, we identify metabolites altered by water scarcity and investigate their participation pathways in more detail. Identifying relevant metabolic networks may help us think more broadly about the drought resistance of these plants and help us comprehend how various root-type alfalfa cope with drought.

2 Materials and methods

2.1 Plant materials and experimental conditions

The alfalfa used in the experiment consisted of rhizomatous-rooted *M. sativa* 'Qingshui' (or QS), tap-rooted *M. sativa* 'Longdong' (or LD), and creeping-rooted *M. varia* 'Gongnong'No. 4 (or GN). Alfalfa seeds that were uniform and plump were selected and disinfected with 5% NaClO and 70% ethanol solution in sequence (20 min) and finally rinsed the remaining solution on the surface of the seeds with distilled water (3 times). Plant the seeds uniformly in

sand-filled pots and grow them in a growth chamber (YSTH-B8-20, ESHENGTAIHE CTRL TECH, China). Growth conditions: 16 h light and 8 h dark cycle, maintain a relative humidity of around 60%, and 450 mol $m^{-2}s^{-1}$ of photosynthetic light flux density from May 10, 2021, to July 26, 2021. The nutrients and water required for alfalfa growth are provided through Hoagland's nutrient solution (1 L Hoagland solution containing 945 mg·L^{-1} $Ca(NO_3)_2{\cdot}4H_2O$, 506 mg·L^{-1} KNO_3, 80 mg·L^{-1} NH_4NO_3, 136 mg·L^{-1} KH_2PO_4, 493 mg·L^{-1} $MgSO_4{\cdot}7H_2O$, 2.78 mg·L^{-1} $FeSO_4{\cdot}7H_2O$, 3.73 mg·L^{-1} EDTA-Na_2, 6.2 mg·L^{-1} HBO_3, 8.6 mg·L^{-1} $ZnSO_4{\cdot}7H_2O$, 0.025 mg·L^{-1} $GuSO_4{\cdot}5H_2O$, 0.83 mg·L^{-1} KI, 22.3 mg·L^{-1} $MnSO_4{\cdot}4H_2O$, 0.25 mg·L^{-1} $Na_2MoO_4{\cdot}2H_2O$, 0.025 mg·L^{-1} $CoCl_2{\cdot}2H_2O$, pH=6), which is watered every two days (Hoagland and Arnon, 1950). When the seedlings reach the two-leaf stage, 20 seedlings with the same growth and uniform distribution should be retained in each pot, for a total of 36 pots.

2.2 Treatment of drought stress

When the average plant height of alfalfa reaches about 40 cm (July 20, 2021), dissolve PEG 6000 in the Hoagland nutrient solution and water each pot to cause osmotic stress in alfalfa. The solution can provide osmotic pressures of 0 MPa (CK, Control), -1.0 MPa (MD, Moderate Drought Stress), and -2.0 MPa (SD, Severe Drought Stress), respectively (Michel and Kaufmann, 1973).

2.3 Sample collection and preservation

After 7 days of stress treatment (July 26, 2021) (Wang et al., 2023a), there was a significant change in leaf morphology, with leaf edges wrinkled and some leaves turning yellow and falling off. Then, to start sample collection, first separate the alfalfa roots from the sand and rinse them with distilled water to absorb the surface moisture. Finally, different repeated root samples of the same treatment were cut and thoroughly mixed, rapidly treated with liquid nitrogen, stored at −80°C, and relevant indicators were measured in the later stage.

2.4 Determining the concentration of phytohormones

① 5 g of the root sample was grounded in 70% chromatography methanol and extracted for 24 h (4°C), repeated the extraction, and merged with the extraction solution (3 times). ② The methanol in the extract was fully evaporated (vacuum conditions), and the residual solution was extracted with ethyl acetate (EA) three times, finally merging the extract and evaporating the EA. ③ The extracts were dissolved again with 70% chromatography methanol (2 mL) and passed through an organic filter (0.22 μm) membrane for the determination of phytohormones by High-Performance Liquid Chromatography (Waters Arc-2998 PDA Waters, Waters Corporation, USA) (Al-Amri, 2021). Test conditions: reversed-phase column (C18); mobile phase A: methanol, mobile phase B: 0.1% phosphorus; pH=3.5, column temperature: 30°C, flow speed: 0.8 mL/min, wavelength: λ GA_3 = 239 nm, λ IAA=255 nm, λ ABA= 208 nm, λ (ZT) = 254 nm.

2.5 Metabolite extraction

① 100 mg of liquid nitrogen-milled samples, put them in 2.0 mL tubes, and add 500 μL of 80% methanol; ② vortex and shake, let it take an ice bath (5 min), and centrifuge it at 12000 rcf (4°C, 20 min); ③ take the supernatant and dilute it with ultrapure water to a methanol content of 53%; ④ collect the supernatant (12000 rcf, 4°C, 20 min), and analyzed by LC-MS (Kumar et al., 2021). Chromatographic conditions: chromatographic column-HypesilGoldcolumn (C18), column temperature: 40°C, flow rate: 0.2 mL/min; mobile phase A: 0.1% formic acid, mobile phase B: methanol; pH 9.0. UHPLC-MS/MS analyses were performed using a Vanquish UHPLC system (Thermo Fisher, Germany).

2.6 Statistical analysis

The detected metabolites were annotated using the KEGG (https://www.genome.jp/kegg/pathway.html). The metabolomics data was processed using the software metaX (Wen et al., 2017) and subjected to principal component analysis (PCA) and partial least squares discriminant analysis (PLS-DA). Calculated the statistical significance (*P*-value) based on the *t*-test and the multiplicity of different Fold Change (FC) of two groups. Criteria for screening: VIP > 1, $P < 0.05$, and FC ≥ 2.

3 Results

3.1 Metabolomic data quality assessment

The higher the correlation of Quality Control (QC) samples (R^2 closer to 1) indicates higher the quality of the obtained raw data. Every sample has an R^2 value above 0.97, which is extremely close to 1 (Figure 1A), indicating that the data are reliable. The six sets of samples from the same experimental treatments under different water stresses clustered together, demonstrating powerful repeatability among the experimental treatments (Figure 1B). Partial Least Squares Discrimination Analysis (PLS-DA) was performed to identify the metabolites that responded to drought stress. R2 and Q2 of each treatment were close to 1, which indicated that the date is robust and accurate, and the subsequent analysis may be performed (Figure 1C).

3.2 Principal component analysis

Drought stress causes significant changes in the metabolic products of three types of root-type alfalfa. The PC1 of QS, LD, and GN (68.04%, 78.62%, and 74.29%) significantly separated the control treatment (CK) from severe drought (SD) (Figure 2). On the score map, individual samples were remarkably far off from one

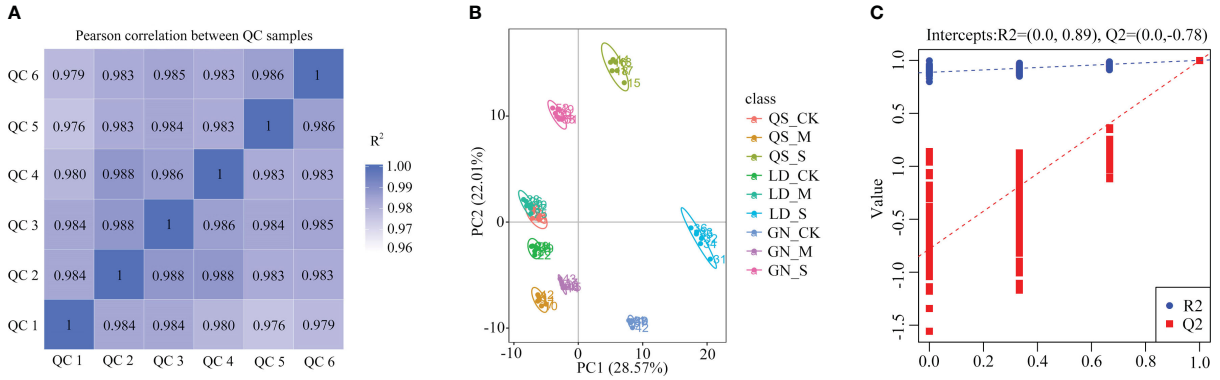

FIGURE 1
Sample correlation analysis **(A)**, sample PCA analysis **(B)** and PLS-DA model plots **(C)**. QC, Quality Control. PC, Principal component. Partial Least Squares Discrimination Analysis (PLS-DA) is a supervised statistical method for discriminant analysis, the method uses partial least squares regression to model the relationship between tabolite expression and sample category to achieve the prediction of sample category, the PLS-DA model of each comparison group was established, and the model evaluation parameters (R2, Q2) obtained by 7-fold cross-validation (seven cycles of crossvalidation, when the number of biological replicates of the samples n<=3, it is k cycles of cross-validation, k=2n), if R2 and Q2 are closer to 1, it indicates that the model is more stable and reliable. QS, rhizomatous-rooted *Medicago sativa* 'Qingshui'; LD, tap-rooted *M. sativa* 'Longdong'; GN, creeping-rooted *M.varia* Martin 'Gongnong No.4'. CK, Control; M, Medium stress; S, Severe stress.

another, indicating obvious variations between samples but not between groups. The PC1 of LD and GN root metabolism in response to drought was more than the variance contribution of QS, demonstrating that the metabolic changes in LD and GN were more significant compared to those in QS under water deficit stress.

3.3 Screening of differentially expressed metabolites

Combining the *t*-test and the PLS-DA method (VIP value) to screen for DEMs. An amount of 796 metabolites were found in three root-type alfalfa under drought conditions (Figure 3). QS, LD, and GN were found to have 265, 333, and 292 DEMs compared to each CK treatment under SD stress. There were 164, 270, and 68 upregulated DEMs, and 101, 63, and 224 downregulated DEMs, respectively. The majority of DEMs were upregulated in QS and LD, which accounted for 61.89% and 81.08% of the total number of metabolites. LD had a greater number of DEMs upregulated as compared to QS and GN. The number of DEMs unique to QS, LD, and GN were 26, 18, and 22 at various degrees of water stress, respectively (Figure 4). The three root-type alfalfa shared 18 species of DEMs under SD stress (Figure 4D), whereas LD and GN had much more special metabolites than QS, with 152, 131, and 103, respectively. This suggests that QS has an excellent ability to adapt to water deficits and drought-stress conditions with less metabolite modification.

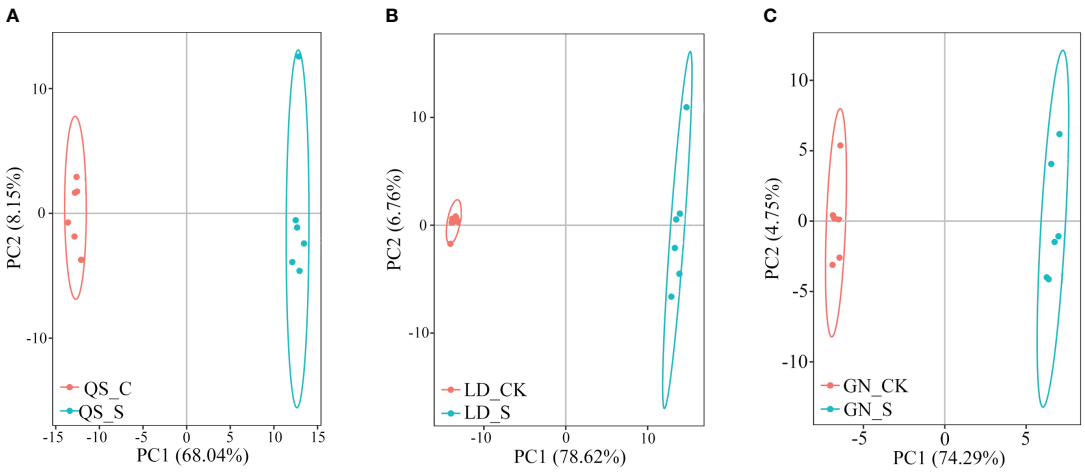

FIGURE 2
Principal component analysis of samples of QS **(A)**, LD **(B)** and GN **(C)** alfalfa under severe stress compared to CK. PC1, Principal component 1; PC2, Principal component 2. QS, rhizomatous-rooted *Medicago sativa* 'Qingshui'; LD, tap-rooted *M. sativa* 'Longdong'; GN, creeping rooted *M.varia* Martin 'Gongnong No.4'. CK, Control; S, Severe stress.

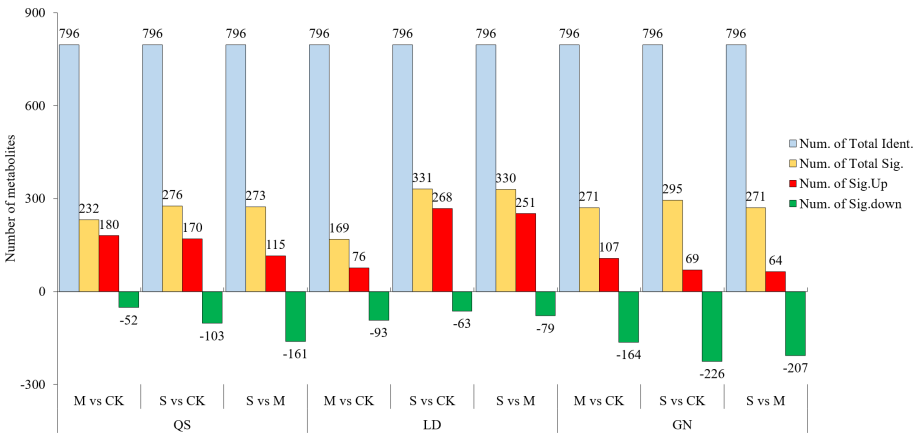

FIGURE 3
Metabolite statistics of QS, LD and GN alfalfa under drought stress. QS, rhizomatous-rooted *Medicago sativa* 'Qingshui'; LD, tap-rooted *M.sativa* 'Longdong'; GN, creeping-rooted *M.varia* Martin 'Gongnong No.4'. CK, Control; M, Medium stress; S, Severe stress.

3.4 Analysis of differential metabolites

The top 20 (upregulated and downregulated) DEMs from the Fold Change (FC) plots of QS, LD, and GN (Figure 5). Illustrate that the metabolites changed dramatically to response aridity coercing and that the same metabolites are present in three root-type alfalfa simultaneously. For instance, metabolite codenames (Com) Com_1614 and Com_2511 simultaneously appeared in QS and GN and all of them showed an upregulated trend. Among the downregulated metabolites Com_739 and Com_2509 simultaneously appeared in QS and GN. As an example, Com_1720, Com_1323, Com_2087, and Com_659 were upregulated in LD alfalfa, while the opposite was true in the GN. This showed that the same varieties of metabolites play various metabolic roles in different alfalfa varieties.

3.5 Functional annotation and enrichment analysis of the differential metabolite KEGG

According to the KEGG database (Figure 6; Table 1), Based on the *P*-value of metabolic pathways, select the top three significantly enriched metabolic pathways in three root types of alfalfa. QS, LD, and GN have 35, 38, and 34 differential metabolites annotated into the first three metabolic pathways, respectively. DEMs (13) including 6-gingero, SA, IAA, GA_4, ABA, and others were dramatically enriched of stilbenoid-diarylheptanoid gingerol biosynthesis (SDG) ($P \leq 0.04$), PST ($P \leq 0.05$), and phenylalanine metabolism (PM) ($P \leq 0.10$) under SD stress in QS (Table 1). The DEMs (15) of sucrose, L-phenylalanine, galacturonic acid, IAA, GA_4, ABA, and others were discovered of ABC-transporters ($P \leq 0.01$), PST ($P \leq 0.06$), and galactose metabolism (GM) ($P \leq 0.13$) in LD (Table 1). The *P*-values of the SDG, PST, and ABC-transporters metabolic pathways in QS and LD were all less than 0.05, indicating that they play a crucial role in the resistance of both alfalfa varieties to drought stress. DEMs (15) including SA, L-tyrosine, L-phenylalanine, succinic acid, and others significantly annotated in GN's metabolic pathways of PM ($P \leq 0.03$), glucosinolate biosynthesis ($P \leq 0.04$), and nicotinate-nicotinamide metabolism ($P \leq 0.10$) (Table 1). The *P*-values of PM and glucose biosynthesis metabolic pathways are both less than 0.05, indicating that they are key metabolic pathways for GN

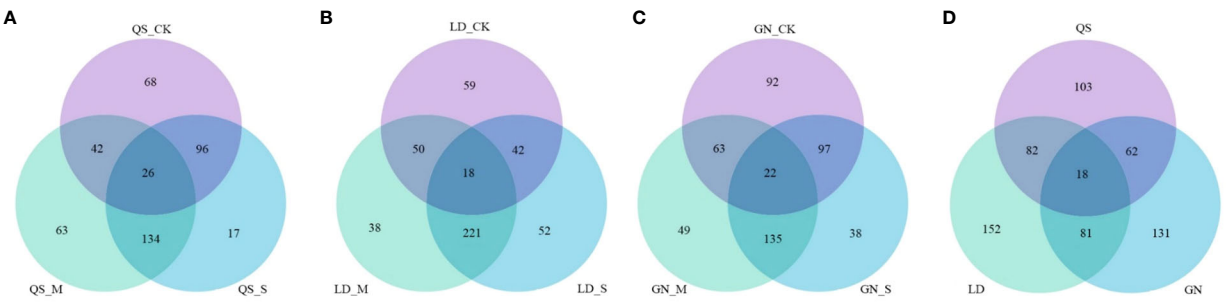

FIGURE 4
Venn plot of differential metabolites unique to QS **(A)**, LD **(B)**, and GN **(C)** and coexisting metabolites **(D)** among the three root types of alfalfa after drought stress. QS, rhizomatous-rooted *Medicago sativa* 'Qingshui'; LD, tap-rooted *M.sativa* 'Longdong'; GN, creeping-rooted *M.varia* Martin 'Gongnong No.4'. CK, Control; M, Medium stress; S, Severe stress.

10.3389/fpls.2024.1341826

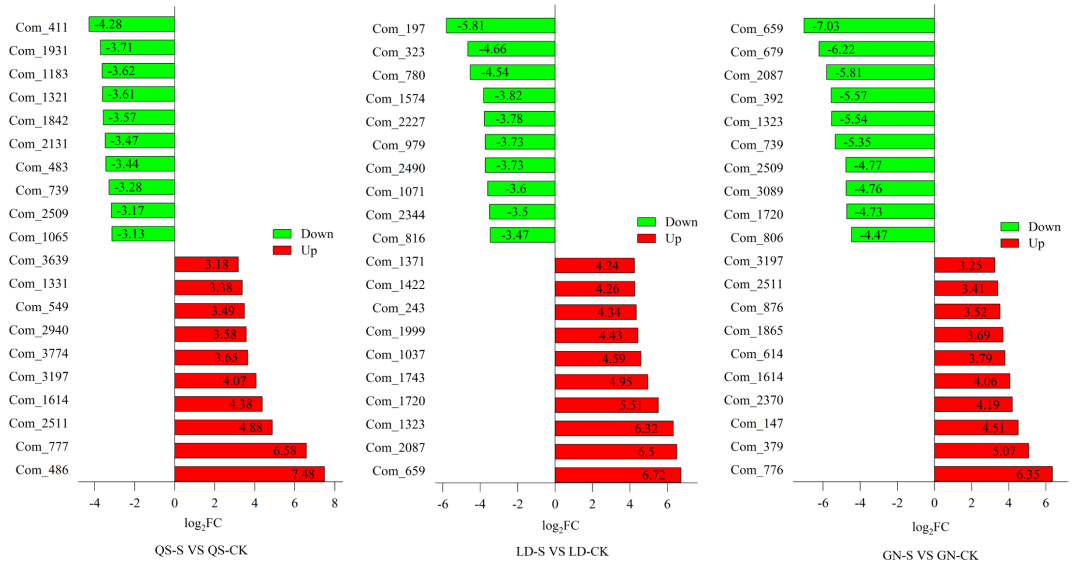

FIGURE 5
Major metabolite statistics for QS, LD and GN alfalfa top 10 after severe drought stress. FC, Fold Change. QS, rhizomatous-rooted *Medicago sativa* 'Qingshui'; LD, tap-rooted *M. sativa* 'Longdong'; GN, creeping rooted *M.varia* Martin 'Gongnong No.4'. CK, Control; M, Medium stress; S, Severe stress.

alfalfa to cope with drought-stress environments. This shows that coping with water deficit stress is closely tied to these metabolic pathways and metabolites, especially the remarkably enriched ABA and SA in three root-type alfalfa, demonstrating that they are crucial to how alfalfa responds to drought.

The top 10 metabolic pathways in QS, LD, and GN were annotated for 28, 31, and 36 metabolites, respectively, and the metabolic pathways mainly classification were SDG, PST, ABC transporters, GM, PM, nicotinate-nicotinamide metabolism (NM) (Figure 7). Up-regulated metabolites account for 28.57%, 83.87%, and 5.6% of the total metabolites, respectively, mainly distributed in the metabolic pathways of tryptophan metabolism (TM), SDG, lysine degradation, starch-sucrose metabolism (SM), PST, and PM (Table 2). The fact that the DEMs annotated in LD and GN are much more abundant than QS alfalfa reveals that QS alfalfa can withstand drought stress with fewer metabolite changes.

3.6 Effects of drought stress on phytohormone contents in alfalfa root

Except for ABA, IAA, GA_3, and ZT, all tended to decrease as the degree of stress increased (Figure 8). The IAA, GA_3, and ZT contents of QS, LD, and GN were considerably lower than those of CK under SD stress, with QS decreasing by 54.13%, 72.76%, and 68.76%; LD decreased by 40.37%, 65.78%, and 58.89%; GN decreased by 80.94%, 81.77%, and 71.14%, respectively. The fact that QS and LD experienced less decline than GN states clearly that they were more drought-resistant and drought-tolerant than GN. The levels of ABA in the three varieties of alfalfa roots exhibited an increasing trend with increasing stress, rising by 177.87%, 75.25%, and 208.89%, respectively. When compared to GN, QS and LD showed lower increases, which demonstrates that they were more capable of enduring the stress of drought than GN.

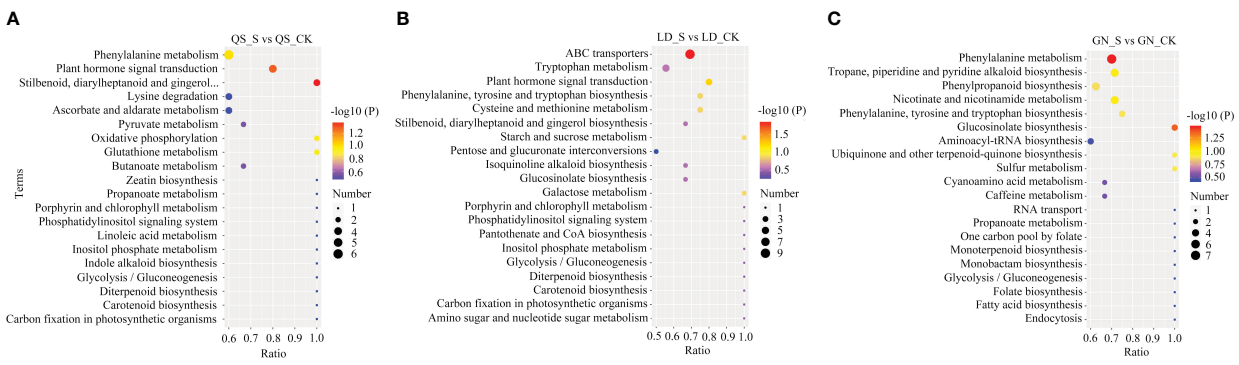

FIGURE 6
KEGG analysis of major metabolic pathways in QS **(A)**, LD **(B)**, and GN **(C)** alfalfa after severe drought stress. QS, rhizomatous-rooted *Medicago sativa* 'Qingshui'; LD, tap-rooted *M.sativa* 'Longdong'; GN, creeping rooted *M.varia* Martin 'Gongnong No.4'. CK, Control; M, Medium stress; S, Severe stress.

TABLE 1 The number of metabolites and metabolic pathways to the top 3.

	Metabolic pathway	*P*	Metabolites
QS	stilbenoid-diarylheptanoid and gingerol biosynthesis	0.04	6-gingerol, piceatannol, chlorogenic acid
	plant hormone signal transduction	0.05	salicylic acid, indole-3-acetic acid, gibberellin A_4, abscisic acid
	phenylalanine metabolism	0.10	salicylic acid, succinic acid, 3-hydroxyphenylacetic acid, trans-cinnamic acid, phenylacetaldehyde, fumaric acid
LD	ABC transporters	0.01	sucrose, L-phenylalanine, galacturonic acid, biotin, betaine, L-cystine, inositol, glutathione
	plant hormone signal transduction	0.06	indole-3-acetic acid, gibberellin A_4, abscisic acid, jasmonic acid
	galactose metabolism	0.13	sucrose, inositol
GN	phenylalanine metabolism	0.03	salicylic acid, L-tyrosine, L-phenylalanine, succinic acid, hippuric acid, trans-cinnamic acid, phenylacetaldehyde
	glucosinolate biosynthesis	0.04	L-tyrosine, L-phenylalanine, methionine
	nicotinate and nicotinamide metabolism	0.10	nicotinuric acid, succinic acid, 1-methylnicotinamide, quinolinic acid

QS, rhizomatous-rooted *Medicago sativa* 'Qingshui'; LD, tap-rooted *M. sativa* 'Longdong'; GN, creeping-rooted *M.varia* Martin 'Gongnong No.4'.

4 Discussion

Osmoregulation is one of the strategies for plants to cope with water deficit stress (Wasaya et al., 2021). High sucrose and sugar alcohol accumulation enhanced plant tolerance and contributed to scavenging free radicals generated by aridity stress (Skalska et al., 2021). The glycolysis or gluconeogenesis pathways were measurably enriched in QS, LD, and GN under SD stress in this study, and arbutin as a natural antioxidant was involved in these pathways were all upregulated, the results show that these pathways are crucial for water deficit. SA, succinic acid, 3-hydroxyphenylacetic acid, trans-cinnamic acid, phenylacetaldehyde, and fumaric acid of QS and GN were all down-regulated in the PM pathway, and one study found that the accumulation of organic acids improves the capacity of *Plumeria rubra* to withstand water shortage conditions (Sun et al., 2023). Research has found that the increase in ABA content under drought stress inhibits the expression of *GmPAL1*, which is the first rate-limiting enzyme encoding the PM pathway, thereby affecting downstream products such as SA and flavonoids (La et al., 2023). SA serves as a signaling molecule to control gene expression to affect physiological properties (Gilani et al., 2020) and enhance the drought resistance of plants (Mubarik et al., 2021; Raza et al., 2023). Succinic acid is a critically important component of the TCA in plants, which can affect their respiration rates and increase their tolerance (Yue et al., 2018; Hijaz and Killiny, 2019), its significant enrichment in QS and GN indicates a positive effect on drought response.

In the phenylalanine-tyrosine and tryptophan biosynthesis pathway, the metabolites of L-phenylalanine, erythrose-4-phosphate, L-tyrosine, and indole were altered but enriched in LD and GN in opposite ways, suggesting that the pathway responds to drought stress in different ways. It was found that tea apoptosis induces high expression of genes related to the synthesis of endogenous hormones, thus affecting changes in their contents (ABA, JA, SA), and that ABA regulates phenylalanine, tyrosine, and tryptophan biosynthesis and phenylalanine metabolism by affecting theanine (Xu et al., 2020). This indicates that changes in ABA levels are in correlation with metabolic pathways, have the ability to control metabolic pathways, and may have an impact on the production of related metabolites. Inositol, the primary metabolite of QS and LD, was decreased significantly during the process of the inositol phosphate metabolism and the phosphoinositide signaling pathway, which mainly manifested as response and adaptation to abiotic stimuli such as cold and arid conditions (Tan et al., 2013). Other studies have found that SA stimulates the expression of genes involved in phosphatidylinositol synthesis in *Arabidopsis*, hence affecting inositol production (Gulabani et al., 2022).

Amino acids are essential osmoregulators for plants under abiotic stress. Research has shown that amino acids can induce stomatal closure and reduce water evaporation under drought stress (Sakata et al., 2023). The tryptophan metabolic pathway was dramatically enriched in LD in this study. Tryptophan and isoleucine indicated that significantly increase with water deficit stress (Ignjatovic-Micic et al., 2015; Kong et al., 2022). However, it has also been demonstrated that only drought-tolerant cultivars have higher tryptophan levels (Bao et al., 2023), and tryptophan metabolites can enhance plant stress resistance under adverse conditions (Hasnain et al., 2023). ABC transporter proteins have certain drought-resistant capabilities under drought stress and provide triacylglycerol to glycerol kinase (Han et al., 2022), which then stimulates the synthesis of sucrose (Sharma and Nayyar, 2014). The accumulation of linoleic acid content can promote the oxidation of fatty acids, and its oxidation products can provide energy for plant growth and enhance the ability of stress tolerance in plants (Goepfert and Poirier, 2007).

Phytohormone content in plants is significantly altered by drought stress due to its impact on phytohormone metabolism (Ghafari et al., 2020; Talaat, 2023). The PST pathway responds simultaneously to water deficit stress in three alfalfa varieties, and there is a close correlation between hormone synthesis and metabolic pathways (Wang et al., 2023b). The trend of IAA and GA_4 is contrary to the enrichment tendency shown by the metabolites of SA and jasmonic acid (JA) in the PST pathway. IAA can promote cell division, elongation, differentiation, and the formation of new organs (Shani et al., 2017), as well as enhance plant adaptability to abiotic stresses by maintaining antioxidant enzyme activity in plant cells (Khan et al., 2021). Reduced IAA levels due to drought stress restrict plant growth. Reduced GA_4 content can improve plant drought resistance (Kang et al., 2011). The growth-promoting hormones of IAA, GA_3, and ZT with low content can slow down

10.3389/fpls.2024.1341826

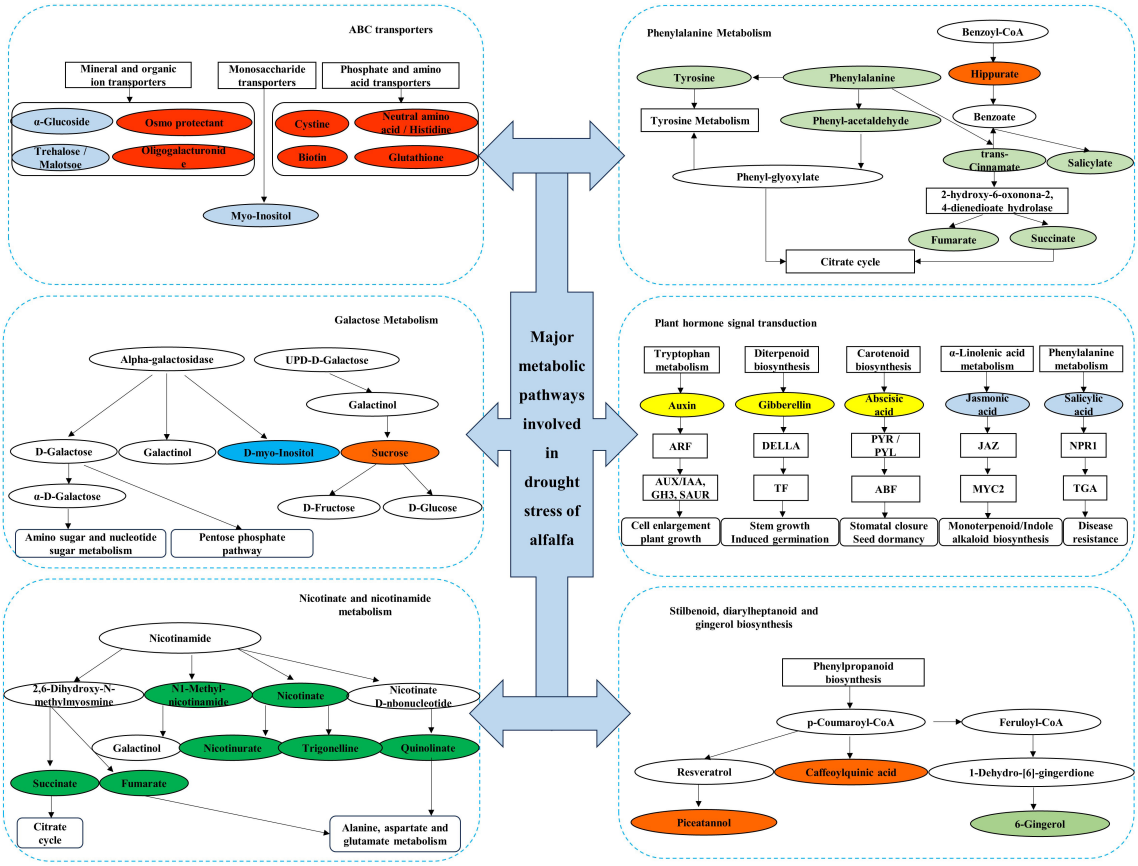

FIGURE 7
Major metabolic pathways involved in drought stress of alfalfa. Boxes in the figure indicate metabolic pathways annotated to drought stress, and ellipses indicate metabolites annotated to drought stress. Green ellipses indicate metabolites down-regulated under relatively severe drought stress in QS and GN, and orange indicates metabolites up-regulated under relatively severe drought stress in the GN; yellow indicates metabolites upregulated under relatively severe drought stress in LD and QS, and light blue indicates metabolites down-regulated under relatively severe drought stress in LD and QS; blue indicates metabolites down-regulated under relatively severe drought stress in LD, and red indicates metabolites upregulated under relatively severe drought stress in LD; and dark green indicates metabolites downregulated under relatively severe drought stress in the GN. QS, rhizomatous-rooted *Medicago sativa* 'Qingshui'; LD, tap-rooted *M.sativa* 'Longdong'; GN, creeping rooted *M.varia* Martin 'Gongnong No.4'. CK, Control; M, Medium stress; S, Severe stress.

TABLE 2 Number of metabolic pathways annotated to differential metabolites.

Number	Metabolic pathway	Number/species of annotated differential metabolites obtained		
		QS	LD	GN
1	ubiquinone and other terpenoid-quinone biosynthesis	0	0	2
2	tryptophan metabolism	0	5	0
3	tropane, piperidine and pyridine alkaloid biosynthesis	0	0	5
4	Sulfur metabolism	0	0	2
5	stilbenoid, diarylheptanoid and gingerol biosynthesis	3	2	0
6	starch and sucrose metabolism	0	2	0
7	propanoate metabolism	2	0	0
8	plant hormone signal transduction	4	4	0
9	phenylalanine biosynthesis	0	0	5

(Continued)

TABLE 2 Continued

Number	Metabolic pathway	Number/species of annotated differential metabolites obtained		
		QS	LD	GN
10	phenylalanine, tyrosine and tryptophan biosynthesis	0	3	3
11	phenylalanine metabolism	6	0	7
12	oxidative phosphorylation	2	0	0
13	nicotinate and nicotinamide metabolism	0	0	5
14	lysine degradation	3	0	0
15	isoquinoline alkaloid biosynthesis	0	2	0
16	glycolysis/gluconeogenesis	1	0	0
17	glutathione metabolism	2	0	0
18	glucosinolate biosynthesis	0	2	3
19	galactose metabolism	0	2	0
20	cyanoamino acid metabolism	0	0	2
21	caffeine metabolism	0	0	2
22	butanoate metabolism	2	0	0
23	ascorbate and aldarate metabolism	3	0	0
24	ABC transporters	0	9	0
Total	total number of differential metabolites annotated	28	31	36
	total number of metabolic pathways annotated	10	9	10

QS, rhizomatous-rooted *Medicago sativa* 'Qingshui'; LD, tap-rooted *M.sativa* 'Longdong'; GN, creeping-rooted *M.varia* Martin 'Gongnong No.4'.

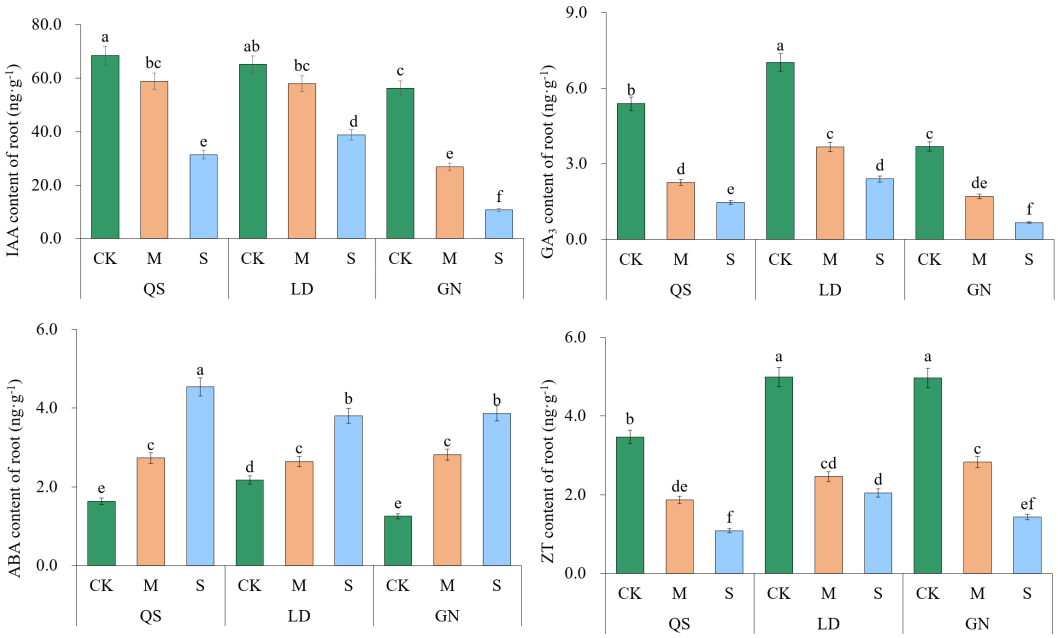

FIGURE 8
Effect of root endogenous hormone contents of alfalfa under drought stress. Different lowercase letters between treatments indicate significant differences ($P<0.05$). QS, rhizomatous-rooted *Medicago sativa* 'Qingshui'; LD, tap-rooted *M. sativa* 'Longdong'; GN, creeping-rooted *M.varia* Martin'Gongnong No.4'. CK, Control; M, Medium stress; S, Severe stress.

plant growth to cope with water deficit. The inhibition hormone of ABA with high content can promote stomatal closure to reduce transpiration loss and promote root water absorption to improve the ability of drought resistance (Zhang et al., 2021b). ABA maintains the growth of the root system under water deficit conditions (Zhang et al., 2020) and promotes the transportation of assimilates to the reservoir (Chen et al., 2020; Zhang et al., 2021b), additionally, phytohormones crosstalk with each other to improve resistance to environment stress (Raza et al., 2023). In this research, the content of three growth-promoting hormones in alfalfa tends to decrease, revealing that the growth is limited by drought. In contrast, the content of growth-inhibiting hormone (ABA) increased with the intensification of drought stress in three root types of alfalfa, which further confirms that ABA can improve plant adaptability to drought stress.

5 Conclusions

Drought stress affects the metabolic pathways and changes in metabolites in alfalfa roots. The main metabolic pathways in three root-type alfalfa are SDG, PST, ABC transporters, PM, NM, and GM. For QS, LD, and GN, the metabolites include amino acids, organic acids, sugars, and alkaloids, mainly involved in osmotic pressure regulation, signal transduction, and ABC transporter proteins. With increasing drought stress, the levels of IAA, GA_3, and ZT were decreased, while ABA content increased in roots. Overall, QS and LD had more resistance than GN under drought stress.

Data availability statement

The raw data supporting the conclusions of this article will be made available by the authors, without undue reservation.

Author contributions

KW: Writing – original draft. LN: Methodology, Writing – review & editing, Data curation. JX: Data curation, Writing – review & editing. SW: Formal analysis, Writing – review & editing. LY: Software, Writing – review & editing.

Funding

The author(s) declare financial support was received for the research, authorship, and/or publication of this article. This work was supported by the National Natural Science Foundation of China (Nos. 32160327), the China Forage and Grass Research System (Nos. CARS-34) and the “Innovation Star” project for outstanding postgraduates in Gansu Province (2023CXZX-624).

Conflict of interest

The authors declare that the research was conducted in the absence of any commercial or financial relationships that could be construed as a potential conflict of interest.

Publisher’s note

All claims expressed in this article are solely those of the authors and do not necessarily represent those of their affiliated organizations, or those of the publisher, the editors and the reviewers. Any product that may be evaluated in this article, or claim that may be made by its manufacturer, is not guaranteed or endorsed by the publisher.

References

Al-Amri, S. M. (2021). Response of growth, essential oil composition, endogenous hormones and microbial activity of mentha piperita to some organic and biofertilizers agents. *Saudi J. Biol. Sci.* 28, 5435–5441. doi: 10.1016/j.sjbs.2021.06.094

Bao, J. B., Liu, Z. Y., Ding, Z. J., Yisilam, G., Wang, Q. Y., and Tian, X. M. (2023). Metabolomic analysis reveals key metabolites and metabolic pathways in under salt and drought stress. *Funct. Plant Biol.* 50, 701–711. doi: 10.1071/Fp23049

Chen, K., Li, G. J., Bressan, R. A., Song, C. P., Zhu, J. K., and Zhao, Y. (2020). Abscisic acid dynamics, signaling, and functions in plants. *J. Integr. Plant Biol.* 62, 25–54. doi: 10.1111/jipb.12899

Epie, K. E., Etesami, M., and Ondoua, R. N. (2019). Characterization and selection for phosphorus deficiency tolerance in 99 spring wheat genotypes in Montana. *J. Plant Nutr.* 42, 595–603. doi: 10.1080/01904167.2019.1567783

Gao, W., Liu, K., Wang, R., Liu, X. G., Li, X. S., Li, P., et al. (2019). Integration of targeted metabolite profiling and sequential optimization method for discovery of chemical marker combination to identify the closely-related plant species. *Phytomedicine* 61, 152829. doi: 10.1016/j.phymed.2019.152829

Ghafari, H., Hassanpour, H., Jafari, M., and Besharat, S. (2020). Physiological, biochemical and gene-expressional responses to water deficit in apple subjected to partial root-zone drying (PRD). *Plant Physiol. Bioch* 148, 333–346. doi: 10.1016/j.plaphy.2020.01.034

Gilani, M., Danish, S., Ahmed, N., Rahi, A. A., Akrem, A., Younis, U., et al. (2020). Mitigation of drought stress in spinach using individual and combined applications of salicylic acid and potassium. *Pak J. Bot.* 52, 1505–1513. doi: 10.30848/Pjb2020-5(18

Goepfert, S., and Poirier, Y. (2007). β-Oxidation in fatty acid degradation and beyond. *Curr. Opin. Plant Biol.* 10, 245–251. doi: 10.1016/j.pbi.2007.04.007

Gulabani, H., Goswami, K., Walia, Y., Roy, A., Noor, J. J., Ingole, K. D., et al. (2022). *Arabidopsis* inositol polyphosphate kinases IPK1 and ITPK1 modulate crosstalk between SA-dependent immunity and phosphate-starvation responses. *Plant Cell Rep.* 41, 347–363. doi: 10.1007/s00299-021-02812-3

Han, B., Wang, F. J., Liu, Z. L., Chen, L., Yue, D. D., Sun, W. N., et al. (2022). Transcriptome and metabolome profiling of interspecific CSSLs reveals general and specific mechanisms of drought resistance in cotton. *Theor. Appl. Genet.* 135, 3375–3391. doi: 10.1007/s00122-022-04174-0

Han, W. Y., Ward, J. L., Kong, Y. Z., and Li, X. (2023). Targeted and untargeted metabolomics for the evaluation of plant metabolites in response to the environment. *Front. Plant Sci.* 14. doi: 10.3389/fpls.2023.1167513

Hasnain, Z., Zafar, S., Usman, S., Zhang, L. H., and Elansary, H. O. (2023). Elucidating role of melatonin foliar spray in ameliorating adverse effects of drought stress on growth and physio-biochemical attributes of Brassica rapa plants. *Sci. Hortic-Amsterdam* 321, 112336. doi: 10.1016/j.scienta.2023.112336

Hijaz, F., and Killiny, N. (2019). Exogenous GABA is quickly metabolized to succinic acid and fed into the plant TCA cycle. *Plant Signal Behav.* 14, e1573096. doi: 10.1080/15592324.2019.1573096

Hoagland, D. R., and Arnon, D. I. (1950). The water-culture method for growing plants without soil. *Calif Agric. Exp. Station Circ.* 347, 357–359. doi: 10.1016/S0140-6736(00)73482-9

Huang, B. M., Zha, Q. L., Chen, T. B., Xiao, S. Y., Xie, Y., Luo, P., et al. (2018). Discovery of markers for discriminating the age of cultivated ginseng by using UHPLC-QTOF/MS coupled with OPLS-DA. *Phytomedicine* 45, 8–17. doi: 10.1016/j.phymed.2018.03.011

Ignjatovic-Micic, D., Vancetovic, J., Trbovic, D., Dumanovic, Z., Kostadinovic, M., and Bozinovic, S. (2015). Grain nutrient composition of maize (*Zea mays* L.) drought-tolerant populations. *J. Agr Food Chem.* 63, 1251–1260. doi: 10.1021/jf504301u

Kang, H. G., Kim, J., Kim, B., Jeong, H., Choi, S. H., Kim, E. K., et al. (2011). Overexpression of *FTL1/DDF1*, an *AP2* transcription factor, enhances tolerance to cold, drought, and heat stresses in *Arabidopsis thaliana*. *Plant Sci.* 180, 634–641. doi: 10.1016/j.plantsci.2011.01.002

Kang, Y., Seminario, A., Udvardi, M., and Annicchiarico, P. (2023). Physiological and biochemical adaptive traits support the specific breeding of alfalfa (*Medicago sativa*) for severely drought-stressed or moisture-favourable environments. *J. Agron. Crop Sci.* 209, 132–143. doi: 10.1111/jac.12600

Khan, R., Ma, X., Zhang, J., Wu, X., Iqbal, A., Wu, Y., et al. (2021). Circular drought-hardening confers drought tolerance via modulation of the antioxidant defense system, osmoregulation, and gene expression in tobacco. *Physiol. Plant* 172, 1073–1088. doi: 10.1111/ppl.13402

Kong, X. G., Guo, Z., Yao, Y., Xia, L. C., Liu, R. X., Song, H. F., et al. (2022). Acetic acid alters rhizosphere microbes and metabolic composition to improve willows drought resistance. *Sci. Total Environ.* 844, 157132. doi: 10.1016/j.scitotenv.2022.157132

Kumar, M., Patel, M. K., Kumar, N., Bajpai, A. B., and Siddique, K. H. M. (2021). Metabolomics and molecular approaches reveal drought stress tolerance in plants. *Int. J. Mol. Sci.* 22, 9108. doi: 10.3390/ijms22179108

La, V. H., Tran, D. H., Han, V. C., Nguyen, T. D., Duong, V. C., Nguyen, V. H., et al. (2023). Drought stress-responsive abscisic acid and salicylic acid crosstalk with the phenylpropanoid pathway in soybean seeds. *Physiol. Plantarum* 175, e14050. doi: 10.1111/ppl.14050

Li, S., Nie, Z. N., Sun, J., Li, X. L., and Yang, G. F. (2022). The physiological role of abscisic acid in regulating root system architecture of alfalfa in its adaptation to water deficit. *Agronomy-Basel* 12, 1882–1899. doi: 10.3390/agronomy12081882

Li, M. F., Yang, Y., Raza, A., Yin, S. S., Wang, H., Zhang, Y. T., et al. (2021). Heterologous expression of *Arabidopsis* thaliana rty gene in strawberry (*Fragaria* × *ananassa* Duch.) improves drought tolerance. *BMC Plant Biol.* 21, 57–77. doi: 10.1186/s12870-021-02839-4

Ma, X. S., Xia, H., Liu, Y. H., Wei, H. B., Zheng, X. G., Song, C. Z., et al. (2016). Transcriptomic and metabolomic studies disclose key metabolism pathways contributing to well-maintained photosynthesis under the drought and the consequent drought-tolerance in rice. *Front. Plant Sci.* 7. doi: 10.3389/fpls.2016.01886

Ma, Q. L., Xu, X., Xie, Y. Z., Huang, T., Wang, W. J., Zhao, L. J., et al. (2021). Comparative metabolomic analysis of the metabolism pathways under drought stress in alfalfa leaves. *Environ. Exp. Bot.* 168, 531–546. doi: 10.1016/j.envexpbot.2020.104329

Marquez-Lopez, R. E., Quintana-Escobar, A. O., and Loyola-Vargas, V. M. (2019). Cytokinins, the Cinderella of plant growth regulators. *Phytochem. Rev.* 18, 1387–1408. doi: 10.1007/s11101-019-09656-6

Michel, B. E., and Kaufmann, M. R. (1973). The osmotic potential of polyethylene glycol 6000. *Plant Physiol.* 51, 914–916. doi: 10.1104/pp.51.5.914

Mubarik, M. S., Khan, S. H., Sajjad, M., Raza, A., Hafeez, M. B., Yasmeen, T., et al. (2021). A manipulative interplay between positive and negative regulators of phytohormones: A way forward for improving drought tolerance in plants. *Physiol. Plantarum* 172, 1269–1290. doi: 10.1111/ppl.13325

Nan, L. L., Nie, Z. N., Zollinger, R., and Guo, Q. E. (2019). Evaluation of morphological and production characteristics and nutritive value of 47 lucerne cultivars/lines in temperate Australia. *Plant Production Sci.* 22, 490–500. doi: 10.1080/1343943x.2019.1608835

Nan, L. L., Shi, S. L., Chen, J. G., Zhu, X. Q., Guo, Q. E., and Zhao, W. H. (2011). Responses and cold-resistance evaluations of different root types of alfalfa in the field during overwintering period. *Chin. J. Eco-Agriculture* 19, 619–625. doi: 10.3724/SP.J.1011.2011.00619

Nan, L. L., Shi, S. L., Guo, Q. E., Tian, F., and Fan, J. J. (2012). Analysis of dynamic variations in crown characteristics of different root-type alfalfa plants. *Chin. J. Eco-Agriculture* 20, 914–920. doi: 10.3724/SP.J.1011.2012.00914

Nan, L. L., Shi, S. L., and Zhang, J. H. (2014). Study on root system development ability of different root-type alfalfa. *Acta Prataculturae Sin.* 23, 117–124. doi: 10.11686/cyxb20140214

Nicolas-Espinosa, J., Garcia-Ibañez, P., Lopez-Zaplana, A., Yepes-Molina, L., Albaladejo-Marico, L., and Carvajal, M. (2023). Confronting secondary metabolites with water uptake and transport in plants under abiotic stress. *Int. J. Mol. Sci.* 24, 2826. doi: 10.3390/ijms24032826

Nyarukowa, C., Koech, R., Loots, T., and Apostolides, Z. (2016). SWAPDT: a method for shorttime withering assessment of probability for drought tolerance in Camellia sinensis validated by targeted metabolomics. *J. Plant Physiol.* 198, 39–48. doi: 10.1016/j.jplph.2016.04.004

Raza, A., Mubarik, M. S., Sharif, R., Habib, M., Jabeen, W., Zhang, C., et al. (2023). Developing drought-smart, ready-to-grow future crops. *Plant Genome-Us* 16, e20279. doi: 10.1002/tpg2.20279

Raza, A., Salehi, H., Rahman, M. A., Zahid, Z., Haghjou, M. M., Najafi-Kakavand, S., et al. (2022). Plant hormones and neurotransmitter interactions mediate antioxidant defenses under induced oxidative stress in plants. *Front. Plant Sci.* 13. doi: 10.3389/fpls.2022.961872

Sakata, N., Ino, T., Hayashi, C., Ishiga, T., and Ishiga, Y. (2023). Controlling stomatal aperture, a potential strategy for managing plant bacterial disease. *Plant Sci.* 327, 111534. doi: 10.1016/j.plantsci.2022.111534

Savoi, S., Wong, D. C. J., Arapitsas, P., Miculan, M., Bucchetti, B., Peterlunger, E., et al. (2016). Transcriptome and metabolite profiling reveals that prolonged drought modulates the phenylpropanoid and terpenoid pathway in white grapes (*Vitis vinifera* L.). *BMC Plant Biol.* 16, 67–84. doi: 10.1186/s12870-016-0760-1

Shani, E., Salehin, M., Zhang, Y., Sanchez, S. E., Doherty, C., Wang, R., et al. (2017). Plant stress tolerance requires auxin-sensitive Aux/IAA transcriptional repressors. *Curr. Biol.* 27, 437–444. doi: 10.1016/j.cub.2016.12.016

Sharma, K. D., and Nayyar, H. (2014). Cold stress alters transcription in meiotic anthers of cold tolerant chickpea (*Cicer arietinum* L.). *BMC Res. Notes* 7, 717–730. doi: 10.1186/1756-0500-7-717

Skalska, A., Beckmann, M., Corke, F., Tuna, G. S., Tuna, M., Doonan, J. H., et al. (2021). Metabolomic variation aligns with two geographically distinct subpopulations of before and after drought stress. *Cells-Basel* 10, 683. doi: 10.3390/cells10030683

Soba, D., Zhou, B., Arrese-Igor, C., Munné-Bosch, S., and Aranjuelo, I. (2019). Physiological, hormonal and metabolic responses of two alfalfa cultivars with contrasting responses to drought. *Int. J. Mol. Sci.* 20, 5099–5118. doi: 10.3390/ijms20205099

Sun, R., Liu, S., Gao, J. L., and Zhao, L. H. (2023). Integration of the metabolome and transcriptome reveals the molecular mechanism of drought tolerance in. *Front. Genet.* 14. doi: 10.3389/fgene.2023.1274732

Talaat, N. B. (2023). Drought stress alleviator melatonin reconfigures water-stressed barley (*hordeum vulgare* L.) plants' photosynthetic efficiency, antioxidant capacity, and endogenous phytohormone profile. *Int. J. Mol. Sci.* 24, 16228. doi: 10.3390/IJMS242216228

Tan, J. L., Wang, C. Y., Xiang, B., Han, R. H., and Guo, Z. F. (2013). Hydrogen peroxide and nitric oxide mediated cold- and dehydration-induced myo-inositol phosphate synthase that confers multiple resistances to abiotic stresses. *Plant Cell Environ.* 36, 288–299. doi: 10.1111/j.1365-3040.2012.02573.x

Tang, W. J., Hazebroek, J., Zhong, C., Harp, T., Vlahakis, C., Baumhover, B., et al. (2017). Effect of genetics, environment, and phenotype on the metabolome of maize hybrids using GC/MS and LC/MS. *J. Agr Food Chem.* 65, 5215–5225. doi: 10.1021/acs.jafc.7b00456

Thorup-Kristensen, K., Halberg, N., Nicolaisen, M., Olesen, J. E., Crews, T. E., Hinsinger, P., et al. (2020). Digging deeper for agricultural resources, the value of deep rooting. *Trends Plant Sci.* 25, 406–417. doi: 10.1016/j.tplants.2019.12.007

Tschaplinski, T. J., Abraham, P. E., Jawdy, S. S., Gunter, L. E., Martin, M. Z., Engle, N. L., et al. (2019). The nature of the progression of drought stress drives differential metabolomic responses in *Populus deltoides*. *Ann. Bot-London* 124, 617–626. doi: 10.1093/aob/mcz002

Wang, Z., Ke, Q., Kim, M. D., Kim, S. H., Ji, C. Y., Jeong, J. C., et al. (2015). Transgenic alfalfa plants expressing the sweetpotato orange gene exhibit enhanced abiotic stress tolerance. *PloS One* 10, e0126050. doi: 10.1371/journal.pone.0126050

Wang, K., Nan, L. L., and Guo, Q. E. (2023a). Changes in root endogenous hormone levels and rhizosphere fungi diversity in alfalfa under drought stress. *Plant Growth Regul.* 10, 874–894. doi: 10.1007/s10725-023-01062-5

Wang, X. S., Yin, J. C., Wang, J., and Li, J. H. (2023b). Integrative analysis of transcriptome and metabolome revealed the mechanisms by which flavonoids and phytohormones regulated the adaptation of alfalfa roots to NaCl stress. *Front. Plant Sci.* 14. doi: 10.3389/fpls.2023.1117868

Wasaya, A., Manzoor, S., Yasir, T. A., Sarwar, N., Mubeen, K., Ismail, I. A., et al. (2021). Evaluation of fourteen bread wheat (*Triticum aestivum* L.) genotypes by observing gas exchange parameters, relative water and chlorophyll content, and yield attributes under drought stress. *Sustainability-Basel* 13, 4799–4814. doi: 10.3390/su13094799

Wen, B., Mei, Z. L., Zeng, C. W., and Liu, S. Q. (2017). metaX: a flexible and comprehensive software for processing metabolomics data. *BMC Bioinf.* 18, 183–197. doi: 10.1186/s12859-017-1579-y

Wu, X. J., Cai, K. F., Zhang, G. P., and Zeng, F. R. (2017). Metabolite profiling of barley grains subjected to water stress: To explain the genotypic difference in drought-induced impacts on malting quality. *Front. Plant Sci.* 8. doi: 10.3389/fpls.2017.01547

Xu, P., Su, H., Zhao, S. Q., Jin, R., Cheng, H. Y., Xu, A. A., et al. (2020). Transcriptome and phytochemical analysis reveals the alteration of plant hormones, characteristic metabolites, and related gene expression in tea (*Camellia sinensis* L.) leaves during withering. *Plants-Basel* 9, 204. doi: 10.3390/plants9020204

Yang, M., Yang, J., Su, L., Sun, K., Li, D. X., Liu, Y. Z., et al. (2019). Metabolic profile analysis and identification of key metabolites during rice seed germination under low-temperature stress. *Plant Sci.* 289, 110282. doi: 10.1016/j.plantsci.2019.110282

Yue, J. Y., Du, C. J., Ji, J., Xie, T. T., Chen, W., Chang, E. M., et al. (2018). Inhibition of α-ketoglutarate dehydrogenase activity affects adventitious root growth in poplar via changes in GABA shunt. *Planta* 248, 963–979. doi: 10.1007/s00425-018-2929-3

Zhang, Y. Q., Kilambi, H. V., Liu, J., Bar, H., Lazary, S., Egbaria, A., et al. (2021b). ABA homeostasis and long-distance translocation are redundantly regulated by ABCG ABA importers. *Sci. Adv.* 7, eabf6069. doi: 10.1126/sciadv.abf6069

Zhang, J., Poudel, B., Kenworthy, K., Unruh, J. B., Rowland, D., Erickson, J. E., et al. (2019b). Drought responses of above-ground and below-ground characteristics in warm-season turfgrass. *J. Agron. Crop Sci.* 205, 1–12. doi: 10.1111/jac.12301

Zhang, C., Shi, S., Liu, Z., Yang, F., and Yin, G. (2019a). Drought tolerance in alfalfa (*Medicago sativa* L.) varieties is associated with enhanced antioxidative protection and declined lipid peroxidation. *J. Plant Physiol.* 232, 226–240. doi: 10.1016/J.JPLPH.2018.10.023

Zhang, Y., Wang, X. P., Luo, Y. Z., Zhang, L., Yao, Y., Han, L., et al. (2020). *Os*ABA8ox2, an ABA catabolic gene, suppresses root elongation of rice seedlings and contributes to drought response. *Crop J.* 8, 480–491. doi: 10.1016/j.cj.2019.08.006

Zhang, F., Wu, J. F., Sade, N., Wu, S., Egbaria, A., Fernie, A. R., et al. (2021a). Genomic basis underlying the metabolome-mediated drought adaptation of maize. *Genome Biol.* 22, 260. doi: 10.1186/s13059-021-02481-1

frontiers | Frontiers in Plant Science

TYPE Original Research
PUBLISHED 08 February 2024
DOI 10.3389/fpls.2024.1342441

OPEN ACCESS

EDITED BY
Dongmei Li,
Shandong Agricultural University, China

REVIEWED BY
Lakshmi Narayana Vemireddy,
Acharya N. G. Ranga Agricultural University, India
Nabin Bhusal,
Agriculture and Forestry University, Nepal

*CORRESPONDENCE
Ramamoorthy Pushpam
pushpamtnau@gmail.com

RECEIVED 21 November 2023
ACCEPTED 18 January 2024
PUBLISHED 08 February 2024

CITATION
Kumar KP, Pushpam R, Manonmani S, Raveendran M, Santhiya S and Senthil A (2024) Enhancing stress resilience in rice (*Oryza sativa* L.) through profiling early-stage morpho-physiological and molecular responses to multiple abiotic stress tolerance. *Front. Plant Sci.* 15:1342441. doi: 10.3389/fpls.2024.1342441

Enhancing stress resilience in rice (*Oryza sativa* L.) through profiling early-stage morpho-physiological and molecular responses to multiple abiotic stress tolerance

Kathiresan Pravin Kumar[1], Ramamoorthy Pushpam[1]*, Swaminathan Manonmani[1], Muthurajan Raveendran[2], Subramanian Santhiya[1] and Alagarsamy Senthil[3]

[1]Centre for Plant Breeding and Genetics, Tamil Nadu Agricultural University (TNAU), Coimbatore, India, [2]Directorate of Research, Tamil Nadu Agricultural University (TNAU), Coimbatore, India, [3]Department of Crop Physiology, Directorate of Crop Management, Tamil Nadu Agricultural University (TNAU), Coimbatore, India

Under changing climatic conditions, crop plants are more adversely affected by a combination of various abiotic stresses than by a single abiotic stress. Therefore, it is essential to identify potential donors to multiple abiotic stresses for developing climate-resilient crop varieties. Hence, the present study was undertaken with 41 germplasm accessions comprising native landraces of Tamil Nadu, Prerelease lines and cultivars were screened independently for drought, salinity, and submergence at the seedling stage during Kharif and Rabi 2022–2023. Stress was imposed separately for these three abiotic stresses on 21-day-old seedlings and was maintained for 10 days. The studied genotypes showed a significant reduction in plant biomass (PB), Relative Growth Index (RGI), relative water content (RWC), leaf photosynthesis, chlorophyll fluorescence, and Chlorophyll Concentration Index (CCI) under drought followed by salinity and submergence. Stress-tolerant indices for drought, salinity, and submergence revealed significant variation for plant biomass. Furthermore, a set of 30 SSR markers linked to drought, salinity, and submergence QTLs has been used to characterize 41 rice germplasm accessions. Our analysis suggests a significantly high polymorphism, with 28 polymorphic markers having a 93.40% in 76 loci. The mean values of polymorphic information content (PIC), heterozygosity index (HI), marker index (MI), and resolving power (RP) were 0.369, 0.433, 1.140, and 2.877, respectively. Jaccard clustering grouped all the genotypes into two major and six subclusters. According to STRUCTURE analysis, all genotypes were grouped into two major clusters, which are concurrent with a very broad genetic base (K = 2). Statistically significant marker-trait associations for biomass were observed for five polymorphic markers, *viz.*, RM211, RM212 (drought), RM10694 (salinity), RM219, and RM21 (submergence). Similarly, significant markers for relative shoot length were observed for RM551 (drought), RM10694 (salinity), and ART5 (submergence). Notably, the genotypes Mattaikar, Varigarudan samba, Arupatham

samba, and APD19002 were identified as potential donors for multiple abiotic stress tolerance. Thus, identifying the genetic potential of germplasm could be useful for enhancing stress resilience in rice.

KEYWORDS

rice, early-stage, multiple abiotic stress, morpho-physiological characters, molecular profiling, marker-trait association

Introduction

Changing climate and growing global population are significant concerns for rice (*Oryza sativa* L) production (Manasa et al., 2023). Climate change disturbs the consistency and intensity of hydrological occurrences, threatening crop yield and food security. Primary regions experiencing these effects include South and Southeast Asia, Sub-Saharan Africa, and Latin America, covering both uplands and shallow rainfed lowlands (Radha et al., 2023). In order to address the challenge of feeding an anticipated global population of nine billion by 2050, we must substantially enhance rice production. To put this into perspective, the current yield stands at 104 million tons, and our target is to generate an additional 160 million tons of rice (www.FAO.org). Amid the changing climate, almost half of the rice cultivation regions are impacted, leading to a 42% decrease in yield worldwide due to various abiotic stresses (Muthu et al., 2020).

Rice is life for millions of farmers and is considered a staple food for over a billion people in the world. Rice cultivation primarily thrives in tropical and subtropical climates, which are mainly affected by drought, salinity, and submergence. On a global scale, 90% of rice production and consumption takes place in Asia (Adhikari et al., 2019). When subjected to drought, crops face a significant reduction in yield, particularly when the stress coincides with the reproductive stage (Garrity and O'Toole, 1994; Oladosu et al., 2020; Verma et al., 2014). Despite Asia being the major producer, approximately 34 Mha of rainfed lowland and 8 Mha of upland rice cultivable area are annually impacted by drought resulting in a yield reduction of 13% to 35% (Panda et al., 2022). Enhancing drought tolerance poses a challenge due to the unpredictable nature of drought stress and the complex response mechanisms of plants (Takahashi et al., 2020). Likewise, salinity is a widespread problem in both coastal and marginal inland environments, limiting rice production in 30% of rice growing area, encompassing 45 million hectares of irrigated land and 32 million hectares of dry land worldwide (Singh et al., 2016; FAO, 2018; Ravikiran et al., 2018). The elevated salt levels disrupt water and nutrient absorption by the roots, causing an imbalance in the plant's metabolism, ultimately resulting in decreased plant growth, leading to a yield loss of up to 35% (Farooq et al., 2015). Although rice is a semi-aquatic plant, it is well-suited for stagnant conditions due to its well-established aerenchyma, enabling oxygen transportation through the roots. However, recurrent flooding in lowland and deep-water rice regions, impacts an area of 12–14 million hectares in India, leading to a yield loss of up to 32% (Oladosu et al., 2020). The ability of tolerance to endure submergence relies on its carbohydrate levels (Alpuerto et al., 2016).

Utilizing natural genetic resources is the primary avenue for advancing stress resilience in rice cultivation (Marone et al., 2021). Studying natural variation not only helps us comprehend the genetic mechanisms underpinning tolerance during crucial growth stages but also advances our understanding of the associated physiological process (Ismail and Horie, 2017). Traditional rice landraces possess a robust genetic foundation that offers enhanced adaptability and protection against various biotic and abiotic stresses (Binodh et al., 2023). Therefore, landraces play a vital role as integral plant genetic resources, holding immense potential as donors for developing multiple stress tolerance. Significant advancements have been made in the past few decades leading to the identification of recognized donors, such as N22 for drought (Vikram et al., 2016), Pokkali for salinity (Singh and Sengar, 2014), and FR13A for submergence (Xu et al., 2006). Currently, due to changing climatic conditions, crops in stress-affected areas are expected to face a combination of abiotic stresses rather than single stresses (Slama et al., 2015; Wani et al., 2016). Thus, breeding for tolerance to a single abiotic stress may be risky, as plant responses to combined stresses differ from individual stress responses. When rice seedlings encounter various abiotic stresses during their initial growth phase, issues may arise due to suboptimal crop establishment, decreased length of roots and shoots, reduced leaf area, and early seedling death (Krishnamurthy et al., 2016). Hence, seedling stage tolerance to multiple abiotic stresses is crucial for better crop establishment, robust vegetative growth, and ultimately higher yield. To tackle this, a trait-based breeding approach in crop improvement programs is more effective than focusing on yield-based breeding (Paleari et al., 2017). Numerous studies have indicated the use of PEG-6000 for drought tolerance (Binodh et al., 2023), sodium chloride (NaCl) for salinity adaptation (Kakar et al., 2019), and the maintenance of a water level ranging from 90 cm to 120 cm for submergence tolerance (Samanta et al., 2022) were employed for quick screening during the seedling stage to identify promising candidates with stress tolerance.

Recent advancements in crop genetics have led to the creation of molecular tools that assist in faster and more efficient breeding techniques. Examining genetic diversity and population structure is

valuable for identifying superior breeding materials and enhancing breeding efficiency. The use of DNA-based markers resulted in the identification of markers linked to QTLs or genic regions of particular traits, making the breeding process quicker and more precise to select preferred plants more rapidly (Singh et al., 2015). Several studies have highlighted specific quantitative trait loci (QTLs) linked to stress tolerance. During the reproductive stage of drought stress, several yield QTLs such as *qDTY 1.1*, *qDTY 2.1*, *qDTY 3.1*, and *qDTY 12.1* were found to be closely associated with particular markers, including RM104 (Ghimire et al., 2012), RM2634 (Muthu et al., 2020), RM168 (Dixit et al., 2014), and RM28166 (Mishra et al., 2013). Moreover, RM3412 is found to be associated with the *saltol* region of seedling stage salinity (Krishnamurthy et al., 2016), and ART5 is found to be associated with the *sub1* region for submergence (Sarkar and Bhattacharjee, 2011). In the present era, rapid changes in climatic conditions emphasize the need for developing broad-spectrum genetic resistance in rice. This genetic resistance, with its inbuilt tolerance to these stresses, offers an economically viable and sustainable option to improve rice productivity under multiple stress conditions. Despite considerable efforts through traditional breeding approaches, molecular introspection of genetic diversity could reveal more precise information about the genetic variation, which would be helpful for genetic improvement breeding by identifying multiple abiotic stress tolerance. Therefore, this study aimed to evaluate the physiological responses and genetic diversity residing among the landraces, prerelease cultures, and cultivars to multiple abiotic stresses in order to identify potential donors to be employed in climate-resilient breeding programs.

Materials and methods

In total, 41 diverse rice genotypes, including native landraces of Tamil Nadu, prerelease lines, and cultivars were evaluated independently for three different abiotic stress tolerance involving respective tolerant checks, *viz*., IR64Drt1 for drought possessing *qDTY 2.2* and *qDTY 4.1* QTL (Binodh et al., 2023), FL478 for salinity having *saltol* QTL (Muthu et al., 2020), and FR13A for submergence having *Sub1* QTL (Xu et al., 2006), whereas IR64 for drought and salinity and IR42 for submergence were used as susceptible checks (Supplementary Table 1). The present investigation was carried out in the Department of Rice, Centre for Plant Breeding and Genetics, Tamil Nadu Agricultural University, Coimbatore, Tamil Nadu, during Kharif and Rabi 2022–2023.

Experimental design for screening

The experiment was carried out in a complete randomized design (CRD) with three independent replications. Uniform-sized seeds were surface sterilized with a 0.1% $HgCl_2$ solution for 5 min and thoroughly washed with distilled water for 10 min. The seeds were then placed in a Petri dish (50 seeds in each petri dish) and soaked in distilled water for 24 h under room temperature (25°C ± 2°C). Pregerminated seeds from each genotype were sown in plastic trays (30 cm × 20 cm × 10 cm) filled with field soil and farmyard manure (3:1 proportion). Twelve seedlings were maintained per genotype at a spacing of 1.5 cm × 1.5 cm. In each tray, the recommended dose of fertilizers, *viz*., urea, single super phosphate (SSP), and murate of potash (MOP) was applied 10 days after sowing. The trays were regularly watered. The average solar radiation throughout the growth period measured was 1,011 ± 40 μmol m^{-2} s^{-1} using a digital pyranometer (PMA2145 Class 1, Solar Light Co. Inc., Philadelphia, USA) with a maximum temperature of 33 ± 4 was measured using a digital thermometer (HTC-1, Aptechdeals, Jipvi tools, China), and relative humidity ranging from 67% to 75% was measured using a digital hygrometer (HTC-1, Aptechdeals, Jipvi tools, China). The seedlings were grown under standard conditions and nurtured for a duration of 21 days. Subsequently, stress was imposed separately, adhering to the specified protocol for each stress (Behera et al., 2023). One set of genotypes was maintained under nonstress conditions (control) until the end of the experiment (Figure 1).

Phenotype screening for drought tolerance

Drought stress was induced by withholding irrigation in plastic trays containing a set of 41 genotypes for a period of 10 days. Plant growth and physiological parameters were recorded upon the completion of the stress period.

Phenotype screening for salinity tolerance

Salinity stress was applied by irrigating the genotypes with saline water with 12 EC dsm^{-1} for a period of 10 days. Plant growth and physiological parameters were recorded upon the completion of the stress period.

FIGURE 1
Experimental procedure for screening seedling stage abiotic stress tolerance.

Phenotype screening for submergence tolerance

For 10 days, 21-day old seedlings were subjected to submergence screening by completely submerging the seedlings in 90 cm ± 5 cm of water. Following submergence, the water was drained, and plants were allowed to recover. Plant growth and physiological parameters were recorded 7 days after de-submergence.

Measurement of plant growth parameter

The measurements of plant growth parameters involved the assessment of shoot length and plant biomass. For biomass determination, whole seedlings were carefully uprooted and oven-dried at 80°C for 48 hours using a hot air oven (LTHOS-4, Labtech, Delhi, India).

The relative shoot length (RSL) was calculated as per Nahar et al. (2018).

$$\text{RSL} = \text{Shoot length under stress} / \text{shoot length under control}$$

The Relative Growth Index (RGI), was calculated by Kumar et al. (2014)

$$\text{RGI} = \text{plant biomass under stress/plant biomass under control}$$

Stress-Tolerant Index for drought, salinity, and bubmergence were calculated following Behera et al. (2023).

$$\text{STI} = \left(\frac{\textit{Plant biomass under stress}}{\textit{Plant biomass under control}}\right) / \left(\frac{\textit{Average plant biomass under stress}}{\textit{Average plant biomass under control}}\right)$$

The Stress Tolerance Index (STI) was used to identify genotypes capable of achieving high yields under both drought stress and non-stress irrigated conditions. A high STI value indicates a greater degree of stress tolerance (Muthuramu and Ragavan, 2020). Based on the values and desirability criteria, various genotypes were categorized as highly tolerant (STI > 1.00), tolerant (STI: 0.76–1.00), moderately tolerant (STI: 0.51–0.75), and susceptible (STI< 0.50).

Measurement of physiological parameters

Several physiological parameters were recorded in control and stress conditions. Relative water content (RWC) was estimated following the protocol of Barik et al. (2018). The second leaf of each plant was used to measure photosynthetic rate (PN), transpiration rate (*e*), and stomatal conductivity (gs) using an open-system photosynthesis gas analyzer (LCi-SD, ADC, UK). Similarly, chlorophyll fluorescence (Fo, Fm, and Fv/Fm) and chlorophyll content (Chlorophyll Content Index) were also measured on the same leaves using chlorophyll fluorometer OS30p (ADC Bioscientific, Hoddesdon, United Kingdom) and CCM (ADC Bioscientific, Hoddesdon, United Kingdom).

Microsatellite marker-based molecular analysis

Microsatellite markers (SSR markers) linked with target traits, *viz*., 14 for drought, eight for salinity, and eight for submergence utilized in this study (Table 1). Details of the linked markers were obtained from earlier reports by Tabkhkar et al. (2018) and Radha et al. (2023), and their respective chromosomal positions and sequence information were sourced from the Gramene marker database (https://archive.gramene.org/markers/).

Genomic DNA isolation and PCR reaction

Genomic DNA was isolated from 14-day-old seedlings using a modified CTAB method (Aboul-Maaty and Oraby, 2019). The purified DNA was dissolved in 50 µl of Tris-EDTA buffer (1×) and stored at −20°C for subsequent handling. The PCR reaction was set up using a Thermal Cycler (Bio-Rad T100). A 10-µl mixture was prepared, comprising 3.5 µl of PCR master mix (2× PCR master Mix-Red, smART Prime), 1 µl of SSR marker, 1 µl of genomic DNA (40 ng/µl), and 4.5 µl of distilled water, following the protocol outlined by Singh et al. (2010).

Analysis of PCR product and genetic similarity analysis

The amplified PCR products were analyzed in the Bio-Rad gel documentation system (USA). Amplified bands were scored manually for the presence (indicated as "1") or absence (indicated as "0") of each SSR marker. The marker traits such as polymorphism information content (PIC), marker index (MI), resolving power (RP), and heterozygosity index (HI) were calculated following Al-Daej et al. (2023). Pairwise genetic similarity between genotypes was calculated using Jaccard's coefficient employing the R Programme (Jaccard, 1908; Prabakaran et al., 2010).

Population structure analysis

To analyze the population structure among rice genotypes, we employed the model-based program STRUCTURE (version 2.3.4) (Zhang et al., 2022). The admixture model was used to determine the ancestry of the population. We adjusted the parameter Lambda, which represents the distribution of allelic frequencies, to 1 for result interpretation. To ensure consistency, we performed five independent runs with a long burn-in and Markov Chain Monte Carlo (MCMC) set at 50,000 iterations each. The number of possible populations (K) was tested, ranging from 1 to 10. The population number was determined by selecting the K value that yielded the highest posterior probability, $\Pr(X = K)$, referred to as $\text{LnP}(D)$ in the STRUCTURE output. The optimal value of K was identified using *ad-hoc* statistics ΔK, as proposed by Evanno et al. (2005), and analyzed using '*Structure Harvester*' https://taylor0.biology.ucla.edu/structureHarvester/.

Identification of marker-trait association

The estimation of marker-trait association was done by single marker analysis with the regression method using single factor

10.3389/fpls.2024.1342441

TABLE 1 List of SSR markers (associated QTLs, trait, chromosome, marker distance/marker region) used for genotyping in the present study.

Marker	AT (°C)	Chr	QTL	Trait	MD/R (cM)	Forward sequence	Reverse sequence	Reference
RM431	55	1	*qDTY 1.1*	Grain yield	12.13	TCCTGCGAACTGAAGAGTTG	AGAGCAAAACCCTGGTTCAC	Vikram et al. (2011)
RM212	55	1	*qDTY 1.1*	Grain yield	19.1	CCACTTTCAGCTACTACCAG	CACCCATTTGTCTCTCATTATG	Sandhu et al. (2018)
RM3825	55	1	*qDTY 1.1*	Grain yield	10.19	AAAGCCCCCAAAAGCAGTAC	GTGAAACTCTGGGGTGTTCG	Prince et al. (2015)
RM11943	55	1	*qDTY 2.1*	Grain yield	17.96	CTTGTTCGAGGACGAAGATAGGG	CTTGTTCGAGGACGAAGATAGGG	Vikram et al. (2011)
RM3412	55	1	*Saltol*	Na^+/K^+ ratio	11.5	AAAGCAGGTTTTCCTCCTCC	CCCATGTGCAATGTGTCTTC	Muthu et al. (2020)
RM8094	55	1	*Saltol*	Na^+/K^+ ratio	60.6	AAGTTTGTACACATCGTATACA	CGCGACCAGTACTACTACTA	Thomson et al. (2010)
RM10694	55	1	*Saltol*	Na^+/K^+ ratio	11	TTTCCCTGGTTTCAAGCTTACG	AGTACGGTACCTTGATGGTAGAAAGG	Thomson et al. (2010)
RM140	55	1	*Saltol*	Na^+/K^+ ratio	10.7	TGCCTCTTCCCTGGCTCCCCTG	GGCATGCCGAATGAAATGCATG	Thomson et al. (2010)
RM7075	55	1	*Saltol*	Na^+/K^+ ratio	74.2	TATGGACTGGAGCAAACCTC	GGCACAGCACCAATGTCTC	Thomson et al. (2010)
RM1287	55	1	*Saltol*	Na^+/K^+ ratio	58.1	GTGAAGAAAGCATGGTAAATG	CTCAGCTTGCTTGTGGTTAG	Thomson et al. (2010)
RM104	55	1	*Sub1*	Na^+/K^+ ratio	8.3	GGAAGAGGAGAGAAAG ATGTGTGTCG	TCAACAGACACACCGCCACCGC	Ghimire et al. (2012)
RM211	55	2	*qDTY 2.2*	Grain yield	14.4	CCGATCTCATCAACCAACTG	CTTCACGAGGATCTCAAAGG	Palanog et al. (2014)
RM250	55	2	*qDTY 2.3*	Grain yield	170.1	GGTTCAAACCAAGCTGATCA	GATGAAGGCCTTCCACGCAG	Palanog et al. (2014)
RM2634	55	2	*qDTY 2.3*	Grain yield	80.95	GATTGAAAATTAGAGTTTGCAC	TGCCGAGATTTAGTCAACTA	Muthu et al. (2020)
RM22	55	3	*qDTY 3.2*	Grain yield	7.7	GGTTTGGGAGCCCATAATCT	CTGGGCTTCTTTCACTCGTC	Vikram et al. (2011)
RM168	55	3	*qDTY 3.1*	Grain yield	37.3	TGCTGCTTGCCTGCTTCCTTT	GAAACGAATCAATCCACGGC	Donde et al. (2020)
RM232	55	3	*qDTY 1.1*	Grain yield	76.7	CCGGTATCCTTCGATATTGC	CCGACTTTTCCTCCTGACG	Palanog et al. (2014)
RM520	55	3	*qDTY 3.1*	Grain yield	138.7	AGGAGCAAGAAAAGTTCCCC	GCCAATGTGTGACGCAATAG	Angaji et al. (2010)
RM7097	55	3	*Saltol*	Na^+/K^+ ratio	115.6	GGGAGGAGGAGAGGAGATTG	TTAGGCCTGCACTTTTGGAG	Angaji et al. (2010)
RM551	55	4	*qDTY 4.1*	Grain yield	143.6	AGCCCAGACTAGCATGATTG	GAAGGCGAGAAGGATCACAG	Malik et al. (2022)
RM204	55	6	*qDTY 6.1*	Grain yield	25.1	GTGACTGACTTGGTCATAGGG	GCTAGCCATGCTCTCGTACC	Donde et al. (2020)
RM589	55	6	*qDTY 6.1*	Grain yield	2.7	ATCATGGTCGGTGGCTTAAC	CAGGTTCCAACCAGACACTG	Venuprasad et al. (2012)
RM11	55	7	*Saltol*	Na^+/K^+ ratio	93.8	TCTCCTCTTCCCCCGATC	ATAGCGGGCGAGGCTTAG	Singh et al. (2021)
RM337	55	8	*Sub1*	Shoot elongation	15.2	GTAGGAAAGGAAGGGCAGAG	CGATAGATAGCTAGATGTGGCC	Xu et al. (2006)
ART5	58	9	*Sub1*	Shoot elongation	6.39	CAGGGAAAGAGATGGTGGA	TTGGCCCTAGGTTGTTTCAG	Muthu et al. (2020)

(Continued)

TABLE 1 Continued

Marker	AT (°C)	Chr	QTL	Trait	MD/R (cM)	Forward sequence	Reverse sequence	Reference
SUB1AB1	60	9	*Sub1*	Shoot elongation	6.4	CATGTTCCATAGCCATCGACT	GAGCGAAGAGAGCTACCTGAA	Septiningsih et al. (2009)
SUB1BC3	60	9	*Sub1*	Shoot elongation	16.72	CATGGGTAAAATTGCCATCC	GCTTGAGGGTGAGTGGAGAG	Septiningsih et al. (2009)
RM219	55	9	*Sub1*	Shoot elongation	5.5	CGTCGGATGATGTAAAGCCT	CATATCGGCATTCGCCTG	Biswas et al. (2013)
RM316	55	9	*Sub1*	Shoot elongation	1.5	CTAGTTGGGCATACGATGGC	ACGCTTATATGTTACGTCAAC	Xu et al. (2006)
RM21	55	11	*Sub1*	Shoot elongation	73.1	ACAGTATTCCGTAGGCACGG	GCTCCATGAGGGTGGTAGAG	Angaji et al. (2010)

standard analysis of variance (Ramchander et al., 2022). The marker-trait association with p-value< 0.05 was identified as significant, and the proportion of phenotypic variance of the trait accounted by the marker was estimated in percent R^2.

Statistical analysis

An analysis of variance (ANOVA) was carried out to assess the variations among plant growth and physiological parameters. Furthermore, for the statistical significance of the parameter's means, we employed the Fisher's least significant difference (LSD) test. All statistical analysis was carried out using the package "*doebioresearch*" in the "R" platform.

Results

Impact of plant growth parameters

The ANOVA of growth patterns from both seasons and pooled analysis revealed significant differences among the genotypes (p< 0.01) for almost all the traits under study across all stress conditions (Table 2). The phenotypic response of individual genotypes under different stress conditions during Kharif and Rabi are shown in Figure 2. The impact of multiple abiotic stresses, *viz*., drought, salinity, and submergence, on plant growth parameters, *viz*., relative shoot length, plant biomass, and relative growth index, exhibited substantial reductions within the studied genotypes, as shown in Supplementary Table 2. When compared to the control, relative shoot length notably increased by 0.5% under submergence under pooled conditions, whereas in the case of drought and salinity, it was decreased by about 7.400% and 0.300%, respectively. In the case of submergence, FR13A was observed to have a lower RSL under both seasons, and the genotype Mattaikar was found to be on par with FR13A. In all the stress conditions, there was a significant reduction in plant biomass of about 13.253% under drought, 16.466% under salinity, and 26.104% under submergence when compared to the control. Similarly, the relative growth index showed a reduction of about 36.900%, 42.00%, and 75.600% under drought, salinity, and submergence, respectively, under both seasons over pooled conditions. Under each stress condition, plant biomass of the genotype exhibited significant differences under both seasons. Notably, under drought, the genotypes APD19002, Arupatham samba, Mattaikar, Norungan, and Varigarudan samba exhibited higher plant biomass when compared to the tolerant check (IR64Drt1). Likewise, under salinity, the genotypes, *viz*., Kappikar, Arupatham samba, Mattaikar, and Norungan, revealed higher biomass compared to the tolerant check (FL478). In the case of submergence, the plant biomass of Mattaikar was found to be on par with the tolerant check (FR13A).

Plant biomass functioned as the basis for calculating various stress tolerance indices, namely the Drought Tolerance Index (DTI), STI, and Submergence Tolerance Index (FTI). The genotypes with a stress-tolerant index above one over the seasons were considered to be tolerant (Figure 3). Over the seasons, nine genotypes (Norungan, APD19002, Anna (R) 4, Arupatham samba, Varigarudan samba, Mattaikar, Ponmani samba, CO53, and Poongar) were found to be superior over the tolerant check IR64Drt1 (1.024), hence these genotypes are grouped as drought tolerant. In the case of salinity, STI varied from 0.460 (CO51) to 1.190 (CO53). Across seasons, the genotypes *viz*., Arupatham samba, CO53, and Norungan exhibited superiority compared to the tolerant check FL478 (1.140), whereas APD19002, Mattaikar, and Varigarudan samba were identified with STI values exceeding 1 in both seasons, classifying them as salinity-tolerant genotypes. Similarly, for submergence, FTI ranged from 0.480 (ADT53) to 1.620 (FR13A) under pooled conditions. Over the seasons, the genotypes, *viz*., Arupatham samba, Mattaikar, APD19002, and Varigarudan samba, were found to be on par with the tolerant check FR13A (1.620), therefore grouped as submergence tolerant. As per the finding from the Stress-Tolerant Index, the genotypes, *viz*., Mattaikar, APD19002, Varigarudan samba, and Arupatham samba, were identified to be multiple abiotic stress tolerant.

Photosystem activities

Photosynthesis activity declined overall under all stress conditions when compared to control. Furthermore, we observed a notable variation among genotypes over the seasons within each

TABLE 2 Analysis of variance (ANOVA) for morpho-physiological parameters of various stresses during Kharif and Rabi during 2022–2023.

Mean sum of square												
Stress	Control			Drought			Salinity			Submergence		
Season	Kharif	Rabi	Pooled	Kharif	Rabi	Pooled	Kharif	Rabi	Pooled	Kharif	Rabi	Pooled
Treatment	41	41	41	41	41	41	41	41	41	41	41	41
DF	40	40	40	40	40	40	40	40	40	40	40	40
PB	0.015***	0.016***	0.0103***	0.014***	0.020***	0.010***	0.014***	0.026***	0.011***	0.016**	0.034***	0.0102
RSL	0	0	0	0.049***	0.032***	0.020**	0.058***	0.047***	0.029***	0.06***	0.015***	0.015
RGI	0	0	0	0.441***	0.19***	0.16***	0.11***	0.094***	0.059***	0.27***	0.045***	0.0672
RWC	311.26***	334.52***	213.31***	442.01***	470.42***	303.60***	313.98***	306.093***	205.05***	288.57***	311.55***	199.19***
TR	1.18***	1.39***	0.85***	0.69***	0.81***	0.50***	2.42***	2.68***	1.69***	0.66***	0.68***	0.45***
SC	0.00086***	0.00091***	0.00041***	0.00072***	0.00073***	0.00048***	0.00063***	0.00068***	0.00058***	0.00080***	0.00082***	0.00053***
PR	1.57***	1.74***	1.10***	2.31***	2.744***	1.67***	2.23***	2.43***	1.55***	1.44***	1.56***	1.003***
CCI	0.10***	0.12***	0.076***	0.633***	0.06***	0.44***	0.20***	0.20***	0.13***	0.32***	0.39***	0.23***
FO	777.58***	891.55***	552.58***	821.10***	899.58***	568.75***	946.80***	973.27***	635.86***	274.33***	328.33***	198.35***
FM	3739.00***	3997.30***	2544.64***	6093.80***	6735.4***	4247***	5385.90***	5499.50***	3612.7***	4423.00***	4866.60***	3067.1***
FV/FM	0.036***	0.04***	0.024***	0.021***	0.020***	0.013***	0.021***	0.02***	0.013***	0.013**	0.043***	0.014***
FV/FO	1.37***	1.46***	0.94***	0.767***	0.825***	0.526***	0.663***	0.74***	0.46***	1.51***	1.71***	1.06***

**0.05 and ***0.01—levels of significance. PB, plant biomass; RSL, relative shoot length; RGI, relative growth index; RWC, relative water content; TR, transpiration rate; SC, stomatal conductance; PR, photosynthetic rate; CCI, chlorophyll content index. Chlorophyll fluorescence: FO, FM, FV/FM, and FV/FO.

10.3389/fpls.2024.1342441

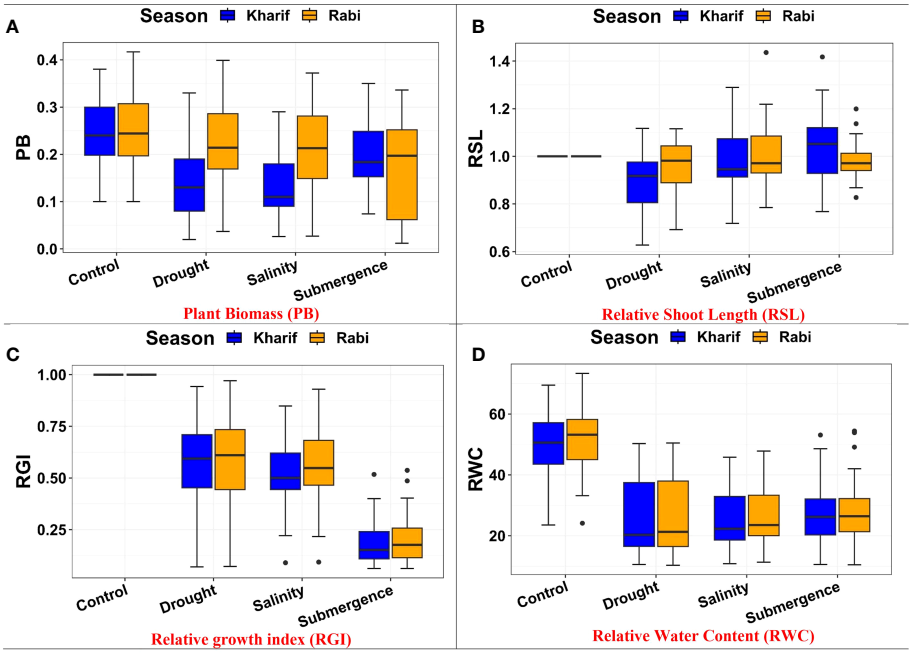

FIGURE 2
Performance of morphology traits: **(A)** plant biomass, **(B)** relative shoot length, **(C)** relative growth index, and **(D)** relative water content under varied stresses during both seasons.

stress condition (Supplementary Table 3). The RWC and CCI were highly affected under stress conditions, and it was found that tolerant genotypes had higher values of RWC and CCI, indicating the adoptive mechanism to unfavorable conditions.

Several leaf gas exchange parameters were measured under all stress conditions. The photosynthetic CO_2 fixation rate in both seasons decreased under the influence of drought, salinity, and submergence conditions (Figure 4). Under pooled conditions, the PN decreased by about 16.394% in drought, 17.434% in salinity, and 50.322% in submergence when compared to the control. The gas exchange parameters, *viz.*, gs and *e* were found to be drastically reduced under stress conditions. Stomatal conductance over the season decreased by

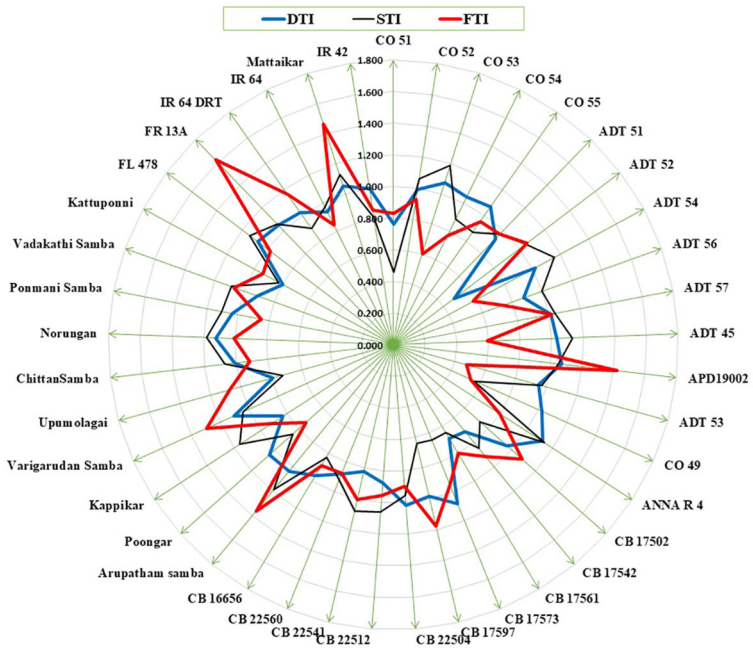

FIGURE 3
Stress tolerance index for drought, salinity, and submergence under combined seasons.

about 17.241% under drought, 31.034% under salinity, and 62.069% under submergence. Similarly, the *e* also decreased by 63.927% under drought, 5.516% under salinity, and 75.565% under submergence over the seasons. Chlorophyll fluorescence parameters of rice seedlings varied under control and stress conditions. Maximal fluorescence (Fm) and Fv/Fm were significantly ($p< 0.01$) reduced under drought, salinity, and submergence conditions (Figure 5). During Kharif, high Fv/Fm was noticed in the genotype Arupatham samba (0.716) under drought, Vadakathi samba (0.720) under salinity, and Mattaikar (0.781) under submergence. Likewise, in Rabi, the genotypes CO51 (0.752), Varigarudan samba (0.753), and FR13A (0.834) exhibited higher Fv/Fm under drought, salinity, and submergence. Likewise, under pooled conditions, the genotypes IR64Drt1 (0.768) under drought, FR13A (0.728) under salinity, and Ponmani samba (0.758) under submergence exhibited higher values for chlorophyll fluorescence, indicating their adoptive mechanisms under unfavorable environment.

Molecular marker profiling

SSR marker profiling employing 30 markers identified 28 markers as polymorphic, whereas RM7075 and RM7097 were found to be monomorphic. QTL-specific markers for drought, salinity, and submergence identified 76 loci across 41 rice germplasm with a mean of 2.37 polymorphic bands/marker (Figure 6). Maximum polymorphic bands were observed for RM8094 (six bands) followed by RM2634 and RM1287 (five bands). The marker attributes of individual SSR markers were assessed by calculating PIC, MI, RP, and HI (Table 3). PIC data varied from 0 to 0.785, with a mean value of 0.37 per primer. The maximum PIC value is obtained by 0.785 (RM8094) followed by RM1287 (0.713) and RM2634 (0.691), and the lowest value is obtained by RM212 (0.124). The HI ranged from 0 to 0.812. HI was found to be at a maximum in RM8094 (0.812), followed by RM1287 (0.755) and RM2634 (0.737), whereas it was lowest in RM316 (0.048) and RM3825 (0.048). The resolving power ranged from 1.85 to 7.805. The resolving power was found to be highest in RM8094 (7.805), followed by RM1287 (6.00) and RM22 (5.70), and the lowest value was observed in SUB_1BC_3 (1.561). The marker index ranged from 0 to 4.70. The marker RM8094 showed a higher marker index of 4.70, followed by the markers RM1287 (3.57) and RM2634 (3.45), and the lowest was observed in RM316 and RM3825 (0.047). Pairwise genetic similarity among 41 rice genotypes estimated using the Jaccard similarity coefficient ranged from 0.149 to 0.644 (Supplementary Table 4). A high genetic similarity was observed between IR64 and Upumolagai (Jc = 0.644). Likewise, the genetic similarity was observed to be low among the genotypes Kattuponni and CO49 (Jc = 0.149). The average genetic distance among the genotypes was found to be 0.443, indicating the considerable level of genetic diversity within the studied rice germplasm.

Principle coordinate analysis

Principle coordinate analysis (PCoA) was conducted to assess the relationship among rice genotypes based on molecular data (Figure 7). The first two principal coordinates collectively accounted for 24.80% of the total variation among the genotypes, with 12.96% attributed to principal coordinate 1 and 11.84% by principal coordinate 2. The distribution of genotypes was analyzed, and they was grouped into four quarters. The first quarter, situated in the top-left region, contained

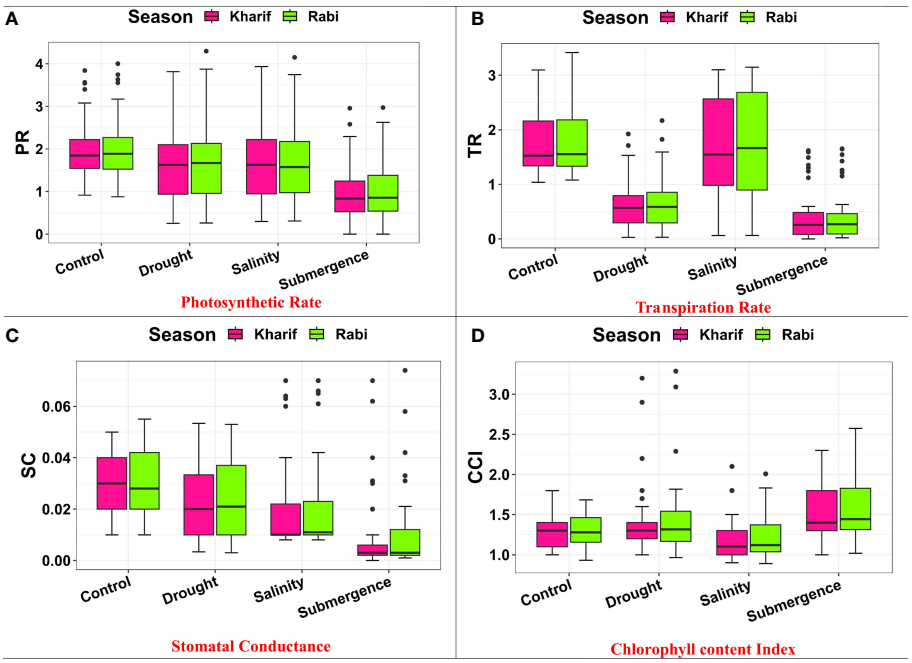

FIGURE 4
Performance of gas exchange parameters: **(A)** photosynthetic rate, **(B)** transpiration rate, **(C)** stomatal conductance, and **(D)** chlorophyll content index under varied stresses during both seasons.

10.3389/fpls.2024.1342441

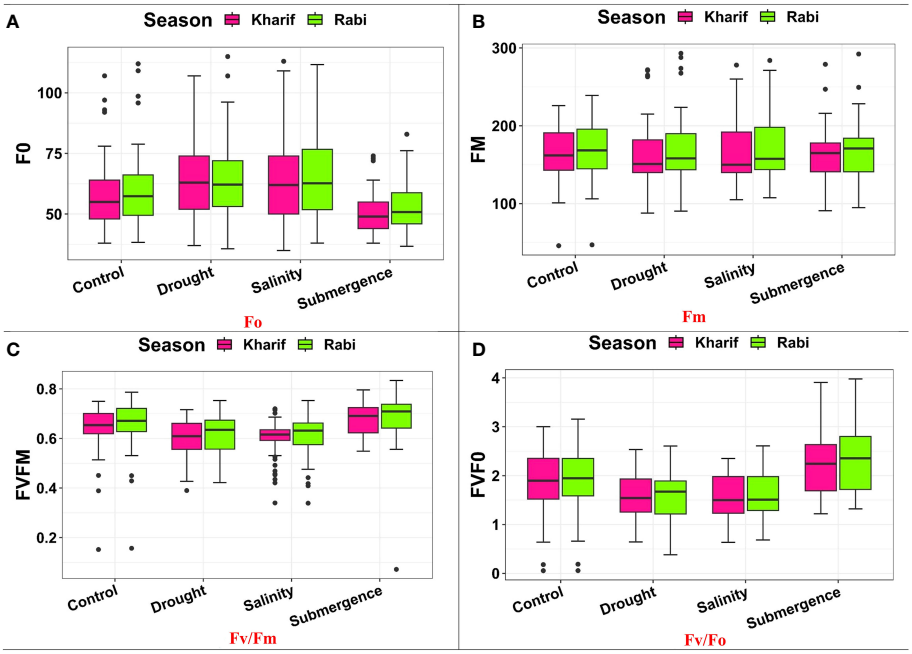

FIGURE 5
Performance of chlorophyll fluorescence parameters: **(A)** Fo, **(B)** Fm, **(C)** FV/Fm, and **(D)** Fv/Fo under varied stresses during both seasons.

12 genotypes (IR64, Vadakathi samba, CB17502, CB17573, CB17597, CB17561, CB17542, CB22541, FL478, Anna (R) 4, Norungan, and ADT54). Likewise, the second quarter in the top-right held 14 genotypes (CO49, CO51, CO52, CO53, CO55, ADT45, ADT51, ADT52, ADT53, ADT56, ADT57, CB 22512, IR42, and Kattuponni), the third quarter in the bottom-right contained eight genotypes (CB22560, CO54, Poongar, Chittansamba, Kappikar, CB16656, Upumlagai, and Arupatham samba), and the remaining seven genotypes (CB22504, Ponmani samba, FR13A, APD19002, Mattaikar, IR64Drt1, and Varigarudan samba) were found in the fourth quarter in the bottom-left.

Population structure analysis

The structure analysis depicted the classification of the 41 rice genotypes based on their SSR marker profile. The STRUCTURE software was applied with an expectation of K = 1, 2, 3…, 10. There were minor differences in consecutive LnP(D) values for the SSR marker data. The likelihood score LnP(D) progressively improved as K increased from 1 to 10, with no distinct peak indicating population assignment. Notably, no Delta-K peak was observed after K = 2 (Figure 8A). The optimal population partition

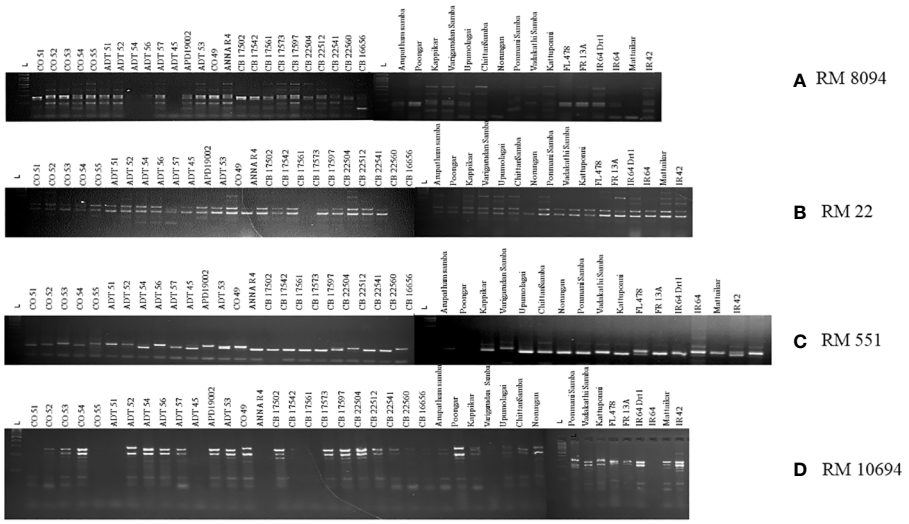

FIGURE 6
Representation of gel images of linked markers: **(A)** RM8094, **(B)** RM22, **(C)** RM551, and **(D)** RM10694.

TABLE 3 SSR marker attributes of polymorphic information content (PIC), marker index (MI), resolving power (RP), and heterozygous index (HI) in studied rice genotypes.

S. No.	Marker	Total number of band	No. of polymorphic band	Polymorphism percentage	PIC	HI	MI	RP
1	RM211	2	1	50	0.175	0.194	0.175	2.244
2	RM431	2	2	100	0.265	0.314	0.530	2.000
3	RM250	2	1	50	0.198	0.223	0.198	2.293
4	RM212	2	2	100	0.124	0.133	0.248	4.000
5	RM3825	1	1	100	0.047	0.048	0.047	1.951
6	RM22	4	4	100	0.664	0.716	2.657	5.707
7	RM168	3	3	100	0.489	0.564	1.467	2.049
8	RM232	2	2	100	0.371	0.493	0.743	2.000
9	RM551	2	2	100	0.126	0.136	0.253	2.000
10	RM204	2	2	100	0.375	0.500	0.750	2.000
11	RM589	2	2	100	0.375	0.500	0.750	3.902
12	RM520	3	3	100	0.373	0.496	1.119	2.098
13	RM3412	2	2	100	0.371	0.493	0.743	2.000
14	RM11943	2	2	100	0.375	0.500	0.750	2.488
15	RM2634	5	5	100	0.691	0.737	3.457	3.024
16	RM11	2	2	100	0.280	0.336	0.560	2.049
17	RM8094	6	6	100	0.785	0.812	4.708	7.805
18	RM10694	4	4	100	0.637	0.697	2.549	4.878
19	RM140	4	4	100	0.608	0.674	2.434	2.488
20	RM7075	1	0	0	0.000	0.000	0.000	1.951
21	RM1287	5	5	100	0.713	0.755	3.563	6.000
22	RM7097	1	0	0	0.000	0.000	0.000	2.000
23	ART5	2	2	100	0.356	0.464	0.713	2.000
24	SUB1AB1	2	2	100	0.364	0.479	0.728	3.317
25	SUB1BC3	2	2	100	0.545	0.623	1.089	1.561
26	RM219	2	2	100	0.339	0.433	0.679	2.000
27	RM316	1	1	100	0.047	0.048	0.047	1.941
28	RM337	3	3	100	0.463	0.525	1.389	2.390
29	RM104	2	1	50	0.375	0.499	0.375	3.854
30	RM21	3	3	100	0.554	0.624	1.661	2.341
	Total	**76**	**71**	**2650**	**0.369**	**0.434**	**1.146**	**2.878**
	Average	**2.53**	**2.37**	**88.33**	**0.37**	**0.43**	**1.15**	**2.88**

(*K*) was determined to be two subgroups, with subgroup 1 comprising 26 genotypes, showing 23 of pure type and three of admixture. Similarly, subgroup 2 comprises 15 genotypes, with 12 being of pure type and three of admixture. The maximum likelihood score for the population was achieved under these conditions (Figure 8B).

The cluster analysis using the neighbor Jaccard similarity coefficient

The dendrogram illustrates the clustering of 41 rice genotypes based on their SSR marker profile into two major clusters and six subclusters, which correlated with the population count obtained

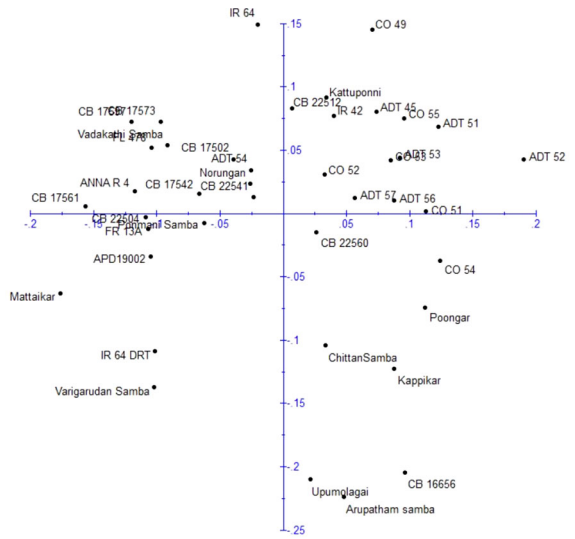

FIGURE 7
Principle coordinate analysis of rice genotypes based on DARwin analysis.

from the STRUCTURE analysis (Figure 9). Major cluster II is the largest, which includes the 29 genotypes comprising susceptible checks IR64 and IR42, along with 12 cultivars, seven prerelease cultures, and eight landraces. Similarly, major cluster I contains 12 genotypes encompassing tolerant checks (IR64Drt1, FL478, and FR13A), two cultivars (ADT54 and Anna (R) 4), four prerelease cultures (CB17502, CB22504, CB17561, and CB17597), and three landraces (Mattaikar, Varigarudan samba, and Vadakathi samba).

Marker trait association for drought, salinity, and submergence

The genetic associations among 28 polymorphic markers and two plant growth parameters, *viz*., plant biomass and relative shoot length, were analyzed using a single-marker analysis. The significant marker-trait association obtained based on *p*-value (< 0.05) along with their corresponding R^2 representing the total phenotypic variation accounted for by each marker for multiple abiotic stress tolerance are presented in Table 4. Markers associated with plant biomass (PB) and RSL under drought conditions were obtained using 14 drought-linked markers. The makers RM211 and RM212 were found highly associated with plant biomass with an R^2 value of 0.237 and 0.173, respectively. Likewise, the maker RM551 was found to be significantly associated with relative shoot length, with an R^2 value of 0.100. In order to find markers associated with traits, *viz*., PB and RSL, with respect to salinity, eight salinity-linked markers were utilized. The results revealed that the marker RM10694 was found to be significantly associated with both traits. Similarly, markers associated with PB and RSL in submergence were analyzed with eight submergence-linked markers, and it was found that the markers RM219 and RM21 were highly associated with plant biomass with R^2 values of 0.255 and 0.257, respectively, and the marker ART5 was found to significantly associated with relative shoot length with an R^2 value of 0.193.

Discussion

Rapid changes in climatic conditions have a significant impact on rice yield, and global food demand is increasingly affected by various abiotic stresses (Ramankutty et al., 2018). In the future development of crops, especially within the context of changing climatic conditions, the focus has shifted toward enhancing climate resilience in the creation of climate-smart crops to ensure food and nutritional security (Salgotra and Chauhan, 2023). Multifaceted abiotic stress tolerance takes on substantial importance in high-yield breeding initiatives. Consequently, there is a need to explore physiological variations and genetic diversity at earlier stages (Muthu et al., 2020). This effort aligns with the primary goal of

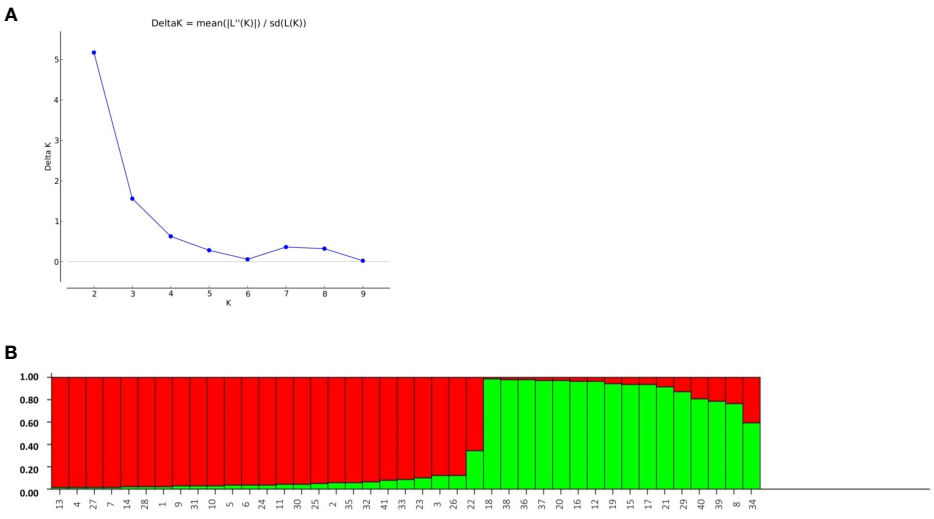

FIGURE 8
(A) Assessment of ad-hoc quantity (Δk) from calculated k and Ln p(D) and **(B)** Bargraph of rice genotypes constructed through population structure analysis.

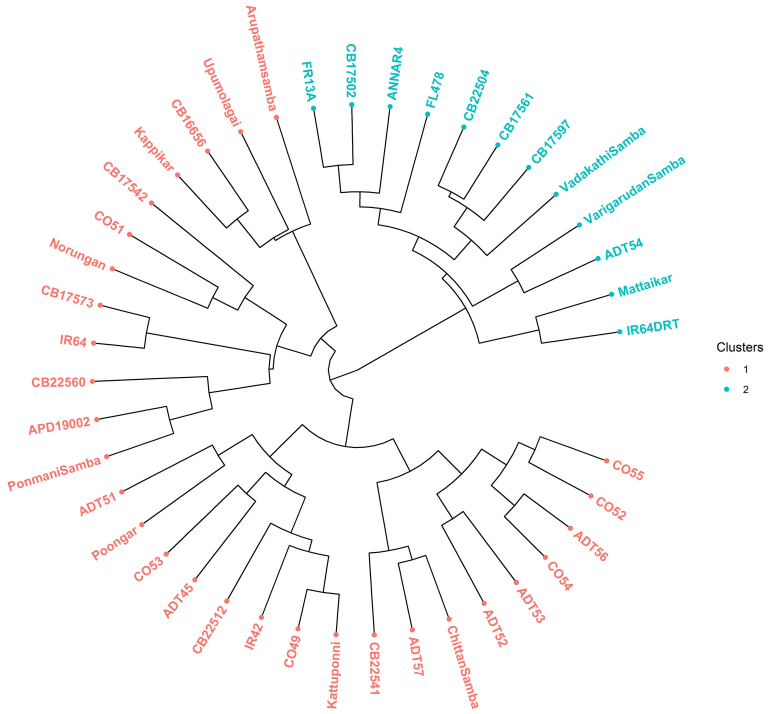

FIGURE 9
Cluster analysis of rice genotypes based on the Jaccard coefficient dendrogram.

enhancing the capacity for stress resilience and productivity, particularly given the dynamic shifts in environmental conditions. In this study, a diverse panel of rice genotypes, including prerelease lines, cultivars, and landraces, underwent screening under drought, salinity, and submergence conditions to evaluate their performance and identify potential donors for climate-resilient variety development.

The present study demonstrates that the resultant reduction in seedling growth parameters, *viz*., plant biomass and RGI, in both seasons leads to a depletion of dry matter content when the rice genotypes are exposed to subsequent stresses like drought, salinity, and submergence. Under all stress conditions, there was a significant reduction in plant biomass over the season of about 13.253% under drought, 16.466% under salinity, and 26.104% under submergence. Likewise, the relative growth index also showed reductions of 36.900%, 42.00%, and 75.600% under drought, salinity, and submergence, respectively. Similarly, Zhao et al. (2014) reported a 46.700% and 56.800% decline in biomass in FL478 and IR64 under salinity stress conditions. The degree of response of genotypes to stress-induced changes in plant growth varies due to a combination of factors, including genetic variations, duration of stress exposure, and developmental stages (Mundada et al., 2020). The seedling biomass obtained under various stress conditions was employed to derive stress-tolerant indices like DTI, STI, and FTI and was subsequently used for identifying tolerant genotypes. Significant divergence in the values of DTI, STI, and FTI indicted wide diversity among the studied genotypes. Generally, higher values of the stress-tolerant index imply their tolerance nature. As per the finding of Muthuramu and Ragavan (2020), the genotypes (*viz*., Norungan, APD19002, Anna (R) 4, Arupatham samba, Varigarudan samba, Mattaikar, Ponmani samba, CO53, and Poongar) with a high DTI value and superiority over the tolerant check IR64Drt1 indicate their ability to grow under limited water conditions. Likewise, the genotypes *viz*., Arupatham samba, CO53,

TABLE 4 Marker-trait association of studied traits under drought, salinity, and submergence conditions.

Trait	Plant biomass			Relative shoot length		
	Marker	*p*-value	R^2	Marker	*p*-value	R^2
Drought	RM211	0.006	0.237	RM551	0.05	0.1
	RM212	0.007	0.173			
Salinity	RM10694	0.02	0.341	RM10694	0.032	0.319
Submergence	RM219	0.001	0.255	ART5	0.004	0.193
	RM21	0.055	0.257			

and Norungan exhibited superiority compared to the tolerant check FL478, whereas APD19002, Mattaikar, and Varigarudan samba were identified with STI values exceeding 1 in both seasons. High STI signifies their potential to be grown in salt-affected areas. Higher values of FTI in the genotypes, *viz*., Arupatham samba, Mattaikar, APD19002, and Varigarudan samba, were found to be on par with the tolerant check FR13A, indicating their ability to withstand flooding situations. The study revealed that the genotypes, *viz*., Mattaikar, APD19002, Varigarudan samba, and Arupatham samba, were found to be multiple stress tolerant (Figure 10). Hence, these genotypes can be employed as potential donors in the development of climate-resilient varieties.

Leaf photosynthesis is an important process in plants and is highly sensitive to various abiotic stresses (Sharma et al., 2020). The results revealed that a gradual reduction in PN was also accompanied by a decrease in *e* and gs in rice seedlings. Under stress conditions, on average, the PN decreased by about 16.394% in drought, 17.434% in salinity, and 50.322% in submergence. Likewise, gs and *e* were found to be drastically reduced under stress conditions. This suggests that stomatal closure upon stress imposition is the major limiting parameter, resulting in declining photosynthesis. This is in accordance with the previous findings of Yamori et al. (2020), where they showed how stomatal conductance affects photosynthesis in rice under changing light conditions using wild-type (WT) rice (*Oryza sativa* L. cv. Taichung 65) and the slac1 mutant (defective in the *OsSLAC1* gene) with a modified stomatal regulation gene (*SLAC1* knockout). Overall, the findings show a considerable impact of drought, salinity, and submergence on key leaf gas exchange parameters, indicating a compromised physiological performance of the plants under these stress conditions in both seasons. The RWC and CCI were highly affected under stress conditions. According to Polash et al. (2018), the accumulation of both organic (proline) and inorganic (K+)

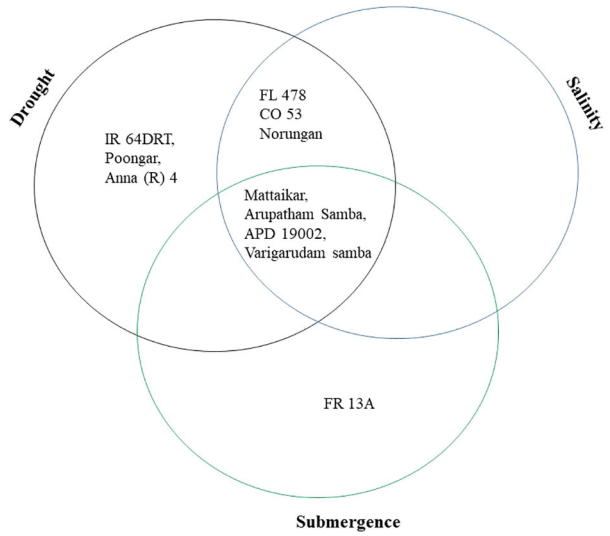

FIGURE 10
Selection of genotypes based on the stress tolerance index of various abiotic stresses under combined seasons.

osmolytes may play a role in stress alleviation by retaining water in the cells. Fluorescence parameters, *viz*., Fm and Fv/Fm, are excellent ways to evaluate the potential of PSII (Faseela et al., 2020). Under all the stress conditions, we observed an increase in Fo values whereas the Fm and Fv/Fm showed a declining trend, suggesting the alteration of PSII activity and photo-inhibition under various stress conditions. Similar results were obtained by Muhammad et al. (2021) for drought, Tsai et al. (2019) for salinity, and Elanchezhian et al. (2015) for submergence. The ability of genotypes to uphold photosynthetic rate and PSII activity determines their tolerance potentiality (Sarkar and Ray, 2016; Pradhan et al., 2019). As a result, the genotypes Mattaikar, Arupatham samba, Varigarudan samba, and Vadakathi samba were identified with higher PSII activity under stress conditions, ultimately leading to better photosynthesis and growth. Based on our experiments, it appears that physiological efficiency is the most indicative parameter for distinguishing genotype responses. Genotypes exhibiting higher physiological efficiency are more likely to tolerate stress conditions, whereas those with lower physiological efficiency are more susceptible.

SSR markers tightly linked to QTLs are amazing molecular tools for the genetic profiling of rice accessions and the identification of tolerant genotypes under multiple abiotic stress conditions. In this study, the genetic diversity of 41 rice genotypes was evaluated by employing 30 markers associated with the target trait. A substantial level of polymorphism was identified in the majority of the SSR markers. A similar result was found in Ram et al. (2007), who assessed genetic diversity and revealed the considerable allelic variability among SSR markers encompassing rice germplasm into cultivars, landraces, and wild relatives, providing valuable insights into genetic variability for future utilization. Based on marker profiling, the SSR primer RM8094, RM1287, RM2634, RM22, RM10694, and RM140 displayed higher values for PIC, MI, and RP, suggesting the potential of further utilization of these markers in investigating genetic diversity of rice accessions. Likewise, Lokeshkumar et al. (2023) identified three landraces (Kuttimanja, Tulasimog, and IET-13713I) as salt-tolerant with strong correlations in morphological and physiological traits under various conditions. Similarly, based on molecular analysis of the *Salto*l region, the markers *viz*., AP3206F, RM10793, and RM3412b, located close to the *SKC1* gene (11.23–12.55 Mb), displayed new alleles in tolerant lines like Kuttimanja, IET-13713I, and Tulasimog, suggesting their potential as candidates for novel genomic regions associated with salinity tolerance, whereas using high-yielding *indica* rice variety as a donor to developing multiple stress-tolerant rice variety through marker-assisted selection by Ali et al. (2017).

The average genetic distance among the genotypes was 0.443, suggesting an elevated magnitude of genetic diversity among the studied rice genotypes, and maximal genetic similarity was observed in the pairwise comparison between germplasm IR64 and Upumolagai. Whereas, the landraces are more genetically diverse than prerelease lines and cultivars. Despite diverse genotypes, rice landraces and cultivars exhibit tolerance to drought, salinity, and submergence. An earlier study of a diverse panel of 148 rice accessions, including 47 cultivars, 59 landraces from Taiwan, and 42 from other countries revealed five subpopulations. Genetic

diversity ranked higher in wild rice than in landraces and cultivars. These landraces exhibited significant genetic diversification, offering a valuable reservoir for future rice breeding (Hour et al., 2020). All genotypes were grouped into two major and seven subclusters by the Jaccard cluster analysis (Figure 9). Furthermore, the identification of tolerant groups was done using their respective tolerant and susceptible checks. Eight rice genotypes, such as CB22504, CB17561, CB17597, CB17502, Vadakathi samba, Varigarudan samba, Mattaikar, and ADT54, were identified to be multiple abiotic stress tolerant as they are grouped together with all the tolerant checks, *viz*., Anna (R) 4 and IR64Drt1 (drought), FL478 (salinity), and FR13A (submergence). A similar grouping pattern was observed in aromatic rice landraces under multiple abiotic stress conditions by Behera et al. (2023). Genotypic diversity attributed to stress tolerance QTLs varies among varieties and is highly affected by the environment (Gaballah et al., 2021). Results from this study identified that the salt-tolerant check (FL478) and submergence-tolerant check (FR13A) are genetically close. It was also reported that FR13A can be a donor for novel alleles, and FR13A can be a donor for new alleles imparting salinity and drought resistance. An earlier study showed that *Porteresia coarctata*, a wild relative of rice, exhibits high salinity and submergence tolerance. Through transcriptome analysis encompassing 375 million reads, 152,367 unique transcripts, including stress-responsive genes and 2,749 transcription factors, were identified. Likewise, key pathways in amino acid and hormone biosynthesis, secondary metabolite biosynthesis, carbohydrate metabolism, and cell wall structures contribute to stress tolerance (Garg et al., 2014). These findings provide insight into the genetic mechanisms of *Porteresia's* tolerance, offering potential strategies for engineering salinity and submergence tolerance in rice. An earlier study reported that genetic network induced in response to submergence and drought tolerance might share some common transcriptional factors at the gene expression level (Fukao et al., 2011), and engineering common transcription factors can ultimately lead to higher multiple stress tolerance (Manna et al., 2021). The genotypes that are identified as genetically close to IR64Drt1, FL478, and FR13A can be used as potential donors for developing climate resilience cultivars (Muthu et al., 2020).

STRUCTURE analysis revealed a very broad genetic base (K = 2) while employing different SSR markers linked to multiple abiotic stress-tolerant QTLs. The higher K value obtained in this study depicts the diverse nature of the population (Figure 8A). Our results were in comparison with the earlier reports of Kimwemwe et al. (2023), who assessed the genetic diversity and population structure of 94 rice genotypes using DArT-based SNP markers. We observed an average PIC of 0.25, identified five subpopulations (K = 5), and found a high average Euclidean genetic distance of 0.87, indicating the existence genetic diversity. The level of genetic diversity found in our study may help to select and conserve rice landraces. Thus, the rice landraces associated with multiple abiotic stress tolerance may be used as parental material in rice breeding to manage rice production in a changing climate.

Marker-assisted breeding programs emphasize the importance of establishing strong marker-trait associations in order to effectively utilize specific markers for trait enhancement (Lakshmi et al., 2021). The genetic associations among 13 polymorphic drought-linked markers and two plant growth parameters, *viz*., plant biomass and relative shoot length, analyzed using a single-marker analysis revealed RM211 and RM212 are closely associated with plant biomass under water-limiting conditions whereas RM551 was closely linked to relative shoot length under water-limiting conditions. Likewise, Salunkhe et al. (2011) reported that RM212, RM302, RM8085, and RM3825 exerted a substantial influence on drought-resistant traits. Similarly, the marker-trait association employing eight salinity-linked polymorphic markers identified RM10694 to be closely linked to plant biomass and relative shoot length under saline conditions. The results are in concordance with Kumari et al. (2019) and Volkova (2017), in which they stated the markers, *viz*., RM302, RM8094, RM10665, RM10694, RM10748, and RM10825, can be employed in validating QTLs for salinity tolerance. The single marker analysis employing seven submergence-linked markers identified RM219 and RM21 to be significantly associated with plant biomass under submergence, whereas ART5 was found to be associated with relative shoot length under submergence. It is worth noting that similar markers (RM219, RM21, and ART5) were reported to be closely linked to submergence, as per earlier findings of Islam et al. (2008); Biswas et al. (2013), and Muthu et al. (2020). Therefore, the abovementioned marker-trait associations could be employed in the identification of tolerant lines in future breeding programs aimed at developing multiple abiotic stress-tolerant varieties.

Conclusion

In the face of climate change and global warming, developing and utilizing genotypes with tolerance to multiple abiotic stresses is of great significance, as it has the potential to boost food production and ensure the stability of rice cultivation. The findings of this study present an opportunity to improve rice cultivars with multiple abiotic stress tolerance, as these germplasms exhibit a wider genetic diversity related to traits enabling them to withstand challenges like drought, salinity, and submergence. Genotypic analysis involving 30 SSR markers revealed substantial genetic similarity among all the studied rice genotypes, indicating a significant level of genetic diversity within the population. STRUCTURE analysis revealed a broad genetic base (K = 2), further emphasizing the suitability of these rice genotypes for coping with environmental stresses. The marker-trait associations suggest that markers RM211, RM212, RM10694, RM219, RM21, and ART5 could be useful for evaluating trait-specific multiple abiotic stress tolerance. The genotypes APD19002, Mattaikar, Varigarudan samba, and Arupatham samba are considered important genetic resources as they exhibit multiple stress tolerance making them a potential donor to be employed in stress resilience breeding.

Data availability statement

The original contributions presented in the study are included in the article/Supplementary Material. Further inquiries can be directed to the corresponding author.

Author contributions

KP: Data curation, Methodology, Software, Visualization, Writing – original draft. RP: Conceptualization, Investigation, Methodology, Resources, Supervision, Writing – review & editing. SM: Investigation, Resources, Writing – review & editing. MR: Writing – review & editing. SS: Data curation, Software, Writing – review & editing. AS: Investigation, Writing – review & editing.

Funding

The author(s) declare that no financial support was received for the research, authorship, and/or publication of this article.

Conflict of interest

The authors declare that the research was conducted in the absence of any commercial or financial relationships that could be construed as a potential conflict of interest.

Publisher's note

Supplementary material

The Supplementary Material for this article can be found online at: https://www.frontiersin.org/articles/10.3389/fpls.2024.1342441/full#supplementary-material

References

Aboul-Maaty, N.-F., and Oraby, H.-S. (2019). Extraction of high-quality genomic DNA from different plant orders applying a modified CTAB-based method. *Bull. Natl. Res. Centre* 43, 1–10. doi: 10.1186/s42269-019-0066-1

Adhikari, M., Adhikari, N. R., Sharma, S., Gairhe, J., Bhandari, R. R., and Paudel, S. (2019). Evaluation of drought tolerant rice cultivars using drought tolerant indices under water stress and irrigated condition. *Am. J. Climate Change* 8, 228–236. doi: 10.4236/ajcc.2019.82013

Al-Daej, M. I., Rezk, A. A., El-Malky, M. M., Shalaby, T. A., and Ismail, M. (2023). Comparative genetic diversity assessment and marker–trait association using two DNA marker systems in rice (Oryza sativa L.). *Agronomy* 13, 329. doi: 10.3390/agronomy13020329

Ali, J., Xu, J.-L., Gao, Y.-M., Ma, X.-F., Meng, L.-J., Wang, Y., et al. (2017). Harnessing the hidden genetic diversity for improving multiple abiotic stress tolerance in rice (Oryza sativa L.). *PloS One* 12, e0172515. doi: 10.1371/journal.pone.0172515

Alpuerto, J. B., Hussain, R. M. F., and Fukao, T. (2016). The key regulator of submergence tolerance, SUB1A, promotes photosynthetic and metabolic recovery from submergence damage in rice leaves. *Plant Cell Environ.* 39, 672–684. doi: 10.1111/pce.12661

Angaji, S. A., Septiningsih, E. M., Mackill, D., and Ismail, A. M. (2010). QTLs associated with tolerance of flooding during germination in rice (O ryza sativa L.). *Euphytica* 172, 159–168. doi: 10.1007/s10681-009-0014-5

Barik, S. R., Pandit, E., Pradhan, S. K., Singh, S., Swain, P., and Mohapatra, T. (2018). QTL mapping for relative water content trait at reproductive stage drought stress in rice. *Indian J Genet Plant Breed* 78 (04), 401–408. doi: 10.31742/IJGPB.78.4.1

Behera, P. K., Kumar, V., Sharma, S. S., Lenka, S. K., and Panda, D. (2023). Genotypic diversity and abiotic stress response profiling of short-grain aromatic landraces of rice (Oryza sativa L. Indica). *Curr. Plant Biol.* 33, 100269. doi: 10.1016/j.cpb.2022.100269

Binodh, A. K., Kathiresan, P. K., Thankappan, S., and Senthil, A. (2023). Acclimatization of non-cultivated rice landraces to early moisture stress mediated by enzymatic antioxidants and osmolyte accumulation. *Biocatalysis Agric. Biotechnol.* 47, 102623. doi: 10.1016/j.bcab.2023.102623

Biswas, T., Das, A., and Bhattacharyya, S. (2013). Marker assisted selection for developing high yielding submergence tolerant rice (Oryza sativa L.) genotypes with slender grain. *Cereal Res. Commun.* 41, 35–44. doi: 10.1556/CRC.2012.0022

Dixit, S., Singh, A., Sta Cruz, M. T., Maturan, P. T., Amante, M., and Kumar, A. (2014). Multiple major QTL lead to stable yield performance of rice cultivars across varying drought intensities. *BMC Genet.* 15, 1–13. doi: 10.1186/1471-2156-15-16

Donde, R., Mohapatra, S., Baksh, S. Y., Padhy, B., Mukherjee, M., Roy, S., et al. (2020). Identification of QTLs for high grain yield and component traits in new plant types of rice. *PloS One* 15, e0227785. doi: 10.1371/journal.pone.0227785

Elanchezhian, R., Haris, A., Kumar, S., and Singh, S. (2015). Positive impact of paclobutrazol on gas exchange, chlorophyll fluorescence and yield parameters under submergence stress in rice. *Indian J. Plant Physiol.* 20, 111–115. doi: 10.1007/s40502-015-0144-9

Evanno, G., Regnaut, S., and Goudet, J. (2005). Detecting the number of clusters of individuals using the software STRUCTURE: a simulation study. *Mol. Ecol.* 14, 2611–2620. doi: 10.1111/j.1365-294X.2005.02553.x

FAO (2018). *FAO and sustainable intensification of rice production for food security* (Rome, Italy: Rome: Food and Agricultural Organization).

Farooq, M., Hussain, M., Wakeel, A., and Siddique, K. H. (2015). Salt stress in maize: effects, resistance mechanisms, and management. A review. *Agron. Sustain. Dev.* 35, 461–481. doi: 10.1007/s13593-015-0287-0

Faseela, P., Sinisha, A., Brestič, M., and Puthur, J. (2020). Chlorophyll a fluorescence parameters as indicators of a particular abiotic stress in rice. *Photosynthetica* 58, 293–300. doi: 10.32615/ps.2019.147

Fukao, T., Yeung, E., and Bailey-Serres, J. (2011). The submergence tolerance regulator SUB1A mediates crosstalk between submergence and drought tolerance in rice. *Plant Cell* 23, 412–427. doi: 10.1105/tpc.110.080325

Gaballah, M. M., Metwally, A. M., Skalicky, M., Hassan, M. M., Brestic, M., El Sabagh, A., et al. (2021). Genetic diversity of selected rice genotypes under water stress conditions. *Plants* 10, 27. doi: 10.3390/plants10010027

Garg, R., Verma, M., Agrawal, S., Shankar, R., Majee, M., and Jain, M. (2014). Deep transcriptome sequencing of wild halophyte rice, Porteresia coarctata, provides novel insights into the salinity and submergence tolerance factors. *DNA Res.* 21, 69–84. doi: 10.1093/dnares/dst042

Garrity, D., and O'Toole, J. (1994). Screening rice for drought resistance at the reproductive phase. *Field Crops Res.* 39, 99–110. doi: 10.1016/0378-4290(94)90012-4

Ghimire, K. H., Quiatchon, L. A., Vikram, P., Swamy, B. M., Dixit, S., Ahmed, H., et al. (2012). Identification and mapping of a QTL (qDTY1. 1) with a consistent effect on grain yield under drought. *Field Crops Res.* 131, 88–96. doi: 10.1016/j.fcr.2012.02.028

Hour, A.-L., Hsieh, W.-H., Chang, S.-H., Wu, Y.-P., Chin, H.-S., and Lin, Y.-R. (2020). Genetic diversity of landraces and improved varieties of rice (Oryza sativa L.) in Taiwan. *Rice* 13, 1–12. doi: 10.1186/s12284-020-00445-w

Islam, M., Singh, R., Salam, M., Hassan, L., and Gregorio, G. (2008). Molecular diversity of stress tolerant rice genotypes using SSR markers. *Sabrao J. Breed Genet.* 40, 127–139.

Ismail, A. M., and Horie, T. (2017). Genomics, physiology, and molecular breeding approaches for improving salt tolerance. *Annu. Rev. Plant Biol.* 68, 405–434. doi: 10.1146/annurev-arplant-042916-040936

Jaccard, P. (1908). Nouvelles recherches sur la distribution florale. *Bull. Soc Vaud. Sci. Nat.* 44, 223–270. doi: 10.5169/seals-268384

Kakar, N., Jumaa, S. H., Redoña, E. D., Warburton, M. L., and Reddy, K. R. (2019). Evaluating rice for salinity using pot-culture provides a systematic tolerance assessment at the seedling stage. *Rice* 12, 1–14. doi: 10.1186/s12284-019-0317-7

Kimwemwe, P. K., Bukomarhe, C. B., Mamati, E. G., Githiri, S. M., Civava, R. M., Mignouna, J., et al. (2023). Population structure and genetic diversity of Rice (Oryza sativa L.) germplasm from the Democratic Republic of Congo (DRC) using DArTseq-Derived single nucleotide polymorphism (SNP). *Agronomy* 13, 1906. doi: 10.3390/agronomy13071906

Krishnamurthy, S., Gautam, R., Sharma, P., and Sharma, D. (2016). Effect of different salt stresses on agro-morphological traits and utilisation of salt stress indices for reproductive stage salt tolerance in rice. *Field Crops Res.* 190, 26–33. doi: 10.1016/j.fcr.2016.02.018

Kumar, S., Dwivedi, S., Singh, S., Jha, S., Lekshmy, S., Elanchezhian, R., et al. (2014). Identification of drought tolerant rice genotypes by analysing drought tolerance indices and morpho-physiological traits. *SABRAO J. Breed. Genet.* 46 (2), 217–230.

Kumari, R., Kumar, P., Sharma, V., and Kumar, H. (2019). Seedling stage salt stress response specific characterization of genetic polymorphism and validation of SSR markers in rice. *Physiol. Mol. Biol. Plants* 25, 407–419. doi: 10.1007/s12298-018-0623-3

Lakshmi, V. I., Sreedhar, M., Lakshmi, V. J., Gireesh, C., and Rathod, S. V. ,. S. (2021). Phenotypic screening and single marker analysis for Brown plant hopper resistance in rice (Oryza sativa L.). *J. Res.* PJTSAU, 49.

Lokeshkumar, B., Krishnamurthy, S., Rathor, S., Warriach, A. S., Vinaykumar, N., Dushyanthakumar, B., et al. (2023). Morphophysiological diversity and haplotype analysis of saltol QTL region in diverse rice landraces for salinity tolerance. *Rice Sci.* 30, 306–320. doi: 10.1016/j.rsci.2023.02.001

Malik, A., Kumar, A., Ellur, R. K., Krishnan S, G., Dixit, D., Bollinedi, H., et al. (2022). Molecular mapping of QTLs for grain dimension traits in Basmati rice. *Front. Genet.* 13, 932166. doi: 10.3389/fgene.2022.932166

Manasa, S., Reddy, S. M., Murthy, K., Meena, A., and Prasad, M. R. (2023). Genetic diversity studies in rice landraces (Oryza sativa L.) based on mahalanobis D2 distance. *Int. J. Environ. Climate Change* 13, 28–34. doi: 10.9734/ijecc/2023/v13i21649

Manna, M., Thakur, T., Chirom, O., Mandlik, R., Deshmukh, R., and Salvi, P. (2021). Transcription factors as key molecular target to strengthen the drought stress tolerance in plants. *Physiologia Plantarum* 172, 847–868. doi: 10.1111/ppl.13268

Marone, D., Russo, M. A., Mores, A., Ficco, D. B., Laidò, G., Mastrangelo, A. M., et al. (2021). Importance of landraces in cereal breeding for stress tolerance. *Plants* 10, 1267. doi: 10.3390/plants10071267

Mishra, K. K., Vikram, P., Yadaw, R. B., Swamy, B. M., Dixit, S., Cruz, M. T. S., et al. (2013). qDTY 12. 1: a locus with a consistent effect on grain yield under drought in rice. *BMC Genet.* 14, 1–10. doi: 10.1186/1471-2156-14-12

Muhammad, I., Shalmani, A., Ali, M., Yang, Q.-H., Ahmad, H., and Li, F. B. (2021). Mechanisms regulating the dynamics of photosynthesis under abiotic stresses. *Front. Plant Sci.* 11. doi: 10.3389/fpls.2020.615942

Mundada, P., Nikam, T., Kumar, S. A., Umdale, S., and Ahire, M. (2020). Morpho-physiological and biochemical responses of finger millet (Eleusine coracana (L.) Gaertn.) genotypes to PEG-induced osmotic stress. *Biocatalysis Agric. Biotechnol.* 23, 101488. doi: 10.1016/j.bcab.2019.101488

Muthu, V., Abbai, R., Nallathambi, J., Rahman, H., Ramasamy, S., Kambale, R., et al. (2020). Pyramiding QTLs controlling tolerance against drought, salinity, and submergence in rice through marker assisted breeding. *PloS One* 15, e0227421. doi: 10.1371/journal.pone.0227421

Muthuramu, S., and Ragavan, T. (2020). Studies on indices and morphological traits for drought tolerance in rainfed rice (Oryza sativa L.). *Electronic J. Plant Breed.* 11, 1–5. doi: 10.37992/2020.1101.001

Nahar, S., Sahoo, L., and Tanti, B. (2018). Screening of drought tolerant rice through morpho-physiological and biochemical approaches. *Biocatalysis Agric. Biotechnol.* 15, 150–159. doi: 10.1016/j.bcab.2018.06.002

Oladosu, Y., Rafii, M. Y., Arolu, F., Chukwu, S. C., Muhammad, I., Kareem, I., et al. (2020). Submergence tolerance in rice: Review of mechanism, breeding and, future prospects. *Sustainability* 12, 1632. doi: 10.3390/su12041632

Palanog, A. D., Swamy, B. M., Shamsudin, N., Dixit, S., Hernandez, J. E., Boromeo, T. H., et al. (2014). Grain yield QTLs with consistent-effect under reproductive-stage drought stress in rice. *Field Crops Res.* 161, 46–54. doi: 10.1016/j.fcr.2014.01.004

Paleari, L., Movedi, E., and Confalonieri, R. (2017). Trait-based model development to support breeding programs. A case study for salt tolerance and rice. *Sci. Rep.* 7, 4352. doi: 10.1038/s41598-017-04022-y

Panda, D., Behera, P. K., Mishra, S., and Mishra, B. S. (2022). Differential drought tolerance responses in short-grain aromatic rice germplasms from Koraput valley of Eastern Ghats of India. *Plant Physiol. Rep.* 27, 119–131. doi: 10.1038/s41598-017-04022-y

Polash, M., Sakil, M. A., Tahjib-Ul-Arif, M., and Hossain, M. A. (2018). Effect of salinity on osmolytes and relative water content of selected rice genotypes. *Trop. Plant Res.* 5, 227–232. doi: 10.22271/tpr.2018.v5.i2.029

Prabakaran, A., Paramasivam, K., Rajesh, T., and Rajarajan, D. (2010). Molecular characterization of rice land races using SSR markers. *Electronic J. Plant Breed.* 1, 512–516.

Pradhan, S. K., Pandit, E., Pawar, S., Baksh, S. Y., Mukherjee, A. K., and Mohanty, S. P. (2019). Development of flash-flood tolerant and durable bacterial blight resistant versions of mega rice variety 'Swarna'through marker-assisted backcross breeding. *Sci. Rep.* 9, 12810. doi: 10.1038/s41598-019-49176-z

Prince, S. J., Beena, R., Gomez, S. M., Senthivel, S., and Babu, R. C. (2015). Mapping consistent rice (Oryza sativa L.) yield QTLs under drought stress in target rainfed environments. *Rice* 8, 1–13. doi: 10.1186/s12284-015-0053-6

Radha, B., Sunitha, N. C., Sah, R. P., Tp, M. A., Krishna, G., Umesh, D. K., et al. (2023). Physiological and molecular implications of multiple abiotic stresses on yield and quality of rice. *Front. Plant Sci.* 13. doi: 10.3389/fpls.2022.996514

Ram, S. G., Thiruvengadam, V., and Vinod, K. K. (2007). Genetic diversity among cultivars, landraces and wild relatives of rice as revealed by microsatellite markers. *J. Appl. Genet.* 48, 337–345. doi: 10.1007/BF03195230

Ramankutty, N., Mehrabi, Z., Waha, K., Jarvis, L., Kremen, C., Herrero, M., et al. (2018). Trends in global agricultural land use: implications for environmental health and food security. *Annu. Rev. Plant Biol.* 69, 789–815. doi: 10.1146/annurev-arplant-042817-040256

Ramchander, S., Leon, M., Souframanien, J., and Arumugam Pillai, M. (2022). Genetic diversity, allelic variation and marker trait associations in gamma irradiated mutants of rice (Oryza sativa L.). *Int. J. Radiat. Biol.* 98, 90–99. doi: 10.1080/09553002.2021.1987568

Ravikiran, K., Krishnamurthy, S., Warraich, A., and Sharma, P. (2018). Diversity and haplotypes of rice genotypes for seedling stage salinity tolerance analyzed through morpho-physiological and SSR markers. *Field Crops Res.* 220, 10–18. doi: 10.1016/j.fcr.2017.04.006

Salgotra, R. K., and Chauhan, B. S. (2023). Genetic diversity, conservation, and utilization of plant genetic resources. *Genes* 14, 174. doi: 10.3390/genes14010174

Salunkhe, A. S., Poornima, R., Prince, K. S. J., Kanagaraj, P., Sheeba, J. A., Amudha, K., et al. (2011). Fine mapping QTL for drought resistance traits in rice (Oryza sativa L.) using bulk segregant analysis. *Mol. Biotechnol.* 49, 90–95. doi: 10.1007/s12033-011-9382-x

Samanta, P., Chakrabarti, A., and Dey, N. (2022). Study on physiological responses with allelic diversity of Sub1A and SK loci in rice seedlings under complete submergence. *Plant Physiol. Rep.* 27, 275–281. doi: 10.1007/s40502-022-00660-1

Sandhu, N., Dixit, S., Swamy, B. M., Vikram, P., Venkateshwarlu, C., Catolos, M., et al. (2018). Positive interactions of major-effect QTLs with genetic background that enhances rice yield under drought. *Sci. Rep.* 8, 1626. doi: 10.1038/s41598-018-20116-7

Sarkar, R., and Ray, A. (2016). Submergence-tolerant rice withstands complete submergence even in saline water: Probing through chlorophyll a fluorescence induction OJIP transients. *Photosynthetica* 54, 275–287. doi: 10.1007/s11099-016-0082-4

Sarkar, R. K., and Bhattacharjee, B. (2011). Rice genotypes with SUB1 QTL differ in submergence tolerance, elongation ability during submergence and re-generation growth at re-emergence. *Rice* 5, 1–11. doi: 10.1007/s12284-011-9065-z

Septiningsih, E. M., Pamplona, A. M., Sanchez, D. L., Neeraja, C. N., Vergara, G. V., Heuer, S., et al. (2009). Development of submergence-tolerant rice cultivars: the Sub1 locus and beyond. *Ann. Bot.* 103, 151–160. doi: 10.1093/aob/mcn206

Sharma, A., Kumar, V., Shahzad, B., Ramakrishnan, M., Singh Sidhu, G. P., Bali, A. S., et al. (2020). Photosynthetic response of plants under different abiotic stresses: a review. *J. Plant Growth Regul.* 39, 509–531. doi: 10.1007/s00344-019-10018-x

Singh, H., Deshmukh, R. K., Singh, A., Singh, A. K., Gaikwad, K., Sharma, T. R., et al (2010). Highly variable SSR markers suitable for rice genotyping using agarose gels. *Mol. Breed.* 25, 359–364. doi: 10.1007/s11032-009-9328-1

Singh, R. K., Kota, S., and Flowers, T. J. (2021). Salt tolerance in rice: seedling and reproductive stage QTL mapping come of age. *Theor. Appl. Genet.* 134, 3495–3533. doi: 10.1007/s00122-021-03890-3

Singh, A., and Sengar, R. (2014). Salinity stress in rice: An overview. *Plant Arch.* 14, 643–648.

Singh, B., Singh, A., Singh, B., and Singh, A. (2015). Marker-assisted selection. *Marker-assisted Plant breeding: principles practices* 259-293.

Singh, R., Singh, Y., Xalaxo, S., Verulkar, S., Yadav, N., Singh, S., et al. (2016). From QTL to variety-harnessing the benefits of QTLs for drought, flood and salt tolerance in mega rice varieties of India through a multi-institutional network. *Plant Sci.* 242, 278–287. doi: 10.1016/j.plantsci.2015.08.008

Slama, I., Abdelly, C., Bouchereau, A., Flowers, T., and Savouré, A. (2015). Diversity, distribution and roles of osmoprotective compounds accumulated in halophytes under abiotic stress. *Ann. Bot.* 115, 433–447. doi: 10.1093/aob/mcu239

Tabkhkar, N., Rabiei, B., Samizadeh Lahiji, H., and Hosseini Chaleshtori, M. (2018). Genetic variation and association analysis of the SSR markers linked to the major drought-yield QTLs of rice. *Biochem. Genet.* 56, 356–374. doi: 10.1007/s10528-018-9849-6

Takahashi, F., Kuromori, T., Urano, K., Yamaguchi-Shinozaki, K., and Shinozaki, K. (2020). Drought stress responses and resistance in plants: From cellular responses to

long-distance intercellular communication. *Front. Plant Sci.* 11, 1407. doi: 10.3389/fpls.2020.556972

Thomson, M. J., De Ocampo, M., Egdane, J., Rahman, M. A., Sajise, A. G., Adorada, D. L., et al. (2010). Characterizing the Saltol quantitative trait locus for salinity tolerance in rice. *Rice* 3, 148–160. doi: 10.1007/s12284-010-9053-8

Tsai, Y.-C., Chen, K.-C., Cheng, T.-S., Lee, C., Lin, S.-H., and Tung, C.-W. (2019). Chlorophyll fluorescence analysis in diverse rice varieties reveals the positive correlation between the seedlings salt tolerance and photosynthetic efficiency. *BMC Plant Biol.* 19, 1–17. doi: 10.1186/s12870-019-1983-8

Venuprasad, R., Bool, M., Quiatchon, L., Sta Cruz, M., Amante, M., and Atlin, G. (2012). A large-effect QTL for rice grain yield under upland drought stress on chromosome 1. *Mol. Breed.* 30, 535–547. doi: 10.1007/s11032-011-9642-2

Verma, S. K., Saxena, R. R., Saxena, R. R., Xalxo, M. S., and Verulkar, S. B. (2014). QTL for grain yield under water stress and non-stress conditions over years in rice ('Oryza sativa'L.). *Aust. J. Crop Sci.* 8, 916–926.

Vikram, P., Swamy, B. M., Dixit, S., Ahmed, H. U., Teresa Sta Cruz, M., Singh, A. K., et al. (2011). qDTY 1.1, a major QTL for rice grain yield under reproductive-stage drought stress with a consistent effect in multiple elite genetic backgrounds. *BMC Genet.* 12, 1–15. doi: 10.1186/1471-2156-12-89

Vikram, P., Swamy, B. M., Dixit, S., Trinidad, J., Sta Cruz, M. T., Maturan, P. C., et al. (2016). Linkages and interactions analysis of major effect drought grain yield QTLs in rice. *PloS One* 11, e0151532. doi: 10.1371/journal.pone.0151532

Volkova, S. (2017). Estimation and selection of parental forms for breeding Kazakhstan salt tolerant rice varieties. *Biol. Agric. J.* 544. doi: 10.15389/agrobiology.2017.3.544eng

Wani, S. H., Kumar, V., Shriram, V., and Sah, S. K. (2016). Phytohormones and their metabolic engineering for abiotic stress tolerance in crop plants. *Crop J.* 4, 162–176. doi: 10.1016/j.cj.2016.01.010

Xu, K., Xu, X., Fukao, T., Canlas, P., Maghirang-Rodriguez, R., Heuer, S., et al. (2006). Sub1A is an ethylene-response-factor-like gene that confers submergence tolerance to rice. *Nature* 442, 705–708. doi: 10.1038/nature04920

Yamori, W., Kusumi, K., Iba, K., and Terashima, I. (2020). Increased stomatal conductance induces rapid changes to photosynthetic rate in response to naturally fluctuating light conditions in rice. *Plant Cell Environ.* 43, 1230–1240. doi: 10.1111/pce.13725

Zhang, Y., He, Q., Zhou, X., Zheng, S., Wang, Y., Li, P., et al. (2022). Genetic diversity and population structure of 93 rice cultivars (lines)(Oryza sativa Xian group) in Qinba in China by 3 types of genetic markers. *BMC Genomics* 23, 550. doi: 10.1186/s12864-022-08707-1

Zhao, X., Wang, W., Zhang, F., Deng, J., Li, Z., and Fu, B. (2014). Comparative metabolite profiling of two rice genotypes with contrasting salt stress tolerance at the seedling stage. *PloS One* 9, e108020. doi: 10.1371/journal.pone.0108020

frontiers | Frontiers in Plant Science

TYPE Original Research
PUBLISHED 12 March 2024
DOI 10.3389/fpls.2024.1326942

OPEN ACCESS

EDITED BY
Dominik K. Großkinsky,
Austrian Institute of Technology (AIT), Austria

REVIEWED BY
Xiang Gao,
Japan International Research Center for Agricultural Sciences (JIRCAS), Japan
Ajay Madhusudan Sorty,
Aarhus University, Denmark

*CORRESPONDENCE
Li Tang
ltang@ynau.edu.cn

†These authors have contributed equally to this work

RECEIVED 24 October 2023
ACCEPTED 26 February 2024
PUBLISHED 12 March 2024

CITATION
Zhou F, Pan Y, Zhang X, Deng G, Li X, Xiong Y and Tang L (2024) Accumulation patterns of tobacco root allelopathicals across different cropping durations and their correlation with continuous cropping challenges.
Front. Plant Sci. 15:1326942.
doi: 10.3389/fpls.2024.1326942

Accumulation patterns of tobacco root allelopathicals across different cropping durations and their correlation with continuous cropping challenges

Fangfang Zhou[1†], Yihong Pan[2†], Xiaolong Zhang[3], Guobing Deng[2], Xiaoting Li[1], Yubin Xiong[1] and Li Tang[1*]

[1]College of Plant Protection, Yunnan Agricultural University, Kunming, China, [2]College of Materials and Chemical Engineering, Southwest Forestry University, Kunming, China, [3]Yunnan Wooja Bio-tech Co.Ltd., Kunming, China

Introduction: Continuous cropping challenges have gradually emerged as pivotal factors limiting the sustainable development of agricultural production. Allelopathicals are considered to be the primary obstacles. However, there is limited information on allelopathic accumulation across various continuous cropping years and its correlation with the associated challenges.

Methods: Tobacco was subjected to varying planting durations: 1 year (CR), 5 years (CC5), 10 years (CC10), and 15 years (CC15).

Results: Our findings unveiled discernible disparities in tobacco growth patterns across diverse continuous cropping periods. Notably, the most pronounced challenges were observed in the CC5 category, characterized by yield reduction, tobacco black shank outbreaks, and a decline in beneficial flora. Conversely, CC15 exhibited a substantial reduction in challenges as the continuous cropping persisted with no significant differences when compared to CR. Within the tobacco rhizosphere, we identified 14 distinct allelopathic compounds, with 10 of these compounds displaying noteworthy variations among the four treatments. Redundancy analysis (RDA) revealed that eight allelopathic compounds exhibited autotoxic effects on tobacco growth, with MA, heptadecanoic acid, and VA ranking as the most potent inhibitors. Interaction network highlighted the pivotal roles of VA and EA in promoting pathogen proliferation and impeding the enrichment of 13 beneficial bacterial genera. Furthermore, a structural equation model elucidated that MA and EA primarily exert direct toxic effects on tobacco, whereas VA fosters pathogen proliferation, inhibits the enrichment of beneficial bacteria, and synergistically exacerbates the challenges associated with continuous cropping alongside EA.

Discussion: These findings suggested discernible disparities in tobacco growth patterns across the various continuous cropping periods. The most pronounced

challenges were observed in CC5, whereas CC15 exhibited a substantial reduction in challenges as continuous cropping persisted. VA may play a pivotal role in this phenomenon by interacting with pathogens, beneficial bacterial genera, and EA.

KEYWORDS

continuous cropping obstacles, allelopathicals, tobacco black shank, beneficial bacteria, rhizosphere

1 Introduction

There is an urgent need to alleviate continuous cropping obstacles worldwide (Li et al., 2019). Long-term continuous cropping leads to crop yield reduction, soil-borne disease outbreaks, and soil degradation (Qin et al., 2017), including nutrient imbalances, soil acidification, and disruptions in microbial community structures (Xi et al., 2019), which threaten the sustainable development of agricultural production (Liu et al., 2018).

It is widely considered that soil nutrient imbalances, disruption of microbial communities, and allelopathic autotoxicity are the most important factors for continuous cropping challenges (Deng et al., 2017; Bai et al., 2019; Ao et al., 2022). Allelochemicals, a form of root exudates, play direct (Bortolo et al., 2018) or indirect (Ren et al., 2017) roles in consecutive monoculture problems. These allelopathic compounds, mainly plant secondary metabolites such as terpenes (Zhao et al., 2018), phenolic acids (Rial et al., 2014), and saponins (Li et al., 2020), contribute to autotoxicity. Numerous allelopathicals have been reported linked to continuous cropping challenges, encompassing vanillic acid, vanillin, cinnamic acid, ferulic acid, saponin, and benzoic acid (Li et al., 2012; Ni et al., 2012; Yeasmin et al., 2014; Deng et al., 2023). In cucumber, cinnamic acid is a primary contributor to the consecutive monoculture problem (Xiao et al., 2020). Autotoxic ginsenosides alter the soil fungal community and lead to replanting failure in Sanqi (Li et al., 2020). Although phytotoxic metabolites released from *Rehmannia gulutinosa* are the main cause of replanting, the specific key allelochemicals remain unknown (Zhang et al., 2019). Eight allelochemicals have been detected in *A. lancea* roots, which exhibit significant autotoxicity during germination and seedling growth (Wang et al., 2023). Tobacco is a globally significant model plant and a major cash crop that contains abundant secondary metabolites, making it more prone to allelopathic activity (Deng et al., 2017). For example, exudates from tobacco rhizosphere soil after 12 consecutive years of continuous cropping negatively affects lettuce and tobacco seedlings, demonstrating strong allelopathy (Wu et al., 2015). Furthermore, di-*n*-butyl phthalate and disobutyl phthalate have been confirmed as autotoxins in tobacco rhizosphere (Deng et al., 2017). These results show that long-term continuous cropping results in the secretion of substances responsible for continuous cropping obstacles. Therefore, it is imperative to explore allelopathic accumulation patterns and the underlying mechanisms causing continuous cropping challenges.

Wu et al. (2015) confirmed that allelopathicals in lily rhizosphere soil increased with continuous cropping years, resulting in the inhibition of beneficial bacterial growth and adverse effects on crop development (Kumar et al., 2017). In the cucumber rhizosphere, vanillic acid, a primary allelopathic compound, modulates the composition and diversity of *Trichoderma* and *Fusarium* spp., thereby affecting plant growth (Zhou and Wu, 2018). Interactions between allelopathicals and pathogenic microorganisms can exacerbate plant diseases. The addition of 0.1 mmol/L benzoic acid externally promoted mycelial growth, sporulation ability, and conidial germination of *Fusarium solani*, causing peanut root rot (Liu et al., 2016). Gallic acid, p-hydroxybenzoic acid, and ortho-hydroxybenzoic acid can trigger soil-borne disease outbreaks, such as *Fusarium wilt* and *Verticillium wilt*, by stimulating pathogen spore germination (Zhang et al., 2012). These have aggravated continuous cropping obstacles. Meanwhile, interactions between allelopathicals and beneficial bacteria may be linked to continuous cropping obstacles. For example, autotoxins can simplify microbial structure and reduce the abundance of dominant microorganisms (Chen et al., 2018).

The above studies confirmed that allelochemicals showed an enrichment trend under continuous cropping and interacted with pathogens, leading to the occurrence of diseases (Chen et al., 2023). Conversely, certain crops exhibit the ability to enrich beneficial microorganisms over prolonged continuous cultivation, creating a soil legacy that protects subsequent crops from pathogenic bacteri (Jos and Raaijmakers, 2016; Bakker et al., 2018). For instance, in the case of continuous wheat cropping, the occurrence of wheat root rot has diminished over several years, attributed to the recruitment of antagonistic fluorescent *Pseudomonas* spp. These microorganisms release the antifungal compound 2,4-diacetylphlologlucino (David et al., 2002). Root exudates, including allelopathic substances, play a significant role in forming a soil legacy that enhances crop disease resistance (Yuan et al., 2018).However, the relationship among allelopathic substances, disease occurrence, and accumulation patterns across different continuous cropping years, and their connection to long-term continuous cropping challenges remain unclear. In this study, we identified 14 allelochemicals in tobacco

rhizosphere using GC-MS. We examined how the accumulation of these allelochemicals changed with the duration of tobacco continuous cropping. Additionally, we analyzed the interplay between these allelochemicals, tobacco growth, major soil-borne diseases, and antagonistic bacteria. The goal was to elucidate the key allelopathicals throughout different durations of continuous cropping and their potential mechanisms in causing continuous cropping obstacles.

2 Materials and methods

2.1 Study area description and soil sampling collection

The experimental plots were located in Baishui Town, Luxi County, Yunnan Province, China (103.8727°E, 24.6657°N). Luxi County is an important tobacco-producing area in Yunnan Province, where approximately 10,000 hm^2 of flue-cured tobacco are cultivated annually. Baishui Town, located in the northeastern part of Luxi County, experiences a subtropical monsoon climate characterized by an annual average temperature of 15°C, annual average precipitation of 1031.7mm, annual average frost-free period lasting 238 days, and an average of 1962.9 h of sunshine annually. These conditions make it well suited for high-quality tobacco leaf production. Four experimental plots were established, each with size of 667 m^2, all located in the same area and managed by the same farmer. The planting scenarios included tobacco planted in the first year (no previous tobacco history, CR), continuous tobacco planting for 5 years (since 2016, CC5), continuous tobacco planting for 10 years (since 2011, CC10), and continuous tobacco planting for 15 years (since 2006, CC15). Tobacco transplantation should occur annually between April 15th and May 10^{th}, with tobacco harvesting being completed before September. All plots used the Yunyan 87, a cultivar known for its moderate resistant to black shank disease (Peng et al., 2015). The natural soil in the region is classified as red soil, according to the Chinese soil classification. The planting density was set at 12,000 tobacco plants per ha. For fertilizer application, a uniform dosage of 105 kg/hm^2 of pure nitrogen to the study area. A compound fertilizer at a rate of 75 kg/hm^2 (N:P_2O_5:K_2O = 12:8:25) was used during transplanting. For the top dressing, 30 kg/hm^2 of compound fertilizer (N:P_2O_5:K_2O = 12:8:25) was applied, followed by 150 kg/hm^2 of potassium sulfate ($K_2O \geq 52\%$) for the second top dressing. The other management practices remained consistent across all plots.

In September 2020, we collected tobacco rhizosphere soil from the four experimental plots. Each soil sample consisted of five-point samples from within each plot, collected in an "S" shape pattern. After carefully excavating the entire tobacco root system and gently removing any large soil clumps, we combined the soil immediately surrounding the root surface from these five locations into a composite sample for each plot. This process was repeated six times for each treatment. To maintain sample quality, we promptly transported the soil to the laboratory in an icebox, passed it through a 2-mm sieve, and then divided it into three portions, all of which were stored at -80°C. One portion was dedicated to DNA extraction, and qPCR was used for quantitative detection of tobacco black shank pathogens. The remaining portion was used to analyze the presence of allelopathicals in the soil.

2.2 Total soil DNA extraction, PCR amplification, and high-throughput sequencing

Soil DNA was extracted using the DNeasy Power Soil Kit (Qiagen, Hilden, Germany). The 16S rRNA genes were amplified using specific primers, namely 338F (5'-ACTCCTACGGGAGMHAMHA-3') and 806R (5'-GGACTACHVGGGTWTCTAAT-3'), along with ITS1F (5'-CTTGGTCATTTAGAGGAAGTAA-3') and ITS2R (5'-MHTMHGTTCTTCATCGATMH-3'). The PCR reaction, amplification process, and purification steps followed the methodology outlined by Yang et al. (2018).

High-throughput sequencing was conducted on an Illumina HiSeq 2500 sequencer at Biomarker Tech. Initially, the raw data underwent paired-end (PE) read splicing using Flash v1.2.7. Subsequently, tags were filtered to obtain high-quality data, a process achieved with Trimmomatic v0.33. Chimeric sequences were eliminated using UCHIME v4.2 software to retain valid data. Tags were then clustered at a 97% similarity level using UCLUST within QIIME software. Operational taxonomic units (OTUs) were assigned for taxonomic annotation by referencing the Silvs and UNITE taxonomic databases. All raw sequencing data from each sample were deposited in the NCBI Sequence Read Archive (SRA) database under the accession number PRJNA719590.

2.3 Determination of rhizosphere soil allelochemicals

Based on reported allelopathic substances (Pervaiz et al., 2020; Chen Y. et al., 2022) and preliminary qualitative test reports, 14 substances with allelopathic potential were selected for quantitative testing. These substances include benzoic acid (BA), vanillin (VA), myristic acid (MA), methyl hexadecanoate (MH), scopoletin (SC), palmitic acid (PA), heptadecanoic acid (HA), linoleic acid (LA), linolenic acid (LIA), stearic acid (SA), arachidic acid (AA), 2,2′-methylenebis (6-tert-butyl-4-methylphenol) (AME), dioctyl phthalate (DOP), and erucylamide (EA).In the soil sample preparation process, a total of 5.00 g of freshly collected soil samples were introduced into a porcelain-evaporating dish, which included dried diatomaceous earth. Subsequently, these components were meticulously ground in a mortar until a homogeneous consistency akin to quicksand was achieved. The processed soil samples were then carefully transferred to an extraction tank, and 20.0 mL of an extraction solution (composed of n-hexane and acetone in a 1:1 ratio) was added. Employing an ASE, the sample was subjected to two pressurized extraction cycles, each entailing agitation at room temperature for 40 min. The resulting extract solution was meticulously decanted into a

concentration bottle. The bottle underwent a sequence of three washes, each employing 3 mL n-hexane, and the washings were subsequently reintroduced into the concentration bottle. Subsequently, the extract solution was concentrated using a rotary evaporator, yielding a final volume within the range of 3–5 mL at an operating temperature of 35°C. In a further step, 20 mL of n-hexane was reintroduced and concentrated to a volume of 3 mL. This process was repeated twice to obtain a concentrated solution with a final volume of 3 mL. The eluate, purified through these procedures, was meticulously collected in a nitrogen-blow tube. Upon reaching a volume of 0.5 mL, ethyl acetate was added to adjust the final volume to 1 mL. The prepared samples were subsequently used for machine-based detection.

For gas chromatography, the inlet temperature was set at 220°C in splitless mode. Helium was employed as the carrier gas at a column flow rate of 1.16 mL/min. The temperature program involved a gradual increase at a rate of 10°C/min until it reached 220°C and was held at this temperature for 2 min. For mass spectrometry, the interface temperature was maintained at 280°C. The ion source temperature was set at 230°C. Data acquisition was performed using ion-selective scanning. The chromatographic column used for this analysis was an Rtx-5MS.

2.4 Fluorescent quantitative PCR of *Phytophthora parasitica* var. *nicotianae* in rhizosphere soil

The total soil DNA was utilized as a template for analysis. The target genes were amplified using specific primers: PF (5'-CGAAMHCAACCATACCACGAA-3') and PR (5'-ATGAAGAACMHTMHGAACTMH-3'). The fluorescent quantitative PCR reaction was conducted in 30 μL reaction mixtures, consisting of 15 μL of qPCR Mix, 0.5 μL of Mg^{2+}, 0.5μL of PF, 0.5μL of PR, 2 μL of DNA template, and ddH_2O to reach a final volume of 30 μL. PCR thermal cycling conditions included an initial denaturation at 95°C for 3 min, followed by 35 cycles of denaturation at 95°C for 15 s, annealing at 65°C for 20 s, and extension at 72°C for 20 s. To quantify the black shank pathogen content in the soil, we constructed a standard curve using the tobacco black shank gene.

2.5 Tobacco agronomic traits, disease investigation, and analysis

For each treatment, we established five sampling points, each consisting of 50 representative tobacco plants. These sampling points were maintained from the time of tobacco transplantation until the harvest phase. Tobacco black shank disease was the main soil borne disease in the region and the word and it outbreaked at high temperature and high humidity condition(Mid-to-late July in Baishui). So a total of 250 plants from each treatment were investigate according to Ao et al. (2022). We conducted surveys every 5 days throughout July 2020 and subsequently calculated the average incidence rate according to the formula. We assessed the agronomic traits of the tobacco fields and determined the maximum leaf area index using the methodology described by Tang et al. (2020). After harvesting, we weighed the flue-cured tobacco leaves in each treatment and calculated the yield.

$$\text{Disease incidence rate}(\%) = \frac{\text{number of susceptible plants}}{\text{total number of investigated plants}} \times 100$$

2.6 Data processing and analysis

Origin 2022 was used to conduct variance analysis, generate heat maps, create correlation mappings, perform RDA analysis, and construct stacked column charts. To construct the interaction network, we utilized the R programming language, and for fitting curve estimation models, we used SPSS26.

3 Results

3.1 Characteristics of tobacco continuous cropping obstacles in different continuous cropping year

3.1.1 Variations in growth and yield of tobacco across different continuous cropping years

Tobacco stem circumference in all three continuous cropping treatments was significantly or extremely significantly lower than that in CR ($P< 0.05$ or $P< 0.01$), and the stem circumference of CC5 was the lowest among the three continuous cropping treatments, exhibiting a significant difference when compared to CC15 (Figure 1A). Additionally, maximum leaf area coefficient, and plant height in CC5 were the lowest and were significantly lower than those in CC15. No significant differences in stem circumference, maximum leaf area coefficient, and plant height were observed between CC10 and CC15 (Figures 1B, C). Significant variations were noted in tobacco yield across different continuous cropping years. CR and CC15 exhibited the highest yields, followed by CC10, while CC5 showed the lowest tobacco yield (Figure 1D). These findings highlight the substantial differences in tobacco growth under various continuous cropping durations. Growth was notably stunted after 5 years of continuous cropping, but with the extension of continuous cropping years, tobacco growth gradually normalized. After 15 years of continuous cropping, both the growth and yield of tobacco were not significantly different from those of tobacco cultivated for just 1 year.

3.1.2 Incidence of tobacco black shank and pathogen accumulation across continuous cropping years

Tobacco black shank, a predominant soil-borne disease in the region, exhibited a higher incidence in the three continuous cropping treatments than in the CR treatment. Notably, CC5 treatment had a significantly higher incidence than CR

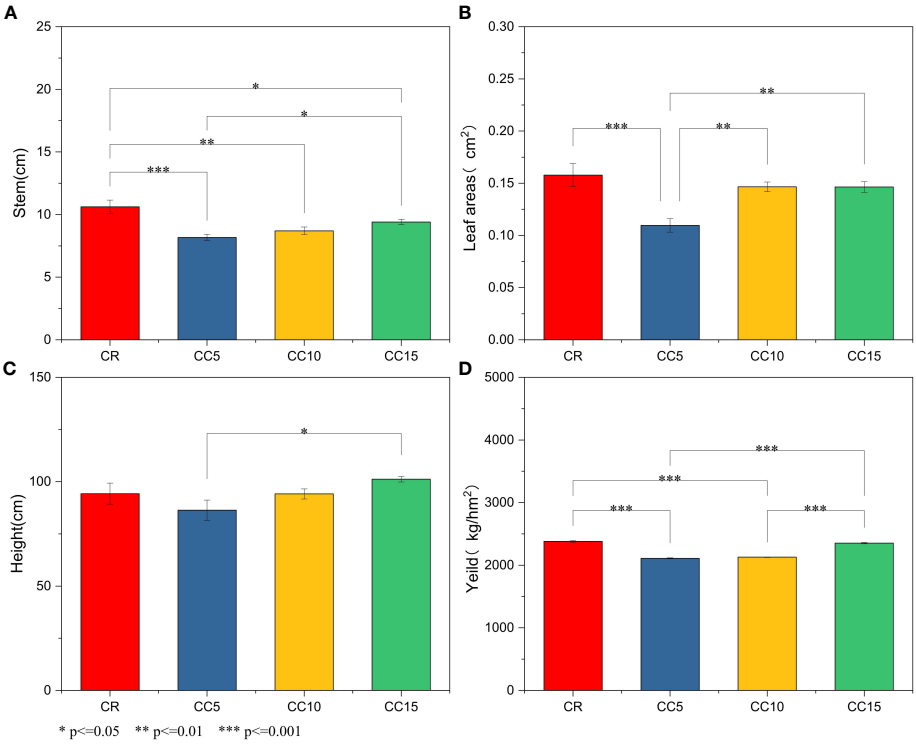

FIGURE 1
Agronomic traits and tobacco yields under different conditions. **(A)** Stem. **(B)** Leaf area. **(C)** Plant height. **(D)** Yield per ha. *, significant difference ($P < 0.05$). **/***, extremely significant difference ($P < 0.01$).

(Figure 2A). Upon comparing the incidence of tobacco black shank within the three continuous cropping treatments, it was observed that CC5 had the highest incidence, which was not significantly different from CC10, but significantly higher than CC15. This pattern of incidence correlated with the accumulation of pathogens, with the highest accumulation of black shank pathogens occurring in CC5, significantly surpassing CC10, CC15, and CR. However, no significant difference was observed between CC10 and CC15. Correlation analysis indicated that there was no significant correlation between the incidence of tobacco black shank and continuous cropping years. Conversely, a negative correlation was observed between the accumulation of black shank pathogens and continuous cropping years. Peak accumulation was noted in CC5, after which pathogen enrichment slowed with the extension of continuous cropping years, gradually leading to a decline in its content (Figure 2B).

3.1.3 Changes in the abundance of antagonistic bacterial flora against tobacco black shank pathogen across continuous cropping years

We constructed an interaction network to identify antagonistic bacterial flora against *Phytophthora parasitica* var. *nicotianae*,

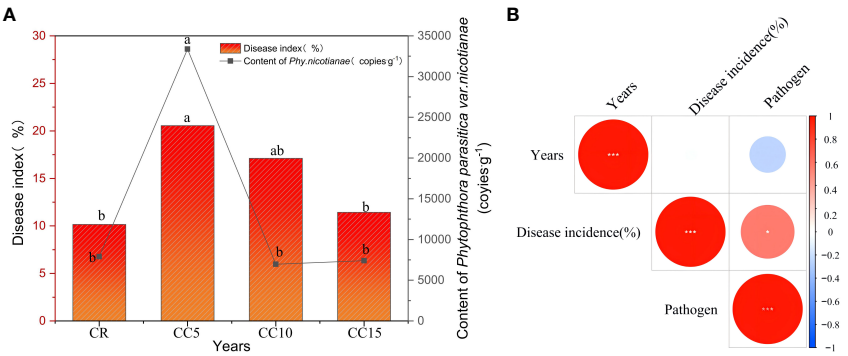

FIGURE 2
Tobacco disease index, pathogen accumulation, and correlation over continuous cropping years. **(A)** Tobacco disease index and pathogen accumulation. **(B)** Correlation among disease index, pathogen accumulation, and continuous cropping years. Different letters indicate significant differences according to the LSD test ($P < 0.05$). *significant correlation ($P < 0.05$). ***, extremely significant correlation ($P < 0.01$).

10.3389/fpls.2024.1326942

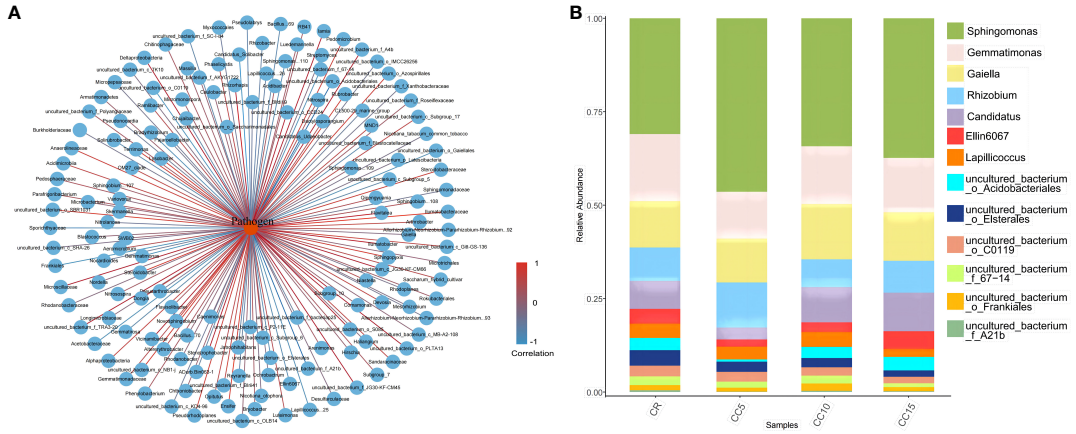

FIGURE 3
Bacteria interactions with *Phytophthora parasitica* var. *nicotianae* and the relative abundance of antagonistic bacteria. **(A)** Interaction network between *Phytophthora parasitica* var. *nicotianae* and bacteria at the genus level (> 0.1%). **(B)** Relative abundance of antagonistic bacterial flora in different continuous cropping years.

focusing on bacterial genera with a relative abundance exceeding 0.1%. Among the 65 bacterial species present in tobacco rhizosphere soil, we found a negative correlation with *Phytophthora parasitica* var. *nicotianae*, which indicated an antagonistic effect. Specifically, 13 bacterial species displayed strong antagonistic relationships with *Phytophthora parasitica* var. *nicotianae* ($P< 0.05$) (Figure 3A). We further analyzed the distribution of these 13 antagonistic bacterial groups across different continuous cropping years (Figure 3B). *Sphingomonas*, *Gemmatimonas*, *Gaiellales*, and *Rhizobium* were the dominant flora across all four treatments, collectively accounting for more than 60%. Notably, *Sphingomonas*, *Gemmatimonas*, and *Gaiellales* exhibited significant differences among treatments. The relative abundance of *Gemmatimonas* and *Gaiellales* in CR was significantly higher than that in CC5, with no significant difference observed compared to CC10 and CC15. For the different planting years, the relative abundance of *Gemmatimonas* and *Gaiellales* in CC10 and CC15 was notably higher. Except for *Lapillicoccus* and uncultured bacterium_o_C0119, the other seven bacterial groups showed significant differences across different continuous cropping years. The relative abundance of uncultured bacterium *Acidobacteriales, Candidatus*, uncultured bacterium_f_67-14, uncultured bacterium_o_*Elsterales*, uncultured bacterium_f_*A21b*, and *Ellin6067* was significantly lower than that in CC10 and CC15 with no significant difference between CC10 and CC15 ($P > 0.05$). These findings underscore the significant variations in the abundance of antagonistic bacteria within the tobacco rhizosphere across different continuous cropping treatments. In particular, the relative abundance of eight antagonistic bacteria in the CC5 treatment was significantly lower than that in CC10 and CC15. Conversely, the antagonistic bacterial flora in CC10 and CC15 exhibited a gradual increase, with no significant difference observed compared to CR.

3.2 Differential allelochemicals across continuous cropping years and their accumulation characteristics

We detected 14 allelopathicals using GC-MS for all four treatments (Figure 4). Variance analysis revealed significant differences in the 10 allelopathicals between CR and various continuous cropping years, except for BA, PA, SA, and LA ($P< 0.05$). Subsequently, we analyzed the allelopathicals across different continuous cropping years. The contents of VA and EA were notably the highest in the CC5 treatment, significantly surpassing that of CC10 and CC15. Moreover, CC15 exhibited significantly higher levels of VA and EA than CC10 did. In contrast, MA, AME, and DOP were most abundant in the CC10 treatment, with significantly higher levels than in the CC5 and CC15 treatments. Additionally, SC, HA, LIA, and MH were significantly more abundant in CC15 than in CC5 or CC10. These findings indicate that all 14 allelochemicals were detectable across the different continuous cropping treatments. Among them, 10 allelochemicals displayed significant differences in three continuous tobacco rhizosphere treatments. Furthermore, these 10 allelochemicals exhibited diverse accumulation trends in various continuous tobacco rhizosphere environments.

We established linear functions for the curve estimation model with the dependent variable (y) representing the 10 allelopathicals that exhibited significant differences between CR and various continuous cropping years. The independent variable (t) represents the tobacco planting years, and this analysis allowed us to examine the accumulation characteristics of these 10 differential allelopathicals. The accumulation trends of VA and EA followed a cubic polynomial curve model (R^2 = 0.978 and R^2 = 0.807). In contrast, the accumulation trends of MA, MH, and DOP conformed to a quadratic polynomial growth model (R^2 = 0836, R^2 = 0.728, and R^2 = 0.935). Additionally, the accumulation trends of SC, HA, LIA, AA, and AME followed a general growth model (Table 1). Based on

10.3389/fpls.2024.1326942

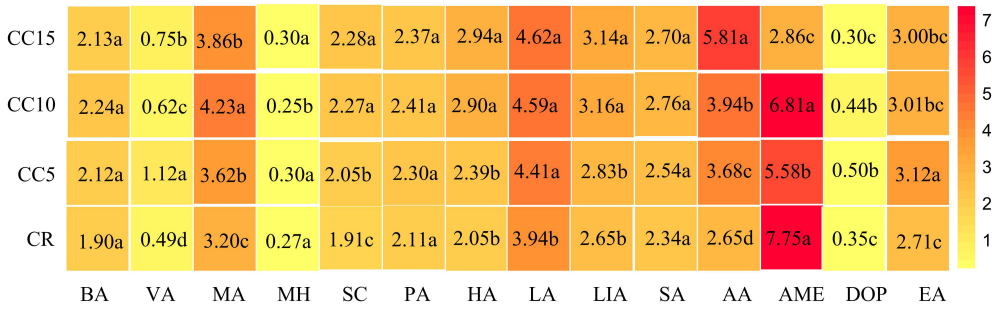

FIGURE 4
Heat map and differential analysis of 14 allelopathicals in tobacco rhizosphere. Different letters indicate significant differences according to the LSD test ($P< 0.05$). BA, benzoic acid; VA, vanillin; MA, myristic acid; MH, methyl hexadecanoate; SC, scopoletin; PA, palmitic acid; HA, heptadecanoic acid; LA, linoleic acid; LIA, linolenic acid; SA, stearic acid; AA, arachidic acid; AME, 2,2′-methylenebis (6-tert-butyl-4-methylphenol); DOP, dioctyl phthalate; EA, erucylamide.

the growth patterns observed in tobacco and the occurrence of diseases, we speculated that VA, MA, MH, DOP, and EA may be related to the continuous cropping obstacles observed in different continuous cropping years.

3.3 Screening key allelopathicals affecting tobacco continuous cropping obstacles

3.3.1 Impact of differential allelopathicals in tobacco rhizosphere on tobacco growth

The RDA analysis revealed that tobacco growth in CR and CC15 was similar, whereas CC5 and CC10 belonged to a distinct group (Figure 5). When considering the effects of the 10 differential allelochemicals on tobacco growth, they ranked from strong to weak impact as follows: MA, HA, VA, LIA, SC, DOP, AA, MH, and EA. Except for MH and AME, the other eight allelochemicals displayed negative correlations with stem circumference, tobacco plant height, and yield. Among these, MA, HA, and VA had the most pronounced negative effects, indicating that MA, HA, and VA significantly contributed to the observed effects on tobacco growth.

3.3.2 Interaction network among differential allelochemicals, *Phytophthora parasitica* var. *nicotianae*, and antagonistic microbial communities

The interaction network analysis revealed specific correlations between allelopathicals and *Phytophthora parasitica* var. *nicotianae* as well as antagonistic microbial flora (Figure 6). VA and EA exhibited positive correlations with *Phytophthora parasitica* var. *Nicotianae* and negative correlations with 13 antagonistic microbial flora ($P< 0.05$). DOP was positively correlated with *Phytophthora parasitica* var. *nicotianae* and negatively correlated with Candidatus, Bradyrhizobium, uncultured_bacteria_f_A21b, and Ellin6067. MA, MH, SC, HA, and LIA were positively correlated with most antagonistic bacteria and negatively correlated with *Phytophthora parasitica* var. *nicotianae.*

TABLE 1 Curve estimation models for 10 differential allelopathicals.

Allelopathicals	Fitting Model	Decisive factor	Significance	regression equation
		R2	P	
VA	cubic polynomial curve	0.978	0.000	$y=-0.015+0.043t^3-0.010t^2+0.001t$
MA	quadratic polynomial growth	0.836	0.000	$y=2.467+0.590t^2-0.045t$
MH	quadratic polynomial growth	0.728	0.003	$y=0.301-0.027t^2+0.003t$
SC	growth model	0.599	0.003	$y=EXP(0.647+0.021t)$
HA	growth model	0.612	0.003	$y=EXP(0.733+0.041t)$
LIA	growth model	0.593	0.003	$y=EXP(0.975+0.020t)$
AA	growth model	0.820	0.000	$y=EXP(1.039+0.079t)$
AME	growth model	0.737	0.000	$y=EXP(2.167-0.100t)$
DOP	quadratic polynomial growth	0.935	0.000	$y=0.255+0.082t^2-0.008t$
EA	cubic polynomial curve	0.807	0.003	$y=-1.059+1.938t^3-0.449t^2+0.027t$

10.3389/fpls.2024.1326942

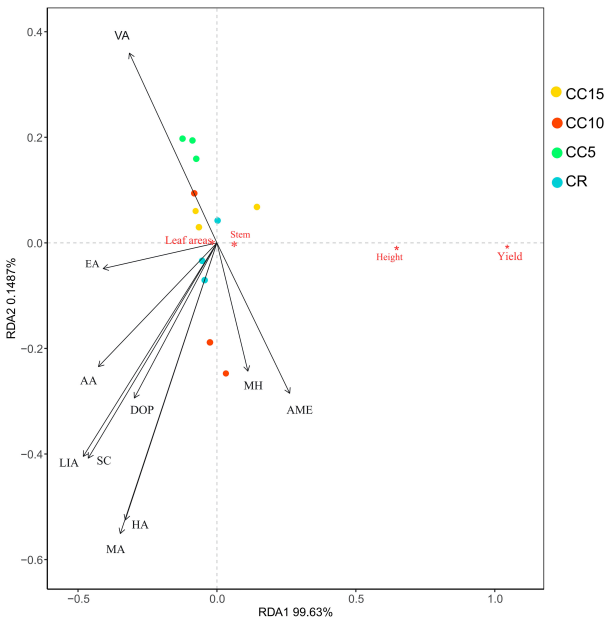

FIGURE 5
RDA analysis of differential allelopathicals and tobacco growth.

3.4 Mechanisms of key allelochemicals in causing tobacco continuous cropping obstacles

Based on the above analysis, MA, VA, and EA were found to be significant allelochemicals. The structural equation model revealed a positive correlation between VA and *Phytophthora parasitica* var. *nicotianae*, directly enhancing its accumulation (Figure 7). Conversely, it hindered the growth of beneficial bacteria, consequently promoting the accumulation of *Phytophthora parasitica* var. *nicotianae* and fostering soil-borne diseases. Furthermore, VA stimulated the accumulation of EA, exacerbating diseases and reducing crop yields. MA, on the other hand, directly impeded tobacco growth, resulting in persistent cropping obstacles. EA contributed to yield reduction by intensifying disease occurrence. These findings underscore the direct and indirect roles of these key allelopathicals in causing obstacles to continuous tobacco cropping. Notably, VA's indirect influence surpassed its direct impact, as it encouraged pathogen proliferation, impeded beneficial bacterial enrichment, and collaborated with EA to compose tobacco continuous cropping obstacles. With its multifaceted action, VA appears to be the most influential allelopathic factor contributing to the persistence of these cropping obstacles.

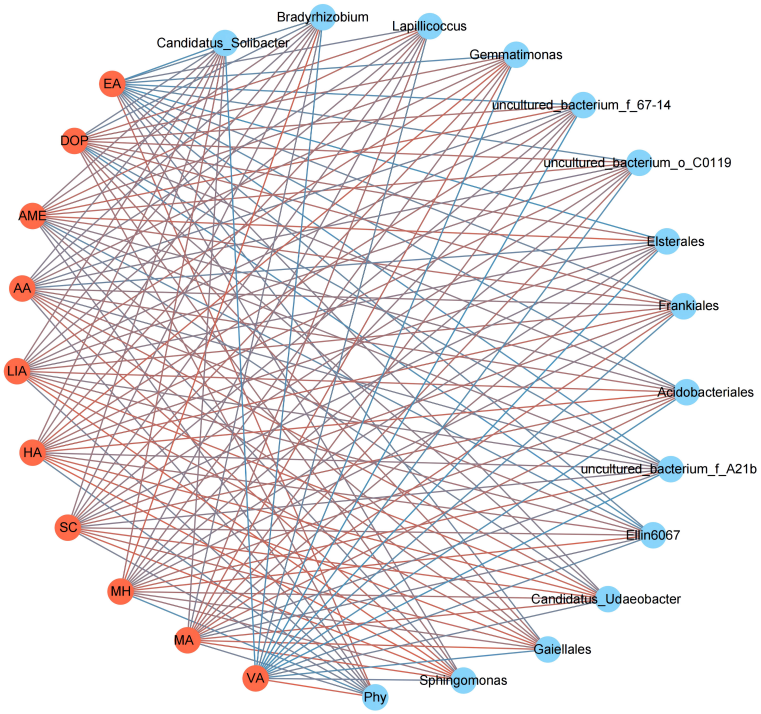

FIGURE 6
Interaction network between 10 differentiated allelopathicals, *Phytophthora parasitica* var. *nicotianae* and antagonistic bacteria. Phy, *Phytophthora parasitica* var. *nicotianae;* Red line, positive correlation; Blue line, negatively correlation ($P < 0.05$).

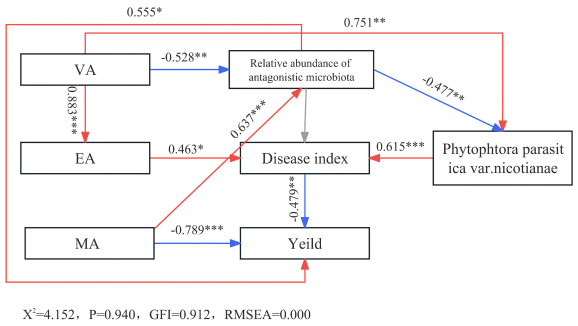

FIGURE 7
Structural equation model of main allelopathicals in tobacco rhizosphere with tobacco disease and yield. *significant correlation ($P < 0.05$). **/***, extremely significant correlation ($P < 0.01$).

4 Discussion

Continuous monoculture leads to the accumulation of soil-borne pathogens, a decline in beneficial bacteria, and disruption of the microbial community, which is often referred to as the plant's second genome. This results in poor crop growth, soil-borne disease outbreaks, and significant economic loss. This phenomenon is widespread across various crops, including food crops (Yao et al., 2020), cash crops (Gao et al., 2019; Xi et al., 2019), vegetables (Gao et al., 2019), and medicinal materials (Deng et al., 2023). In our study, we observed that tobacco growth was severely hindered after 5 years of continuous cropping, marked by a high incidence of tobacco black shank and pathogen accumulation, indicating noticeable obstacles. After 15 years of continuous cropping, we observed an improvement in tobacco growth and a reduction in disease occurrence, in contrast to the findings of Chen et al. (2018), who reported obstacles to continuous cropping 25 years after tobacco planting. This discrepancy may be attributed to the influence of the different varieties. Previous studies have demonstrated significant variations in soil microbial structure among different genotypes of the same crop (Weinert et al., 2011), influencing responses to continuous cropping by affecting soil nutrient content and crop disease resistance (Priyanka et al., 2020; Maria-Soledad et al., 2021). For example, studies on soybean varieties have revealed that tolerant varieties exhibit higher levels of beneficial bacteria, increased available nutrient content, and enhanced activities of nitrogen and phosphorus cycling enzymes than sensitive varieties (Liu et al., 2023). Microbial functions may serve as the primary mechanisms explaining these phenomena. Long-term continuous cropping in the wheat rhizosphere enriches antagonistic *Pseudomonas fluorescens* and triggers the secretion of antifungal compounds, mitigating the challenges associated with continuous cropping (Berendsen et al., 2012). In this study, we observed that the relative abundance of nine antagonistic bacterial groups in the 15-year continuous cropping rhizosphere was higher than in the 5-year continuous cropping treatment. There was no significant difference in the relative abundance of antagonistic bacterial genera in the tobacco rhizosphere after 1 and 10 years of continuous cropping. This may explain the increasing severity of tobacco continuous cropping obstacles after 5 years but their alleviation after 15 years. Analysis of antagonistic bacterial groups revealed relatively abundant genera, such as *Gemmatimonas, Gaiellales, Candidatus*, and *Ellin6067*. *Gemmatimonas* promotes plant growth and pathogen resistance (Xiong et al., 2015; Yang et al., 2018; Karthika et al., 2020). *Gaiellales* thrives in healthy plants, particularly in soils with high organic matter content (Lin et al., 2019; Pang et al., 2022). *Candidatus* is a crucial microbial community in wheat rhizospheres that positively influences crop yields and soil functions (Fan et al., 2021) and participates in soil pollutant transformations (Chen C. et al., 2022). *Ellin6067* aids in pollutant degradation and enhances plant growth (Yang et al., 2021). These results suggest that long-term continuous cropping promotes resilience of beneficial bacteria to adverse conditions, enriching bacterial groups related to plant growth, pathogen resistance, and pollutant degradation. This enrichment contributes to the formation of disease-suppressing soils and helps mitigate continuous cropping obstacles. However, the underlying reasons for the changes in tobacco rhizosphere microbial community structure with varying continuous cropping years remain unclear. Further exploration is needed to deepen our understanding of the mechanisms underlying obstacles to tobacco continuous cropping.

A study by Rial et al. (Rial et al., 2014) demonstrated that long-term continuous cropping plants release substances known as autotoxic allelopathicals into their rhizosphere, inhibiting their own growth. As continuous cropping years increase, these autotoxic allelopathicals accumulate along with soil acidification, hindering the growth and reproduction of beneficial microorganisms (Wu et al., 2015). These allelopathicals are likely the root cause of changes in rhizosphere microorganisms of continuously cropped plants, ultimately affecting plant growth. We identified 14 allelopathicals using GC-MS, of which 10 exhibited significant differences across various continuous cropping years. Further analysis revealed that the levels of VA and EA were highest after 5 years of continuous cropping, followed by a downward trend as continuous cropping years extended, conforming to a cubic polynomial growth pattern. Conversely, the levels of MA, AME, and DOP were the highest after 10 years of continuous cropping, with the accumulation of MA and DOP following a quadratic polynomial growth pattern. Allelochemicals adhering to quadratic or cubic polynomial growth patterns appeared to correlate more closely with tobacco growth and disease occurrence trends, potentially playing a role in tobacco continuous cropping obstacles. The results of the RDA indicated that MA, HA, and VA were the top three allelopathicals that significantly inhibited tobacco growth. Chen et al. (2011) verified that elevated VA concentration (1–4 nmol/L) notably inhibits eggplant seedling growth and increases the incidence of verticillium wilt disease. Myristic acids contribute to the

exacerbation of tobacco bacterial wilt by facilitating the colonization of pathogenic bacteria, consequently affecting tobacco growth (Li et al., 2016). Over short-term continuous cropping years, HA exhibits an enrichment trend correlated with an increase in tobacco continuous cropping years, potentially linked to the occurrence of continuous cropping obstacles (Pan et al., 2023). However, the current evidence lacks direct confirmation of the autotoxicity of this substance, necessitating further investigation. Network analysis further revealed that VA and EA could stimulate the accumulation of *Phytophthora parasitica* var. *nicotianae* while inhibiting the enrichment of 13 antagonistic bacteria. This may be attributed to allelopathicals serving as carbon sources that boost the proliferation of pathogenic microorganisms (Carrara et al., 2018), enabling them to dominate ecological niches, suppress beneficial bacteria growth, trigger disease outbreaks, and contribute to continuous cropping obstacles (Furtak and Gajda, 2018). In light of these findings, it is evident that MA, VA, and EA are likely key allelopathicals responsible for disrupting the rhizosphere microbial community structure, impeding tobacco growth, and leading to tobacco black shank disease.

Wu et al. (Wu, 2010) isolated several allelopathicals, including VA, from tobacco rhizosphere. Bioassays indicated that vanillin had a weaker inhibitory effect on tobacco seedlings than benzoic acid or p-hydroxybenzoic acid. Our findings suggest that the direct inhibitory effect of vanillin on tobacco growth was less pronounced than that of MA. This implies that different allelopathicals affect tobacco differently, underscoring the importance of identifying key allelopathicals and elucidating their mechanisms of action for more in-depth analysis of their pathways. Structural equation model results revealed that MA and EA primarily induced continuous cropping obstacles through direct toxicity to tobacco. VA featured prominently in the model due to its multifaceted actions. On one hand, it promoted the accumulation of *Phytophthora parasitica* var. *nicotianae*, inhibited beneficial bacterial enrichment, disrupted the tobacco rhizosphere microbial community, and exacerbated obstacles to continuous cropping. For example, low concentrations of VA encouraged eggplant Fusarium wilt, whereas high concentrations enhanced eggplant autotoxicity and inhibited eggplant growth (Chen et al., 2011). On the other hand, VA can stimulate the accumulation of EA, intensifying its direct inhibitory effect on tobacco. Wu et al. (Wu et al., 2016) confirmed that a mixture of syringic acid and phenolic acid exhibited a stronger allelopathic effect on *Radix pseudostellariae* than a single allelopathic effect, highlighting the interactions between substances that affect continuous cropping obstacles. In summary, our results indicate that MA and EA primarily impact tobacco growth through direct toxicity, whereas VA disrupts the microbial community structure and promotes EA accumulation, jointly exacerbating continuous cropping obstacles. Regardless of the scenario, key allelopathicals consistently play a pivotal role in the crop rhizosphere, serving as crucial links between rhizosphere allelopathicals, microorganisms, and crop growth, ultimately influencing the occurrence of continuous cropping obstacles. Based on our findings, we speculated that VA may be a key allelopathical in the tobacco rhizosphere, and its changing content over continuous cropping years could serve as an essential internal mechanism to alleviate obstacles in 15 years of continuous cropping.

5 Conclusion

The most pronounced challenges were observed in the CC5 category, with yield reduction, tobacco black shank outbreaks, and diminished beneficial flora. In contrast, CC15 exhibited a substantial reduction in challenges as the continuous cropping persisted. This was marked by tobacco growth recovery, a reduction in disease incidence, and an increased abundance of beneficial bacteria. This phenomenon was closely mirrored by allelochemical accumulation patterns in the tobacco rhizosphere. Notably, among these allelochemicals, VA exhibited significant variation in the tobacco rhizosphere across different planting years, following a cubic polynomial curve model. Although its direct inhibitory effect on tobacco was weaker than that of MA, VA played a pivotal role in fostering pathogen proliferation, inhibiting the enrichment of beneficial bacteria, and synergistically exacerbating the challenges associated with continuous cropping, particularly with EA. This mechanism is essential for understanding the occurrence and alleviation of continuous cropping obstacles in tobacco, particularly 15 years after planting.

Data availability statement

The datasets presented in this study can be found in online repositories. The names of the repository/repositories and accession number(s) can be found below: NCBI Sequence Read Archive (SRA) database under the accession number PRJNA719590.

Author contributions

FZ: Conceptualization, Data curation, Formal analysis, Investigation, Methodology, Resources, Validation, Visualization, Writing – original draft, Writing – review & editing. YP: Formal analysis, Investigation, Methodology, Resources, Writing – review & editing, Data curation. XZ: Formal analysis, Resources, Validation, Writing – review & editing. GD: Methodology, Resources, Validation, Writing – review & editing. XL: Data curation, Formal analysis, Writing – review & editing. YX: Data curation, Formal analysis, Writing – review & editing. LT: Conceptualization, Funding acquisition, Project administration, Resources, Supervision, Validation, Writing – review & editing.

Funding

The author(s) declare financial support was received for the research, authorship, and/or publication of this article. This study was financially supported by the National Key Research and Development Program of China (2022YFD1901503) and the Major Science and Technology Special Project of Yunnan Province (202202AE090025).

Acknowledgments

This is a short text to acknowledge the contributions of specific colleagues, institutions, or agencies that aided the efforts of the authors.

Conflict of interest

Author XZ was employed by Yunnan Wooja Bio-tech Co. Ltd.

The remaining authors declare that the research was conducted in the absence of any commercial or financial relationships that could be construed as a potential conflict of interest.

Publisher's note

References

Ao, J., Wang, Z., Yang, Q., Li, B., Li, Y., and Li, Y. (2022). Differentially enriched fungal communities in root rot resistant and susceptible varieties of tobacco (Nicotiana tabacum L.) under continuous monoculture cropping. *Front. Microbiol.* 13, 1036091. doi: 10.1111/j.1574-6941.2010.01025.x

Bai, Y., Wang, G., Cheng, Y., Shi, P., Yang, C., Yang, H., et al. (2019). Soil acidification in continuously cropped tobacco alters bacterial community structure and diversity via the accumulation of phenolic acids. *Sci. Rep.* 9, 12499. doi: 10.1038/s41598-019-48611-5

Bakker, P., Pieterse, C. M. J., De Jonge, R., and Berendsen, R. L. (2018). The soil-borne legacy. *Cell* 172, 1178–1180. doi: 10.1016/j.cell.2018.02.024

Berendsen, R. L., Pieterse, C. M., and Bakker, P. A. (2012). The rhizosphere microbiome and plant health. *Trends Plant Sci.* 17, 478–486. doi: 10.1016/j.tplants.2012.04.001

Bortolo, T. D. S. C., Marchiosi, R., Viganó, J., Siqueira-Soares, R. C., Ferro, A. P., Barreto, G. E., et al. (2018). Trans-aconitic acid inhibits the growth and photosynthesis of Glycine max. *Plant Physiol. Biochem.* 132, 490–496. doi: 10.1016/j.plaphy.2018.09.036

Carrara, J. E., Walter, C. A., Hawkins, J. S., Peterjohn, W. T., Averill, C., and Brzostek, E. R. (2018). Interactions among plants, bacteria, and fungi reduce extracellular enzyme activities under long-term N fertilization. *Glob. Chang Biol.* 24, 2721–2734. doi: 10.1111/gcb.14081

Chen, Y., Du, J., Li, Y., Tang, H., Yin, Z., Yang, L., et al. (2022). Evolutions and managements of soil microbial community structure drove by continuous cropping. *Front. Microbiol.* 13, 839494. doi: 10.3389/fmicb.2022.839494

Chen, S., Qi, G., Luo, T., Zhang, H., Jiang, Q., Wang, R., et al. (2018). Continuous-cropping tobacco caused variance of chemical properties and structure of bacterial network in soils. *Land Degradation Dev.* 29, 4106–4120. doi: 10.1002/ldr.3167

Chen, C., Yang, B., Gao, A., Yu, Y., and Zhao, F. J. (2022). Transformation of arsenic species by diverse endophytic bacteria of rice roots. *Environ. pollut.* 309, 119825. doi: 10.1016/j.envpol.2022.119825

Chen, Y., Yang, L., Zhang, L., Li, J., Zheng, Y., Yang, W., et al. (2023). Autotoxins in continuous tobacco cropping soils and their management. *Front. Plant Sci.* 14, 1106033. doi: 10.3389/fpls.2023.1106033

Chen, S., Zhou, B., Lin, S., Xia, L., and Xueling, Y. (2011). Accumulation of cinnamic acid and vanillin in eggplant root exudates and the relationship with continuous cropping obstacle. *Afr. J. Biotechnol.* 10, 2659–2665. doi: 10.5897/AJB

David, M. W., Raaijimakers, J. M., Gardener, B. B. M., and Linda, S. T. (2002). Microbial population responsible for specific soil suprressive ness to plant pathogens. *Annu. Rev. Phytopathol.* 40, 309.

Deng, L., Luo, L., Li, Y., Wang, L., Zhang, J., Zi, B., et al. (2023). Autotoxic ginsenoside stress induces changes in root exudates to recruit the beneficial Burkholderia Strain B36 as revealed by transcriptomic and metabolomic approaches. *J. Agric. Food Chem.* 71, 4536–4549. doi: 10.1021/acs.jafc.3c00311

Deng, J., Zhang, Y., Hu, J., Jiao, J., Hu, F., Li, H., et al. (2017). Autotoxicity of phthalate esters in tobacco root exudates: effects on seed germination and seedling growth. *Pedosphere* 27, 1073–1082. doi: 10.1016/S1002-0160(17)60374-6

Fan, K., Delgado-Baquerizo, M., Guo, X., Wang, D., Zhu, Y. G., and Chu, H. (2021). Biodiversity of key-stone phylotypes determines crop production in a 4-decade fertilization experiment. *ISME J.* 15, 550–561. doi: 10.1038/s41396-020-00796-8

Furtak, K., and Gajda, A. M. (2018). Activity and variety of soil microorganisms depending on the diversity of the soil tillage system. *Sustain. Agroecol.* 45, 45–61. doi: 10.5772/intechopen.72966

Gao, Z., Han, M., Hu, Y., Li, Z., Liu, C., Wang, X., et al. (2019). Effects of continuous cropping of sweet potato on the fungal community structure in rhizospheric soil. *Front. Microbiol.* 10, 2269. doi: 10.3389/fmicb.2019.02269

Jos, M., and Raaijmakers, M. M. (2016). ECOLOGY. Soil immune responses. *Science* 352, 1392–1393. doi: 10.1126/science.aaf3252

Karthika, S., Midhun, S. J., and Jisha, M. S. (2020). A potential antifungal and growth-promoting bacterium Bacillus sp. KTMA4 from tomato rhizosphere. *Microb. Pathog.* 142, 104049. doi: 10.1016/j.micpath.2020.104049

Kumar, S., Jakhar, S. R., Dahiya, S., Jangir, C. K., and Meena, R. S. (2017). Soil sickness and productivity from ecological aspects. *J. Pharmacogn. Phytochem.* 6, 827–831.

Li, S., Xu, C., Wang, J., Guo, B., Yang, L., Chen, J., et al. (2016). Cinnamic, myristic and fumaric acids in tobacco root exudates induce the infection of plants by Ralstonia solanacearum. *Plant and Soil.* 412 (1-2), 381–395. doi: 10.1007/s11104-016-3060-5

Li, Y., Dai, S., Wang, B., Jiang, Y., Ma, Y., Pan, L., et al. (2020). Autotoxic ginsenoside disrupts soil fungal microbiomes by stimulating potentially pathogenic microbes. *Appl. Environ. Microbiol.* 86, e00130–e00120. doi: 10.1128/AEM.00130-20

Li, Y., Wang, B., Chang, Y., Yang, Y., Yao, C., Huang, X., et al. (2019). Reductive soil disinfestation effectively alleviates the replant failure of Sanqi ginseng through allelochemical degradation and pathogen suppression. *Appl. Microbiol. Biotechnol.* 103, 3581–3595. doi: 10.1007/s00253-019-09676-4

Li, Z. F., Yang, Y. Q., Xie, D. F., Zhu, L. F., Zhang, Z. G., and Lin, W. X. (2012). Identification of autotoxic compounds in fibrous roots of Rehmannia (Rehmannia glutinosa Libosch.). *PloS One* 7, e28806. doi: 10.1371/journal.pone.0028806

Lin, Y., Ye, G., Kuzyakov, Y., Liu, D., Fan, J., and Ding, W. (2019). Long-term manure application increases soil organic matter and aggregation, and alters microbial community structure and keystone taxa. *Soil Biol. Biochem.* 134, 187–196. doi: 10.1016/j.soilbio.2019.03.030

Liu, J., Li, X., Jia, Z., Zhang, T., and Wang, X. (2016). Effect of benzoic acid on soil microbial communities associated with soilborne peanut diseases. *Appl. Soil Ecol.* 110, 34–42. doi: 10.1016/j.apsoil.2016.11.001

Liu, H., Pan, F., Han, X., Song, F., Zhang, Z., Yan, J., et al. (2018). Response of soil fungal community structure to long-term continuous soybean cropping. *Front. Microbiol.* 9, 3316. doi: 10.3389/fmicb.2018.03316

Liu, W., Wang, N., Yao, X., He, D., Sun, H., Ao, X., et al. (2023). Continuous-cropping-tolerant soybean cultivars alleviate continuous cropping obstacles by improving structure and function of rhizosphere microorganisms. *Front. Microbiol.* 13. doi: 10.3389/fmicb.2022.1048747

Maria-Soledad, B., Patrick, M. E., Shannon, L. O., and Lehman, R. M. (2021). Rhizosphere microbial communities explain positive effects of diverse crop rotations on maize and soybean performance. *Soil Biol. Biochem.* 159, 108309. doi: 10.1016/j.soilbio.2021.108309

Ni, L., Acharya, K., Hao, X., and Li, S. (2012). Isolation and identification of an anti-algal compound from Artemisia annua and mechanisms of inhibitory effect on algae. *Chemosphere* 88, 1051–1057. doi: 10.1016/j.chemosphere.2012.05.009

Pan, Y., Ji, X., Zhou, F., Li, X., Zhang, X., Peng, Q., et al. (2023). Long term monocropping effects tobacco yield by regulating rhizosphere allelochemicals and microbial community. *J. Biobased Mater. Bioenergy*. 17, 65–78. doi: 10.1166/jbmb.2023.2244

Pang, Z., Mao, X., Xia, Y., Xiao, J., Wang, X., Xu, P., et al. (2022). Multiomics reveals the effect of root rot on polygonati rhizome and identifies pathogens and biocontrol Strain. *Microbiol. Spectr.* 10, e0238521. doi: 10.1128/spectrum.02385-21

Peng, Shicheng, Yang, Zheng, Li, Cai, et al. (2015). Resistance identification of different flue-cured tobacco varieties against black shank. *Plant Dis. Pests*. 6, 15–18.

Pervaiz, Z. H., Iqbal, J., Zhang, Q., Chen, D., Wei, H., and Saleem, M. (2020). Continuous cropping alters multiple biotic and abiotic indicators of soil health. *Soil Syst.* 4, 59. doi: 10.3390/soilsystems4040059

Priyanka, A., Balendu Shekher, G., and Radha, R. (2020). Unravelling the role of rhizospheric plant-microbe synergy in Phytoremediation: A Genomic Perspective. *Curr. Genomics*. 21, 334–342. doi: 10.2174/1389202921999200623133240

Qin, S., Yeboah, S., Cao, L., Zhang, J., Shi, S., and Liu, Y. (2017). Breaking continuous potato cropping with legumes improves soil microbial communities, enzyme activities and tuber yield. *PloS One* 12, e0175934. doi: 10.1371/journal.pone.0175934

Ren, X., He, X., Zhang, Z., Yan, Z., Jin, H., Li, X., et al. (2017). Correction to isolation, identification, and autotoxicity effect of allelochemicals from rhizosphere soils of flue-cured tobacco. *J. Agric. Food Chem.* 65, 3783–3783. doi: 10.1021/acs.jafc.7b01914

Rial, C., Novaes, P., Varela, R. M., G. Molinillo, J. M., and Macias, F. A. (2014). Phytotoxicity of Cardoon *(Cynara cardunculus)* allelochemicals on standard target species and weeds. *J. Agric. Food Chem.* 62, 6699. doi: 10.1021/jf501976h

Tang, Z., Chen, L., Chen, Z., Fu, Y., Sun, X., Wang, B., et al. (2020). Climatic factors determine the yield and quality of Honghe flue-cured tobacco. *Sci. Rep.* 10, 19868. doi: 10.1038/s41598-020-76919-0

Wang, M., Deng, J., Duan, G., Chen, L., Huang, X., Wang, W., et al. (2023). Insights into the impacts of autotoxic allelochemicals from rhizosphere of Atractylodes lancea on soil microenvironments. *Front. Plant Sci.* 14. doi: 10.3389/fpls.2023.1136833

Weinert, N., Yvette, M. P., Guo-Chun, D., Remo, M., Holger, H., Gabriele, B., et al. (2011). PhyloChip hybridization uncovered an enormous bacterial diversity in the rhizosphere of different potato cultivars: many common and few cultivar-dependent taxa. *FEMS Microbiol. Ecol.* 75, 497–506. doi: 10.1111/fem.2011.75.issue-3

Wu, W. (2010). *Research on Tobacco autotoxic substances and their effects on rhizosphere soil microorganisms* (Fuzhou, China: Maste's Thesis, Fujian Agriculture and Forestry University).

Wu, H., Wu, L., Wang, J., Zhu, Q., Lin, S., Xu, J., et al. (2016). Mixed phenolic acids mediated proliferation of pathogens Talaromyces helicus and Kosakonia sacchari in continuously monocultured radix pseudostellariae rhizosphere Soil. *Front. Microbiol.* 7, 335. doi: 10.3389/fmicb.2016.00335

Wu, Z. J., Xie, Z. K., Yang, L., Wang, R. Y., Guo, Z. H., Zhang, Y. B., et al. (2015). Identification of autotoxins from root exudates of Lanzhou lily *(Lilium davidii* var. *Unicolor Allelopathy J.* 35, 35–48.

Xi, H., Shen, J., Qu, Z., Yang, D., Liu, S., Nie, X., et al. (2019). Effects of long-term cotton continuous cropping on soil microbiome. *Sci. Rep.* 9, 18297. doi: 10.1038/s41598-019-54771-1

Xiao, X., Lv, J., Xie, J., Feng, Z., Ma, N., Li, J., et al. (2020). Transcriptome analysis reveals the different response to toxic stress in rootstock grafted and non-grafted cucumber seedlings. *Int. J. Mol. Sci.* 21, 774. doi: 10.3390/ijms21030774

Xiong, W., Zhao, Q., Zhao, J., Xun, W., Li, R., Zhang, R., et al. (2015). Different continuous cropping spans significantly affect microbial community membership and structure in a vanilla-grown soil as revealed by deep pyrosequencing. *Microb. Ecol.* 70, 209–218. doi: 10.1007/s00248-014-0516-0

Yang, X., Lai, J. L., Zhang, Y., Luo, X. G., Han, M. W., and Zhao, S. P. (2021). Microbial community structure and metabolome profiling characteristics of soil contaminated by TNT, RDX, and HMX. *Environ. pollut.* 285, 117478. doi: 10.1016/j.envpol.2021.117478

Yang, L., Tan, L., Zhang, F., Gale, W. J., Cheng, Z., and Sang, W. (2018). Duration of continuous cropping with straw return affects the composition and structure of soil bacterial communities in cotton fields. *Can. J. Microbiol.* 64, 167–181. doi: 10.1139/cjm-2017-0443

Yao, Y., Yao, X., An, L., Bai, Y., and Wu, K. (2020). Rhizosphere bacterial community response to continuous cropping of Tibetan Barley. *Front. Microbiol.* 11, 551444. doi: 10.3389/fmicb.2020.551444

Yeasmin, R., Nakamatsu, K., Matsumoto, H., Motoki, S., Nishihara, E., and Yamamoto, S. (2014). Inference of allelopathy and autotoxicity to varietal resistance of asparagus ('Asparagus officinalis' L.). *Aust. J. Crop Sci.* 8, 251–256.

Yuan, J., Zhao, J., Wen, T., Zhao, M., Li, R., Goossens, P., et al. (2018). Root exudates drive the soil-borne legacy of aboveground pathogen infection. *Microbiome* 6, 156. doi: 10.1186/s40168-018-0537-x

Zhang, Y., Wang, L., Yao, Y., Yan, J., and He, Z. (2012). Phenolic acid profiles of Chinese wheat cultivars. *J. Cereal Sci.* 56, 629–635. doi: 10.1016/j.jcs.2012.07.006

Zhang, B., Weston, P. A., Gu, L., Zhang, B., Li, M., Wang, F., et al. (2019). Identification of phytotoxic metabolites released from Rehmannia glutinosa suggest their importance in the formation of its replant problem. *Plant Soil* 441, 439–454. doi: 10.1007/s11104-019-04136-4

Zhao, Y. M., Cheng, Y. X., Ma, Y. N., Chen, C. J., Xu, F. R., and Dong, X. (2018). Role of phenolic acids from the rhizosphere soils of *Panax notoginseng* as a double-edge sword in the occurrence of root-rot disease. *Molecules* 23, 819. doi: 10.3390/molecules23040819

Zhou, X., and Wu, F. (2018). Vanillic acid changed cucumber *(Cucumis sativus L.)* seedling rhizosphere total bacterial, Pseudomonas and Bacillus spp. communities. *Sci. Rep.* 8, 4929. doi: 10.1038/s41598-018-23406-2

frontiers | Frontiers in Plant Science

TYPE Original Research
PUBLISHED 03 May 2024
DOI 10.3389/fpls.2024.1354413

OPEN ACCESS

EDITED BY
Dongmei Li,
Shandong Agricultural University, China

REVIEWED BY
Yusuf Khan,
Oslo University Hospital, Norway
Cengiz Toker,
Akdeniz University, Türkiye

*CORRESPONDENCE
Gulmira Khassanova
khasanova-gulmira@mail.ru
Yuri Shavrukov
yuri.shavrukov@flinders.edu.au

RECEIVED 12 December 2023
ACCEPTED 17 April 2024
PUBLISHED 03 May 2024

CITATION
Khassanova G, Oshergina I, Ten E, Jatayev S, Zhanbyrshina N, Gabdola A, Gupta NK, Schramm C, Pupulin A, Philp-Dutton L, Anderson P, Sweetman C, Jenkins CLD, Soole KL and Shavrukov Y (2024) Zinc finger knuckle genes are associated with tolerance to drought and dehydration in chickpea (*Cicer arietinum* L.).
Front. Plant Sci. 15:1354413.
doi: 10.3389/fpls.2024.1354413

Zinc finger knuckle genes are associated with tolerance to drought and dehydration in chickpea (*Cicer arietinum* L.)

Gulmira Khassanova[1,2*], Irina Oshergina[2], Evgeniy Ten[2], Satyvaldy Jatayev[1], Nursaule Zhanbyrshina[1], Ademi Gabdola[1], Narendra K. Gupta[3], Carly Schramm[4], Antonio Pupulin[4], Lauren Philp-Dutton[4], Peter Anderson[4], Crystal Sweetman[4], Colin L.D. Jenkins[4], Kathleen L. Soole[4] and Yuri Shavrukov[4*]

[1]Faculty of Agronomy, S.Seifullin Kazakh AgroTechnical Research University, Astana, Kazakhstan, [2]Department of Crop Breeding, A.I.Barayev Research and Production Centre of Grain Farming, Shortandy, Kazakhstan, [3]Department of Plant Physiology, Sri Karan Narendra (SNK) Agricultural University, Jobster, Rajastan, India, [4]College of Science and Engineering (Biological Sciences), Flinders University, Adelaide, SA, Australia

Chickpea (*Cicer arietinum* L.) is a very important food legume and needs improved drought tolerance for higher seed production in dry environments. The aim of this study was to determine diversity and genetic polymorphism in zinc finger knuckle genes with *CCHC* domains and their functional analysis for practical improvement of chickpea breeding. Two *CaZF-CCHC* genes, *Ca04468* and *Ca07571*, were identified as potentially important candidates associated with plant responses to drought and dehydration. To study these genes, various methods were used including Sanger sequencing, DArT (Diversity array technology) and molecular markers for plant genotyping, gene expression analysis using RT-qPCR, and associations with seed-related traits in chickpea plants grown in field trials. These genes were studied for genetic polymorphism among a set of chickpea accessions, and one SNP was selected for further study from four identified SNPs between the promoter regions of each of the two genes. Molecular markers were developed for the SNP and verified using the ASQ and CAPS methods. Genotyping of parents and selected breeding lines from two hybrid populations, and SNP positions on chromosomes with haplotype identification, were confirmed using DArT microarray analysis. Differential expression profiles were identified in the parents and the hybrid populations under gradual drought and rapid dehydration. The SNP-based genotypes were differentially associated with seed weight per plant but not with 100 seed weight. The two developed and verified SNP molecular markers for both genes, *Ca04468* and *Ca07571*, respectively, could be used for marker-assisted selection in novel chickpea cultivars with improved tolerance to drought and dehydration.

KEYWORDS

CCHC domain, chickpea, DArT analysis, drought and dehydration, gene expression, seed yield, SNP, zinc finger knuckle gene

Introduction

Chickpea (*Cicer arietinum* L.) is an important food legume in many countries due to high levels of seed proteins and high nutrient value (Didinger and Thompson, 2022; Koul et al., 2022). The chickpea plant shows a degree of tolerance to several abiotic stresses, including drought, dehydration, heat, and salinity, making it a versatile crop plant (Arriagada et al., 2022; Asati et al., 2022; Karalija et al., 2022). However, there is room for development of new chickpea cultivars with improved growth in harsh environments, higher yield, and better seed quality (Eker et al., 2022a, Eker et al., 2022b). To achieve this goal most efficiently, the identification of the most important genes requires molecular breeding tools (Jain et al., 2023). The genomic and genetic study of chickpea is very well established (Varshney et al., 2021; Ali et al., 2022; Bohra et al., 2022) with fully sequenced genomes of cv. Frontier (Kabuli ecotype) and the accession ICC-4958 (Desi ecotype) now publicly available to researchers in databases Legume Information System (LIS, https://www.legumeinfo.org) and Chickpea Portal (http://www.cicer.info/databases.php). Within these databases, genes with zinc finger motifs can be identified.

Gene families with zinc finger (ZF) sequences form a large group and are widely distributed in all living organisms. Within these, zinc finger knuckles with CCHC (or C_2HC) domain are less well characterized compared to other ZF families. Initially, ZF-CCHC was reported in retroviruses like HIV, where nucleocapsid proteins containing CCHC domains play important roles in the viral lifecycle (Armas and Calcaterra, 2012). The CCHC domain is highly conserved with a simple consensus sequence as follows: Cys–X_2–Cys–X_4–His–X_4–Cys, where X can be any amino acid. Any change in the critical zinc-binding amino acids, i.e., any of the three Cys or His, results in a protein that is defective for RNA binding and viral packaging. ZF-CCHC proteins are found in microorganisms, yeast, plants, animals, and humans and can contain as few as 1 CCHC domain or as many as 11. These proteins play essential functions in the metabolism of nucleic acids and mediation of protein–protein interactions (Liew et al., 2000). CCHC domains, when located in the N-termini of ZF proteins, are often involved in homodimerization of transcription factors resulting either in activation or repression of various biological processes in animals based on the example of a mouse model (Grabarczyk et al., 2018).

In plants, ZF-CCHC proteins were first described as RNA-binding proteins, and they have since been found to play important roles in plant growth, development, and stress responses (Reviewed in: Lee and Kang, 2016). Recently, in a comprehensive study of bread wheat (*Triticum aestivum* L.), 50 TaZF-CCHC proteins and their corresponding genes were identified and found to be distributed in nine clusters in a molecular dendrogram (Sun et al., 2022). The authors studied 38 out of the 50 genes, and 32 of them were found to be either up- or downregulated in response to drought, heat stress, or both. Some, but not all, of the genes had similar expression patterns (Sun et al., 2022).

Individual *ZF-CCHC* genes have been functionally described for various plant species. Arginine/serine (RS)-rich splicing factors with a CCHC domain, AdRSZ21 and AtRSZp22, were confirmed to be related to plant defense and cell death via the hypersensitive response to pathogen infection found in *Arachis diogoi* (Kumar and Kirti, 2012) and in *Arabidopsis thaliana* with homologs in mammals and humans (Lopato et al., 1999). Other glycine-rich RNA-binding proteins (RZ) play an important role in plant growth regulation and improving plant resistance to bacterial infections in bread wheat (Xu et al., 2015) and to ascochyta blight in chickpea (Iruela et al., 2009). Similar RZ proteins were identified in the genus *Eucalyptus*, but their function remains unclear (Bocca et al., 2005).

The specific ZF-CCHC genes, *AIR1* and *AIR2*, encode arginine methyltransferase-interacting proteins with five CCHC domains, and they were described as important RNA-binding proteins in yeast acting as nuclear cofactors for RNA degradation via exosomes (Fasken et al., 2011; Lange and Gagliardi, 2022). Similarly, gene *GIS2*, glucose inhibition of gluconeogenic growth-suppressor 2, was first described in yeast as encoding a cytoplasmic ZF protein with seven "retroviral"-type CCHC domains and predicted to interact with DNA and possibly RNA (Scherrer et al., 2011). The AIR1, AIR2, and GIS2 proteins were not described in *A. thaliana* (L.) Heynh (Aceituno-Valenzuela et al., 2020), but similar proteins were found in bread wheat and rice (Sun et al., 2022).

Much better known are glycine-rich proteins (GRP) containing both a CCHC and a cold shock domain (CSD). This group of cold shock proteins (CSP) or cold shock domain proteins (CSDP) is very wide and intensively studied in many plant species in response to cold and freezing but not in other abiotic stresses (Sasaki and Imai, 2012). For example, in *A. thaliana*, GRP2 proteins contain both zinc finger CCHC and a cold shock domain (Kingsley and Palis, 1994), and contribute to the enhancement of freezing tolerance (Kwak et al., 2011). The expression levels of many of these genes in *A. thaliana* were upregulated by cold stress but not by drought or salinity (Kim et al., 2007, Kim et al., 2010, Kim et al., 2013).

In other plant species, for example, in saltwater cress (*Eutrema salsugineum* Pall.), CSDP proteins with a varying number of CCHC-domains in the C-terminus were found to be similar to CSDP1 and CSDP2 in *A. thaliana* (Taranov et al., 2018). In bread wheat, the gene *WCSP1* (wheat cold shock protein 1) was reported to be gradually upregulated after cold treatment but otherwise not affected by other abiotic stresses, like drought, salinity, or heat stress (Karlson et al., 2002). In rice (*Oryza sativa* L.), two genes encoding cold shock domain proteins, *OsCSP1* and *OsCSP2*, also showed increased expression, but only after a very short exposure of 0.5–1 h of cold with a subsequent return back to the initial level (Chaikam and Karlson, 2008). In cabbage (*Brassica oleracea* L.), genetic polymorphism in the *BoCSDP5* gene did not affect the gene expression levels, but other ZF-proteins were produced, with varying numbers of CCHC domains, in plants with different alleles of the *BoCSDP5* gene (Song et al., 2020).

Additionally, CSDP1 and CSDP2 proteins with seven and two CCHC domains, respectively, had an important effect on seed germination in *Arabidopsis*. The overexpression of the corresponding genes rescued a mutant for glycine-rich RNA-binding protein from cold damage (Park et al., 2010). Significantly earlier-flowering transgenic *Arabidopsis* plants were reported after silencing of the similar gene *AtGRP2* encoding a glycine-rich protein with both CSD and CCHC domains (Fusaro et al., 2007). In poplar (*Populus* × *xiaohei*

T.S. Hwang et Liang), "Zn-finger (CCHC)" genes were identified in RNA-seq transcriptome profiling of seed germination, but exact identification of the genes and encoded ZF-CCHC proteins were not provided (Qu et al., 2019).

Proteins containing a group of three amino acids: glycine–arginine–phenylalanine, designated by "GRF," encoding GRF-type ZF proteins are widely distributed throughout eukaryotes, but in plants, their structure is very different to yeast and humans sharing similarity only in the main components (Aceituno-Valenzuela et al., 2020). In *Xenopus*, protein ZF-CCHC4 with a GRF domain binding a Zn^{2+} ion plays a central structural role in coordination with a partner CCHC domain (Wallace et al., 2017). GRF-ZF proteins are involved in DNA damage response, transcriptional regulation, and RNA metabolism both in animals and plants (Aceituno-Valenzuela et al., 2020; Sun et al., 2022).

Attention has to be paid to the zinc finger CCHC-type protein in the model legume species *Medicago truncatula* Gaertn (Radkova et al., 2019, Radkova et al., 2021). This MtZF-CCHC protein (ABE91952) was unique and related to flower morphology and seed size in transgenic *M. truncatula* and *A. thaliana* lines. Overexpression of the *MtZF-CCHC* transgene caused taller plants with larger seed size, whereas the exact opposite effect was demonstrated in knockdown expression in RNAi lines, with strongly reduced seed size accompanied by shorter stem length and internodes (Radkova et al., 2019, Radkova et al., 2021).

ZF-CCHC genes have been reported to play important roles in plant responses to various abiotic stresses. For example, in rice, the nuclear-localized protein encoded by the *OsZFP6* gene was upregulated in response to abiotic factors like salinity, alkalinity, and H_2O_2 oxidative stress. These results were confirmed with transgenic yeast and *Arabidopsis* plants with *OsZFP6* overexpression, where tolerance to these abiotic stresses was significantly increased (Guan et al., 2014). The *OsZFP6* gene (LOC_Os02g34760 = LOC4329640) belongs to the retrotransposon GAG polyprotein (Sun et al., 2022). Additionally, two genes, *OsCSP1* and *OsCSP2*, were upregulated in roots and downregulated in shoots of rice seedlings exposed to dehydration (Chaikam and Karlson, 2008). Ecotypes of the reed, *Phragmites communis* Trin, a hydrophytic species can adapt well to harsh drought conditions, and proteomics analysis indicated that at least two groups of ZF-CCHC proteins are present during plant adaptation (Li et al., 2021). They include a serine-/arginine-rich protein, similar to wheat described above (Sun et al., 2022), and chloroplastic protein DEAD-box ATP-dependent RNA helicase with homology to rice, Os03t0827700 (Sun et al., 2022), *Arabidopsis*, and maize (*Zea mays* L.) (Aceituno et al., 2020).

In plant research, assessment of genetic diversity is mostly based on single-nucleotide polymorphism (SNP) analysis, with an enormous number of publications completed to date (Reviewed in: Huq et al., 2016; Morgil et al., 2020), and more specifically in chickpea (Basu et al., 2018). There are many methods available for plant genotyping based on SNP analysis (Schramm et al., 2019), including next-generation sequencing (Shavrukov et al., 2014). These include more traditional and manual techniques that are slow and have low throughput to more expensive methods like cleaved amplified polymorphic sequences (CAPS), which requires the following three steps: PCR-based amplification of a specific genetic fragment, digestion with a restriction enzyme where the recognition site specifically targets the SNP, and separation of digested fragments on gels (Reviewed in: Shavrukov, 2016). In general, it is much faster to work with medium throughput methods, for example, based on fluorescence (Förster) resonance energy transfer (FRET). Recently, allele-specific qPCR (ASQ) methods for plant genotyping have been developed that are also suitable for chickpea (Kalendar et al., 2022; Amangeldiyeva et al., 2023). Microarray technology employing thousands of simultaneous reactions on a microchip represents the next generation of plant genotyping (Varshney et al., 2012), and diversity array technology (DArT) is also very powerful and popular for the identification of SNP and haplotypes (a group of closely located SNPs) in genetic regions of entire genomes (James et al., 2008; Deres and Feyissa, 2022), including chickpea (Roorkiwal et al., 2014; Thudi et al., 2014).

However, for functional analysis, it is important to show how gene expression is changed in response to stress treatment or during plant development. RT-qPCR or RNA-seq technology thus becomes a reasonable requirement for gene studies in plants (Upton et al., 2023), including chickpea (Nguyen et al., 2015; Borhani et al., 2020). Based on genotyping and gene expression analysis, the final step for "proof of a hypothesis" is to show how selected genotypes are more tolerant to stresses and how seed yield and quality are improved. This is a classical combination of marker-assisted selection (MAS) with proven functional analysis of the candidate genes (Boopathi, 2020), and such a strategy is applicable for crop improvement in general (Ben-Ari and Lavi, 2012) and for chickpea specifically (Basu et al., 2018; Chahande et al., 2021).

The current study represents the first step in determining the diversity and genetic polymorphism in *CaZF-CCHC* and their functional analysis for practical improvement of chickpea breeding. The following strategies were used: (1) molecular–phylogenetic analysis of CaZF-CCHC proteins in chickpea and other legume species, (2) SNP analysis in two *CaZF-CCHC* genes (*Ca04468* and *Ca07571*) selected as potential candidates for improved plant response to drought, (3) SNP genotyping using ASQ and CAPS markers in parents and hybrid breeding lines of chickpea, (4) 6K DArT microarray analysis for haplotypes of genetic regions in the selected hybrid breeding lines, (5) RT-qPCR expression analysis of *Ca04468* and *Ca07571* genes in parents and hybrid breeding lines under drought and dehydration, and (6) evaluation of yield-related traits in chickpea genotypes in field trials in Kazakhstan under mild and strong drought conditions.

Materials and methods

Identification of zinc finger genes with CCHC domains, *Ca04468* and *Ca07571*, and encoded proteins

A candidate gene from the family *CaZF-CCHC* in chickpea with a potential role in tolerance to abiotic stresses was identified in the NCBI database for SNP in *C. arietinum* L. (https://

www.ncbi.nlm.nih.gov/snp). The gene family with full-length nucleotide sequences and corresponding polypeptide sequence was retrieved from the same database and used for both BLASTN and BLASTP in databases NCBI and GenomeNet, Kyoto University, Japan (https://www.genome.jp/tools/blast). After the identified *CaZF-CCHC* gene family was studied, based on differences in SNP databases, two genes, *Ca04468* and *Ca07571*, with a specific combination of Zn-finger domains, were selected for further analysis as the most suitable candidates for plant response to drought and dehydration. All sequences of genes and encoded proteins in chickpea and other legume species were identified and downloaded from GenomeNet and NCBI databases. Chromosome locations, positions on the physical map, and gene identification for chickpea was found in the Legume Information System database (LIS) using BLAST, cv. Frontier v1.0 assembly (https://www.legumeinfo.org/taxa/cicer).

The molecular–phylogenetic dendrogram was constructed using CLUSTALW Multiple Sequence Alignment at GenomeNet Database Resources (https://www.genome.jp/tools/blast) with the ETE3 FastTree program. The result file was converted into a "nex" file for further use in SplitsTree4 version 4.14.4 from algorithms in the bioinformatics website at the University of Tübingen, Germany (https://uni-tuebingen.de).

Plant material and hybridization

Initially, six chickpea germplasm accessions were studied, including three Kabuli-type cultivars, Kamila, Krasnokutsky-123, and Looch, and three Desi-type accessions, ICC-1083, ICC-10945, and ICC-12654. Additionally, accession ICC-4958 was used as a reference genotype. Seeds of the Kabuli-type cultivars were obtained from the collection of S.Seifullin Kazakh AgroTechnical Research University, Astana, Kazakhstan, and included locally adapted genotypes originating from both Russia and Kazakhstan. The remaining chickpea accessions were obtained from the ICRISAT Reference set collection, India, and distributed for research purposes in Australia.

Selected chickpea accessions were crossed using manual emasculation and controlled pollination. The true hybrid F_1 plants were confirmed by flower color, with maternal and paternal parents bearing white and colored flowers, as well as PCR analysis of the marker KATU-C22 developed earlier (Khassanova et al., 2019). Each F_2 plant was used as the progenitor of breeding line families, and F_6 breeding lines were used in the analysis. For the purpose of this study, two hybrid populations were studied as follows: (1) ♀ Krasnokutsky-123 × ♂ ICC-12654 and (2) ♀ ICC-10945 and ♂ Looch. Cultivars Krasnokutsky-123 (with dark seeds) and Looch (with light seeds), Kabuli-type, originated from Russia and Kazakhstan, respectively. Chickpea ICRISAT accessions, ICC-12654 and ICC-10945, both with dark seeds, Desi-type, originated from Ethiopia and India, respectively. In hybrid populations 1 and 2, originally 12 F_6 breeding lines were developed in each population with subsequent selection of six and seven, respectively, for DArT analysis, and three and four for qPCR and field trial testing, respectively.

Drought and dehydration experiments

Seeds were sown in 6-L plastic pots filled with BioGro, Australia, potting media with the addition of "NoduleN" chickpea legume inoculant, New Edge Microbial, Australia. For each genotype, four plants per pot and two pots per treatment were grown in a greenhouse with 26°C/18°C day/night, with natural light and, on cloudy days, supplemented with LED with a photon flux density of 800 μmol $m^{-2}{\cdot}s^{-1}$. The relative humidity was controlled at 40%, and pots were watered with tap water twice per week. Placement of plants in the greenhouse was fully randomized.

For slowly developed drought, plants were grown for 1 month in well-watered conditions. Four time-points were designated for sampling starting from "day 0," before the start of drought treatment, and 5, 7, and 9 days after watering was withdrawn. Leaf wilting symptoms in stress-treated plants were observed gradually. Watering was continued unchanged for control plants. Leaf samples were collected from three randomly selected plants (three biological replicates) for each time-point, genotype, and treatment, then frozen in liquid nitrogen and stored at −80°C for further analyses.

For rapid dehydration of detached leaves, a separate set of 1-month-old well-watered plants was used. For each genotype, leaf samples were split into four batches, designated as 0, 2, 4, and 6 h, with three biological replicates in each batch. The first group of samples (0 h) was frozen immediately in liquid nitrogen, whereas other leaf samples were exposed to dehydration on paper towel on the lab bench at room temperature (22°C). Consequently, after 2, 4, and 6 h of exposure to dehydration, leaf samples were frozen in liquid nitrogen and stored for further analyses.

DNA extraction, sequencing, and SNP identification

DNA was extracted as described earlier (Weining and Langridge, 1991; Khassanova et al., 2019) with the following adjustments. Leaf samples were collected in 10-ml tubes from individual plants and frozen in liquid nitrogen. They were ground with two 8-mm stainless ball bearings using a Vortex mixer. One microliter of DNA was checked on a 1% agarose gel to assess quality, and concentration was measured by Nano-Drop (Thermo Fisher Scientific, USA).

To identify SNPs in the identified gene fragments, they were compared with reference genotypes of cv. Frontier and accession ICC-4958, then primers were designed in coding regions and promoters (Supplementary Material S1) covering approximately 1 kb of amplification fragments. PCR was performed in 60-μl-volume reactions containing 6 μl of template DNA adjusted to 50 ng/ml and with the following components in their final concentrations as listed: 1× PCR buffer, 2 mM of $MgCl_2$, 0.2 mM each of dNTPs, 0.25 mM of each primer, and 4.0 U of GoTaq Flexi DNA polymerase (Promega, USA) in each reaction. PCR was conducted on a Thermal iCycler (Bio-Rad, USA) using a program with the following steps:

initial denaturation, 94°C, 2 min; 35 cycles of 94°C for 15 s, 55°C for 15 s, 72°C for 1 min, and a final extension of 72°C for 3 min. Single bands of the expected size were confirmed after visualization of 5 µl of the PCR product in 1% agarose gel. The remaining PCR reaction volume (55 µl) was purified using a FavorPrep PCR Purification kit (Favorgene Biotec Corp., Taiwan) following the manufacturer's protocol. The concentrations of purified PCR products were measured using NanoDrop (Thermo Fisher Scientific, USA) and later used as a template for Sanger sequencing at the Australian Genome Research Facility (AGRF), Adelaide, Australia. SNPs were visualized using the Chromas computer software program version 2.0 with manual comparison and SNP identification.

SNP genotyping using ASQ and CAPS methods

The ASQ method was used for plant genotyping following the protocol described recently (Amangeldiyeva et al., 2023). In brief, option A with a short 4-bp tag was used, and two allele-specific forward primers and one reverse primer were developed targeting two SNPs, *Ca04468*-SNP1 and *Ca07571*-SNP4. The sequence of the primers and three universal probes with attached FAM, HEX, and quencher Dabcyl are presented in Supplementary Material S1. Primers and universal probes were ordered from Sigma-Merck (Australia). Master-mix preparation was the same as described by Amangeldiyeva et al. (2023). Each reaction had a 10-µl cocktail in total and was loaded in a 96-well BioRad microplate sealed with clear tape prior to amplification in a CFX96 Real-Time PCR Detection System (Bio-Rad, USA) with automatically recorded fluorescence using the described protocol (Amangeldiyeva et al., 2023). Amplification of FAM and HEX was checked and controlled, whereas genotyping results were determined in a post-run step automatically using the software CFX Manager accompanying the qPCR instrument.

The CAPS method was used for verification of *Ca07571*-SNP4. Primers were re-designed to make the amplicon shorter to avoid multiple cutting. Sequences of the primers are present in Supplementary Material S1. The PCR reaction mix was as described above for sequencing but reduced 2× proportionally for all components with a total PCR volume of 30 µl. The PCR amplification protocol was also adjusted for shorter steps but maintained the same temperatures as follows: initial denaturation, 94°C, 2 min; 35 cycles of 94°C for 10 s, 55°C for 10 s, 72°C for 25 s, and final extension, 72°C for 1 min. After amplification, the entire 30-µl reaction was subjected to digestion with 4 µl (20 U of enzyme activity) of *Mnl*I (NEBiolab, England), 4 µl of supplied 10× CutSmart buffer, and 2 µl of sterile water making 40 µl of total digestion mix volume. After 2 h of digestion in an incubator at 37°C, digested PCR products were separated by running in 12% polyacrylamide gel, visualized with ethidium bromide using a GelDoc imaging system (BioRad, USA). In both ASQ and CASP methods, the sources of potential error could be related to the accuracy of instruments, "human error," and reproducibility of the received results. All experiments were carried out with three biological replicates (plants) and two technical replicates (repeated runs) for each studied sample, so that all potential errors are eliminated in the preliminary steps.

DArT microarray analysis

DNA extracted from leaves of individual plants as described above was adjusted to 100 ng/µl and aliquoted into 50-µl volumes and submitted to Diversity Array Technology Co., Canberra, Australia (https://www.diversityarrays.com) for genotyping using chickpea DArTseq (1.0) with 6K DArT clones. Results were presented in two major files with the Silico-DArT and SNP map used for further analysis.

RNA extraction and RT-qPCR analysis of gene expression

Leaf samples were collected from individual plants, frozen, and ground as described for DNA extractions. TRIzol-like reagent was used for RNA extraction following the protocol developed earlier (Shavrukov et al., 2013), then cDNA synthesis and RT-qPCR analysis as described previously (Sweetman et al., 2020). Briefly, after 1 µl of DNase treatment (NEBiolab, England) and reverse transcription with 2 µg of RNA using the Protoscript Reverse Transcriptase kit (NEBiolab, England), cDNA samples were diluted with sterile water (1:10), resulting in a DNA quantity of around 10 ng of cDNA, and used for RT-qPCR analysis. KAPA SYBR Fast Universal Mix (KAPA Biosystems, USA), was used in 10-µl total volume containing 0.5 µM primers and 3 µl of cDNA, and run in a CFX96 Real-Time qPCR system (BioRad, USA). Thermal cycling conditions involved an initial melt at 95°C for 3 min, followed by 40 cycles of 95°C, 5 s, and 60°C, 20 s, with post-PCR melt curve from 60°C to 95°C increasing by 0.5°C increments every 5 s. Expression levels of target genes were normalized relative to the geometric average of two reference gene transcript levels (Bustin et al., 2009): *CaELF1α*, elongation factor 1-alpha (AJ004960) and *CaHsp90*, and heat shock protein 90 (GR406804) (Garg et al., 2010). Sequences of all gene-specific and reference primers are present in Supplementary Material S1. At least three biological replicates (individual plants) and two technical repeats were used for each genotype and treatment.

Field experiments and seed-related traits analysis

For field experiments, the same three F_6 breeding lines and parents were used from hybrid population 1 (♀ Krasnokutsky-123 × ♂ ICC-12654) and four F_6 breeding lines and parents from hybrid population 2 (♀ ICC-10945 × ♂ Looch). Field experiments were carried out in 2021 and 2022 in the Akmola region (Kazakhstan) in a research field of S.Seifullin Kazakh AgroTechnical Research University. Volumetric water content (VWC) in the soil was

measured using a portable Moisture meter (Model CS616, Campbell Scientific, Australia). At the stage of fully developed plants (45 days since seed sowing), VWC value was decreased from 80% field capacity (sowing time) to 48% (mild drought) in 2021 and to 35% (strong drought) in 2022, respectively. These mild and strong drought conditions corresponded to 10% and 30% less precipitation during the crop growth period recorded in 2021 and 2022 compared to the average for many previous years.

Chickpea seeds of the selected genotypes were included in the field test and sown at the regular scheduled time, in 10–13 May. Plots were 1 m^2 with a density of 10 plants per m^2. Each genotype had three replicated plots in a randomized block design. Seeds sown manually were watered once immediately after sowing with no further watering. Seed-related traits were measured individually in each plant after harvesting, as used in other chickpea studies (Purdy et al., 2023; Tiwari et al., 2023). For the purpose of this study, only two traits were considered as follows: seed weight per plant (SWP) and hundred seed weight (HSW), which was measured and calculated directly for the seeds of each plant.

Statistical treatment

Excel 365 (Microsoft) and SPSS 25.0.0.0 (IBM) packages were used to calculate and analyze means, standard errors, and significance levels using unpaired *t*-test, ANOVA, and *post-hoc* Tukey test. Three biological and two technical replicates were used for RT-qPCR experiments, whereas two repeats were used for seed yield traits and field trials.

Results

Molecular phylogenetic analysis of ZF-CCHC proteins in chickpea and other legumes

Based on bioinformatic analysis for chickpea, 21 zinc finger proteins with a CCHC domain were identified (Supplementary Material S2). The molecular-phylogenetic tree was constructed for chickpea and several legume species, generating six clades, A-E (Figure 1). Clade A represents a diverse group among legumes but almost all proteins contained six CCHC domains and are annotated as ZF-CCHC protein 7. In chickpea, two genes were identified as belonging to Clade A. The first protein, Ca10268, contains seven CCHC domains while the more typical second protein, Ca07571, had six CCHC domains.

Stronger similarity of ZF-CCHC proteins among legumes was found in Clade B, with all of them containing five CCHC domains. However, the annotations of these proteins (e.g. NCBI, https://www.ncbi.nlm.nih.gov) were quite variable. In chickpea, only a single gene, *Ca4468*, was found in Clade B encoding ZF-CCHC domain protein 9. In contrast, Clade C contained five loosely related chickpea proteins, together with two proteins from *M. truncatula*. Two genes in Clade C, *Ca11100* and *Ca25010*, encoded zinc knuckle proteins with a single CCHC domain, but other genes with three CCHC domains had different annotations and variable functions. Clade D appears isolated, where all proteins in legumes clustered very tightly, including a single chickpea gene *Ca04752* encoding a ZF-protein with nine CCHC domains. All genes in Clade D were

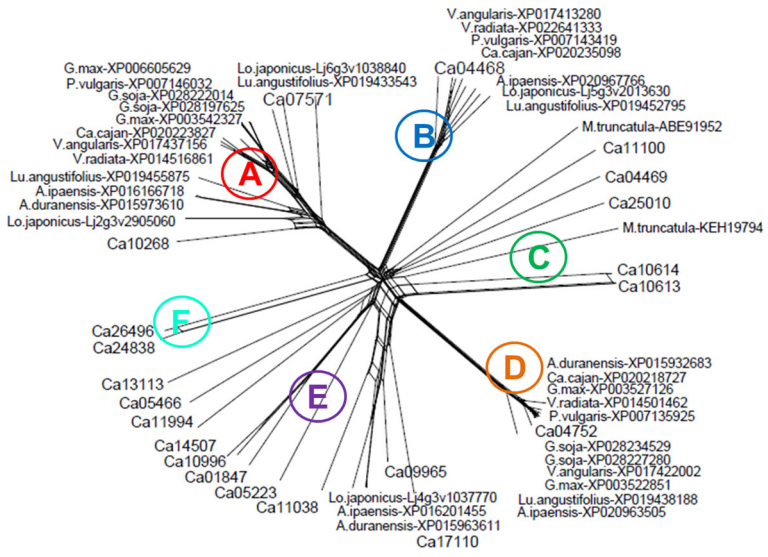

FIGURE 1
Molecular-phylogenetic tree of zinc finger proteins containing CCHC domains in chickpea and other legume plant species. The chickpea proteins are coded as Ca, *Cicer arietinum* with the following species in alphabetical order: A.duranensis, *Arachis duranensis* (wild ancestor peanut, A genome); A.ipaensis, *Arachis ipaensis* (wild ancestor peanut, B genome); Ca.cajan, *Cajanus cajan* (pigeon pea); G.max, *Glycine max* (soybean); G.soja, *Glycine soja* (wild soybean); Lo.japonicus, *Lotus japonicus* (wild model legume); Lu.angustifolius, *Lupinus angustifolius* (narrowleaf, blue lupine); M.truncatula, *Medicago truncatula* (barrelclover); P.vulgaris, *Phaseolus vulgaris* (common bean); V.angularis, *Vigna angularis* (adzuki bean); V.radiata, *Vigna radiata* (mung bean). The proteins were retrieved from the NCBI database (https://www.ncbi.nlm.nih.gov), and chickpea proteins were converted into those annotated in LIS, the Legume Information System database (https://www.legumeinfo.org). The full sequence of the chickpea and other legume proteins are presented in Supplementary Material S2.

annotated as *GIS2*, Glucose inhibition of gluconeogenic growth suppressor 2, and are involved in interaction with DNA.

Clade E contained the largest number of proteins, including several from chickpea, and these were annotated as CSDP, cold shock domain proteins, and GRP, Glycine-rich RNA-binding proteins RZ1. The proteins in this Clade contained a diverse number of CCHC domains with as many as 11 domains in Ca17110 to the more typical five domains in Ca09965, and the rest contained only one or two CCHC domains. The last Clade F contained only two chickpea proteins, Ca24838 and Ca26496, and was identified as a typical Zinc knuckle family protein with two CCHC domains but unrelated to CSP or GRP.

For this study, two chickpea genes, *Ca07571* and *Ca04468*, from Clades A and B, respectively, different in a combination of zinc finger domains, were selected for further analysis and functional characterization representing genes potentially responsive to drought and dehydration (Figure 1; Supplementary Material S2). The first gene, *Ca07571* (accession: XM_012716319), encoded "Zinc finger CCHC domain-containing protein 7" with six CCHC motifs, 528 aa (accession: XP_004502023), UniProt: A0A1S2YAP2. The gene *Ca07571* was located in the annotated reference genome of chickpea cv. Frontier, Ca5: 40,504,781–40,507,811, and has similarity with two genes in *A. thaliana*, At3g43590 and At5g36240, annotated as "Zinc knuckle (CCHC-type) family protein".

The second selected gene, *Ca04468* (accession: XM_004496505), encoded "Zinc finger CCHC domain-containing protein 9" with five CCHC motifs, 262 aa (accession: XP_004496562), UniProt: A0A1S2XZY1. The gene was located in the reference genome of chickpea cv. Frontier, Ca4: 12,446,515–12,449,051, and has a similarity with the *A. thaliana* gene, At5g52380, annotated as "Vascular-related NAC-domain protein 6".

Sequencing and SNP identification in the promoter regions of two genes, *Ca04468* and *Ca07571*, encoding ZF-CCHC proteins in chickpea

Sanger sequencing results for open reading frames (ORF) of both genes, *Ca04468* and *Ca07571*, in six chickpea germplasm accessions as follows: Kamila, Krasnokytsky-123, and Looch (Kabuli type) and ICC-1083, ICC-10945, and ICC-12654 (Desi type) revealed strong conservation, and no SNPs were identified (data not shown). In contrast, promoter regions of both genes contained four SNPs each (Figure 2; Supplementary Material S3). The distribution of the identified SNP was different in each gene among chickpea accessions in comparison to two reference chickpea genomes cv. Frontier (Kabuli type) and accession ICC-4958 (Desi type).

For gene *Ca04468*, in chromosome Ca4, all four SNP were present in the reference genomes of cv. Frontier and accession ICC-4958 (Figure 2A). SNP1 [C/T] was widely distributed among the accessions, while SNP2 [T/C], SNP3 and SNP4 [both A/T] also represented haplotypes for Frontier and ICC-4958, respectively.

For gene *Ca07571*, in chromosome Ca5 (Figure 2B), the first three SNPs, at the greatest distance from the Start codon, represented rare alleles and occurred in a single accession only, i.e., SNP1 [A/T] and SNP3 [A/T] in cv. Looch, while a "doubled" SNP2 (two very closely located SNP with just five bp between them), both [T/C], was found only in cv. Kamila. These SNPs were not found in either reference chickpea genome. In contrast, SNP4 [G/A], the most proximally located to the ORF (–261 bp) was equally distributed among six accessions: three Kabuli-type cultivars (Kamila, Krasnokutsky-123, and Looch) had SNP4 [G] similar to reference cv. Frontier, while SNP4 [A], as in reference genome of ICC-4958, was also identified in three Desi-type accessions (ICC-1083, ICC-10945, and ICC-12654). Additionally, SNP5 [T/C] was common between the reference genomes of cv. Frontier and accession ICC-4958, but all six studied chickpea germplasms were monomorphic for SNP5 [C] (Figure 2B).

Finally, one SNP was selected for each gene and confirmed in the parents of two hybrid populations as follows: *Ca04468*-SNP1 [C/T] was suitable for parents, ♀ Krasnokutsky-123 and ♂ ICC-12654, labeled as hybrid population 1, while *Ca07571*-SNP4 [A/G] was selected for the other parents, ♀ ICC-10945 and ♂ Looch, hybrid population 2 (Figure 3).

SNP genotyping of chickpea plants using the ASQ method for two targeted genes, *Ca04468* and *Ca07571*

Genotyping of chickpea plants was carried out based on SNP in each targeted gene, *Ca04468*-SNP1 and *Ca07571*-SNP4, as described above. Parents and breeding lines developed from the progenies were examined. For *Ca04468*-SNP1, hybrid population 1 [♀ Krasnokutsky-123 and ♂ ICC-12654] was used, while hybrid population 2 [♀ ICC-10945 × ♂ Looch] was selected for *Ca07571*-SNP4 genotyping.

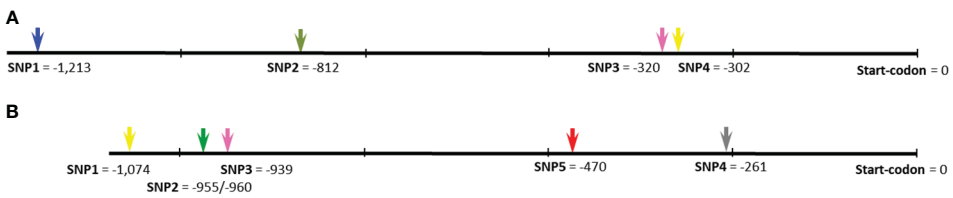

FIGURE 2
SNP identified in the promoter regions of two *ZF-CCHC* genes, *Ca04468* **(A)** and *Ca07571* **(B)**, in chromosomes Ca4 and Ca5, respectively. The position of each SNP is indicated by the number of nucleotides before the Start-codon. Full description of the identified SNP, corresponding sequences from two reference genomes, cv. Frontier and accession ICC-4958, and their comparisons are present in Supplementary Material S3.

10.3389/fpls.2024.1354413

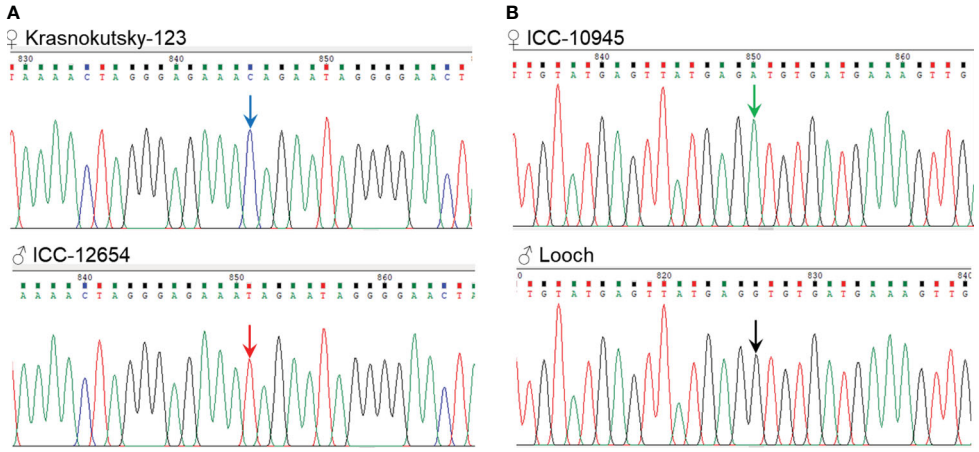

FIGURE 3
Fragments of Sanger sequencing with two SNPs selected for further study. **(A)** SNP1 [C/T] in gene *Ca04468* in the parents of hybrid population 1, ♀ Krasnokutsky-123 and ♂ ICC-12654, and **(B)** SNP4 [A/G] in gene *Ca07571* in the parents of hybrid population 2, ♀ ICC-10945 and ♂ Looch. The SNP is designated by arrows in the corresponding color.

The parents of both hybrid populations were used as reference genotypes for comparison with their breeding lines (Figure 3).

Genotyping was based on the ASQ method and examples of clear amplification of FAM or HEX fluorescence in parents Krasnokutsky-123 or ICC-12654 for *Ca04468* gene are shown (Figures 4A, B). Examples of allele discrimination are shown in Figures 4C, D for genes *Ca04468* and *Ca07571*, respectively. Results of SNP genotyping for *Ca04468* and *Ca07571* genes are present in Supplementary Material S4.

Validation of SNP genotyping for the *Ca07571* gene using a CAPS marker

The results from SNP genotyping via the ASQ method were confirmed using CAPS, but only for SNP4 in the *Ca07571* gene, because there was no suitable restriction enzyme site targeting the SNP1 fragment in the *Ca04468* gene.

For CAPS marker *Ca07571*-SNP4, a *Mnl*I restriction site was suitable, with the recognition sequence "CCTC" and "GGAG" (in

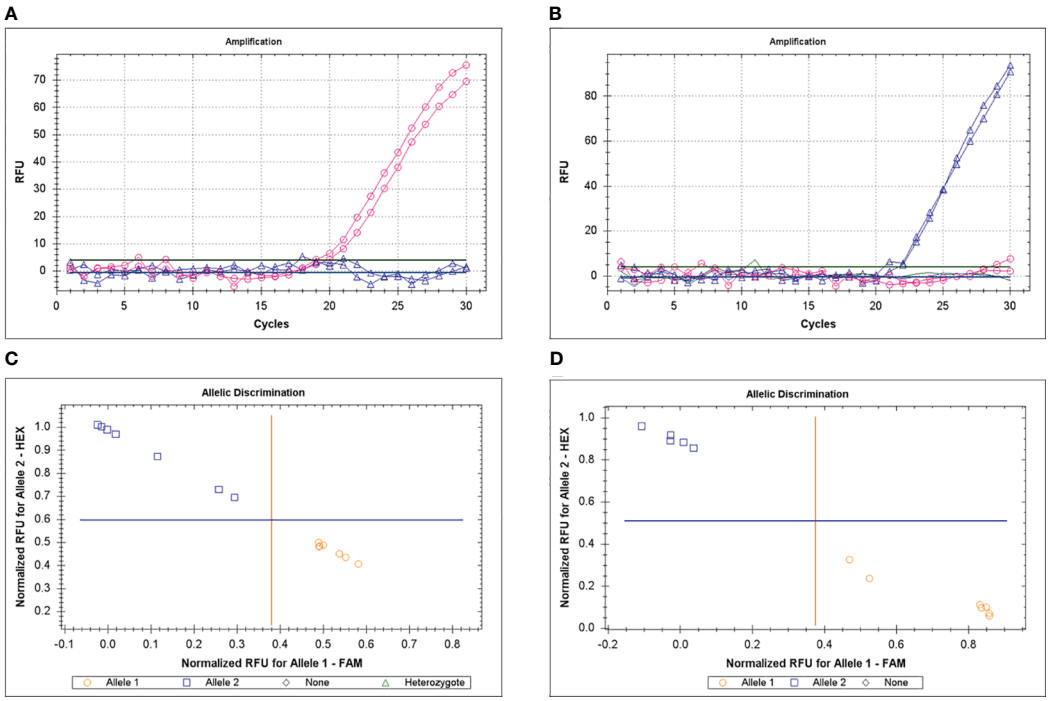

FIGURE 4
Example of genotyping for *Ca04468* gene in parents, Krasnokutsky-123 and ICC-12654, with FAM **(A)** and HEX **(B)**, respectively, using the ASQ method. Examples of allele discrimination for genes *Ca04468* **(C)** and *Ca07571* **(D)**, respectively, in two hybrid populations, 1 and 2, respectively.

the complemented strain). Due to the presence of several recognition sites in the region surrounding the SNP, a shorter amplification fragment was designed producing a 77-bp digested fragment easily visible for allele [G] in Kabuli-type chickpea (Kamila, Krasnokutsky-123, and Looch). In contrast, there was no such fragment in genotypes with allele [A] in Desi-type chickpea (ICC-1083, ICC-10945, and ICC-12654).

Results of CAPS marker analysis of ICC-10945 and Looch, parents of hybrid population 2, and eight of their breeding lines are shown in Figure 5 after separation either in agarose or in polyacrylamide gels. The paternal genotype Looch and three breeding lines confirmed the [G] allele in *Ca07571*-SNP4.

Analysis of 6K Diversity Array Technology (DArT) markers for haplotype study in *Ca04468* and *Ca07571* genes

DArT-seq analysis was applied to study genetic polymorphism and variability among a set of chickpea accessions and several hybrid populations, including hybrid populations 1 and 2, described above. After an initial filtration of the 6,000 DArT markers, 3,600 of them were polymorphic, and following that, 1,600 DArT markers had known mapping locations in the chickpea genome. For this study, DArT markers identified in the physical map of chromosomes Ca4 and Ca5 cv. Frontier were used for further analysis (Figure 6). Sequences and genetic positions of the used DArT markers and raw-data for DArT microarray analysis are present in Supplementary Materials S5, S6, respectively.

Among 298 DArT markers in chromosome Ca4 with approximately 59M bp in length, five major genetic blocks were found indicating differences in the haplotypes between parents of hybrid population 1, Krasnokutsky-123, and ICC-12654. These DArT haplotype blocks varied in size from 0.22M bp (Block 2) to 5.9M bp (Block 3), and blocks 1–3 and 4–5 were located in opposite arms of chromosome Ca4 (Figure 6A).

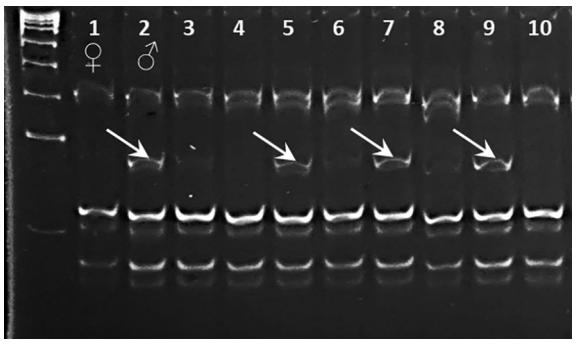

FIGURE 5
Validation of SNP genotyping for *Ca07571* gene using CAPS marker Ca07571-SNP4-*MnlI* separated in 12% polyacrylamide gel, in parents (lanes 1 and 2) and selected breeding lines (lanes 3–10) from hybrid population 1 [♀ ICC-10945 × ♂ Looch]. Fragments of 77 bp after digestion with *MnlI* are indicated by arrows.

For chromosome Ca5, which is approximately 69M bp in length, only 176 DArT markers were suitable for the analysis. Haplotypes of ICC-10945 and Looch, parents of hybrid population 2, were also characterized by five major genetic blocks. Blocks 5 and 2 were the shortest and longest DArT haplotype blocks and accounted for about 1M and 5.3M bp, respectively. The five haplotype blocks were distributed relatively similarly along chromosome Ca5 and without a tendency for concentration on the chromosome arms (Figure 6B). The density of DArT markers in chromosome Ca5 was fewer by 1.7-fold, compared to chromosome Ca4, and resulted in less identified SNPs in each haplotype block in chromosome Ca5 compared to chromosome Ca4, respectively.

A more detailed zoom of the genetic regions is shown in Figure 6C. For gene *Ca04468* in chromosome Ca4, the region between DArT markers 13146196 and 10263426 covered approximately a 1.8M-bp fragment of the chromosome. DArT markers 50759538 and 5824740 were identified as flanking the target gene *Ca04468*. Based on the flanking genetic region, four out of six hybrid breeding lines had a DArT haplotype identical to the maternal parent cv. Krasnokutsky-123. The haplotypes of two breeding lines H18-1 and H18-5 were identical to the paternal parent ICC-12654. All recombination events in the entire genetic region took place in four breeding lines, but all in the proximal part, i.e., between DArT markers 5825634 and 10263417 in lines H18-1 and H18-4, and between DArT markers 5824874 and 5826066 in lines H18-5 and H18-6 (Figure 6C).

Similarly, for gene *Ca07571* in chromosome Ca5, the region between DArT markers 10269623 and 35486562 covered a chromosome fragment of approximately 1.9M bp. The flanking DArT markers 23889105 and 23886128 surrounded the target gene *Ca07571*. Three hybrid breeding lines (H35-1, H35-5, and H35-7) had a DArT haplotype identical to the maternal parent ICC-10945. The haplotype of the paternal parent cv. Looch was found in the remaining four hybrid breeding lines. Four breeding lines, H35-2, H35-4, H35-6, and H35-7, have undergone various recombination events in the entire genetic region, both in proximal and distal parts from the target gene *Ca07571* (Figure 6C).

For further studies on gene expression, the following genotypes were selected: (1) the first three breeding lines (H18-1, H18-2, and H18-3) from hybrid population 1 together with their parents, Krasnokutsky-123 and ICC-12654; and (2) the first four breeding lines (H35-1, H35-2, H35-3, and H35-4) from hybrid population 2 and their parents, ICC-10945, and Looch.

RT-qPCR expression analysis of *Ca04468* and *Ca07571* genes in response to drought and dehydration in chickpea parents and breeding lines

Under drought stress, chickpea plants from the parental accessions and breeding lines from hybrid populations 1 and 2 showed both some similarities and differences. The expression of the *Ca04468* gene was diverse among genotypes in each hybrid population (Figure 7A). For example, in parent Krasnokutsky-123, the expression level of *Ca04468* was significantly higher at all time-points of drought treatment compared to Controls. A similar pattern

10.3389/fpls.2024.1354413

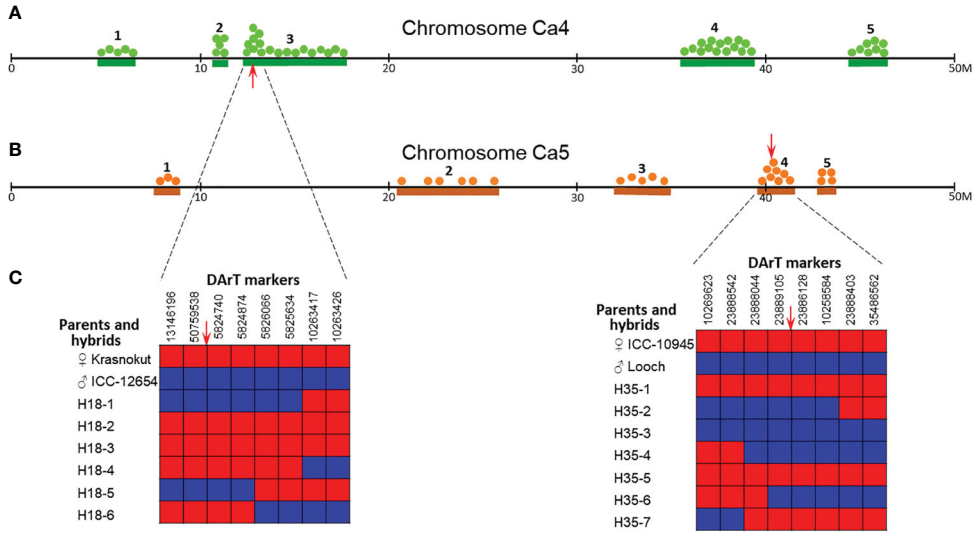

FIGURE 6
Distributions of DArT haplotype blocks in chromosomes Ca4 **(A)** and Ca5 **(B)** in parents and selected breeding lines from hybrid population 1 (Krasnokutsky-123 and ICC-12654) and hybrid population 2 (ICC-10945 and Looch), respectively. Five identified haplotype blocks with numbers above are designated by green and brown lines according to the position on the physical map of chickpea cv. Frontier, 50M bp in each chromosome. Green and brown dots correspond to SNPs found in parents and their breeding lines. Red arrows indicate positions of the target genes *Ca04468* in chromosome Ca4 **(A)** and *Ca07571* in chromosome Ca5 **(B)**. Representative "zoom" of these genetic regions with both target genes **(C)** shows the distribution of eight surrounding DArT markers in parents and hybrid breeding lines. Maternal and paternal alleles are designated by red and blue boxes, respectively. Sequences and genetic positions of the used DArT markers are present in Supplementary Material S5.

was observed in breeding line H18-3, and it was very high in line H18-2 especially after 7 days of drought stress. In contrast, no changes in *Ca04468* expression under drought was found in parent ICC-12654 and breeding line H18-1. A different situation was found in hybrid population 2, where both parents, ICC-10945 and Looch, as well as two breeding lines, H35-2 and H35-3, showed increased mRNA level and corresponding gene expression. Unexpectedly, no changes in *Ca04468* expression were found in line H35-1, while only delayed increase in expression was recorded in line H35-4 after 9 days of drought treatment. The reference genotype ICC-4958 with a high level of mRNA production was closer to genotypes of Looch and ICC-10945 rather than to ICC-12654 (Figure 7A).

The situation was dramatically different when the genes were studied in plants after dehydration treatment (Figure 7B). For the *Ca07571* gene, the parents and breeding lines of hybrid population 1 showed constantly low expression and downregulation in some

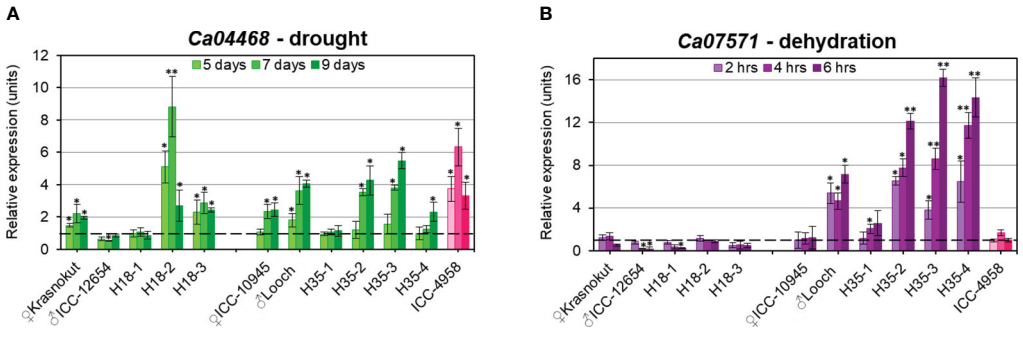

FIGURE 7
RT-qPCR expression analysis of *Ca04468* under drought stress **(A)** and *Ca07571* after dehydration treatment **(B)** in chickpea plants of parents and selected breeding lines from two hybrid populations. On the left-hand side of each panel, parents Krasnokutsky-123 and ICC-12654 and three breeding lines H18 represent hybrid population 1, while parents ICC-10945 and Looch and four breeding lines H35, on the right-hand side of the panels, belong to hybrid population 2. Plants of ICC-4958 were included as a reference genotype with a fully sequenced genome and are indicated in pink. For drought, leaf samples were collected from soil-grown plants when water was withdrawn, whereas detached leaves were exposed to dehydration on paper-towel at room temperature. Four consecutive time-points were used for sampling, and "point 0" was arranged as controls in both treatments. For all genotypes and experiments, the expressions of controls were set as unit level 1, indicated by dashed lines. Expression data were normalized using two reference genes, *CaELF1α* (elongation factor 1-alfa) and *CaHSP90* (heat shock protein 90), and are present as the average ± SE of three biological replicates (individual plants) and two technical repeats for each genotype and treatment. Significant differences (*p < 0.05 and **p< 0.01) from level 1 were calculated using two-way ANOVA with *post-hoc* Tukey test.

cases. However, the *Ca07571* mRNA level was quite different in the parents and breeding lines from hybrid population 2. The parent ICC-10945 had no change in *Ca07571* expression, while parent Looch and three breeding lines, in contrast, had a high increase in gene expression. The exception is in breeding line H35-1, which showed an increased expression level after 4 h of dehydration, but it was still much smaller than the other three breeding lines in hybrid population 2. The reference genotype ICC-4958 showed no changes in *Ca07571* expression under dehydration, similar to the majority of the studied genotypes, but differing from Looch (Figure 7B).

Seed-related traits in parents and selected breeding lines based on *Ca04468* and *Ca07571* genes

The parents and selected breeding lines from hybrid populations 1 and 2 were evaluated for seed-related traits (seed weight per plant, SWP; and 100-seed weight, HSW) in field experiments in Northern Kazakhstan for 2 years under mild and strong drought conditions (Figure 8).

SWP did not vary significantly among genotypes during mild drought stress in 2021 regardless of their alleles of both *Ca04468* and *Ca07571* (Figure 8A). In contrast, clear discrimination for SWP was found between genotypes in conditions of strong drought in the field study in 2022. Parent ICC-12654 and breeding line H18-1 showed a significantly lower SWP, and they also shared the same allele *Ca04468*-SNP1, which can be described as "unfavorable" for this trait. Other breeding lines H18-2 and H18-3 with *Ca04468*-SNP1 allele identical to the maternal parent Krasnokutsky-123 showed significantly higher SWP. Similarly, in hybrid population 2, a significantly lower SWP was recorded in maternal parent ICC-10945 and one breeding line H35-1. They have the same allele *Ca07571*-SNP4, which is also unfavorable for this trait. Another allele is present in the paternal parent Looch and the remaining three breeding lines H35 with a significantly higher SWP (Figure 8A).

Different results were found for HSW, where alleles of *Ca04468* and *Ca07571* were not associated with this trait (Figure 8B). In hybrid population 1, the seeds of paternal parent ICC-12654 and breeding line H18-2 showed a significantly smaller HSW, while other genotypes had a significantly higher HSW. In hybrid population 2, no significant differences were recorded for HSW among all genotypes, while the maternal parent ICC-10945 recorded a slightly lower HSW, probably the result of smaller seeds, but not significantly lower compared to other genotypes. The results indicate that alleles of *Ca04468* and *Ca07571* did not affect the HSW trait in chickpea genotypes under conditions of mild and strong drought (Figure 8B).

Discussion

Genes encoding zinc finger proteins with CCHC domains are important in various processes of plant life, but little information is available about their function in chickpea. The two genes selected for this study, *Ca04468* and *Ca07571*, belong to different Clades B and A in a molecular–phylogenetic tree (Figure 1). They encode zinc finger CCHC domain-containing proteins 7 and 9 with unknown functions in chickpea plants. Forward and reverse genetic approaches are often used to address this issue. Instead of going from phenotype to sequence as in forward genetics, reverse genetics works in the opposite direction—from known sequence toward assigned gene function (Alonso and Ecker, 2006). However, reverse genetics was used in a different way in our study. We focused on genes described in *Arabidopsis* and other plants species that showed a high degree of similarity to the genes in chickpea, *Ca04468* and *Ca07571*, and these were characterized for the first time in the current research. These two selected candidate genes with a specific combination of Zn finger domains were shown to be expressed in the chickpea genome (Supplementary Material S2). Therefore, our research leverages selected genes studied earlier in other plants species for the discovery of novel genes in chickpea;

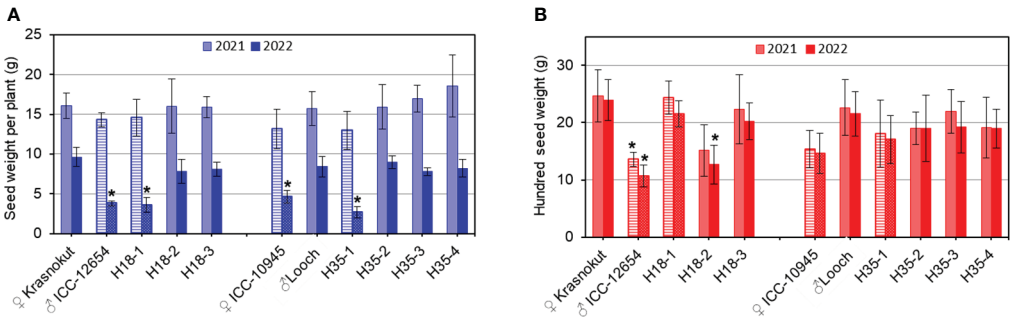

FIGURE 8
Seed-related traits: seed weight per plant **(A)** and hundred seed weight **(B)** in parents and selected breeding lines from hybrid populations 1 and 2. Data were calculated as the average of the plants grown in the field experiments, 1 m^2 plot (n = 10), with three replicates, in the Akmola region, Northern Kazakhstan, over 2 years, 2021 (lighter color) and 2022 (darker color) with mild and strong drought, respectively. Parents and breeding lines that carried unfavorable alleles of *Ca04468* and *Ca07571* genes are shown in bars with stripes and dots. Error bars represent standard errors. Significant differences (*p < 0.05) are shown for genotypes compared to another parent and breeding lines in each hybrid population, and were calculated using two-way ANOVA with *post-hoc* Tukey test.

and this method is very different from forward genetics with QTL and linkage analysis (Aklilu, 2021).

However, a confusing situation exists in cluster 6 with wheat and rice ZF-CCHC proteins, where the same or similar proteins have different annotations (Sun et al., 2022). For example, protein LOC_Os04g46920, of 277 aa in length, was described as a "Zinc knuckle domain-containing protein" (Rice Genome Annotation Project: http://rice.uga.edu), while the same protein sequence, NP_001406677 = LOC129456122 = Os04g0555800, was annotated as "Arginine methyltransferase-interacting protein" (NCBI: https://www.ncbi.nlm.nih.gov). Furthermore, the closest homolog in *A. thaliana*, At5g52380, was annotated as "Vascular-related NAC-domain 6," 268 aa in length (Yamaguchi et al., 2008). Such dissimilar protein descriptions reflect the complexity and wide diversity of ZF-CCHC proteins, including those containing NAC-domains or interactivity with arginine methyltransferase, perhaps relating to different motifs and structural elements within the proteins.

The other chickpea *ZF-CCHC* genes do not have clear similarity with wheat and rice homologs. For example, genes from Clade E in chickpea (cold shock proteins and glycine-rich proteins with CCHC domains) were similar to several clusters in wheat and rice, including clusters 7 (CSP) and 1–3 (GRP), respectively (Figure 1). Proteins in Clade C had altogether weak similarity with ZF-CCHC proteins in clusters with wheat and rice (Sun et al., 2022).

Based on the ORF sequences of the two selected genes, *Ca04468* and *Ca07571*, their encoded proteins were highly conserved. Nevertheless, our results demonstrate significant genetic polymorphism in the promoter regions of several chickpea accessions (Figures 2, 3). This could indicate that the regulation of *Ca04468* and *Ca07571* genes occurs via additional transcription factors differentially binding the promoters of these genes to enhance or inhibit their expression. However, there is no evidence for this yet, but this may be a promising area for future experiments, where potential transcriptional factors regulating the studied *ZF-CCHC* genes may be identified using, for example, RNA-seq technology. Any SNP in coding or non-coding regions of genes can be used for molecular marker development and further plant genotyping, as demonstrated by previous successful applications for molecular breeding in chickpea (Hiremath et al., 2012; Kujur et al., 2015; Shimray et al., 2017), including marker KATU-C22 developed by the authors (Khassanova et al., 2019). In the current study, suitable SNPs, *Ca04468*-SNP1 and *Ca07571*-SNP4, were identified in promoter regions of the genes (Figures 2, 3).

In the current study, the ASQ method was adapted and successfully used for the first time for the genotyping of chickpea plants. In the established hybrid populations, two parents (vs. Krasnokutsky-123 and Looch), known to be well-adapted to the dry environments of Kazakhstan, were crossed with germplasm accessions with superior seed quality and protein content. Based on plant genotyping performed using the ASQ method and verified via CAPS markers, parents and hybrid breeding lines were assessed for alleles of *Ca04468*-SNP1 and *Ca07571*-SNP4 in two *CaZF-CCHC* genes in chickpea. The ASQ method based on fluorescence measurement showed strong amplification of either FAM or HEX signals (Figure 4). The allele discrimination and genotyping results are clear using this ASQ method with medium throughput working effectively in 96- or 384-well microplates and qPCR instruments. Successful results for the ASQ method were recorded earlier in the genotyping of barley (Kalendar et al., 2022), sugar beet, and tomato (Amangeldiyeva et al., 2023).

CAPS markers are useful for the verification of genotyping results. However, the CAPS method has also significant limitations. For example, only one marker, *Ca07571*-SNP4-*Mnl*I, was developed with a single restriction enzyme. In the current study, this CAPS marker was generated and used, but the application of this CAPS marker was much slower and more expensive. For the other marker, *Ca04468*-SNP1, there was no restriction enzyme available with a recognition site targeting the SNP. In this situation, it may have been possible to develop a dCAPS marker (derived CAPS), where a restriction site can be introduced at the SNP position using specific primers. However, this additional step further complicates the process. In a comparison between both methods, ASQ genotyping definitely has an advantage. Nevertheless, in chickpea research, both CAPS and dCAPS markers have also been used effectively (Gujaria et al., 2011; Jaganathan et al., 2015). They remain slower and more expensive compared to other modern methods of plant genotyping.

DArT-seq microarray analysis is a very different and powerful approach. Our results demonstrated that the genetic regions with the identified SNPs were included in the DArT-based haplotype groups. Therefore, microarray and DArT markers confirmed the genotyping results for the two genes studied using an alternative technology. A similar DArT method was used for the mapping and identification of genetic regions with candidate genes in chickpea hybrid populations (Thudi et al., 2011; Atieno et al., 2021).

RT-qPCR analysis revealed that the gene *Ca04468* was strongly expressed in both hybrid populations under slowly developed drought, and it was associated with *Ca04468*-SNP1 genotypes in parents and breeding lines of hybrid population 1. In contrast, under rapid dehydration, no change, or downregulation of *Ca04468*, gene expression was evident in genotypes of hybrid population 1, while a strong association was found in parents and breeding lines of hybrid population 2 associated with *Ca07571*-SNP4 genotypes exposed to dehydration. Therefore, both genes, *Ca04468* and *Ca07571*, were specific in their expression to drought and dehydration, and genotype-dependent in hybrid populations 1 and 2, respectively.

The expression analysis of the two studied genes was associated with genotyping results using ASQ markers, *Ca04468*-SNP1 and *Ca07571*-SNP4. These markers were developed based on SNP in promoter regions of the genes, and at the current stage, we can hypothesize that chickpea haplotypes with different SNPs can confer the regulation of gene expression in plants under drought and dehydration. Additionally, in further experiments, the two ASQ molecular markers, *Ca04468*-SNP1 and *Ca07571*-SNP4, developed for the studied genes, must be tested in broader application in chickpea breeding programs, with analysis of their advantages and potential limitations.

Finally, from seed-related traits, SWP was strongly associated with *Ca04468* expression in plants of hybrid population 1, while a similar significant association with *Ca07571* was found in hybrid population 2. This indicates that both genes play an important role in plants grown under mild and especially severe drought conditions. However, their mechanisms of action differed in soil-based drought and under dehydration in detached leaves. These results are similar to many others published earlier during comparisons of the slow drying of soil or substrate, where plants can adapt to drought gradually, or dehydration shock, with the sudden detaching of leaves or removal of plants from hydroponics. For example, drought and dehydration have different effects for aquaporin genes in resurrection plants (*Craterostigma plantagineum* Hochst.) (Mariaux et al., 1998), two genes encoding enzymes of the abscisic acid biosynthesis pathway in tomato (*Lycopersicon esculentum* Mill.) (Thompson et al., 2000), ascorbate peroxidase genes in cowpea [*Vigna unguiculata* (L.) Walp.] (D'Arcy-Lameta et al., 2006), dehydrin genes in Bermuda grass [*Cynodon dactylon* (L.) Pers.] (Hu et al., 2010), and several antioxidant-related genes and transcription factors in barley (*Hordeum vulgae* L.) (Gürel et al., 2016). It can be concluded that experiments with drought and dehydration must be considered very differently.

In our study, seeds were analyzed in individual plants grown in real field experiment under different levels of drought, and this method is used often in chickpea (Chetariya et al., 2022; Patil et al., 2023; Sundaram et al., 2023). Seed-related traits are complex (Sundaram et al., 2018), where many genes are involved, including chickpea (Shimray et al., 2017; Kivrak et al., 2020). For the SWP trait, *Ca09705*, an ABC transporter gene for glutathione conjugates was reported and mapped to chromosome Ca2 in chickpea collections and hybrid populations (Basu et al., 2019). The authors reported an enormous 20% increase in seed yield in hybrid plants with favorable haplotypes of the *CaABC* transporter gene under growing conditions without drought or dehydration. In the same chromosome Ca2, another gene *Ca03044*, encoding a pentatricopeptide repeat (PPR)-containing protein, was closely associated with SWP in chickpea using genome-wide genotyping of informative SNPs under non-stressed conditions (Basu et al., 2018).

Seed number per pod was not analyzed in this study, but it ultimately relates to seed yield in chickpea, and was regulated by the *Ca17942* gene, cellulose synthase, *CesA3*, mapped to chromosome Ca5 (Kujur et al., 2015). It was found during genome-wide SNP scanning for strong association in a chickpea grown without stresses. In proteomics analysis, drought-tolerant and sensitive chickpea genotypes showed changes in 29 and 30 proteins, respectively, under drought stress (Vessal et al., 2020). Such massive changes need careful analysis of the identified proteins and encoding genes. Among more than 430K studied SNPs, the NAC transcription factor (*Ca05696*, chromosome Ca6) and possible downregulated gene-encoded histone H3 protein (*Ca15001*, chromosome Ca2) harbor the major QTL for seed yield under drought in chickpea (Sharma et al., 2019). Therefore, many genes have been identified as involved in seed yield in chickpea, both in normal conditions and under drought; in our study, *CaZF-CCHC* genes for the first time showed some promising results for seed weight per plant grown in a dry environment. Additionally, phenotypic variability of seed-related traits and tolerance to drought and dehydration must be studied and verified in different chickpea accessions and breeding lines grown in diverse environments in future experiments.

No associations between *ZF-CCHC* genes and seed yield in plant species have been published to our knowledge. However, in an interspecific cross between bread wheat and *Triticum spelta* (3338 × Di7), the glycine-rich protein with RNA-binding and CCHC domains, AG5, was very strongly indicated in young leaves of F_1 hybrid plants compared to both parents (Ni et al., 2000). These hybrid plants showed 40% more grain yield compared to the high-yielding wheat parent 3338. The authors hypothesized about the *AG5* gene role in wheat heterosis, but they also indicated that many other genes were expressed specifically in this hybrid (Ni et al., 2000). The *AG5* was reported to have a strong similarity to the *RZ1* gene in tobacco and belongs to cluster 3 in the wheat study by Sun et al. (2022). We identified from NCBI, the wheat protein, accession AAK01176, identical to AG5 and annotated it as "RNA-binding protein with zinc knuckle CCHC domain," with the corresponding gene accession AF315811. BLAST comparison revealed that the closest homolog of AG5 protein in chickpea was Ca05223 (accession: XP004504758), which is located in Clade E (Figure 1). This discovery indicates the very diverse functions of *ZF-CCHC* genes in different crop species, and each candidate gene needs careful evaluation in future analysis.

In our study, both genes, *Ca04468* and *Ca07571*, showed no influence on HSW. These results differed from those published earlier for chickpea, where two genes, *Ca04364* and *Ca04607*, were identified as strongly associated with HSW. These genes were mapped to chromosome Ca4 and encoded a cell division protein kinase and a transmembrane protein, respectively (Singh et al., 2016), and a very different chickpea hybrid population was used in that study [ICC 4958 × ICC1882].

The HSW trait is presumably directly related to seed size. Our findings were also different from those for the *MtZF-CCHC* gene in *Medicago truncatula*, where seed size was significantly enlarged in plants with overexpression of this gene (Radkova et al., 2019, Radkova et al., 2021). However, the MtZF-CCHC protein was similar to those in Clade C presented here (Figure 1) and very different from Clades A and B including the chickpea proteins encoded by *Ca04468* and *Ca07571*.

In summary, the two genes, *Ca04468* and *Ca07571*, which code for zinc finger knuckle motifs with CCHC domains, were identified as potential important candidate genes associated with plant response to drought and dehydration. The SNP-based genotypes had different roles in traits of seed weight per plant but not 100-seed weight. The developed and verified two SNP molecular markers for both genes, *Ca04468* and *Ca07571*, could be used for marker-assisted selection for improving tolerance to drought and dehydration and may be applied to the production of novel chickpea cultivars in the future.

Data availability statement

The original contributions presented in the study are included in the article/Supplementary Material, further inquiries can be directed to the corresponding authors.

Author contributions

GK: Investigation, Writing – original draft. IO: Data curation, Writing – review & editing. ET: Software, Writing – review & editing. SJ: Funding acquisition, Writing – review & editing. NZ: Validation, Writing – review & editing. AG: Visualization, Writing – review & editing. NG: Writing – review & editing, Resources. CSc: Writing – review & editing, Writing – original draft. AP: Resources, Writing – review & editing. LP-D: Visualization, Writing – review & editing. PA: Methodology, Writing – review & editing. CSw: Formal analysis, Writing – review & editing. CJ: Funding acquisition, Writing – review & editing. KS: Supervision, Writing – review & editing. YS: Conceptualization, Writing – original draft.

Funding

The author(s) declare that financial support was received for the research, authorship, and/or publication of this article. This research was funded by the Science Committee of the Ministry of Science and Higher Education, Republic of Kazakhstan, AP14869777, for GK, IO, ET, SJ, and AG; and the International Bolashak Fellowships 15/1-267 for GK. Open access funding for the publication was provided by the Ministry of Science and Higher Education, Republic of Kazakhstan.

Acknowledgments

We want to thank the staff and students of our universities and the Research Institute for their support in this research and help with critical comments to the manuscript.

Conflict of interest

The authors declare that the research was conducted in the absence of any commercial or financial relationships that could be construed as a potential conflict of interest.

Publisher's note

Supplementary material

The Supplementary Material for this article can be found online at: https://www.frontiersin.org/articles/10.3389/fpls.2024.1354413/full#supplementary-material

SUPPLEMENTARY MATERIAL S1
Sequences and information about primers and molecular probes used for: (1) Sequencing of fragments in coding regions and promoters; (2) ASQ genotyping; (3) CAPS markers; (4) RT-qPCR gene specific and reference gene primers.

SUPPLEMENTARY MATERIAL S2
Sequences and information about 21 Zinc-finger proteins with CCHC domain in chickpea as similar genes in legumes.

SUPPLEMENTARY MATERIAL S3
Promoter regions of two studied genes, *Ca04468* and *Ca07571*, with identified SNP in chickpea.

SUPPLEMENTARY MATERIAL S4
Results of SNP genotyping of *Ca04468* and *Ca07571* genes using ASQ method.

SUPPLEMENTARY MATERIAL S5
Sequences and genetic positions of the used DArT markers for the analysis of *Ca04468* and *Ca07571* genes.

SUPPLEMENTARY MATERIAL S6
The raw-data of DArT microarray analysis.

References

Aceituno-Valenzuela, U., Micol-Ponce, R., and Ponce, M. R. (2020). Genome-wide analysis of CCHC-type zinc finger (ZCCHC) proteins in yeast, Arabidopsis, and humans. *Cell. Mol. Life Sci.* 77, 3991–4014. doi: 10.1007/s00018-020-03518-7

Aklilu, E. (2021). Review on forward and reverse genetics in plant breeding. *All Life* 14, 127–135. doi: 10.1080/26895293.2021.1888810

Ali, A., Altaf, M. T., Nadeem, M. A., Karaköy, T., Shah, A. N., Azeem, H., et al. (2022). Recent advancement in OMICS approaches to enhance abiotic stress tolerance in legumes. *Front. Plant Sci.* 13. doi: 10.3389/fpls.2022.952759

Alonso, J. M., and Ecker, J. R. (2006). Moving forward in reverse: genetic technologies to enable genome-wide phenomic screens in *Arabidopsis*. *Nat. Rev. Genet.* 7, 524–536. doi: 10.1038/nrg1893

Amangeldiyeva, A., Baidyussen, A., Kuzbakova, M., Yerzhebayeva, R., Jatayev, S., and Shavrukov, Y. (2023). "Modified allele-specific qPCR (ASQ) genotyping," in *Plant Genotyping: Methods and Protocols. Methods in Molecular Biology*, vol. 2638 . Ed. Y. Shavrukov (SpringerNature, New York), 231–247. doi: 10.1007/978-1-0716-3024-2_16

Armas, P., and Calcaterra, N. B. (2012). "Retroviral zinc knuckles in eukaryotic cellular proteins," in *Zinc fingers: Structure, properties, and applications*. Eds. R. Ciofani and L. Makrlik (Nova Science Publishers, NY), 51–80.

Arriagada, O., Cacciuttolo, F., Cabeza, R. A., Carrasco, B., and Schwember, A. R. (2022). A comprehensive review on chickpea (*Cicer arietinum* L.) breeding for abiotic stress tolerance and climate change resilience. *Int. J. Mol. Sci.* 23, 6794. doi: 10.3390/ijms23126794

Asati, R., Tripathi, M. K., Tiwari, S., Yadav, R. K., and Tripathi, N. (2022). Molecular breeding and drought tolerance in chickpea. *Life* 12, 1846. doi: 10.3390/life12111846

Atieno, J., Colmer, T. D., Taylor., J., Li, Y., Quealy, J., Kotula, L., et al. (2021). Novel salinity tolerance loci in chickpea identified in glasshouse and field environments. *Front. Plant Sci.* 12. doi: 10.3389/fpls.2021.667910

Basu, U., Srivastava, R., Bajaj, D., Thakro, V., Daware, A., Malik, N., et al. (2018). Genome-wide generation and genotyping of informative SNPs to scan molecular signatures for seed yield in chickpea. *Sci. Rep.* 8, 13240. doi: 10.1038/s41598-018-29926-1

Basu, U., Upadhyaya, H. D., Srivastava, R., Daware, A., Malik, N., Sharma, A., et al. (2019). ABC transporter-mediated transport of glutathione conjugates enhances seed yield and quality in chickpea. *Plant Physiol.* 180, 253–275. doi: 10.1104/pp.18.00934

Ben-Ari, G., and Lavi, U. (2012). "Marker-assisted selection in plant breeding," in *Plant Biotechnology and Agriculture*. Eds. A. Altman and P. M. Hasegawa (Academic Press, Amsterdam), 163–184. doi: 10.1016/B978-0-12-381466-1.00011-0

Bocca, S. N., Magioli, C., Mangeon, A., Junqueira, R. M., Cardeal, V., Margis, R., et al. (2005). Survey of glycine-rich proteins (GRPs) in the *Eucalyptus* expressed sequence tag database (ForEST). *Genet. Mol. Biol.* 28, 608–624. doi: 10.1590/S1415-47572005000400016

Bohra, A., Bansal, K. C., and Graner, A. (2022). The 3366 chickpea genomes for research and breeding. *Trends Plant Sci.* 27, 217–219. doi: 10.1016/j.tplants.2021.11.017

Boopathi, N. M. (2020). Genetic Mapping and Marker Assisted Selection. Basics, Practice and Benefits (Singapore: Springer-Nature). doi: 10.1007/978-981-15-2949-8

Borhani, S., Vessal, S., Bagheri, A., and Shokouhifar, F. (2020). Differential gene expression pattern of drought responsive transcription factors in chickpea: An expressional analysis. *J. Plant Growth Regul.* 39, 1211–1220. doi: 10.1007/s00344-019-10056-5

Bustin, S. A., Benes, V., Garson, J. A., Hellemans, J., Huggett, J., Kubista, M., et al. (2009). The MIQE guidelines: Minimum information for publication of quantitative real-time PCR experiments. *Clin. Chem.* 55, 611–622. doi: 10.1373/clinchem.2008.112797

Chahande, R. V., Kulwal, P. L., Mhase, L. B., and Jadhav, A. S. (2021). Validation of the markers linked with drought tolerance related traits for use in MAS programme in chickpea. *J. Genet.* 100, 74. doi: 10.1007/s12041-021-01324-z

Chaikam, V., and Karlson, D. (2008). Functional characterization of two cold shock domain proteins from *Oryza sativa*. *Plant Cell Environ.* 31, 995–100. doi: 10.1111/j.1365-3040.2008.01811.x

Chetariya, C. P., Pithia, M. S., Rehavar, P., Chaitanya, A. K., and Chavadhari, R. M. (2022). Association analysis of morpho-phenological traits and yield in desi chickpea lines evaluated under normal and late sown conditions. *J. Food Legumes* 35, 145–150.

D'Arcy-Lameta, A., Ferrari-Iliou, R., Contour-Ansel, D., Pham-Thi, A. T., and Zuily-Fodil, Y. (2006). Isolation and characterization of four ascorbate peroxidase cDNAs responsive to water deficit in cowpea leaves. *Ann. Bot.* 97, 133–140. doi: 10.1093/aob/mcj010

Deres, D., and Feyissa, T. (2022). Concepts and applications of diversity array technology (DArT) markers for crop improvement. *J. Crop Improv.* 37, 913–933. doi: 10.1080/15427528.2022.2159908

Didinger, C., and Thompson, H. J. (2022). The role of pulses in improving human health: A review. *Legume Sci.* 4, e147. doi: 10.1002/leg3.147

Eker, T., Sari, H., Sari, D., Canci, H., Arslan, M., Aydinoglu, B., et al. (2022b). Advantage of multiple pods and compound leaf in Kabuli chickpea under heat stress conditions. *Agronomy* 12, 557. doi: 10.3390/agronomy12030557

Eker, T., Sari, D., Sari, H., Tosun, H. S., and Toker, C. (2022a). A kabuli chickpea ideotype. *Sci. Rep.* 12, 1611. doi: 10.1038/s41598-022-05559-3

Fasken, M. B., Leung, S. W., Banerjee, A., Kodani, M. O., Chavez, R., Bowman, E. A., et al. (2011). Air1 zinc knuckles 4 and 5 and a conserved IWRXY motif are critical for the function and integrity of the Trf4/5-Air1/2-Mtr4 polyadenylation (TRAMP) RNA quality control complex. *J. Biol. Chem.* 286, 37429–37445. doi: 10.1074/jbc.M111.271494

Fusaro, A. F., Bocca, S. N., Ramos, R. L. B., Barrôco, R. M., Magioli, C., Jorge, V. C., et al. (2007). AtGRP2, a cold-induced nucleo-cytoplasmic RNA-binding protein, has a role in flower and seed development. *Planta* 225, 1339–1351. doi: 10.1007/s00425-006-0444-4

Garg, R., Sahoo, A., Tyagi, A. K., and Jain, M. (2010). Validation of internal control genes for quantitate gene expression studies in chickpea (*Cicer arietinum* L.). *Biochem. Biophys. Res. Commun.* 396, 283–288. doi: 10.1016/j.bbrc.2010.04.079

Grabarczyk, P., Winkler, P., Delin, M., Sappa, P. K., Bekeschus, S., Hildebrandt, P., et al. (2018). The N-terminal CCHC zinc finger motif mediates homodimerization of transcription factor BCL11B. *Mol. Cell. Biol.* 38, e00368–e00317. doi: 10.1128/MCB.00368-17

Guan, Q. J., Wang, L. F., Bu, Q. Y., and Wang, Z. Y. (2014). The rice gene *OsZFP6* functions in multiple stress tolerance responses in yeast and Arabidopsis. *Plant Physiol. Biochem.* 82, 1–8. doi: 10.1016/j.plaphy.2014.04.021

Gujaria, N., Kumar, A., Dauthal, P., Dubey, A., Hiremath, P., Prakash, A. B., et al. (2011). Development and use of genic molecular markers (GMMs) for construction of a transcript map of chickpea (*Cicer arietinum* L.). *Theor. Appl. Genet.* 122, 1577–1589. doi: 10.1007/s00122-011-1556-1

Gürel, F., Öztürk, N. Z., Yörük, E., Uçarlı, C., and Poyraz, N. (2016). Comparison of expression patterns of selected drought-responsive genes in barley (*Hordeum vulgare* L.) under shock-dehydration and slow drought treatments. *Plant Growth Regul.* 80, 183–193. doi: 10.1007/s10725-016-0156-0

Hiremath, P. J., Kumar, A., Penmetsa, R. V., Farmer, A., Schlueter, J. A., Chamarthi, S. K., et al. (2012). Large-scale development of cost-effective SNP marker assays for diversity assessment and genetic mapping in chickpea and comparative mapping in legumes. *Plant Biotechnol. J.* 10, 716–732. doi: 10.1111/j.1467-7652.2012.00710.x

Hu, L., Wang, Z., Du, H., and Huang, B. (2010). Differential accumulation of dehydrins in response to water stress for hybrid and common Bermudagrass genotypes differing in drought tolerance. *J. Plant Phys.* 167, 103–109. doi: 10.1016/j.jplph.2009.07.008

Huq, A., Akter, S., Nou, S., Kim, H. T., Jung, Y. J., and Kang, K. K. (2016). Identification of functional SNPs in genes and their effects on plant phenotypes. *J. Plant Biotechnol.* 43, 1–11. doi: 10.5010/JPB.2016.43.1.1

Iruela, M., Pistón, F., Cubero, J. I., Millán, T., Barro, F., and Gil, J. (2009). The marker SCK13603 associated with resistance to ascochyta blight in chickpea is located in a region of a putative retrotransposon. *Plant Cell Rep.* 28, 53–60. doi: 10.1007/s00299-008-0609-7

Jaganathan, D., Thudi, M., Kale, S., Azam, S., Roorkiwal, M., Gaur, P. M., et al. (2015). Genotyping-by-sequencing based intra-specific genetic map refines a "QTL-hotspot" region for drought tolerance in chickpea. *Mol. Genet. Genom.* 290, 559–571. doi: 10.1007/s00438-014-0932-3

Jain, S. K., von Wettberg, E. J., Punia, S. S., Parihar, A. K., Lamichaney, A., Kumar, J., et al. (2023). Genomic-mediated breeding strategies for global warming in chickpeas (*Cicer arietinum* L.). *Agriculture* 13, 1721. doi: 10.3390/agriculture13091721

James, K. E., Schneider, H., Ansell, S. W., Evers, M., Robba, L., Uszynski, G., et al. (2008). Diversity arrays technology (DArT) for pan-genomic evolutionary studies of non-model organisms. *PloS One* 3, e1682. doi: 10.1371/journal.pone.0001682

Kalendar, R., Baidyussen, A., Serikbay, D., Zotova, L., Khassanova, G., Kuzbakova, M., et al. (2022). Modified "Allele-specific qPCR" method for SNP genotyping based on FRET. *Front. Plant Sci.* 12. doi: 10.3389/fpls.2021.747886

Karalija, E., Vergata, C., Basso, M. F., Negussu, M., Zaccai, M., Grossi-de-Sa, M. F., et al. (2022). Chickpeas' tolerance of drought and heat: Current knowledge and next steps. *Agronomy* 12, 2248. doi: 10.3390/agronomy12102248

Karlson, D., Nakaminami, K., Toyomasu, T., and Imai, R. (2002). A cold-regulated nucleic acid-binding protein of winter wheat shares a domain with bacterial cold shock proteins. *J. Biol. Chem.* 277, 35248–35256. doi: 10.1074/jbc.M205774200

Khassanova, G., Kurishbayev, A., Jatayev, S., Zhubatkanov, A., Zhumalin, A., Turbekova, A., et al. (2019). Intracellular vesicle trafficking genes, *RabC*-GTP, are highly expressed under salinity and rapid dehydration but down-regulated by drought in leaves of chickpea (*Cicer arietinum* L.). *Front. Genet.* 10. doi: 10.3389/fgene.2019.00040

Kim, J. Y., Kim, W. Y., Kwak, K. J., Oh, S. H., Han, Y. S., and Kang, H. (2010). Zinc finger-containing glycine-rich RNA-binding protein in *Oryza sativa* has an RNA chaperone activity under cold stress conditions. *Plant Cell Environ.* 33, 759–768. doi: 10.1111/j.1365-3040.2009.02101.x

Kim, J. S., Park, S. J., Kwak, K. J., Kim, Y. O., Kim, J. Y., Song, J., et al. (2007). Cold shock domain proteins and glycine-rich RNA-binding proteins from *Arabidopsis thaliana* can promote the cold adaptation process in *Escherichia coli*. *Nucleic Acids Res.* 35, 506–516. doi: 10.1093/nar/gkl1076

Kim, M. H., Sato, S., Sasaki, K., Saburi, W., Matsui, H., and Imai, R. (2013). Cold shock domain protein 3 is involved in salt and drought stress tolerance in Arabidopsis. *FEBS Open Bio* 3, 438–442. doi: 10.1016/j.fob.2013.10.003

Kingsley, P. D., and Palis, J. (1994). GRP2 proteins contain both CCHC zinc fingers and a cold shock domain. *Plant Cell* 6, 1522–1523. doi: 10.1105/tpc.6.11.1522

Kivrak, K. G., Eker, T., Sari, H., Sari, D., Akan, K., Aydinoglu, B., et al. (2020). Integration of extra-large-seeded and double-podded traits in chickpea (*Cicer arietinum* L.). *Agronomy* 10, 901. doi: 10.3390/agronomy10060901

Koul, B., Sharma, K., Sehgal, V., Yadav, D., Mishra, M., and Bharadwaj, C. (2022). Chickpea (*Cicer arietinum* L.) biology and biotechnology: From domestication to biofortification and biopharming. *Plants* 11, 2926. doi: 10.3390/plants11212926

Kujur, A., Bajaj, D., Upadhyaya, H. D., Das, S., Ranjan, R., Shree, T., et al. (2015). A genome-wide SNP scan accelerates trait-regulatory genomic loci identification in chickpea. *Sci. Rep.* 5, 11166. doi: 10.1038/srep11166

Kumar, K. R. R., and Kirti, P. B. (2012). Novel role for a serine/arginine-rich splicing factor, AdRSZ21 in plant defense and HR-like cell death. *Plant Mol. Biol.* 80, 461–476. doi: 10.1007/s11103-012-9960-8

Kwak, K. J., Park, S. J., Han, J. H., Kim, M. K., Oh, S. H., Han, Y. S., et al. (2011). Structural determinants crucial to the RNA chaperone activity of glycine-rich RNA-binding proteins 4 and 7 in *Arabidopsis thaliana* during the cold adaptation process. *J. Exp. Bot.* 62, 4003–4011. doi: 10.1093/jxb/err101

Lange, H., and Gagliardi, D. (2022). Catalytic activities, molecular connections, and biological functions of plant RNA exosome complexes. *Plant Cell* 34, 967–988. doi: 10.1093/plcell/koab310

Lee, K., and Kang, H. (2016). Emerging roles of RNA-binding proteins in plant growth, development, and stress responses. *Mol. Cells* 39, 179–185. doi: 10.14348/molcells.2016.2359

Li, H., Lin, W. F., Shen, Z. J., Peng, H., Zhou, J. J., and Zhu, X. Y. (2021). Physiological and proteomic analyses of different ecotypes of reed (*Phragmites communis*) in adaption to natural drought and salinity. *Front. Plant Sci.* 12. doi: 10.3389/fpls.2021.720593

Liew, C. K., Kowalski, K., Fox, A. H., Newton, A., Sharpe, B. K., Crossley, M., et al. (2000). Solution structures of two CCHC zinc fingers from the FOG family protein

U-shaped that mediate protein-protein interactions. *Structure* 8, 1157–1166. doi: 10.1016/S0969-2126(00)00527-X

Lopato, S., Gattoni, R., Fabini, G., Stevenin, J., and Barta, A. (1999). A novel family of plant splicing factors with a Zn knuckle motif: Examination of RNA binding and splicing activities. *Plant Mol. Biol.* 39, 761–773. doi: 10.1023/A:1006129615846

Mariaux, J. B., Bockel, C., Salamini, F., and Bartels, D. (1998). Desiccation- and abscisic acid-responsive genes encoding major intrinsic proteins (MIPs) from the resurrection plant *Craterostigma plantagineum*. *Plant Mol. Biol.* 38, 1089–1099. doi: 10.1023/A:1006013130681

Morgil, H., Gercek, Y. C., and Tulum, I. (2020). "Single nucleotide polymorphisms (SNPs) in plant genetics and breeding," in *The Recent Topics in Genetic Polymorphisms*. Ed. M. Çalışkan (InTech Open, London), 825–400. doi: 10.5772/intechopen.91886

Nguyen, K. H., Ha, C. V., Watanabe, Y., Tran, U. T., Esfahani, M. N., Nguyen, D. V., et al. (2015). Correlation between differential drought tolerability of two contrasting drought-responsive chickpea cultivars and differential expression of a subset of *CaNAC* genes under normal and dehydration conditions. *Front. Plant Sci.* 6. doi: 10.3389/fpls.2015.00449

Ni, Z., Sun, Q., Liu, Z., Wu, L., and Wang, X. (2000). Identification of a hybrid-specific expressed gene encoding novel RNA-binding protein in wheat seedling leaves using differential display of mRNA. *Mol. Gen. Genet.* 263, 934–938. doi: 10.1007/PL00008693

Park, S. J., Kwak, K. J., Jung, H. J., Lee, H. J., and Kang, H. (2010). The C-terminal zinc finger domain of Arabidopsis cold shock domain proteins is important for RNA chaperone activity during cold adaptation. *Phytochemistry* 71, 543–547. doi: 10.1016/j.phytochem.2009.12.006

Patil, S., Patil, B. S., Hanamaratti, N. G., and Kulkarni, V. R. (2023). Genetics of yield contributing traits with emphasis on seed traits in segregating generations of chickpea (*Cicer arietinum* L.). *Vegetos*. doi: 10.1007/s42535-023-00729-8

Purdy, S. J., Fuentes, D., Ramamoorthy, P., Nunn, C., Kaiser, B. N., and Merchant, A. (2023). The metabolic profile of young, watered chickpea plants can be used as a biomarker to predict seed number under terminal drought. *Plants* 12, 2172. doi: 10.3390/plants12112172

Qu, C., Zhang, Y., Chen, J., Zhang, S., Yu, J., Yang, C., et al. (2019). A weighted mean value analysis to identify biological pathway activity changes during poplar seed germination. *Forests* 10, 664. doi: 10.3390/f10080664

Radkova, M., Revalska, M., Kertikova, D., and Iantcheva, A. (2019). Zinc finger CCHC-type protein related with seed size in model legume species *Medicago truncatula*. *Biotechnol. Biotechnol. Equip.* 33, 278–285. doi: 10.1080/13102818.2019.1568914

Radkova, M., Revalska, M., Zhiponova, M., and Iantcheva, A. (2021). Evaluation of the role of *Medicago truncatula* Zn finger CCHC type protein after heterologous expression in *Arabidopsis thaliana*. *Biotechnol. Biotechnol. Equip.* 35, 1686–1695. doi: 10.1080/13102818.2021.2006786

Roorkiwal, M., von Wettberg, E. J., Upadhyaya, H. D., Warschefsky, E., Rathore, A., and Varshney, R. K. (2014). Exploring germplasm diversity to understand the domestication process in *Cicer* spp. using SNP and DArT markers. *PloS One* 9, e102016. doi: 10.1371/journal.pone.0102016

Sasaki, K., and Imai, R. (2012). Pleiotropic roles of cold shock domain proteins in plants. *Front. Plant Sci.* 2. doi: 10.3389/fpls.2011.00116

Scherrer, T., Femmer, C., Schiess, R., Aebersold, R., and Gerber, A. P. (2011). Defining potentially conserved RNA regulons of homologous zinc-finger RNA-binding proteins. *Genome Biol.* 12, R3. doi: 10.1186/gb-2011-12-1-r3

Schramm, C., Shavrukov, Y., Anderson, P., Kurishbaev, A., and Jatayev, S. (2019). "Development of Single nucleotide polymorphism (SNP) markers for cereal breeding and crop research: Current methods and future prospects," in *Advances in Breeding Techniques for Cereal Crops*. Eds. F. Ordon and W. Friedt (BD Publishing, Cambridge), 327–362. doi: 10.19103/AS.2019.0051.16

Sharma, A., Basu, U., Malik, N., Daware, A., Thakro, V., Narnoliya, L., et al. (2019). Genome-wide cis-regulatory signatures for modulation of agronomic traits as exemplified by drought yield index (DYI) in chickpea. *Funct. Integr. Genom.* 19, 973–992. doi: 10.1007/s10142-019-00691-2

Shavrukov, Y. (2016). CAPS markers in plant biology. *Russ. J. Genet. Appl. Res.* 6, 279–287. doi: 10.1134/S2079059716030114

Shavrukov, Y., Bovill, J., Afzal, I., Hayes, J. E., Roy, S. J., Tester, M., et al. (2013). *HVP10* encoding V-PPase is a prime candidate for the barley *HvNax3* sodium exclusion gene: evidence from fine mapping and expression analysis. *Planta* 237, 1111–1122. doi: 10.1007/s00425-012-1827-3

Shavrukov, Y., Suchecki, R., Eliby, S., Abugalieva, A., Kenebayev, S., and Langridge, P. (2014). Application of Next-generation sequencing technology to study genetic diversity and identify unique SNP markers in bread wheat from Kazakhstan. *BMC Plant Biol.* 14, 258. doi: 10.1186/s12870-014-0258-7

Shimray, P. W., Bajaj, D., Srivastava, R., Daware, A., Upadhyaya, H. D., Kumar, R., et al. (2017). Identifying transcription factor genes associated with yield traits in chickpea. *Plant Mol. Biol. Rep.* 35, 562–574. doi: 10.1007/s11105-017-1044-0

Singh, V. K., Khan, A. W., Jaganathan, D., Thudi, M., Roorkiwal, M., Takagi, H., et al. (2016). QTL-seq for rapid identification of candidate genes for 100-seed weight and root/total plant dry weight ratio under rainfed conditions in chickpea. *Plant Biotechnol. J.* 14, 2110–2119. doi: 10.1111/pbi.12567

Song, H., Kim, H. R., Hwang, B. H., Yi, H., and Hur, Y. (2020). Natural variation in glycine-rich region of *Brassica oleracea cold shock domain protein 5 (BoCSDP5)* is associated with low temperature tolerance. *Genes Genom.* 42, 1407–1417. doi: 10.1007/s13258-020-01010-x

Sun, A., Li, Y., He, Y., Zou, X., Chen, F., Ji, R. Z., et al. (2022). Comprehensive genome-wide identification, characterization, and expression analysis of CCHC-type zinc finger gene family in wheat (*Triticum aestivum* L.). *Front. Plant Sci.* 13. doi: 10.3389/fpls.2022.892105

Sundaram, P., Samineni, S., Sajja, S. B., Singh, S. P., Sharma, R. N., and Gaur, P. M. (2018). Genetic studies for seed size and grain yield traits in Kabuli chickpea. *Euphytica* 214, 63. doi: 10.1007/s10681-018-2147-x

Sundaram, P., Samineni, S., Sajja, S. B., Singh, S. P., Joshi, P., Shweta, et al. (2023). Identification of transgressive segregants and variability studies in segregating generations of four crosses in chickpea. *Legume Res.* 46, 25–31. doi: 10.18805/LR-4163

Sweetman, C., Khassanova, G., Miller, T. K., Booth, N. J., Kurishbayev, A., Jatayev, S., et al. (2020). Salt-induced expression of intracellular vesicle trafficking genes, *CaRab*-GTP, and their association with Na^+ accumulation in leaves of chickpea (*Cicer arietinum* L.). *BMC Plant Biol.* 20, 183. doi: 10.1186/s12870-020-02331-5

Taranov, V. V., Zlobin, N. E., Evlakov, K. I., Shamustakimova, A. O., and Babakov, A. V. (2018). Contribution of *Eutrema salsugineum* cold shock domain structure to the interaction with RNA. *Biochemistry* 83, 1369–1379. doi: 10.1134/S000629791811007X

Thompson, A. J., Jackson, A. C., Parker, R. A., Morpeth, D. R., Burbidge, A., and Taylor, I. B. (2000). Abscisic acid biosynthesis in tomato: Regulation of zeaxanthin epoxidase and 9-cis-epoxycarotenoid dioxygenase mRNAs by light/dark cycles, water stress and abscisic acid. *Plant Mol. Biol.* 42, 833–845. doi: 10.1023/A:1006448428401

Thudi, M., Bohra, A., Nayak, S. N., Varghese, N., Shah, T. M., Penmetsa, R. V., et al. (2011). Novel SSR markers from BAC-end sequences, DArT arrays and a comprehensive genetic map with 1,291 marker loci for chickpea (*Cicer arietinum* L.). *PloS One* 6, e27275. doi: 10.1371/journal.pone.0027275

Thudi, M., Upadhyaya, H. D., Rathore, A., Gaur, P. M., Krishnamurthy, L., Roorkiwal, M., et al. (2014). Genetic dissection of drought and heat tolerance in chickpea through genome-wide and candidate gene-based association mapping approaches. *PloS One* 9, e96758. doi: 10.1371/journal.pone.0096758

Tiwari, P. N., Tiwari, S., Sapre, S., Babbar, A., Tripathi, N., Tiwari, S., et al. (2023). Screening and selection of drought-tolerant high-yielding chickpea genotypes based on physio-biochemical selection indices and yield trials. *Life* 13, 1405. doi: 10.3390/life13061405

Upton, R. N., Correr, F. H., Lile, J., Reynolds, G. L., Falaschi, K., Cook, J. P., et al. (2023). Design, execution, and interpretation of plant RNA-seq analyses. *Front. Plant Sci.* 14. doi: 10.3389/fpls.2023.1135455

Varshney, R. K., Kudapa, H., Roorkiwal, M., Thudi, M., Pandey, M. K., Saxena, R. K., et al. (2012). Advances in genetics and molecular breeding of three legume crops of semi-arid tropics using next-generation sequencing and high-throughput genotyping technologies. *J. Biosci.* 37, 811–820. doi: 10.1007/s12038-012-9228-0

Varshney, R. K., Roorkiwal, M., Sun, S., Bajaj, P., Chitikineni, A., Thudi, M., et al. (2021). A chickpea genetic variation map based on the sequencing of 3,366 genomes. *Nature* 599, 622–627. doi: 10.1038/s41586-021-04066-1

Vessal, S., Arefian, M., and Siddique, K. H. M. (2020). Proteomic responses to progressive dehydration stress in leaves of chickpea seedlings. *BMC Genom.* 21, 523. doi: 10.1186/s12864-020-06930-2

Wallace, B. D., Berman, Z., Mueller, G. A., Lin, Y., Chang, T., Andres, S. N., et al. (2017). APE2 Zf-GRF facilitates 3'-5' resection of DNA damage following oxidative stress. *Proc. Natl. Acad. Sci. U.S.A.* 114, 304–309. doi: 10.1073/pnas.1610011114

Weining, S., and Langridge, P. (1991). Identification and mapping of polymorphisms in cereals based on the polymerase chain reaction. *Theor. Appl. Genet.* 82, 209–216. doi: 10.1007/BF00226215

Xu, T., Lee, H., Sy, N. D., and Kang, H. (2015). Wheat (*Triticum aestivum*) zinc finger-containing glycine-rich RNA-binding protein TaRZ1 affects plant growth and defense response in *Arabidopsis thaliana*. *Plant Growth Regul.* 76, 243–250. doi: 10.1007/s10725-014-9994-9

Yamaguchi, M., Kubo, M., Fukuda, H., and Demura, T. (2008). Vascular-related NAC-domain7 is involved in the differentiation of all types of xylem vessels in Arabidopsis roots and shoots. *Plant J.* 55, 652–664. doi: 10.1111/j.1365-313X.2008.03533.x

frontiers | Frontiers in Plant Science

TYPE Original Research
PUBLISHED 01 August 2024
DOI 10.3389/fpls.2024.1356272

OPEN ACCESS

EDITED BY
Dongmei Li,
Shandong Agricultural University, China

REVIEWED BY
Waqar Shafqat,
Mississippi State University, United States
Sanna Sevanto,
Los Alamos National Laboratory (DOE), United States

*CORRESPONDENCE
Antonios Petridis
apetridis@food.au.dk

RECEIVED 15 December 2023
ACCEPTED 19 July 2024
PUBLISHED 01 August 2024

CITATION
Davoudi M, Kalantzis S and Petridis A (2024) Adaptive responses to elevated CO_2 in fruit species with different phloem loading mechanisms.
Front. Plant Sci. 15:1356272.
doi: 10.3389/fpls.2024.1356272

Adaptive responses to elevated CO_2 in fruit species with different phloem loading mechanisms

Marzieh Davoudi, Spyridon Kalantzis and Antonios Petridis*

Department of Food Science, Aarhus University, Aarhus, Denmark

Introduction: It has been suggested that the mechanism of phloem loading, that is apoplastic or symplastic loading, may affect a plant's ability to adapt to elevated CO_2 levels. Strawberry (*Fragaria* × *ananassa*) and tomato (*Solanum lycopersicum*) are two fruit crops that use different mechanisms to load sugars into the phloem – the former symplastically and the latter apoplastically – yet both species can increase their yields when grown in a CO_2-enriched environment. In this study, we subjected strawberry and tomato plants to long-term CO_2 enrichment to determine the morphological and physiological adaptations that enable them to increase their yields in response to higher CO_2 levels.

Methods: Transplanted tomato and strawberry plants were subjected to ambient (400 ppm) and elevated (800 ppm) CO_2 for three months. We examined various parameters associated with growth, yield, photosynthesis, and carbon allocation by means of phenotyping, gas exchange analysis, and ^{13}C labelling combined with isotope ratio mass spectrometry.

Results: We found that CO_2 enrichment promoted growth and reproductive development in both species, resulting in more flowers per plant (tomato and strawberry), larger crown (strawberry), and, eventually, higher yields. Gas exchange analysis and A/c_i curves revealed that elevated CO_2 increased carbon assimilation rate in strawberry, but not in tomato – the latter being limited by Rubisco's carboxylation efficiency. Finally, whereas both species prioritized fruit development over the development of other sink organs, they were both limited by carbon export at elevated CO_2, since new photoassimilates were equally distributed to various sinks between CO_2 treatments.

Discussion: The findings suggest that both species will benefit from future increases in CO_2 levels and support current glasshouse practices entailing CO_2 enrichment. Those benefits probably stem from an enhanced performance of both species at early developmental stages, as differences in carbon assimilation rate (tomato) and carbon allocation between treatments at late developmental stages were absent. Moreover, crop adaptation to elevated CO_2 seems to depend on the ability of each species to respond to elevated CO_2, rather than on the phloem loading mechanism per se.

KEYWORDS

apoplastic loader, carbon dioxide, carbon allocation, fruit crops, phloem loading mechanism, photosynthesis, symplastic loader

1 Introduction

Phloem loading is the first step in photoassimilate translocation from source leaves to heterotrophic sink organs (e.g., roots, flowers, and fruits), comprising the transport of photoassimilates from photosynthetic mesophyll cells to the long-distance transport tissue, the phloem (Rennie and Turgeon, 2009; Ainsworth and Lemonnier, 2018). Depending on the species, plants use primarily two distinct routes to load sugars (mainly sucrose) into the phloem, involving either an apoplastic or a symplastic pathway. In apoplastic loading, sucrose moves from mesophyll cells to the cell wall space (apoplast) and is subsequently loaded energetically into the phloem by the action of specific transport proteins, including members of the SWEET and sucrose transporter (SUCs or SUTs) protein families. In symplastic loading, sucrose moves cell-to-cell towards phloem through numerous narrow cytoplasmic channels, called plasmodesmata (Rennie and Turgeon, 2009; Braun et al., 2014; Ainsworth and Lemonnier, 2018).

Current evidence suggests that several features associated with phloem loading and carbon export are subject to environmental control to balance source supply with sink demand (Amiard et al., 2005; Adams et al., 2007; Bishop et al., 2018; Xu et al., 2018). These responses to environmental cues involve anatomical and molecular changes and depend on the mode of phloem loading. For example, growth under high light conditions resulted in a higher number of cell wall invaginations in minor vein companion cells to facilitate more sugar transporters (apoplastic loaders), or in a higher vein density to increase total plasmodesmatal frequency (symplastic loaders), ensuring in both cases greater delivery of photoassimilates to heterotrophic organs as a result of higher photosynthetic rates (Adams et al., 2007). Similarly, environmental stresses that limit carbon assimilation rate reduced SUTs expression in various apoplastic species (Xu et al., 2018).

A current gap in our knowledge is how plants with different phloem loading mechanisms respond to elevated CO_2 with only few studies having dealt with this question so far (Körner et al., 1995; Bishop et al., 2018). Körner et al. (1995) investigated the accumulation of non-structural carbohydrates in leaves of apoplastic and symplastic species to test the hypothesis that symplastic species are less efficient than apoplastic species in exporting carbohydrates into the phloem for long distance transport to heterotrophic organs. The authors additionally hypothesized that if symplastic species were limited in their ability to export carbohydrates into the phloem, then they would have exhibited an excess of non-structural carbohydrates in their leaves when subjected to elevated CO_2 conditions (Körner et al., 1995). Indeed, the authors found a higher accumulation of non-structural carbohydrates in the leaves of most symplastic species, but they did not investigate further what would be the impact of this differential accumulation of non-structural carbohydrates between symplastic and apoplastic species on their photosynthesis or other important agronomic parameters such as yield. Likewise, Bishop et al. (2018) examined the impact of elevated CO_2 levels on photosynthesis and carbohydrate accumulation in leaves of three apoplastic (pea, beet, and sugar beet) and three symplastic species (strawberry, melon and peony). The authors concluded that species differing in phloem loading mechanism had similar photosynthetic responses to elevated CO_2, while, contrarily to Körner et al. (1995), they did not observe a higher sucrose build up in the leaves of symplastic species compared to apoplastic species. Again, however, there was no information about the distribution of photoassimilates to different sink organs or changes in yield in response to elevated CO_2.

Strawberry (*Fragaria* × *ananassa*) and tomato (*Solanum lycopersicum*) are two important fruit crops that use different mechanisms to load sugars into the phloem – strawberry is a symplastic loader (Rennie and Turgeon, 2009; Bishop et al., 2018) and tomato is an apoplastic loader (Osorio et al., 2014) – yet both species benefit from CO_2 enrichment by increasing their yields (Mamatha et al., 2014; Tagawa et al., 2022). In this study, we investigated the long-term effects of CO_2 enrichment on strawberry and tomato plants to determine the morphological and physiological adaptations that enable these two contrasting crops to adapt and benefit from elevated CO_2 levels. Determining how these two species respond to elevated CO_2 levels could eventually inform practices involving CO_2-enrichment in the glasshouse and reveal potential barriers that may limit their productivity.

2 Materials and methods

2.1 Plant material and growth conditions

The experiment took place at the glasshouse facilities of the Department of Food Science, Aarhus University, from November 2022 to March 2023. Seeds of tomato (*Solanum lycopersicum*) cultivar 'Roma' were obtained from a commercial supplier (SeedCom A/S, Denmark), sown directly in peat substrate in 96-cell plastic trays, and grown to ~ 4-week-old seedling stage according to standard protocols. The everbearing strawberry (*Fragaria* × *ananassa*) cultivar 'Bravura' was propagated from our own stock (initial plants were obtained by SW Horto A/S, Denmark) by cutting runner tips from mother plants and planting them in 50-cell plastic trays to develop roots.

In mid-November 2022, newly established tomato and strawberry plants were transplanted in 5.5 L plastic pots containing commercial peat substrate (Pindstrup 2; Pindstrup Mosebrug A/S, Ryomgaard, Denmark) and transferred to two separate but adjacent glasshouse rooms, corresponding to each of the two CO_2 treatments. For each fruit species and each treatment, we placed 13 plants in the glasshouse rooms that were selected based on their uniformity and vigor. In the control treatment, CO_2 was applied at 400 ppm concentration, while in the elevated CO_2 treatment, CO_2 was applied at 800 ppm concentration, the latter corresponding to projected CO_2 levels for the year 2100 (Valone, 2021). Both species were grown under long-day conditions (16 h light and 23-25°C day-temperature/8 h dark and 18-20°C night temperature) with natural and supplemental artificial light (~320 to ~ 720 µmol m^{-2} s^{-1}), the latter provided via LED lamps (FL300 Grow, Senmatic A/S, Søndersø, Denmark). The relative humidity in the glasshouse was maintained between 50-60%. All plants were fertigated with fertilizer suitable for tomatoes and strawberries by

flooding the tabletop for 12 minutes twice a day. To ensure pollination of strawberry and tomato plants, flowers of both species were brushed at the full bloom stage using a paint brush. Since plants were flowering throughout the experimental period, we ensured that plants were brushed two to three times per week until the end of the experiment. Any damaged or diseased plants were excluded from further analysis. Finally, tomato plants were only lightly pruned to reduce the probability for disease infections but at the same time resemble how they are being produced in the field for industrial purposes.

2.2 Plant phenotypic analysis

Phenotypic analysis was performed to confirm the beneficial effect of elevated CO_2 on growth and productivity of both species, and to determine which phenotypic characteristics may have contributed to any of those benefits. For most traits and both species, phenotypic analysis was performed at weekly intervals. This time-course evaluation of certain phenotypic traits was necessary in order to determine how they change in time in response to CO_2 enrichment, which in turn would indicate the timing in which potential benefits may occur for both crops. Besides a basic understanding of when the two crops can capitalize on CO_2 enrichment, this knowledge is also important because it can inform management practices in the glasshouse (e.g., to inform the duration of CO_2 enrichment period).

For tomatoes, we measured primary shoot length (length between first leaf and apical meristem), number of inflorescences per plant, number of open flowers, closed flowers and fruits, flowering time, and yield. For strawberries, we measured leaf length and width, crown diameter, flower number, and yield.

Regarding tomato phenotypic traits, primary shoot length was measured with standard 30 cm or 100 cm rulers, while the number of inflorescences and flowers/fruits per inflorescence were measured by counting. Fruit yield was measured by weighing all fruits of a plant when 75% of the fruits had turned red.

For strawberry phenotypic traits, leaf length and width were measured using a ruler, while crown diameter using a digital caliper (Fowler, Cole Parmer, UK). Yield was measured by weighing all berries of a plant when the most mature fruits of the plant were on the 'brick red' stage.

2.3 Photosynthetic gas exchange measurements

Gas exchange measurements were conducted at the fruiting stage on the youngest, fully developed leaf of tomato and strawberry plants according to Petridis et al. (2018) with minor modifications related to temperature and gas flow rate. For each species and treatment, we used three independent replicate plants. Net carbon assimilation rate (A), stomatal conductance (g_s), and intercellular CO_2 concentration (c_i) were measured using a GFS-3000 portable gas exchange system (Heinz Walz GmbH, Effeltrich, Germany) equipped with a 2.5 cm^2 leaf cuvette, which provided light through an integrated LED light unit. Leaf temperature was maintained at 23°C and relative humidity at 60%. Except for A/c_i curves, CO_2 concentration was supplied at 400 (for control) or 800 (for elevated CO_2) μmol mol^{-1} with a gas flow rate of 300 mL min^{-1}.

A/c_i curves were generated at 1200 μmol m^{-2} s^{-1} using the following stepwise gradients: 400, 200, 100, 50, 400, 500, 600, 800, 1000, 1200, 1400, and 1600 μmol mol^{-1} (Petridis et al., 2018).

2.4 Labeling with ^{13}C isotope

Labeling with ^{13}C isotope was performed in both tomato and strawberry plants. In total, we used five tomato (three replicates for eCO_2 and two replicates for control treatments) and five strawberry plants (three replicates for eCO_2 and two replicates for control treatments). Whole plants were enclosed in transparent plastic bags, transferred in a growth chamber, and labelled for 2 hours. To generate $^{13}CO_2$, 3 ml of 70% lactic acid was injected into glass vials, containing 1 g of $NaH^{13}CO_3$ ($^{13}CO_2$, treated plants) or $NaH^{12}CO_3$ ($^{12}CO_2$, control plants). The glass vials were mounted on the pots before covering the plants with the bags. When the labelling period ended, the bags were removed. ^{13}C was chased for 24 h before harvesting the plants.

After chasing for 24 h, the above ground organs (fully developed and developing leaves, flowers, fruits, and crown) were separated and immediately frozen in liquid N_2. The roots were washed to remove soil and then frozen to liquid N_2 too. Frozen samples were placed in an oven at 70°C for 3 days, milled to fine powder, and stored at room temperature until elemental analysis.

The stable carbon isotopic composition (δ ^{13}C) and carbon content of lyophilized powdered material were analyzed by OEA Laboratories LTD (Callington, UK) using a dual-pumped Sercon 20-20 isotope ratio mass spectrometer (IRMS, Sercon Ltd, Crewe, UK) coupled to a Thermo EA110 elemental analyzer (Thermo Fisher Scientific, Waltham, MA, USA). For each sample, approximately 0.94-1.2 mg of tissue were weighed, and 2 standards were used to calibrate the data (USGS L-glutamic acid and USGS41a L-glutamic acid). Excess δ ^{13}C (%) of a given organ was calculated by subtracting δ ^{13}C values after 24 hours of chasing from δ ^{13}C values of control plants.

2.5 Data analysis

The exact number of individuals (n) used for quantitative analysis are presented in each figure. Depending on the examined parameter, we used a minimum of 3 and a maximum of 13 replicates, with the only exception of the control treatment of ^{13}C labeling experiment in which we used 2 replicates. In the latter case the analysis is valid, but the statistical power is lower. Data analysis and calculation of 95% confidence interval of the CO_2 response curves were performed using GraphPad Prism, version 9.5.1 (Dotmatics, Boston MA, USA). Data from ^{13}C labeling experiment were subjected to two-way analysis of variance (ANOVA). Significant differences ($P \leq 0.05$) between means were determined using either Tukey's test or unpaired t-test.

3 Results

3.1 Phenotypic responses to elevated CO_2

To determine the effect of elevated CO_2 on tomato and strawberry plants, we assessed several parameters associated with vegetative growth and productivity, across the entire experimental period. Specifically, for tomato we measured plant height, number of inflorescences per plant, number of flowers and fruits per plant, and yield, whereas for strawberry leaf length and width, crown diameter, number of flowers and fruits per plant, and yield.

Overall, tomato plants grown under elevated CO_2 levels had a higher growth rate compared with plants grown under ambient CO_2 levels, specifically during the first month of the experiment, corresponding to the vegetative growth stage (Figure 1A).

Regarding the generative structures, tomato plants grown at elevated CO_2 had more inflorescences per plant compared with plants grown at ambient CO_2 (Figure 1B). However, the number of fruits per inflorescence was similar between treatments (Figure 1C). In addition, CO_2 enrichment accelerated transition to fruiting, as evidenced by the lower number of closed flowers and the higher number of fruits measured in the elevated CO_2 treatment compared with the control treatment. Finally, CO_2 enrichment resulted in a 37.7% yield improvement (Figure 1E), presumably as a result of the greater number of inflorescences measured in that treatment (Figure 1B).

Like tomato, eCO_2 treatment promoted vegetative and generative growth of strawberry plants (Figure 2). Specifically, elevated CO_2 levels resulted in increased leaf size as evidenced primarily by the increased leaf width and to a lesser extent the increased leaf length (Figure 2A). Elevated CO_2 levels also increased crown diameter (Figure 2B), a trait that is positively correlated with yield, and the number of flowers per plant, especially after the second half of the flowering period (Figure 2C). The better performance of strawberry under elevated CO_2 conditions (Figures 2A–C), was reflected on yield, which increased by 64.1% as a result of CO_2 enrichment (Figure 2D).

3.2 Photosynthetic responses to elevated CO_2

To determine the effect of elevated CO_2 on photosynthetic responses of tomato and strawberry plants, we measured carbon assimilation rate (A), stomatal conductance (g_s) and intercellular CO_2 concentration (c_i).

Tomato plants grown under elevated CO_2 conditions had higher intercellular CO_2 concentration in their leaves compared with plants grown under ambient CO_2 conditions (Figure 3). The percentage increase in intercellular CO_2 concentration in response to CO_2 enrichment was 103%.Carbon assimilation rate and stomatal conductance, however, were similar between the two CO_2 treatments (Figure 3).

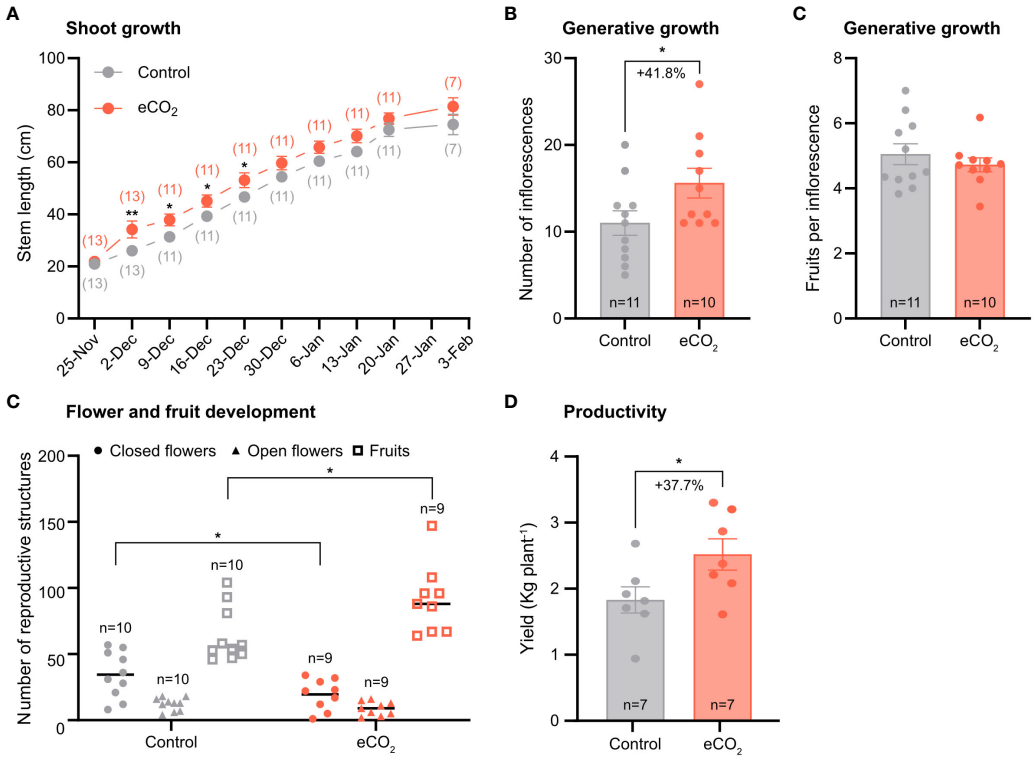

FIGURE 1
The effect of elevated CO_2 on growth and yield-related parameters of tomato plants. **(A)** Stem length. The numbers in parentheses indicate the number of plants used in the analysis. **(B)** Number of inflorescences per plant and fruits per truss. n, number of plants used in the analysis. **(C)** Number of fruits per inflorescence **(D)** Total number of reproductive structures. **(E)** Yield. Error bars indicate the mean standard error, while dots in each bar represent the number of replicates. Percentage indicates changes in number of inflorescences and yield in response to CO_2 enrichment. Significant differences ($P \leq 0.05$) between means were determined using t-test. The asterisks above data points indicate significant differences (*$P \leq 0.05$, **$P \leq 0.01$).

10.3389/fpls.2024.1356272

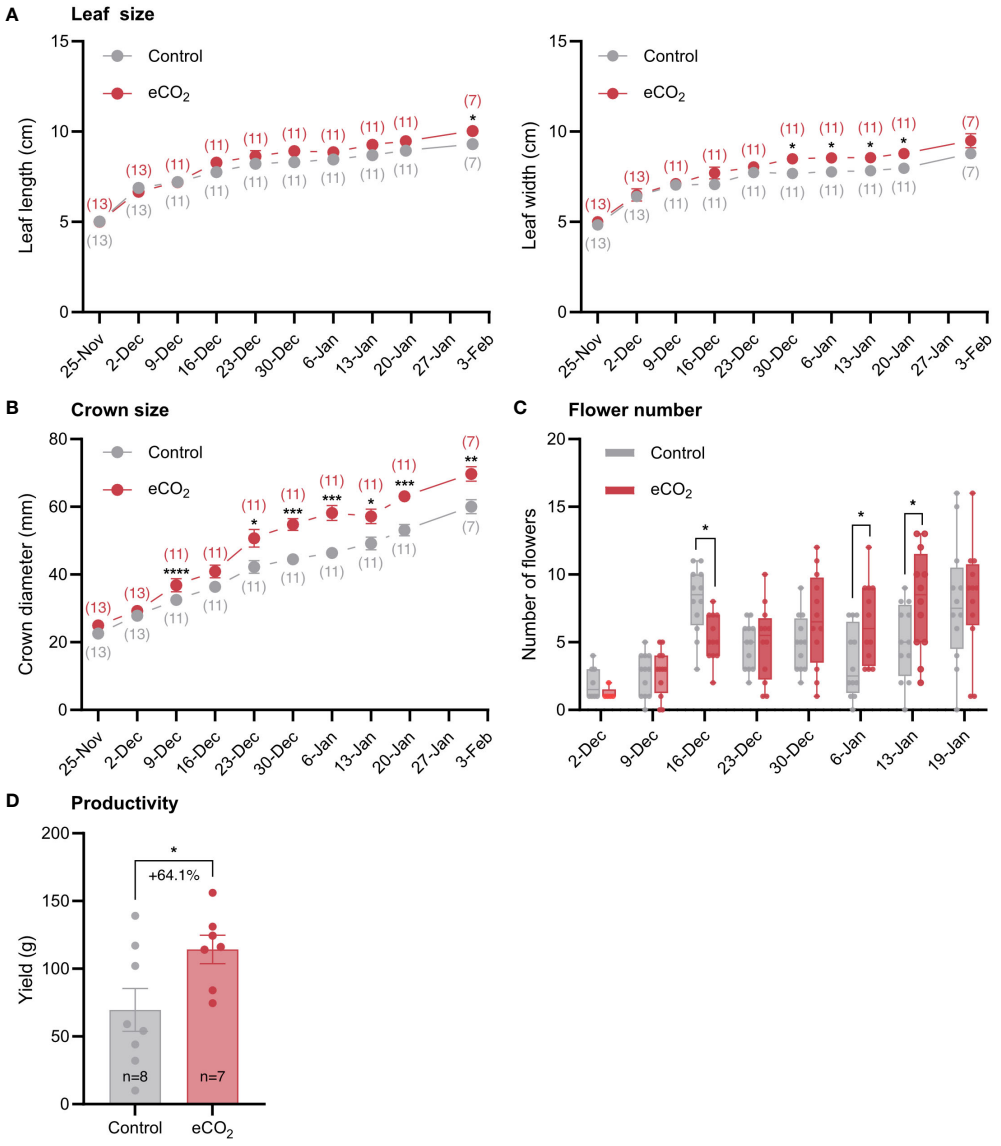

FIGURE 2
The effect of elevated CO_2 on growth and yield-related parameters of strawberry plants. **(A)** Leaf length and width. The numbers in parentheses indicate the number of plants used in the analysis. **(B)** Crown diameter. **(C)** Number of flowers per plant. **(D)** Yield. n, number of plants used in the analysis. Error bars indicate the mean standard error, while dots in each bar represent the number of replicates. Percentage indicates changes in yield in response to CO_2 enrichment. Significant differences ($P \leq 0.05$) between means were determined using t-test. The asterisks above data points indicate significant differences (*$P \leq 0.05$, **$P \leq 0.01$, ***$P \leq 0.001$, ****$P \leq 0.0001$).

In contrast, strawberry plants grown under elevated CO_2 conditions had higher carbon assimilation rate and intercellular CO_2 concentration compared with plants grown under ambient CO_2 conditions (Figure 3). The percentage increase in carbon assimilation rate and intercellular CO_2 concentration was 43.6% and 109%, respectively. No differences were observed in stomatal conductance between the two CO_2 treatments (Figure 3).

To assess the extent to which Rubisco carboxylation efficiency influences carbon assimilation rate in tomato and strawberry, we estimated carbon assimilation rate as a function of CO_2 concentration (A/c_i curves) at saturating light intensity (Figure 4). For both species, carbon assimilation rate increased with increasing CO_2 levels until a certain concentration after which it reached a plateau. The CO_2 concentration in which carbon assimilation rate saturated was lower in tomato compared to strawberry. Upon that, carbon assimilation rate was lower at elevated-CO_2-grown tomato plants compared with ambient-CO_2-grown plants at any given CO_2 concentration, whereas the opposite trend was observed for strawberry plants (Figure 4).

3.3 Partitioning of newly assimilate carbon (^{13}C) during fruit development under elevated CO_2

Having established how elevated CO_2 affects the phenotypic and photosynthetic responses in tomato and strawberry, we then

10.3389/fpls.2024.1356272

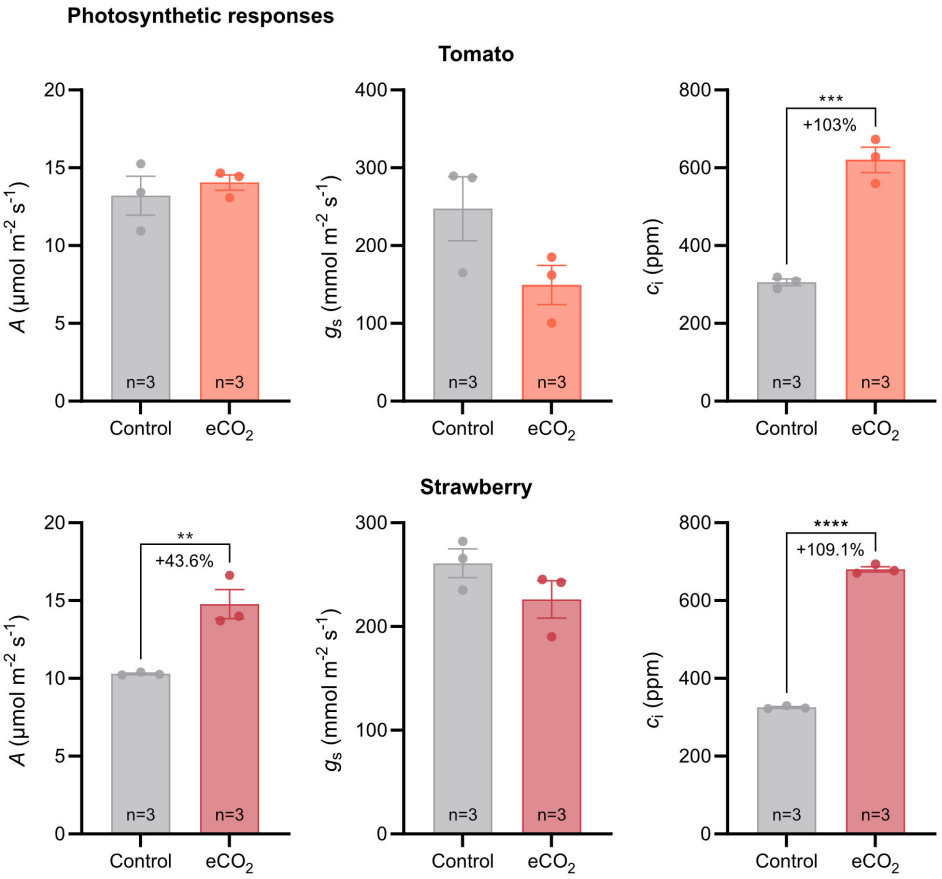

FIGURE 3
Photosynthetic responses of tomato and strawberry plants grown under ambient and elevated CO_2 conditions. Error bars indicate the mean standard error, while dots in each bar represent the number of replicates (n). Percentage indicates changes in photosynthetic parameters in response to CO_2 enrichment. Significant differences ($P \leq 0.05$) between means were determined using t-test. The asterisks above data points indicate significant differences (**$P \leq 0.01$, ***$P \leq 0.001$, ****$P \leq 0.0001$). *A*, CO_2 assimilation rate; g_s, stomatal conductance; c_i, internal CO_2 concentration.

labelled plants with ^{13}C to understand how elevated CO_2 influences the distribution of newly assimilated carbon to different organs.

In tomato, under ambient CO_2 conditions, all organs recovered a similar concentration of ^{13}C, except for roots, which had the lowest ^{13}C concentration (Figure 5A). Under elevated CO_2 conditions, the highest concentration of ^{13}C was found in developing (sink) leaves, followed by flowers, fruits and developed (source) leaves, and lastly roots (Figure 5A).

A similar allocation pattern to that found in tomato, was also observed in strawberry under ambient CO_2 conditions (Figure 5A). However, under elevated CO_2 conditions, all organs had a similar ^{13}C concentration, except for roots, which again had the lowest concentration (Figure 5A).

When considering the mass of the different organs to estimate the relative distribution of newly assimilated carbon, we found that, in tomato, the majority of new assimilates remained associated with the developed (source) leaves or were allocated to fruits in both CO_2 treatments, indicating that fruits are stronger sinks than other organs (Figure 5B).

Similarly, in strawberry, most new assimilates were allocated to fruits, regardless of CO_2 treatment. For the remaining organs, new assimilates were equally distributed among them in both CO_2 treatments (Figure 5B).

4 Discussion

One of the key findings of this study is that elevated CO_2 treatment promoted growth and reproductive development in both tomato and strawberry. In tomato, the higher yield (Figure 1E) can be attributed to the higher number of inflorescences (Figure 1B), but not to the number of fruits per inflorescence (Figure 1C). In strawberry, the higher yield at elevated CO_2 conditions (Figure 2D) can be attributed to increased crown growth (Figure 2B), which enabled the formation of more flowers (Figure 2C), and presumably the number of fruits per plant. The findings agree with those of other studies that found an increase in flower and fruit number in both tomato and strawberry under elevated CO_2 (Deng and Woodward, 1998; Mamatha et al., 2014; Rangaswamy et al., 2021; Tagawa et al., 2022). Overall, these data suggest that elevated CO_2 levels in the atmosphere will have a positive impact on the yield of field-grown tomato and strawberry crops in the future and support

10.3389/fpls.2024.1356272

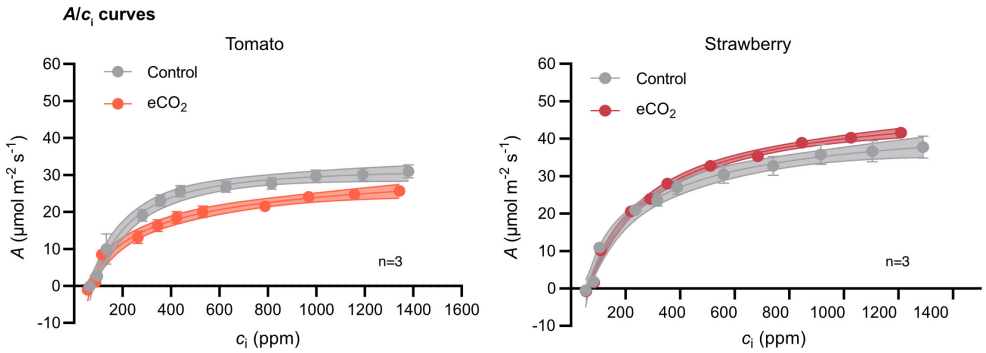

FIGURE 4
CO_2 assimilation rate (*A*) as a function of internal CO_2 concentration (c_i) in tomato and strawberry plants grown under ambient and elevated CO_2 conditions. A/c_i curves were generated using a photosynthetic photon flux density of (PPFD) of 1200 µmol m^{-2} s^{-1} and leaf temperature of 23°C. Each data point represents the mean value of three replicates ± SE, n=3. Dotted lines denote the 95% confidence interval.

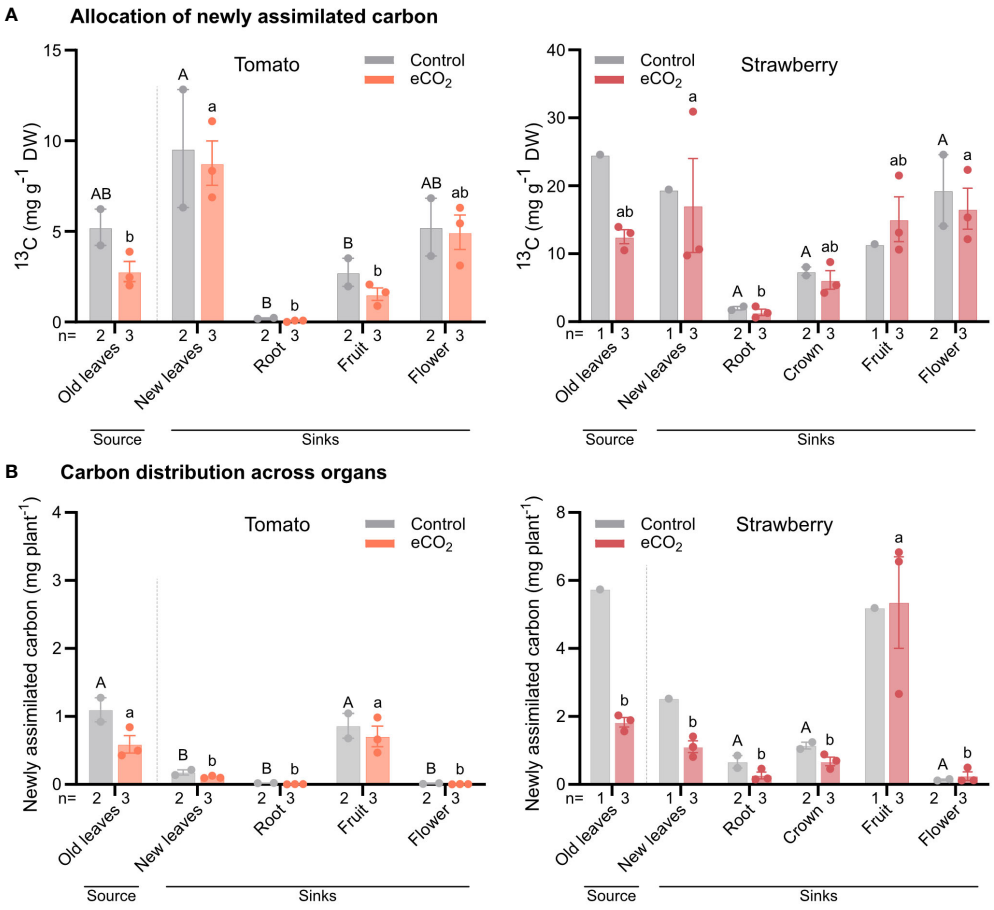

FIGURE 5
Newly assimilated carbon in individual organs of tomato and strawberry plants grown under ambient and elevated CO_2 conditions. Plants were labelled for 2 h with $^{13}CO_2$ and harvested after chasing for 24 h. ^{13}C concentration was estimated in each individual organ **(A)**, and data were used to estimate the mean total ^{13}C-assimilation in plants normalized to whole plant fresh weight **(B)**. Dashed lines separate source from sink tissues. Bars for control plants are the mean value of two replicates (n) ± SE, while bars for elevated CO_2 plants are the mean value of three replicates (n) ± SE. Data were subjected to two-way ANOVA and significant differences ($P \leq 0.05$) between means were determined using Tukey's test. Uppercase and lowercase letters denote differences between tissues from plants grown under ambient and elevated CO_2 levels, respectively.

current glasshouse management practices entailing CO_2 enrichment.

To determine the underlying mechanisms responsible for yield improvements under elevated CO_2 conditions and to identify potential barriers limiting yield, we examined tomato and strawberry photosynthetic responses to ambient and elevated CO_2 conditions. Interestingly, gas exchange analysis showed that carbon assimilation rate was higher in strawberry plants under elevated CO_2, but there was no difference between tomato plants grown under ambient and elevated CO_2 (Figure 3), despite the higher levels of CO_2 in the mesophyll cells of elevated-CO_2-treated tomato plants (Figure 3). The latter could be explained by the decrease in Rubisco's carboxylation efficiency of tomato plants subjected to elevated CO_2 compared with plants grown under ambient CO_2, as evidenced by the lower CO_2 assimilation rate of the former to increasing CO_2 levels (Figure 4). In contrast, strawberry plants subjected to elevated CO_2 conditions not only had higher CO_2 concentration in the mesophyll space of their leaves, but also higher Rubisco carboxylation efficiency compared with plants grown under ambient CO_2 conditions. The latter observation indicates that the symplastic loader, strawberry, can better adjust its photosynthesis to elevated CO_2 levels than the apoplastic loader, tomato. Ainsworth and Lemonnier (2018) reported the results of a meta-analysis in which they compared the photosynthetic acclimation of apoplastic and symplastic species that had been studied to date in Free Air CO_2 Enrichment (FACE) experiments. They found that the light-saturated photosynthetic rate, the maximum rate of Rubisco carboxylation ($V_{c,\ max}$), and the maximum rate of electron transport (J_{max}) of symplastic species were significantly higher than that of apoplastic species, and they attributed those differences to the better adaptation of passive loaders to high mesophyll sugar concentrations, which in turn renders them less susceptible to carbohydrate-mediated downregulation of photosynthesis. The findings of this study agree with those of Ainsworth and Lemonnier (2018).

In agreement with this study, Bishop et al. (2018) observed an increase in carbon assimilation rate in strawberry plants grown at elevated CO_2 conditions; however, they also found an increase in carbon assimilation rate in all three apoplastic species as a result of elevated CO_2 levels in the atmosphere. This contrasts with the findings of our work, in which we observed a similar carbon assimilation rate between tomato plants grown under either ambient or elevated CO_2 conditions. One reason for that discrepancy might be associated with differences among apoplastic species in altering their photosynthetic responses to elevated CO_2 levels. Another reason could be related to the fact that tomato plants in this study were only lightly pruned, resulting in higher shoot-to-root ratio and thus lower sink strength. This alteration in source-sink relationship in tomatoes may have disrupted the balance between production of sugars in source leaves and their utilization in sink organs. Indeed, as Arp (1991) indicated, whereas photosynthesis of C3 plants is stimulated when the CO_2 levels in the atmosphere increase, their photosynthetic capacity is often reduced after long-term exposure to elevated CO_2 levels, especially under conditions of low sink strength. The latter explanation is further supported by the data from ^{13}C-labelling experiment in which we found that the distribution of newly assimilated carbon to sink organs was similar between tomato plants grown under ambient and elevated CO_2 conditions (Figure 5B), suggesting that tomato plants are sink limited under elevated CO_2. Hence, future breeding efforts, focusing on improving tomato productivity at elevated CO_2 conditions, could revolve around enhancing sink strength, particularly that of flowers and fruits, and therefore the utilization of photoassimilates by harvestable organs.

Photosynthesis is generally considered a major determinant of yield, providing heterotrophic organs with carbon skeletons and energy for growth and development (Jones et al., 2013; Ort et al., 2015; Petridis et al., 2018). Here, we found that carbon assimilation rate was unaffected in tomato, but increased in strawberry, in response to long-term CO_2 enrichment (Figure 3). Hence, based on their photosynthetic response, one would expect that tomato plants grown under elevated CO_2 would have had similar yields to those grown under ambient CO_2, whereas CO_2 enriched strawberry plants would have had higher yields compared to those grown under ambient CO_2. However, we found that not only strawberry plants, but also tomato plants had higher yields as a result of CO_2 enrichment (Figures 1, 2). In addition, we also observed that carbon distribution across organs was similar between treatments in both species (Figure 5B). If both species increase their yield in response to elevated CO_2, irrespective of carbon assimilation rate and carbon distribution, then a question that arises is what triggers them. Although further research is needed to answer this question, we speculate that the yield benefits may arise from early developmental events, probably prior to photosynthetic acclimation to elevated CO_2, promoting floral initiation and differentiation and thus the formation of more flowers. If this hypothesis is true, then it would be interesting to investigate the connection between photosynthesis and early stages of development, especially in relation to the maturation rate of shoot apical meristem, as this process can be a major driver of yield by altering inflorescence architecture and the number of flowers on inflorescences (Lippman et al., 2008; Park et al., 2012, 2014).

5 Conclusions

Our work confirms previous studies indicating that CO_2 enrichment enhances strawberry and tomato yields (Mamatha et al., 2014; Tagawa et al., 2022). For both species this improvement in yield was the result of greater vegetative growth and flower formation. We also found that at elevated CO_2 conditions carbon assimilation rate in tomato was limited by Rubisco's carboxylation efficiency, but this limitation was not observed in strawberry. Furthermore, in both species most newly assimilated carbon had been allocated to fruits during fruit ripening; however, neither species allocated more carbon to sink organs of CO_2-enriched plants, suggesting that the observed yield improvements in response to CO_2 may have resulted from differences between treatments at earlier developmental stages. The similar response between strawberry and tomato plants, that is both species had similar levels of newly assimilated carbon in their sink organs between the two CO_2 treatments, may additionally suggest that symplastic and apoplastic species are limited by their ability to export carbon at elevated CO_2 conditions, at least at later developmental stages. Finally, based on

this as well as previous studies (Bishop et al., 2018), we conclude that the phloem loading mechanism does not seem to affect crop adaptation to elevated CO_2 per se, but any potential differences among species should be attributed to the individual ability of a species to adapt to elevated CO_2.

Data availability statement

The raw data supporting the conclusions of this article will be made available by the authors, without undue reservation.

Author contributions

AP: Conceptualization, Funding acquisition, Investigation, Project administration, Resources, Supervision, Writing – original draft. MD: Data curation, Formal analysis, Investigation, Methodology, Writing – review & editing. SK: Data curation, Formal analysis, Investigation, Writing – review & editing.

Funding

The author(s) declare financial support was received for the research, authorship, and/or publication of this article. Financial support was received by the Department of FOOD Science, Aarhus University.

Acknowledgments

We thank Thomas Bak-Østerby and Yannick Valentine El Khoury for technical assistance with plant care and photosynthetic equipment.

Conflict of interest

The authors declare that the research was conducted in the absence of any commercial or financial relationships that could be construed as a potential conflict of interest.

Publisher's note

References

Adams, W. W., Watson, A. M., Mueh, K. E., Amiard, V., Turgeon, R., Ebbert, V., et al. (2007). Photosynthetic acclimation in the context of structural constraints to carbon export from leaves. *Photosynth Res.* 94, 455–466. doi: 10.1007/s11120-006-9123-3

Ainsworth, E. A., and Lemonnier, P. (2018). Phloem function: a key to understanding and manipulating plant responses to rising atmospheric [CO2]? *Curr. Opin. Plant Biol.* 43, 50–56. doi: 10.1016/j.pbi.2017.12.003

Amiard, V., Mueh, K. E., Demmig-Adams, B., Ebbert, V., Turgeon, R., and Adams, W. W. (2005). Anatomical and photosynthetic acclimation to the light environment in species with differing mechanisms of phloem loading. *Proc. Natl. Acad. Sci.* 102, 12968–12973. doi: 10.1073/pnas.0503784102

Arp, W. J. (1991). Effects of source-sink relations on photosynthetic acclimation to elevated CO2. *Plant Cell Environ.* 14, 869–875. doi: 10.1111/j.1365-3040.1991.tb01450.x

Bishop, K. A., Lemonnier, P., Quebedeaux, J. C., Montes, C. M., Leakey, A. D. B., and Ainsworth, E. A. (2018). Similar photosynthetic response to elevated carbon dioxide concentration in species with different phloem loading strategies. *Photosynth Res.* 137, 453–464. doi: 10.1007/s11120-018-0524-x

Braun, D. M., Wang, L., and Ruan, Y.-L. (2014). Understanding and manipulating sucrose phloem loading, unloading, metabolism, and signalling to enhance crop yield and food security. *J. Exp. Bot.* 65, 1713–1735. doi: 10.1093/jxb/ert416

Deng, X., and Woodward, F. I. (1998). The Growth and Yield Responses ofFragaria ananassato Elevated CO2and N Supply. *Ann. Bot.* 81, 67–71. doi: 10.1006/anbo.1997.0535

Jones, R., Ougham, H., Thomas, H., and Waaland, S. (2013). *The Molecular Life of Plants* (Wiley). Available online at: https://www.wiley.com/en-dk/The+Molecular+Life+of+Plants-p-9781118315989 (Accessed December 8, 2023). *Wiley.com*.

Körner, Ch., Pelaez-Riedl, S., and Van Bel, A. J. E. (1995). CO2 responsiveness of plants: a possible link to phloem loading. *Plant Cell Environ.* 18, 595–600. doi: 10.1111/j.1365-3040.1995.tb00560.x

Lippman, Z. B., Cohen, O., Alvarez, J. P., Abu-Abied, M., Pekker, I., Paran, I., et al. (2008). The making of a compound inflorescence in tomato and related nightshades. *PLoS Biol.* 6, e288. doi: 10.1371/journal.pbio.0060288

Mamatha, H., Srinivasa Rao, N. K., Laxman, R. H., Shivashankara, K. S., Bhatt, R. M., and Pavithra, K. C. (2014). Impact of elevated CO2 on growth, physiology, yield, and quality of tomato (Lycopersicon esculentum Mill) cv. Arka Ashish. *Photosynthetica* 52, 519–528. doi: 10.1007/s11099-014-0059-0

Ort, D. R., Merchant, S. S., Alric, J., Barkan, A., Blankenship, R. E., Bock, R., et al. (2015). Redesigning photosynthesis to sustainably meet global food and bioenergy demand. *Proc. Natl. Acad. Sci.* 112, 8529–8536. doi: 10.1073/pnas.1424031112

Osorio, S., Ruan, Y.-L., and Fernie, A. R. (2014). An update on source-to-sink carbon partitioning in tomato. *Front. Plant Sci.* 5. doi: 10.3389/fpls.2014.00516

Park, S. J., Eshed, Y., and Lippman, Z. B. (2014). Meristem maturation and inflorescence architecture—lessons from the Solanaceae. *Curr. Opin. Plant Biol.* 17, 70–77. doi: 10.1016/j.pbi.2013.11.006

Park, S. J., Jiang, K., Schatz, M. C., and Lippman, Z. B. (2012). Rate of meristem maturation determines inflorescence architecture in tomato. *Proc. Natl. Acad. Sci.* 109, 639–644. doi: 10.1073/pnas.1114963109

Petridis, A., van der Kaay, J., Chrysanthou, E., McCallum, S., Graham, J., and Hancock, R. D. (2018). Photosynthetic limitation as a factor influencing yield in highbush blueberries (Vaccinium corymbosum) grown in a northern European environment. *J. Exp. Bot.* 69, 3069–3080. doi: 10.1093/jxb/ery118

Rangaswamy, T. C., Sridhara, S., Ramesh, N., Gopakkali, P., El-Ansary, D. O., Mahmoud, E. A., et al. (2021). Assessing the impact of higher levels of CO2 and temperature and their interactions on tomato (Solanumlycopersicum L.). *Plants* 10, 256. doi: 10.3390/plants10020256

Rennie, E. A., and Turgeon, R. (2009). A comprehensive picture of phloem loading strategies. *Proc. Natl. Acad. Sci.* 106, 14162–14167. doi: 10.1073/pnas.0902279106

Tagawa, A., Ehara, M., Ito, Y., Araki, T., Ozaki, Y., and Shishido, Y. (2022). Effects of CO2 enrichment on yield, photosynthetic rate, translocation and distribution of photoassimilates in strawberry 'Sagahonoka.'. *Agronomy* 12, 473. doi: 10.3390/agronomy12020473

Valone, T. F. (2021). Linear global temperature correlation to carbon dioxide level, sea level, and innovative solutions to a projected 6°C warming by 2100. *J. Geosci. Environ. Prot.* 9, 84–135. doi: 10.4236/gep.2021.93007

Xu, Q., Chen, S., Yunjuan, R., Chen, S., and Liesche, J. (2018). Regulation of sucrose transporters and phloem loading in response to environmental cues. *Plant Physiol.* 176, 930–945. doi: 10.1104/pp.17.01088

frontiers | Frontiers in Plant Science

TYPE Original Research
PUBLISHED 26 August 2024
DOI 10.3389/fpls.2024.1324144

OPEN ACCESS

EDITED BY
Antonella Castagna,
University of Pisa, Italy

REVIEWED BY
Avneesh Kumar,
SRM University, Sikkim, India
Santosh Kumar,
Sikkim University, India

*CORRESPONDENCE
Shimei Sun
sunshimei@jlju.edu.cn

RECEIVED 19 October 2023
ACCEPTED 06 August 2024
PUBLISHED 26 August 2024

CITATION
Li M, Wang S and Sun S (2024) Mechanism of emergency phytoremediation technology based on a 3D-QSAR pharmacological model. *Front. Plant Sci.* 15:1324144. doi: 10.3389/fpls.2024.1324144

Mechanism of emergency phytoremediation technology based on a 3D-QSAR pharmacological model

Minghao Li[1], Siming Wang[2] and Shimei Sun[1]*

[1]School of Emergency Science and Engineering, Jilin Jianzhu University, Changchun, China, [2]XingYe Environmental Group Co., Ltd., Harbin, China

Introduction: The ability of transgenic plants to respond to sudden environmental pollution accidents has become viable. Nonetheless, there is a dearth of research regarding the mechanism by which transgenic plants degrade organic pollutants. Hence, this study aimed to elucidate the process of organic pollutant degradation by plants, offering theoretical support for the application of transgenic plant emergency phytoremediation technology.

Methods: In this investigation, we developed a 3D-QSAR pharmacophore model to represent the collective impact of plant resistance and phytodegradation. This was achieved by employing integrated effect values following treatment with a sine function approach. Moreover, we have undertaken an inaugural exploration of the coregulatory mechanism involved in plant resistance and pollutant degradation within plants. Additionally, we applied virtual molecular modification techniques for analysis and validation, striving for a more indepth understanding of the molecular-level enhancement mechanism related to the degradation of pollutants within plant organisms.

Results and discussion: The mechanism analysis results of the Hypo 1 pharmacophore model were verified, indicating that hydrophobic characteristics affect the resistance and degradation of PCBs in plants, significantly affecting the degradation effect of pollutants in plants.

KEYWORDS

sudden environmental pollution accidents, emergency phytoremediation techniques, plant resistance, phytodegradability, molecular dynamics, quantitative molecular surface analysis

1 Introduction

With the rapid advancement of industrialization, human social activities have significantly expanded, leading to a surge in the frequency of sudden environmental

pollution accidents (SEPAs). These incidents pose a substantial threat to human development and ecological security due to their high uncertainty, intricate evolution, rapid propagation, and severe wide-ranging damage (Lei et al., 2018; Wang and Wang, 2021). In light of the increase in environmental pollution, finding a method capable of promptly eliminating pollutants at their source and addressing pollution issues arising from SEPA holds vital practical significance for global ecological wellbeing and sustainable human development.

The primary techniques for addressing environmental pollution include physical, chemical, biological, and integrated remediation methods (Li and Sun, 2022). Among these, phytoremediation, as a biological approach, offers the advantages of simplicity and cost-effectiveness compared to traditional methods, with the added benefit of minimizing secondary pollution. However, traditional phytoremediation suffers from protracted remediation cycles (Terzaghi et al., 2019). With the maturation of transgenic technology, scientists have begun enhancing phytoremediation efficiency from a transgenic standpoint to overcome its lengthy remediation time. For instance, Kong et al. (2022) introduced the N-demethylase gene into soybeans, resulting in the removal of 98% and 84% of isoproturon from water and soil within 5 and 14 days, respectively, in transgenic soybeans. This achievement outpaced that of conventional soybeans, underscoring the efficacy of transgenic plants in organic matter remediation (Kong et al., 2022). The researchers incorporated two bacterial genes designed to degrade RDX, a military explosive residue, into *Panicum virgatum*, demonstrating its ability to remove and degrade RDX at a rate of 27 kg per hectare (Cary et al., 2021). These studies illustrate the potential of transgenic plants for addressing SEPA, yet there is limited research on the mechanism of pollutant degradation within phytoremediation technology. Therefore, this paper aims to investigate the mechanism of organic pollutant degradation by plants, providing a theoretical foundation for the use of transgenic plants in emergency remediation technology.

The activity of the plant antioxidant system closely correlates with the development of stress tolerance. During plant growth, various abiotic stresses can increase intracellular reactive oxygen species concentrations, leading to oxidative stress and plant damage (Gechev et al., 2006). In response to oxidative damage, plants have evolved various antioxidant mechanisms, including peroxidase (POD), which significantly influences plant stress resistance (Kawano, 2003). When organic pollutants infiltrate plants, they can induce oxidation in cell membranes and various organelles, inhibiting POD enzyme activity and compromising plant health (Zhang et al., 2017). Additionally, during the degradation of organic pollutants by plants, plants can secrete bioxygenases related to organic pollutant degradation, affecting the overall degradation efficiency (Mohammadi et al., 2007). Among these pollutants, polychlorinated biphenyls (PCBs) are among the 12 persistent organic pollutants (POPs) regulated under the Stockholm Convention due to their environmental persistence, high biotoxicity, substantial bioconcentration, and long-range transport characteristics (Hayat et al., 2019; Terzaghi et al., 2020). Nevertheless, PCBs continue to leach into the soil environment as by-products of incinerating chlorinated compounds or producing and using chlorine-containing chemicals, potentially causing sudden environmental incidents. In summary, the enzymatic structures of peroxidase (1CCK), an enzyme related to plant resistance, and dioxygenase (3GZX), an enzyme related to plant degradability, were derived from the Protein Data Bank (http://www1.rcsb.org), and these enzymes were utilized as target enzymes to jointly analyze phytoremediation techniques using PCB molecules as representatives of the degradation mechanism.

3D-QSAR models integrate structural information of molecules in three dimensions with their biological activities, enabling a more accurate and comprehensive understanding of the underlying mechanisms involved in phytoremediation. Given the complexity and diversity of POPs, there is a pressing need for the development of advanced 3D-QSAR models tailored specifically for phytoremediation. These models could not only help researchers select the most promising plant species for remediation but also guide the design of novel virtual modifications to pollutants that could improve their degradability by plants. In this paper, we established a 3D-QSAR pharmacophore model for predicting the plant resistance and phytodegradability of PCBs based on their molecular structural parameters. We selected PCBs with documented plant resistance and phytodegradability data as dependent variables and employed molecular structural parameters as independent variables to construct the model. Furthermore, we validated the model by incorporating molecular virtual modification techniques, molecular dynamics methods, and quantitative molecular surface analysis. Based on these results, additionally, it provides a theoretical reference for the genetic modification of highly efficient repair plants in the future.

2 Materials and methods

2.1 Characterization of plant resistance receptor enzymes and plant degradative enzymes that bind to PCBs—molecular docking

From the PDB database, we selected a representative plant resistance receptor enzyme (PDB ID: 1CCK) and a plant degradation receptor enzyme (PDB ID: 3GZX) as acceptors, along with 60 PCBs as ligands. These proteins were loaded into Discovery Studio 2020 software for analysis. The LibDock module was employed to investigate the interaction between the receptor enzymes and the ligand molecules (Zhang et al., 2019). Using the LibDock module, we defined the two selected enzymes as two enzyme receptors. Subsequently, molecular docking was conducted for each of the 60 PCB ligands with these two enzyme receptors using the "Find Sites from Receptor Cavities" option under the Define module to identify potential binding sites within the receptors. Docking preferences were configured as custom, Max Hit to Save was set to 10, and all other settings remained at their default values. The resulting

10.3389/fpls.2024.1324144

TABLE 1 Calculated values for the combined effect of plant resistance and degradability for 60 PCBs.

PCBs (IUPAC)	Plant resistance	Phytodegradability	Comprehensive effect value
1	75.426	71.577	1.865
2	81.624	73.685	1.91
4	73.822	76.604	1.867
6	83.766	78.019	1.929
7	83.786	74.232	1.923
8	87.006	76.220	1.943
9	80.980	71.669	1.900
10	72.398	77.082	1.857
11	87.533	74.788	1.943
12	88.323	78.408	1.952
13	88.073	75.084	1.946
14	87.991	73.595	1.942
16	69.318	79.249	1.836
17	83.794	77.495	1.929
18	71.252	70.436	1.831
20	79.668	76.524	1.905
23	82.007	71.477	1.905
25	89.403	74.420	1.950
28	89.893	75.407	1.954
31	86.392	67.811	1.913
33	90.196	75.792	1.956
36	91.012	68.505	1.936
39	90.431	71.216	1.944
40	73.154	80.691	1.865
46	65.282	78.958	1.803
52	67.751	77.703	1.822
59	79.861	74.233	1.901
61	93.144	76.448	1.968
67	92.454	60.891	1.896
74	85.467	70.231	1.919
77	99.318	73.871	1.98
81	99.705	75.858	1.985
85	64.546	70.043	1.775
90	75.506	62.585	1.820
95	70.561	78.021	1.844
101	71.570	65.686	1.811
105	99.271	65.437	1.945
110	71.019	56.458	1.740
114	98.329	66.982	1.951
118	85.897	72.296	1.928
123	95.620	70.652	1.960
126	105.165	69.209	1.973
128	66.586	64.601	1.765
130	72.689	72.932	1.850
135	72.564	74.071	1.852
138	69.900	58.690	1.750
153	67.731	55.717	1.708
156	89.360	51.817	1.803
157	88.695	51.693	1.799
164	73.038	48.786	1.677
167	89.597	55.942	1.844
169	109.961	49.844	1.825
174	67.737	43.346	1.571
180	72.489	44.462	1.622
189	84.203	53.788	1.799
196	74.020	44.223	1.629
200	76.580	53.269	1.749
201	70.293	47.688	1.644
207	76.815	56.916	1.785
209	79.575	53.317	1.769

(Continued)

scoring function values $X_{i,1}$ and $X_{i,2}$ (i = 1, 2), the principal parameters of the LibDock module, were separately computed to better characterize the interaction between the two plant receptor enzymes and the 60 PCB ligands, and the results are presented in Table 1.

2.2 Comprehensive effect values for plant resistance and degradability of PCBs corrected by the sine normalization method

The scoring function is normalized using Equation 1 as follows:

$$X_{i,1} = \frac{xi,1}{x1max}; X_{i,2} = \frac{xi,2}{x2max} \quad (i = 1,\ 2,\ 3, \ldots, 23) \qquad (1)$$

Following the normalization of Equation 1, a simple sine function was chosen to further normalize the data. A lower score after docking with plant resistance enzymes indicates a lower toxicity of PCBs to plants. Conversely, higher SFs after docking with plant degradation enzymes suggest that PCBs are less resistant to degradation by these enzymes, thus enhancing their

environmental remediation potential. To ensure consistency in the direction of change for both effects, a negative sign was introduced before the scoring function of PCBs and plant resistance enzymes. This produced a combined activity value reflecting the synergy of the two effects in an inverse direction. The sine method (Wang et al., 2017; Julien et al., 2007; Liu and Marukawa, 2004) generated a combined score k_i (i = 1, 2, 3, 4,…,60), representing the impact of PCBs on both types of plant receptor enzymes, as shown in Equation 2:

$$k_i = 1 - sin(\frac{\pi X_{i,\,1}}{2}) + sin(\frac{\pi X_{i,\,2}}{2}) \quad (i = 1,\ 2) \tag{2}$$

The calculated values of the combined effect of resistance and degradability of the PCB plants after sine normalization treatment are shown in Table 1.

2.3 Pharmacophore modeling of the comprehensive effects of plant resistance and PCB degradability

A "pharmacophore" represents the molecular structure of a wide range of active features common to PCB congeners (Langer, 2010). These pharmacophore elements can include hydrophobic groups, specific chemical groups, etc (Huang et al., 2014; Feng et al., 2016). The development of 3D-QSAR pharmacophore models helps reveal the relationship between PCB activity and structural characteristics, aiding mechanistic analysis (Kubo et al., 2003). We employed the combined effect of PCB resistance and degradation as the dependent variable and PCB structure as the independent variable. The 3D-QSAR Pharmacophore Generation module within Discovery Studio 2020 was utilized to construct the 3D-QSAR model for the combined effect of PCB resistance and degradation. This module allowed us to investigate the mechanisms influencing the combined effect of PCB resistance and degradation.

The selected 3D-QSAR pharmacophore features included hydrogen bond acceptors, hydrogen bond donors, hydrophobic groups, hydrophobic–aliphatic groups, and aromatic rings. The module parameters were set as follows: Fast for conformation generation, an energy threshold of 20 kcal/mol, maximum conformations per homolog set to the default 255, and minimum interference distance set to 0. The energy threshold for similarity conformation generation was set to 10 (Zhao et al., 2021; Zhang et al., 2021).

The HypoGen module within Discovery Studio 2020 software was chosen to evaluate the constructed 3D-QSAR pharmacophore model for the combined effects of plant resistance and degradation of PCBs. The cost function, a key metric, reflects the model's suitability and includes its complexity, chemical properties, and error between predicted and experimental data (Chen and Li, 2021). According to Occam's Razor, the optimal pharmacophore model should have the lowest total cost among all models and be close to the fixed cost value (Vincent and Bellini, 2002). Another significant parameter is the configuration cost, which is determined by the model's spatial complexity. A meaningful pharmacophore model should possess a configuration cost value of no more than 17 (Arooj et al., 2011).

2.4 Molecular dynamics methods

The magnitude of the binding of plant resistance receptor enzymes (1CCK) and plant degrading enzymes (3GZX) to PCBs indicates the strength of the interaction between contaminants and enzymes (Gu et al., 2020). In this study, we performed molecular dynamics simulations using Gromacs software for PCB molecules and enzymes before and after modification utilizing the Dell PowerEdge R7425 server. Each complex was placed in a periodic dodeca cube with a side length of 10 nm. Molecular confinement was conducted using the GROMOS96 43a1 force field, and Na^+ ions were added to neutralize the system charge. The PCB–enzyme complex system underwent energy minimization simulations via the steepest gradient method, with 50,000 simulation steps. The simulation duration for both the hot and pressure baths was set to 100 ps, with the pressure bath size maintained at a constant standard atmospheric pressure of 1 bar. Kinetic simulations lasting 200 ps were performed for each step group to calculate the changes in binding energy between PCBs and enzymes. Finally, the binding energy data generated via the molecular dynamics method were combined with quantitative molecular surface analysis to analyze the phytoremediation capacity.

2.5 Quantitative molecular surface analysis

Interactions between proteins and ligands are typically governed by weak interactions among biomolecules (Xie et al., 2006). Common weak interactions include van der Waals forces, hydrogen bonding forces, and hydrophobic forces (Johnson et al., 2010). In this study, we utilized the quantitative molecular surface analysis function of Multiwfn software (Lu and Chen, 2012a, b) to calculate the van der Waals surface area before and after molecular modification, with the electron density of the equivalent surface set to 0.002 a.u. We analyzed the reasons for changes in van der Waals forces resulting from alterations in indicators before and after PCB molecular modification. Subsequently, we investigated the factors influencing changes in the binding energy between plant resistance receptor enzymes and plant-degrading enzymes and PCBs.

3 Results and discussion

3.1 Construction and evaluation of a 3D-QSAR pharmacophore model for the comprehensive effects of plant resistance and degradability of PCBs

The program generated a total of nine 3D-QSAR pharmacophore models for the combined effect of plant resistance and degradation of PCBs, as outlined in Table 2.

10.3389/fpls.2024.1324144

TABLE 2 Nine pharmacophore models and their statistical data.

Hypo No. 1	Total cost	RMS	Correlation	Features
1	216.167	0.05	0.6	H, RA*2
2	216.065	0	0	HA, RA*2
3	216.173	0.06	0.5	H, RA*2
4	216.065	0	0	H, RA*2
5	216.178	0.06	0.5	RA*2
6	216.065	0	0	RA*2
7	216.182	0.06	0.48	H*2, RA
8	216.065	0	0	H*4
9	216.888	0.16	−0.01	HA, H, RA
Configuration	13.12	Fixed cost	201.816	
Null cost	227.037			

HBA, hydrogen bond acceptor; HBD, hydrogen bond donor; H, hydrophobic group; HA, hydrophobic aliphatic group; RA, aromatic ring.

Based on the parameter values of the nine 3D-QSAR pharmacophore models (Table 2), five valid models (Hypo 1, Hypo 3, Hypo 5, Hypo 7, and Hypo 9) were selected because their RMS (Root mean square) and correlation values were both greater than zero. Among the five effective 3D-QSAR pharmacophore models, Hypo 1 exhibited the most promising performance. Its Total cost value (216.167) was closest to the Fixed cost value (201.816) and the Nullcost value (227.037). The RMS value (0.05) and Total cost value (216.167) were also the smallest among the five models. These parameters collectively indicated that Hypo 1 outperformed the others in representing the combined pharmacophore characteristics of plant resistance and degradation of PCBs. The configuration parameter, which should be less than 17 for a pharmacophore model to be considered significant, was 13.12 for the Hypo 1 model, confirming its significance. Table 3 shows that the error values of the predicted values from the Hypo 1 pharmacophore model for the combined effect values of the 60 PCBs were less than 2, which falls within an acceptable error range. This outcome further validated the reliability of the Hypo 1 pharmacophore model and its ability to represent the combined pharmacophore characteristics of plant resistance and degradation of PCBs.

3.2 Mechanistic analysis of the effect of PCBs on plant resistance and degradation based on the characteristic map of the 3D-QSAR pharmacophore model

The Hypo 1 pharmacophore model comprised one hydrophobic and two aromatic ring features. Figure 1 shows an overlay of the Hypo 1 pharmacophore model with the three-dimensional spatial relationships of PCBs, where blue represents hydrophobic features and yellow represents aromatic ring features.

TABLE 3 Statistical data of 60 PCBs based on Hypo 1.

PCBs (IUPAC)	Fit value	Est value	Act value	Error
1	3.881	1.061	1.104	−1.040
2	3.896	1.026	1.072	−1.045
4	3.858	1.117	1.127	−1.009
5	3.870	1.089	1.087	1.002
7	3.865	1.101	1.061	1.038
8	3.867	1.096	1.049	1.045
9	3.883	1.055	1.069	−1.013
10	3.864	1.102	1.138	−1.032
11	3.898	1.021	1.044	−1.023
12	3.922	0.966	1.046	−1.083
13	3.899	1.017	1.043	−1.025
14	3.919	0.972	1.039	−1.069
16	3.870	1.089	1.163	−1.068
17	3.873	1.081	1.067	1.013
18	3.870	1.088	1.129	−1.038
20	3.871	1.085	1.089	−1.004
23	3.865	1.100	1.063	1.035
25	3.888	1.043	1.035	1.007
28	3.867	1.096	1.036	1.058
31	3.886	1.047	1.025	1.022
33	3.892	1.034	1.035	−1.001
36	3.898	1.021	1.008	1.013
39	3.895	1.028	1.022	1.006
40	3.866	1.099	1.135	−1.033
46	3.867	1.095	1.196	−1.093
52	3.872	1.084	1.175	−1.084
59	3.870	1.089	1.083	1.005
61	3.896	1.025	1.025	−1.000
67	3.889	1.041	0.958	1.086
74	3.883	1.057	1.040	1.016
77	3.922	0.965	1.003	−1.040
81	3.952	0.902	1.006	−1.116
85	3.901	1.012	1.182	−1.168
90	3.873	1.082	1.057	1.023
95	3.877	1.071	1.153	−1.077
101	3.874	1.077	1.104	−1.025
105	3.901	1.013	0.968	1.046
110	3.872	1.083	1.042	1.040

(Continued)

10.3389/fpls.2024.1324144

TABLE 3 Continued

PCBs (IUPAC)	Fit value	Est value	Act value	Error
114	3.923	0.963	0.978	−1.016
118	3.920	0.971	1.045	−1.077
123	3.912	0.988	1.002	−1.014
126	3.953	0.899	0.977	−1.087
128	3.879	1.067	1.137	−1.066
130	3.899	1.017	1.127	−1.109
135	3.875	1.075	1.131	−1.052
138	3.869	1.091	1.069	1.021
153	3.869	1.092	1.061	1.029
156	3.938	0.930	0.889	1.046
157	3.887	1.047	0.891	1.175
164	3.878	1.067	0.949	1.125
167	3.931	0.945	0.928	1.018
169	3.953	0.898	0.825	1.088
174	3.933	0.941	0.924	1.019
180	3.884	1.054	0.901	1.170
189	3.917	0.976	0.933	1.046
190	3.880	1.063	1.013	1.050
200	3.899	1.017	0.972	1.046
201	3.884	1.053	0.957	1.101
207	3.882	1.058	1.005	1.053
209	3.880	1.063	0.954	1.114

Using PCB-46, which had the highest combined effect value, and PCB-1, which had the lowest number of chlorine atoms, as examples, the positions of the hydrophobic and aromatic ring features were visualized (Figure 1). Although the number of molecules with varying aromatic ring features differed slightly, all the molecules contained these two features. This indicated that these two features had a significant impact on the combined effect of plant resistance and degradation of PCBs. Since the aromatic ring is an inherent property of PCB structures, modifying the hydrophobic features of PCBs in plants can further mitigate their resistance and enhance their phytodegradability.

Furthermore, the aromatic ring feature reflects the susceptibility of PCBs to electrophilic substitution reactions, where they tend to lose electrons in this region. Previous studies have shown that the E_{HOMO} parameter, which measures the electron loss ability (reducibility) of PCBs, can influence plant resistance to some extent (Li et al., 2021). Therefore, the aromatic ring indirectly reflects the E_{HOMO} parameter of PCBs (electron loss property or reducibility). Hydrophobic features represent hydrophobic functions contained in aliphatic atoms. The literature indicates that the primary influential parameter for plant degradation of PCBs *in vivo* is Log*P*, which measures the hydrophobicity of organic compounds (Li et al., 2021). Hydrophobic features partially reflect the influence of Log*P* parameters on PCB plant degradability. In summary, the 3D-QSAR pharmacophore model for the combined effect of plant resistance and degradation of PCBs somewhat corroborates the literature findings (Li et al., 2021). However, further analysis is needed to understand how the hydrophobic characteristics of pollutants indirectly affect PCB resistance in plants.Figure 1 shows that the hydrophobic feature significantly influences PCB plant resistance and degradability and is located at the 2′ position of the benzene ring, indicating that the hydrophobic group at this position can affect PCB plant resistance and degradability. Therefore, this chapter validates the mechanism of the effect of hydrophobic features on PCB plant resistance and degradability using molecular virtual modification techniques.

3.3 Validation and investigation of the mechanism analysis results based on molecular virtual modification technology

3.3.1 Validation of the mechanism analysis results using molecular virtual modification techniques

We selected three common hydrophobic groups as substituents: hydroxymethylol (-CH_2OH), trifluoromethyl (-CF_3), and nitryl

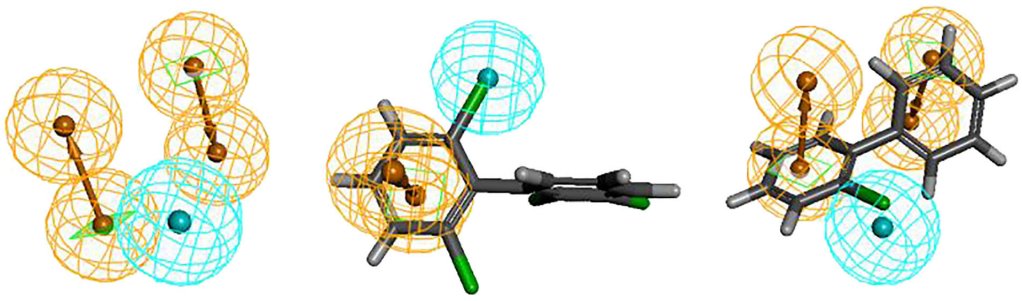

FIGURE 1
Spatial relationship of Hypo1 and alignment with PCBs, PCB-1 and PCB-46.

(-NO_2). PCB-46, which had the greatest comprehensive effect, served as the template molecule for molecular virtual modification to adjust PCB resistance and degradation. We conducted molecular virtual modification to adjust PCB resistance and degradation using PCB-46 as the template molecule. The Hypo 1 pharmacophore model was used to predict the combined effects of three molecules (2′-CH_2OH-PCB-46, 2′-CF_3-PCB-46, and 2′-NO_2-PCB-46) after virtual modification of PCB-46 (Figure 2).

Table 4 presents the changes in the combined effect values of plant resistance tolerance and degradability before and after PCB-46 modification. The combined effects of all three PCB-46 virtual modification molecules (2′-CH_2OH-PCB-46, 2′-CF_3-PCB-46, and 2′-NO_2-PCB-46) tended to increase, with changes of 10.03%, 50.92%, and 97.66%, respectively. These changes indicated significant alterations in plant resistance and degradability after introducing hydrophobic feature group modifications to PCBs, confirming the results from the mechanistic analysis of the Hypo 1 pharmacophore model, which indicated that hydrophobic features significantly affected PCB resistance and degradability changes.

Using the 2D-QSAR model of plant resistance and plant degradability of PCBs constructed in previous literature (Li et al., 2021), we further predicted and analyzed the plant resistance and plant degradability data for the three molecules after virtual modification of PCB-46 (Table 5). The results revealed that 2′-CH_2OH-PCB-46 exhibited improved plant stress resistance and plant degradability, consistent with the trend of the combined effect values. Hence, we employed 2′-CH_2OH-PCB-46 as an illustrative case study to conduct an in-depth examination of plant stress resistance and plant degradability alterations before and after virtual modification with PCBs. Thus, we selected 2′-CH_2OH-PCB-46 as a representative example to scrutinize the changes in plant stress resistance and enhancement in phytodegradability mechanisms before and after PCB modification.

TABLE 4 Changes in the comprehensive effect before and after virtual modification of PCB-46.

No.	PCBs	Comprehensive effect value	Change (%)
1	PCB-46	1.196	
2	2′-CH_2 OH-PCB-46	1.316	10.03
3	2′-CF_3 -PCB-46	1.805	50.92
4	2′-NO_2 -PCB-46	2.364	97.66

Based on the results from the 2D-QSAR model analysis of PCB phytodegradability [31], reducing hydrophobic interactions and increasing hydrophilic interactions between PCBs and phytodegradable enzyme binding facilitated PCB degradation. An analysis of the phytodegradability improvement mechanism of 2′-CH_2OH-PCB-46 revealed that although the hydrophobic -CH_2OH group was introduced, the hydrophobicity of 2′-CH_2OH-PCB-46 decreased to 4.81 after this addition, showing a slight decrease compared to the hydrophobicity of PCB-46 (4.83). This decrease improved the affinity of 2′-CH_2OH-PCB-46 for plant degradation enzymes, leading to enhanced plant degradability of the molecule. Similarly, in comparison to that of PCB-46, the hydrophobicity of 2′-NO_2-PCB-46 (4.68) decreased, while that of 2′-CF_3-PCB-46 (6.30) increased, resulting in opposite trends in the phytodegradability changes for both, with 2′-NO_2-PCB-46 and 2′-CH_2OH-PCB-46 demonstrating positive trends in phytodegradability improvement.

3.3.2 Analysis of the mechanism using molecular docking and molecular dynamics

Reactions between enzymes and ligands are typically governed by intermolecular forces (Li et al., 2022). Common weak interaction forces include van der Waals forces, hydrogen bonding forces, and hydrophobic forces, among others (Johnson et al., 2010). To analyze the mechanism of plant resistance improvement by PCBs, the "Show 2D Diagram" function in the "View Interaction" module of Discovery Studio 2020 software was used to extract the active pockets of PCB-46 and 2′-CH_2OH-PCB-46 bound to plant resistance enzymes. This allowed us to analyze the virtual modification of PCB-46 before and after the changes in weak forces within the active pocket. Green represents interactions involving van der Waals forces between amino acid residues and the molecule, light pink indicates electrostatic forces, purple signifies π–π stacking, red represents unfavorable donor–donor interactions, and yellow signifies π–cation interactions.

Van der Waals forces, as attractive forces, become stronger as the distance between the molecule and the protein decreases (Staahlberg et al., 1992). We extracted the situation near the binding site between PCB molecules and plant enzymes, and found that the van der Waals force is the highest. Figure 3 illustrates that the main force around PCB-46 binding to plant resistance enzymes is van der Waals forces (involving amino acid residues SER81, ARG48, TRP191, THR180, SER185, TYR187, and TRP51), followed by electrostatic forces (involving amino acid residues HIS52, LEU144, HIS175, LEU232, ALA147, and PRO145). After docking, 2′-CH_2OH-PCB-46 with plant resistance enzymes exhibited peripheral forces, including van der Waals forces

TABLE 5 Changes in plant resistance and phytodegradability before and after PCB-46 modification.

Molecular	Plant resistance	Range of variation (%)	Phytodegradability	Range of variation (%)
PCB-46	65.2815		78.9577	
2′-CH_2OH-PCB-46	41.1463	−36.97	87.0085	10.20
2′-CF_3-PCB-46	10.3862	−84.09	59.4146	−24.75
2′-NO_2-PCB-46	115.2215	76.50	90.5838	14.72

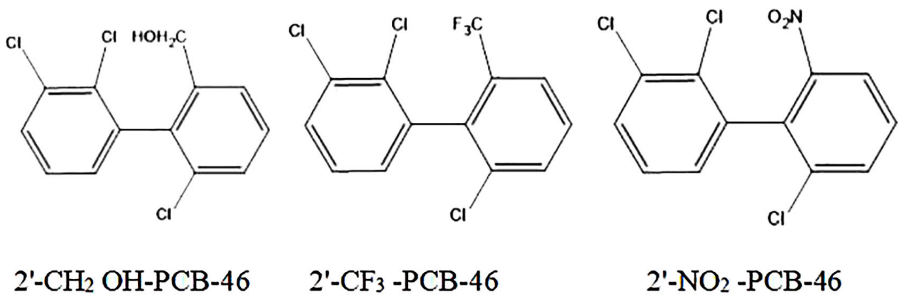

FIGURE 2
2D structure diagram of three PCB-46 virtual modification molecules.

(involving amino acid residue HIS181), electrostatic forces (involving amino acid residues HIS175 and LEU232), π–π stacking (involving amino acid residue TPR191), unfavorable interactions (involving amino acid residue ASN184), and π–cation interactions (involving amino acid residue ARG48).

Molecular dynamics methods were used to calculate the binding energies and van der Waals forces of PCB-46 and 2′-CH_2OH-PCB-46 with plant resistance enzymes. The results showed that PCB-46 had a binding energy of 122.444 kJ/mol and van der Waals force of 149.006 kJ/mol with plant resistance enzymes, while 2′-CH_2OH-PCB-46 had a binding energy of 110.059 kJ/mol and van der Waals force of 128.887 kJ/mol with plant resistance enzymes. Compared to PCB-46, 2′-CH_2OH-PCB-46 exhibited a decrease in binding energy and a significant decrease (by 13.50%) in the surrounding van der Waals forces. These results from molecular dynamics calculations further supported the idea that PCB-46 had a greater binding energy due to greater surrounding van der Waals forces, resulting in an opposite effect for 2′-CH_2OH-PCB-46, where the reduced van der Waals forces led to increased distance between the molecule and the enzyme, resulting in weaker binding and reduced toxicity of 2′-CH_2OH-PCB-46 on plants.

Furthermore, an analysis of the impact of introducing the -CH_2OH group on the changes in van der Waals forces of PCB-46 revealed that the molecular volume of 2′-CH_2OH-PCB-46 increased by 3.84% compared to that of PCB-46, with volumes of 71.95 cm^3/mol and 69.29 cm^3/mol, respectively. A larger molecular volume increases the distance between the molecule and the protein, weakening the van der Waals forces and attraction between the protein and the molecule (Roth et al., 1996). Therefore, the introduction of the -CH_2OH group resulted in an increased molecular volume and weakened van der Waals forces of 2′-CH_2OH-PCB-46, ultimately improving its plant resistance compared to PCB-46.

Additionally, the van der Waals surface area fraction of the virtually modified fragments in PCB-46 and 2′-CH_2OH-PCB-46 was calculated using the "Quantitative Molecular Surface Analysis" function of Multiwfn software (Qu et al., 2012), with the electron density of the equivalent surface set to 0.002 a.u. In this study, the -Cl substituent region of PCB-46 was designated fragment 1, and the -CH_2OH substituent region of 2′-CH_2OH-PCB-46 was designated fragment 2. Figure 4 illustrates the van der Waals surface effects of PCB-46. The calculations revealed that the van der Waals surface area of fragment 1 (depicted in blue) constituted 1.91% of the total van der

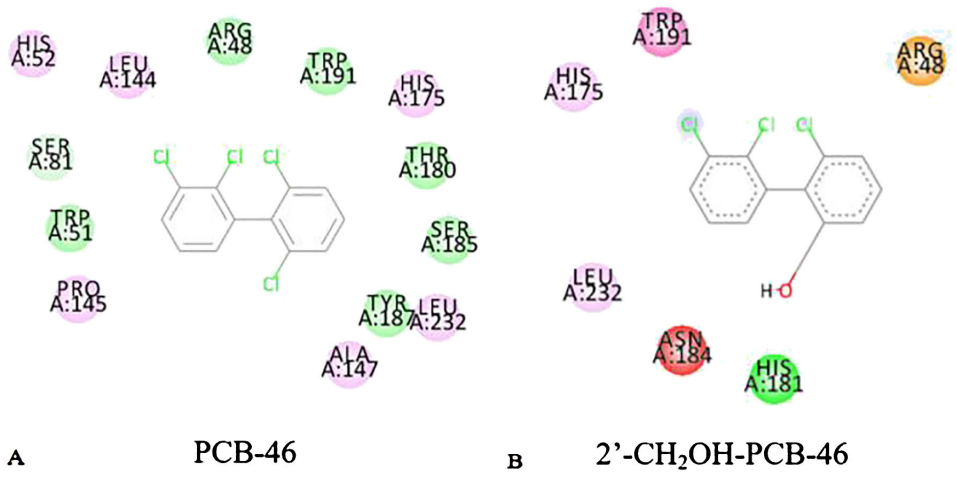

FIGURE 3
2D diagram of PCB-46 **(A)** and 2′-CH_2OH-PCB-46 **(B)** binding to plant-degrading enzymes.

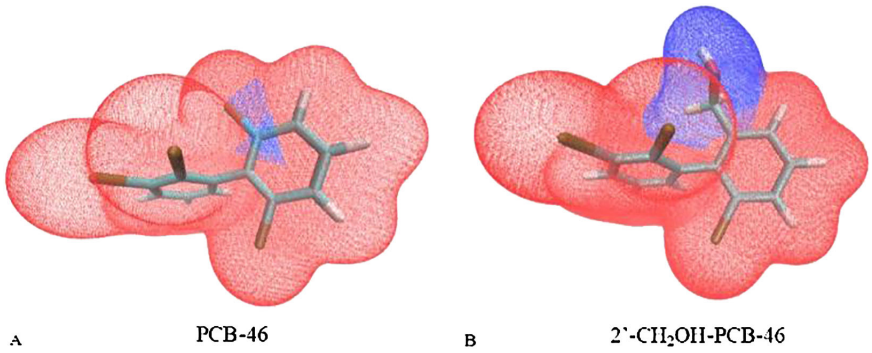

FIGURE 4
Van der Waals surface area of segments 1 and 2 of PCB-46 **(A)** and 2′-CH2OH-PCB-46 **(B)**.

Waals surface area of PCB-46, while the van der Waals surface area of fragment 2 (depicted in blue) constituted 17.93% of the total van der Waals surface area of 2′-CH_2OH-PCB-46. Dispersion forces, an important form of van der Waals forces, exist between all molecules or atoms (Roth et al., 1996). The greater the molecular weight of a molecule is, the greater its deformability, leading to stronger intermolecular dispersion forces (Liu et al., 2019). Compared with fragment 1 of PCB-46, the reduction in the molecular weight of fragment 2 results in a decrease in the dispersion force exhibited by 2′-CH_2OH-PCB-46. Additionally, fragment 2 occupies a larger portion of the limited total van der Waals surface, further diminishing the dispersion force of 2′-CH_2OH-PCB-46 and reducing the van der Waals force. The reduction of molecular weight leads to a decrease in the energy of dispersion forces, while the larger molecular volume occupies a greater area within the limited van der Waals surface area, thus resulting in an overall decrease in the van der Waals force. Consequently, when introducing hydrophobic groups, it is important to consider both the molecular weight of the group itself and the alteration in molecular volume following virtual modification. This approach is beneficial for enhancing plant resistance to PCBs.

4 Conclusion

A 3D-QSAR pharmacophore model for the combined effects of PCBs on plant stress resistance and degradation was constructed, which can better express the combined pharmacophore characteristics of PCBs on plant stress resistance and degradation. The Hypo 1 pharmacophore model contains one hydrophobic and two aromatic ring features, indicating that these two features have a significant impact on the combined effects of pollutants on plant stress resistance and degradation. Since the aromatic ring feature is a characteristic of PCB structure, adjusting the hydrophobic characteristics of PCBs in plants can further alleviate PCB stress resistance and improve PCB degradation.

Using PCB-46 with the highest comprehensive effect value as a template molecule, molecular virtual modification technology was used to improve the resistance and degradation of PCBs in plants. The mechanism analysis results of the Hypo 1 pharmacophore model were verified, indicating that hydrophobic characteristics affect the resistance and degradation of PCBs in plants, significantly affecting the degradation effect of pollutants in plants.

In-depth analysis of the mechanism changes in plant stress resistance and plant degradation improvement before and after virtual modification of PCBs revealed that hydrophobic groups have a greater impact on plant degradation of pollutants. The improvement in plant degradation is biased toward hydrophobic groups with weaker hydrophobicity compared to chlorine atoms, while the improvement of plant stress resistance tends to be associated with hydrophobic groups with smaller molecular weights compared to chlorine atoms and an increase in the overall molecular volume after virtual modification.

Data availability statement

The original contributions presented in the study are included in the article/supplementary material. Further inquiries can be directed to the corresponding author.

Author contributions

ML: Conceptualization, Data curation, Formal analysis, Investigation, Methodology, Software, Validation, Visualization, Writing – original draft. SW: Conceptualization, Formal analysis, Investigation, Writing – review & editing. SS: Investigation, Writing – review & editing.

Funding

The author(s) declare that no financial support was received for the research, authorship, and/or publication of this article.

Acknowledgments

We thank Sagesci company (www.sagesci.cn) for English language editing.

Conflict of interest

Author SW was employed by XingYe Environmental Group Co., Ltd.

The remaining authors declare that the research was conducted in the absence of any commercial or financial relationships that could be construed as a potential conflict of interest.

Publisher's note

References

Arooj, M., Thangapandian, S., and John, S. (2011). 3D QSAR pharmacophore modeling, in silico screening, and density functional theory (DFT) approaches for identification of human chymase inhibitors. *Int. J. Mol. Sci.* 12, 9236–9264. doi: 10.3390/ijms12129236

Cary, T., Rylott, E., Zhang, L., Routsong, R., Palazzo, A., Strand, S., et al. (2021). Field trial demonstrating phytoremediation of the military explosive RDX by XplA/XplB-expressing switchgrass. *Nat. Biotechnol.* 39, 1216–1219. doi: 10.1038/s41587-021-00909-4

Chen, X., and Li, Y. (2021). Toxicity remission of PAEs on multireceptors after molecular modification through a 3D-QSAR pharmacophore model coupled with a gray interconnect degree method. *Turk. J. Chem.* 45, 307–322. doi: 10.3906/kim-2008-38

Feng, L., Xin, M. F. U., and Chao, W. (2016). QSAR, molecular docking and molecular dynamics of 3C-like protease inhibitors. *Acta Phys-Chim. Sinica.* 32, 2693–2708. doi: 10.3866/PKU.WHXB201608121

Gechev, T., Breusegem, F., Stone, J., and Laloi, D. (2006). Reactive oxygen species as signals that modulate plant stress responses and programmed cell death. *BioEssays* 28, 1091–1101. doi: 10.1002/bies.20493

Gu, W., Zhao, Y., Li, Q., and Li, Y. (2020). Plant-microorganism combined remediation of polychlorinated naphthalenes contaminated soils based on molecular directed transformation and Taguchi experimental design-assisted dynamics simulation. *J. hazard. Mater.* 396, 122753. doi: 10.1016/j.jhazmat.2020.122753

Hayat, A., Hussain, I., Soja, G., Iqbal, M., Shahid, N., Syed, J. H., et al. (2019). Organic and chemical amendments positively modulate the bacterial proliferation for effective rhizoremediation of PCBs-contaminated soil. *Ecol. Eng.* 138, 412–419. doi: 10.1016/j.ecoleng.2019.07.038

Huang, H. J., Lee, C. C., and Chen, Y. C. (2014). Pharmacological chaperone design for reducing risk factor of Parkinson's disease from traditional Chinese. *Evid-based. Compl. Alt.* 4, 1–12. doi: 10.1155/2014/830490

Johnson, E. R., Keinan, S., Morisánchez, P., Contreras-García, J., Cohen, A. J., and Yang, W. (2010). Revealing noncovalent interactions. *J. Am. Chem. Soc* 132, 6498–6506. doi: 10.1021/ja100936w

Julien, O., Macabiau, C., and Cannon, M. (2007). ASPeCT: Unambiguous sine-BOC (n,n) acquisition/tracking technique for navigation applications. *IEEE T aero. Elec. Sys.* 43, 150–162. doi: 10.1109/TAES.2007.357123

Kawano, T. (2003). Roles of the reactive oxygen species-generating peroxidase reactions in plant defense and growth induction. *Plant Cell Rep.* 21, 829–837. doi: 10.1007/s00299-003-0591-z

Kong, X., Lv, N., Liu, S., Xu, H., Huang, J., Xie., X., et al. (2022). Phytoremediation of isoproturon-contaminated sites by transgenic soybean. *Plant Biotechnol. J.* 21, 342–353. doi: 10.1111/pbi.13951

Kubo, I., Chen, Q. X., and Nihei, K. I. (2003). Molecular design of antibrowning agents: antioxidative tyrosinase inhibitors. *Food Chem.* 81, 241–247. doi: 10.1016/S0308-8146(02)00418-1

Langer, T. (2010). Pharmacophores in drug research. *Mol. Inform.* 29, 470–475. doi: 10.1002/minf.201000022

Lei, Y., Zhou, X., and Xie, L. (2018). Emergency monitoring and disposal decision support system for sudden pollution accidents based on multimedia information system. Multimed. *Tools. Appl.* 78, 11047–11071. doi: 10.1007/s11042-018-6665-2

Li, M., He, W., Han, Z., Zhou, M., Chen, X., and Li, Y. (2021). Mechanism analysis of the phytotoxicity and phytodegradation of PCBs based on the 2D-QASR model and sensitivity analysis method. *J. Environ. Chem. Eng.* 9, 106241. doi: 10.1016/j.jece.2021.106241

Li, M. H., and Sun, S. M. (2022). Technological developments and remediation mechanisms for phytoremediation of PCB-contaminated soils. *Sustainability* 14, 13582. doi: 10.3390/su142013582

Li, X., He, W., Zhao, Y., Chen, B., Zhu, Z., Kang, Q., et al. (2022). Dermal exposure to synthetic musks: Human health risk assessment, mechanism, and control strategy. *Ecotox. Environ. Safe.* 236, 113463. doi: 10.1016/j.chemosphere.2015.06.078

Liu, C. L., and Marukawa, K. (2004). "Global shape normalization for handwritten Chinese character recognition: a new method," in *Ninth International Workshop on Frontiers in Handwriting Recognition*, Comput Sci. IEEE. Kokubunji, Japan. Vol. 1. 300–305. doi: 10.1109/IWFHR.2004.47

Liu, J., Xu, L., and Bai, J. (2019). Ethyl carbazole-grafted polysiloxane as stationary phase for gas chromatography. *Chromatographia* 82, 671–682. doi: 10.1007/s10337-019-03694-0

Lu, T., and Chen, F. W. (2012a). Multiwfn: A multifunctional wavefunction analyzer. *J. Comput. Chem.* 33, 580–592. doi: 10.1002/jcc.22885

Lu, T., and Chen, F. W. (2012b). Quantitative analysis of molecular surface based on improved Marching Tetrahedra algorithm. *J. Mol. Graph. Model.* 38, 314–323. doi: 10.1016/j.jmgm.2012.07.004

Mohammadi, M., Chalavi, V., Novakova-Sura, M., Laliberte, J., and Sylvestre, M. (2007). Expression of bacterial biphenyl-chlorobiphenyl dioxygenase genes in tobacco Plants. *Biotechnol. Bioeng.* 97, 496–505. doi: 10.1002/bit.21188

Qu, R., Liu, H., Feng, M., Yang, X., and Wang, Z. (2012). Investigation on intramolecular hydrogen bond and some thermodynamic properties of polyhydroxylated anthraquinones. *J. Chem. Eng. Data* 57, 2442–2455. doi: 10.1021/je300407g

Roth, C., Neal, L., and Lenhoff, A. (1996). van der Waals interactions involving proteins. *Biophys. J.* 70, 977–987. doi: 10.1016/S0006-3495(96)79641-8

Staahlberg, J., Joensson, B., and Horvath, C. (1992). Combined effect of coulombic and van der Waals interactions in the chromatography of proteins. *Anal. Chem.* 64, 3118–3124. doi: 10.1021/ac00048a009

Terzaghi, E., Vergani, L., Mapelli, F., Borin, S., and Guardo, A. D. (2019). Rhizoremediation of weathered PCBs in a heavily contaminated agricultural soil. Results of a biostimulation trial in semi field conditions. *Sci. Total Environ.* 686, 484–496. doi: 10.1016/j.scitotenv.2019.05.458

Terzaghi, E., Vitale, C. M., Salina, G., and Guardo, A. D. (2020). Plants radically change the mobility of PCBs in soil: Role of different species and soil conditions. *J. Hazard. Mater.* 388, 121786. doi: 10.1016/j.jhazmat.2019.121786

Vincent, L. R., and Bellini, L. M. (2002). William of Occam and Occam's razor. *Ann. Intern. Med.* 136, 634–635. doi: 10.7326/0003-4819-136-8-200204160-00022

Wang, X., Luo, Y., Zhai, Z., Yang, L., and He, T. (2017). "Algorithm for sine wave cure fit based on frequency precise estimation," in *2017 International Conference on Mechanical, System and Control Engineering (ICMSC)*, Vol. 7. 357–361. doi: 10.1109/ICMSC.2017.7959501

Wang, D., and Wang, Y. (2021). Emergency capacity of small towns to endure sudden environmental pollution accidents: construction and application of an evaluation model. *Sustainability* 13, 5511. doi: 10.3390/su13105511

Xie, Y., Zhang, J., Yin, S., and Loo, J. (2006). Top-down ESI-ECD-FT-ICR mass spectrometry localizes noncovalent protein-ligand binding sites. *J. Am. Chem. Soc* 128, 14432–14433. doi: 10.1021/ja063197p

Zhang, C. Y., Feng, Y., Liu, H., Chang, Z., and Li, J. (2017). Uptake and translocation of organic pollutants in plants: a review. *J. Integr. Agr.* 16, 11–20. doi: 10.1016/S2095-3119(16)61590-3

Zhang, H., Shen, C., and Zhang, H. R. (2021). Discovery of novel DGAT1 inhibitors by combination of machine learning methods, pharmacophore model and 3D-QSAR model. *Mol. Divers.* 25, 1–15. doi: 10.1007/s11030-021-10247-x

Zhang, Q., Li, R., and Peng, W. (2019). Identification of the active constituents and significant pathways of Guizhi-Shaoyao-Zhimu decoction for the treatment of diabetes mellitus based on molecular docking and network pharmacology. *Comb. Chem. High T. scr.* 22, 584–598. doi: 10.1016/10.2174/1386207322666191022101613

Zhao, S., Li, X., and Peng, W. (2021). Ligand-based pharmacophore modeling, virtual screening and biological evaluation to identify novel TGR5 agonists. *RSC Adv.* 11, 9403–9409. doi: 10.1039/D0RA10168K

Frontiers in
Plant Science

Cultivates the science of plant biology and its applications

The most cited plant science journal, which advances our understanding of plant biology for sustainable food security, functional ecosystems and human health.

Discover the latest Research Topics

See more →

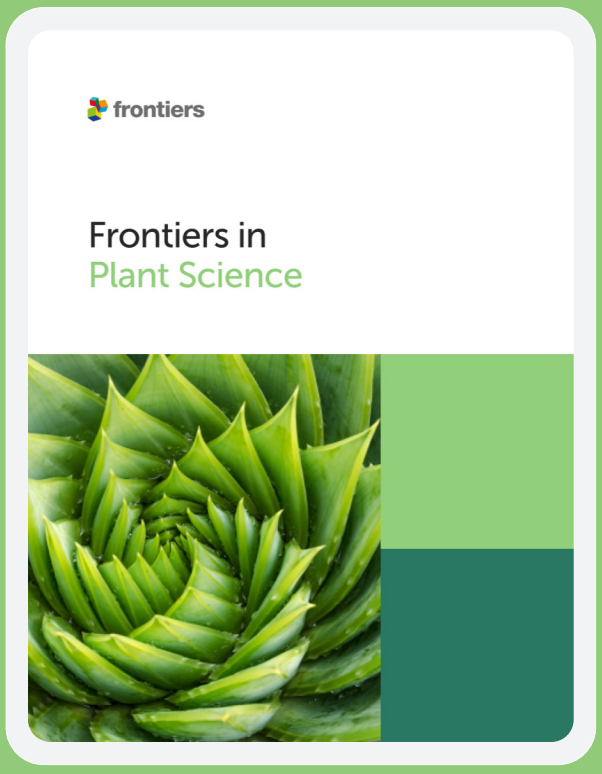

Frontiers

Avenue du Tribunal-Fédéral 34
1005 Lausanne, Switzerland
frontiersin.org

Contact us

+41 (0)21 510 17 00
frontiersin.org/about/contact